Monometallic and multimetallic complexes as precatalysts in the hydroformylation of olefins

Shepherd Siangwata

University of Cape Town

January 2020

Monometallic and multimetallic complexes as precatalysts in the hydroformylation of olefins

A thesis submitted to the

University of Cape Town

In fulfilment of the requirements for the degree of

Doctor of Philosophy

by

Shepherd Siangwata

Supervisor: Assoc. Professor Gregory S. Smith

Co-supervisor: Dr Neill J. Goosen

Department of Chemistry,

University of Cape Town,

South Africa

Declaration

I know the meaning of Plagiarism and declare that all of the work in the document "**Monometallic and multimetallic complexes as precatalysts in the hydroformylation of olefins**" is my own, save for that which is properly acknowledged by means of a reference. It is to the best of my knowledge that this work has never been reported or submitted for any degree or examination by any university.

Shepherd Siangwata …… Signed by candidate

Date …… 10 January 2020

Acknowledgements

Firstly, I would like to thank God for the gift of life, for this work and the blessings with which my future is set.

I also wish to express my deepest gratitude and appreciation to my supervisor, Assoc. Prof. Gregory Smith, and my co-supervisor, Dr Neill Goosen, for their invaluable support and cutting-edge guidance that I received throughout the period of my doctoral studies. I owe an immeasurable debt of gratitude and appreciation for their expertise, kindness, help and advice that undoubtedly leads to a sound career progression.

Specific heartfelt appreciation extends to my mentor, Dr Siyabonga Ngubane for his encouragement, and unwavering first-class academic support throughout this project. The substantial guidance and knowledge offered in unparralled.

I would also like to express my special acknowledgement and gratitude to my friends, Dr Leah Matsinha, Dr Nicholas Breckwoldt, and Ms Latisa Maqeda for their foundational support leading to this work, and consistent encouragement over the years.

My indebtedness extends to the organometallic research group members, both former and current members with whom I have shared laboratory space and grown to build a life-long friendship. I trust that they know just how greatly I cherish our interaction during the period of my study.

I would also like to express my special acknowledgement and gratitude to the central office personnel in the Department of Chemistry, as well as Mr Pete Roberts and the workshop personnel for their great job throughout my studies.

For funding, I would like to give thanks to the University of Cape Town and the DST-NRF Centre of Excellence in Catalysis (c*change).

Finally, I would like to thank my parents, family and friends for their prayers, support, inspiration and encouragement throughout the period of my study.

Abstract

A series of new aryl ether salicylaldimine-based monomeric, dimeric, trimeric and hexameric triazolyl ligands have been synthesised. The *N,O*-chelating ligands were synthesised *via* Schiff base condensation reactions of salicylaldehyde with the bromopropylamine hydrobromide salt, followed by the azidation of the resultant *N*-3-bromopropylsalicylaldimine. Click chemistry reactions of the azido propyl salicylaldimine with the appropriate phenolic-alkyne afforded the mono-, di-, tri- and hexameric aryl ether salicylaldimine-based triazolyl ligands. The ligands were characterised using various analytical and spectroscopic techniques. Complexation of the monomeric and trimeric ligands with the dimeric rhodium precursor $[RhCl(COD)]_2$ yielded new aryl ether *N,O*-chelate mononuclear and trinuclear Rh(I) complexes. The complexes were characterised using nuclear magnetic resonance spectroscopy, infrared spectroscopy, mass spectrometry and melting point determinations.

The mononuclear and trinuclear complexes were successfully evaluated as catalyst precursors in the hydroformylation of higher olefins. The reaction conditions were optimised using the mononuclear precatalyst at 85 °C, 40 bar syngas pressure for 4 h with 2.87 x 10^{-3} mmol Rh loading and a substrate (1-octene) to catalyst ratio of 2500 : 1. These conditions gave good aldehyde chemoselectivity (90%), excellent conversion of the substrate (99%) and good catalytic activity (554 h^{-1}). Comparable catalytic performance of both precatalysts was obtained when milder reaction conditions (85 °C, 20 bar for 4 h) were adopted in the evaluation of the mononuclear complex against the low generation dendritic trinuclear complex. The mercury poisoning experiments revealed a dual catalytically influenced system, emanating from a combination of homogeneous and heterogeneous catalytic species. The mononuclear catalyst precursor was also evaluated successfully in the hydroformylation of internal olefins 7-tetradecene and *trans*-4-octene. The catalyst precursor gave good conversions of both internal olefins (> 80%) under the optimum reaction conditions (85 °C, 40 bar for 4 h). Catalyst recyclability studies in the hydroformylation of 1-octene conducted using the Organic Solvent Nanofiltration (OSN) strategy demonstrated five successful recycles with consistently good catalytic performance from both catalyst precursors. Inductively coupled plasma optical emission spectrometry (ICP-OES) experiments revealed a near perfect (99%) membrane retention of the rhodium metal. Kinetic studies using the mononuclear precatalyst were investigated by evaluating the effect of temperature, syngas total pressure and catalyst loading on the rate of hydroformylation. The activation energy for the hydroformylation of 1-octene

was calculated to be 62 kJ mol^{-1} and the experimental rate constants were found to be in good agreement with the predicted rate data obtained using a modified fundamental mechanism-based rate model.

The synthesis and characterisation of new water-soluble, sulfonated aryl ether salicylaldimine-based mono- and trimeric ligands has also been described. The ligands were prepared following a series of amine and Boc-protection and deprotection procedures, Schiff base condensation reactions and Williamson ether synthesis. The water-soluble *N,O*-chelating aryl ether ligands were characterised using various spectroscopic and analytical techniques. Subsequently, complexation reactions of the ligands with the dimeric $[RhCl(COD)]_2$ gave the corresponding new water-soluble mononuclear and trinuclear Rh(I) complexes. The complexes were characterised using nuclear magnetic resonance spectroscopy, infrared spectroscopy, mass spectrometry and melting point determinations. The complexes show appreciably good solubility in water, 15.7 mg/mL (mononuclear complex) and 8.6 mg/mL (trinuclear complex).

The new water-soluble mono- and trinuclear complexes were successfully evaluated as precursors in the aqueous biphasic hydroformylation of higher olefins. Optimisation experiments using the mononuclear precatalyst gave the best results at 85 °C, 50 bar syngas pressure for 4 h with 2.87 x 10^{-3} mmol Rh loading and a substrate (1-octene) to catalyst ratio of 2500 : 1. Both catalyst precursors gave near quantitative catalytic conversion of 1-octene, good activities (> 550 h^{-1}) and attractive aldehyde chemoselectivity (> 85%). A substrate and product-distribution time study showed a positive dendritic effect in relation to the trinuclear complex over the mononuclear complex. The mercury poisoning experiments were suggestive of a system that is catalysed by a dual effect of homogeneous and heterogeneous catalytic species. Recyclability experiments were successfully conducted over 5 cycles, with a gradual decline in catalytic performance for both complexes. The dendrimer stabilised trinuclear precatalyst showed improved recyclability in "neat", monophasic hydroformylation experiments, while the mononuclear precatalyst showed a reduced overall performance. The bias towards the linear aldehyde for the dendritic trinuclear complex was tunable by addition of excess bulkier trimeric water-soluble ligand into the catalytic system. Inductively coupled plasma optical emission spectrometry experiments showed moderate losses of the metal from the aqueous phase to the organic layer. Both catalyst precursors also showed good catalytic activity (> 450 h^{-1}) and a total bias to aldehyde chemoselectivity (no hydrogenation products) in the aqueous biphasic hydroformylation of styrene.

Publications and Conference contributions

Journal Articles

1. Aqueous olefin hydroformylation using water-soluble mono- and trinuclear *N,O*-chelate rhodium(I)-aryl ether precatalysts.
   Shepherd Siangwata, Neill J. Goosen and Gregory S. Smith, *Appl. Catal. A Gen*., 2020, **603**, 117736.

2. Olefin hydroformylation and kinetic studies using mono- and trinuclear *N,O*-chelate rhodium(I)-aryl ether precatalysts.
   Shepherd Siangwata, Nicholas C. C. Breckwoldt, Neill J. Goosen, and Gregory S. Smith, *Appl. Catal. A Gen.,* 2019, **585**, 117179.

3. Aqueous biphasic hydroformylation of olefins: From classical phosphine-containing systems to emerging strategies based on water-soluble non-phosphine ligands.
   Leah C. Matsinha, **Shepherd Siangwata**, Gregory S. Smith and Banothile C. E. Makhubela, *Cat. Rev. - Sci. Eng*., 2019, 61, 111–133.

Conference Contributions

1. *Recoverable and recyclable mono- and multinuclear Rh(I)-salicylaldimine aryl ether-based complexes for olefin hydroformylation* (Poster Presentation). CATSA Conference, Club Mykonos, Langebaan (10 – 13 November 2019).
   Shepherd Siangwata, Nicholas C. C. Breckwoldt, Neill J. Goosen, and Gregory S. Smith.

2. *Mononuclear and multinuclear Rh(I) N,O-chelate complexes and their evaluation as pre-catalysts for 1-octene hydroformylation* (Poster Presentation). ICOMC, Florence, Italy (15 – 21 July 2018).
   Shepherd Siangwata and Gregory S. Smith.

3. *N,O-chelate Rh(I) complexes conjugated on the periphery of aryl ether dendritic synthons for 1-octene hydroformylation* (Poster presentation). CATSA Conference, Pilanesberg, South Africa (19 – 22 November 2017).
   Shepherd Siangwata and Gregory S. Smith.

4. *Recoverable and recyclable water-soluble mono- and binuclear organometallic complexes in the aqueous biphasic hydroformylation of 1-octene* (Poster presentation). Green Chemistry Symposium and Workshop (G_2C_2), Chengdu, Sichuan University, China (18 – 19 July 2016).
   Shepherd Siangwata, Percy van der Gryp and Gregory Smith.

List of Abbreviations

Acac	acetylacetone
Ar	aromatic or aryl
ATR-IR	attenuated total reflectance infrared spectroscopy
br s	broad signal
°C	degrees celsius
δ	chemical shift
ν	wavenumber
ν_{max}	maximum wavelength
$^{13}C\{^{1}H\}$ NMR	proton-decoupled carbon-13 nuclear magnetic resonance
calcd.	calculated
$CDCl_3$	deuterated chloroform
cm^{-1}	wavenumber (reciprocal centimetres)
COD	1,5-cyclooctadiene
COSY	correlation spectroscopy
d	doublet
DAB	1,4-diaminobutane
dd	doublet of doublets
DCM	dichloromethane
DMF	dimethylformamide
DMSO	dimethyl sulfoxide
EA	elemental analysis
EI-MS	electron impact mass spectrometry
ESI-MS	electrospray ionisation mass spectrometry

EtOH	ethanol
FT-IR	Fourier transform infrared spectroscopy
g	gram(s)
GC	gas chromatography
h	hour
^{1}H NMR	proton nuclear magnetic resonance
HSQC	heteronuclear single quantum correlation
Hz	hertz
ICP-OES	inductively coupled optical emission spectrometry
IL	ionic liquid
IR	infrared
J	coupling constant
m	multiplet for nuclear magnetic resonance
MeOH	methanol
mg	milligram(s)
MHz	megahertz
mL	millilitre
mmol	millimole(s)
M.P.	melting point
MS	mass spectrometry
m/z	mass to charge ratio
NMR	nuclear magnetic resonance
PGMs	platinum group metals
ppm	parts per million

ppb	part per billion
q	quartet
quin	quintet
r.t.	room temperature
s	singlet
sext	sextet
$scCO_2$	supercritical carbon dioxide
Syngas	synthesis gas
t	triplet
^{t}Bu	tertiary butyl
TOF	turnover frequency
TPP	triphenylphosphine
TPPMS	monosulfonated triphenylphosphine
TPPTS	triphenylphosphine trisulfonate

Table of Contents

Chapter 1

Background and literature review on catalysis: A focus on hydroformylation

This Chapter forms part of a review publication, titled "*Aqueous biphasic hydroformylation of olefins: From classical phosphine-containing systems to emerging strategies based on water-soluble non-phosphine ligands*", cited as:
L. C. Matsinha, **S. Siangwata**, G. S. Smith and B. C. E. Makhubela, *Cat. Rev. - Sci. Eng.*, 2019, **61**, 111–133.

1.1 Introduction

The approach of acceleration of chemical reactions *via* catalysis has developed to be the fundamental backbone to industrially relevant chemical transformations. Dating back to the 18th century, catalysis has unarguably played a significant role in the chemical industry, impacting immensely on the economic and environmental principles of manufacturing.[1–5] The growing global demand for energy-efficient and eco-friendly industrial processes has over the years led to improved strategies in catalyst design and development for medium to large scale applications. Key industries that thrive on the use of catalysts are in sectors such as the automobile (for example, exhaust catalytic converters),[6,7] agrochemicals (for example, pesticide production),[8–10] pharmaceuticals (for example, through asymmetric catalysis),[11–13] as well as the petrochemicals sector (for example, catalytic cracking of hydrocarbons).[14–16]

The availability of synthetic hydrocarbons (alkanes and alkenes) from the catalysed conversion of syngas (a mixture of CO and H_2) *via* the Fischer-Tropsch Process at Sasol is very attractive, creating avenues for further value-addition of these hydrocarbons through catalysis. Moreover, the process is increasingly attractive owing to the ease of access of syngas from several sources, such as natural gas, coal gasification as well as from biomass. This translates to huge economic benefits that culminate from the downstream processing of the resultant hydrocarbons, often utilising transition metal-based catalysts. Several transition metal-catalysed reactions are based on the rare, relatively expensive, moisture and air stable second and third–row transition metals, for example, the Platinum Group Metals (PGMs).[17–19]

The availability of PGMs in Southern Africa (Merensky and Upper Group 2 (UG2) Reefs in South Africa, and the Great Dyke in Zimbabwe) necessitates beneficiation of these expensive and fast-depleting metals through application in downstream hydrocarbon catalytic transformations. Such strategies are aimed at adding more value to the metals while also transforming the low-value hydrocarbons (< C6) to high-value sources (> C7). This can be achieved through the design and synthesis of novel catalyst precursors that are more efficient, active, highly selective towards the desired product, and operate under mild reaction conditions. These highly desirable characteristics are more-often from a combination of the two types of catalytic systems, heterogeneous and homogeneous catalysis (Table 1.1).[20,21] The two systems are easily distinguished by the phases present during a reaction. Moreover, of particular note is the often-cumbersome separation and recovery of a catalyst from the product and solvent that differentiates homogeneous catalysis from heterogeneous catalysis.

Table 1.1 Comparison of homogeneous catalysis against heterogeneous catalysis.[20,21]

Property	**Homogeneous catalysis**	**Heterogeneous catalysis**
1. Phase	Liquid	Solid/liquid ; Solid/gas
2. Activity	Moderate	High
3. Selectivity	High	Low
4. Working temperature / thermal stability	Low (< 250 ºC)	High (250 – 500 ºC)
5. Catalyst recovery	Difficult and expensive	Easy and cheap
6. Product separation	Difficult	Easy
7. Diffusion problems	Facile	May be encountered
8. Resistance to catalyst poisoning	High	Low
9. Heat transfer	Easy	Can be problematic

It is generally recognised that many industrial reactions that use catalysts are carried out *via* heterogeneous catalysis, owing to the ease of catalyst separation from the product, as well as the high activities associated with the surface area of the supported solid catalyst. However, high reaction temperatures and poor selectivity characterises heterogeneous catalysis. On the other hand, homogeneous catalysis offers good selectivity towards the desired products under mild reaction conditions, with the major drawback being the recovery of the often-expensive

catalyst from the product.[20,21] In view of the challenges that characterise both systems, it has become prudent to explore strategies that bridge the gap between heterogeneous catalysis and homogeneous catalysis. This would be of benefit to highly important homogeneous catalysed reactions in industry, such as carbonylation[22–25], hydrogenation[26–28] and hydroformylation reactions.[29–31]

1.2 Hydroformylation

The hydroformylation reaction was discovered by Otto Roelen in 1938, while investigating the oxygenated side products of the cobalt-catalysed Fischer-Tropsch reaction.[32,33] This atom-economic transition metal catalysed reaction is also known as the "Oxo process" and involves the production of aldehydes from the addition of syngas to olefins (Scheme 1.1). Further conversion of these aldehydes following appropriate reduction, oxidation and condensation reactions leads to intermediates known as the oxo intermediates (specialty esters, carboxylic acids, polyols, alcohols and amines). The oxo intermediates are then transformed into a wide array of products which are in the bulk and fine chemicals industries, ranging from detergents, pharmaceuticals, plasticisers, agrochemicals to fragrances.[34]

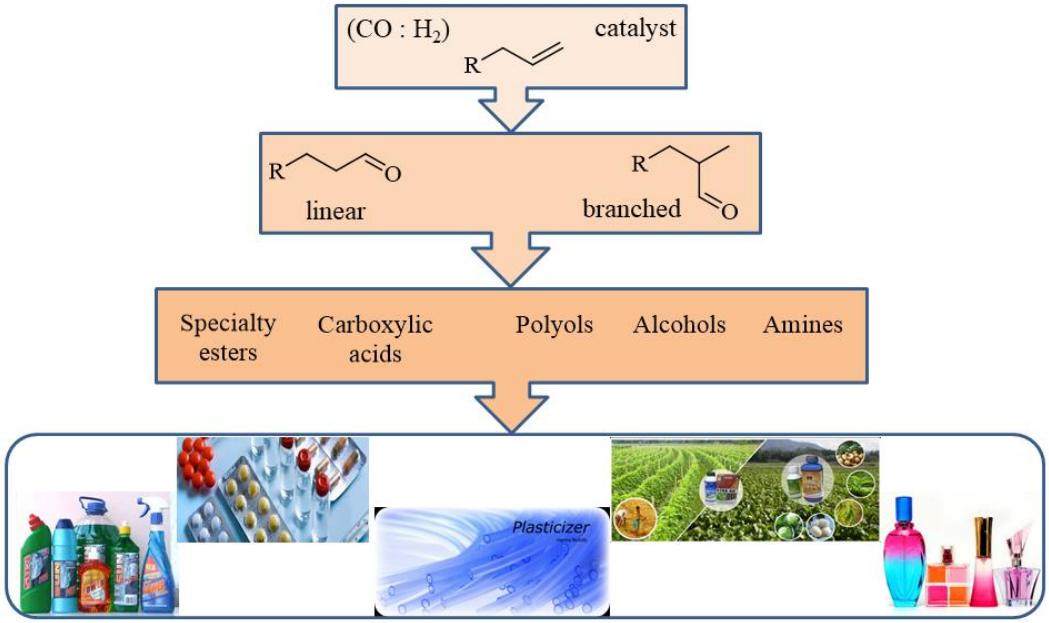

Scheme 1.1 Illustrating the hydroformylation process and the downstream products.[34]

The initial hydroformylation catalyst was based on the cobalt carbonyl complex $[Co(CO)_4H]$. However, the use of the cobalt-based catalyst had certain drawbacks which included: i) fouling of industrial reactors due to the formation of undesirable cobalt clusters, ii) the need for high temperature and pressure to attain average linear selectivity of 80%, and iii) ease of volatility of the catalytically active species (resulting in difficulties in catalyst separation and recovery through the conventional distillation process). Modified cobalt and rhodium catalysts were then introduced to circumvent some of these drawbacks as demand for the oxo products grew. The introduction of rhodium as a metal of choice proved to be beneficial due to its high reactivity and regioselectivity under mild reaction conditions. The superiority of the rhodium metal over other transition metals in the hydroformylation of olefins has been reported in the literature:[35]

$$Rh >> Co > Ir, Ru > Os > Pt > Pd >> Fe > Ni$$

The good catalytic activity of organorhodium complexes in the hydroformylation reaction can be ascribed to the ease of oxidative addition of the metal to tetra coordinate rhodium(I) and the reductive elimination from octahedral rhodium(III). Such redox properties are shown in the catalytic cycle for the rhodium-catalysed hydroformylation mechanism (Scheme 1.2), where L represents PPh_3.[36]

The catalytic cycle begins with the generation of a 16 electron Rh-H fragment **(1.1)** followed by the coordination of an olefin to a vacant coordination site on Rh to form a 5-coordinate species **(1.2)**. Migratory insertion of the olefin into Rh-H gives rise to a 4 coordinate Rh-alkyl intermediate **(1.3a)** or **(1.3b)** which coordinates a molecule of carbon monoxide in **(1.4a)** or **(1.4b)**. Migratory insertion of CO into the Rh-alkyl species results in a Rh-acyl complex **(1.5a)** or **(1.5b)**. Anti-Markovnikov addition of hydride onto compound **(1.5b)** gives the linear aldehyde product whereas Markovnikov addition onto compound **(1.5a)** leads to the branched aldehyde product. The hydrogenolysis of the Rh-acyl complex is also accompanied with the regeneration of the Rh-H complex **(1.1)**.[45] The selectivity of the hydride addition is controlled by the hydride acidity and the steric constraints of the ligands. It is therefore expected that sterically demanding ligands such as triarylphosphines will be more inclined to the formation of linear aldehydes through anti-Markovnikov addition.

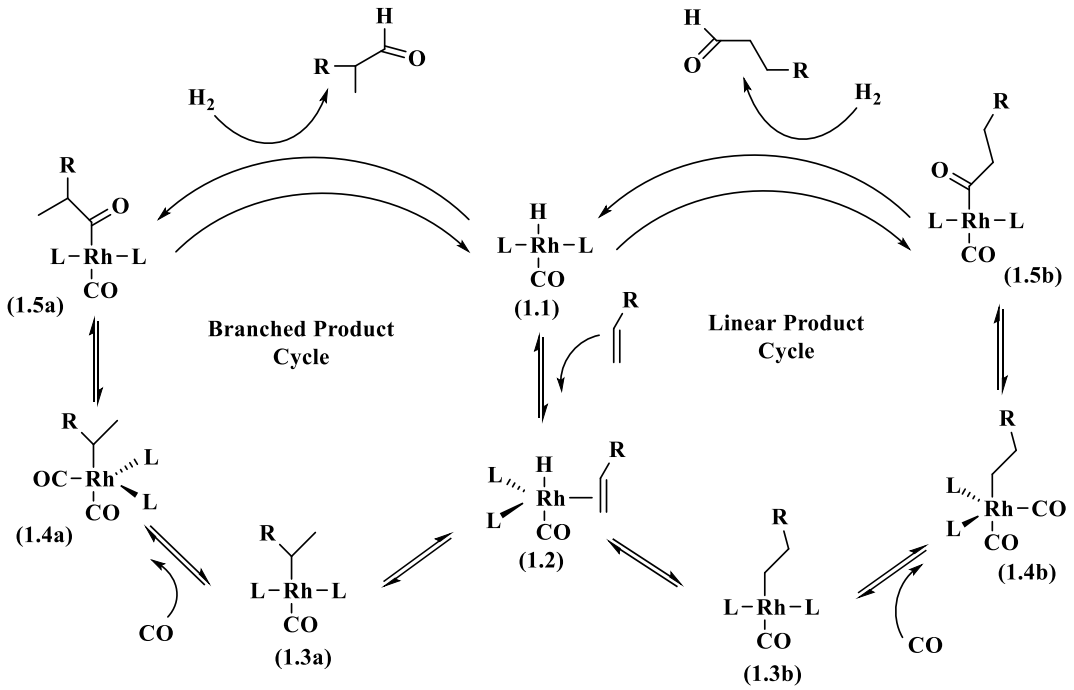

Scheme 1.2 Mechanism of Rh-catalysed hydroformylation.[36]

The understanding of the hydroformylation catalytic cycle is imperative as this creates potential to manipulate the selectivity of a catalyst towards a desired product, minimising the formation of side products that emanate from competing reactions such as isomerisation.[37] Moreover, improving the catalyst efficiency through recoverable and recyclable catalyst precursors is highly-sought after. Several recovery strategies that have been developed are based on the immobilisation of the catalyst onto organic or inorganic supports, and more commonly catalyst immobilisation in multiphase media (catalysis using two or more different phases).[38–41]

1.3 Multiphase media in hydroformylation

Immobilisation of a catalyst in a different phase to that of the substrate has been carried out over the years, mainly for catalyst recovery and reuse.[42] More often, this technique has been applied in a two-phase system, wherein the catalyst is heterogenised in one phase, and the substrate is in a different and immiscible phase at room temperature.[43] In a typical biphasic system, application of heat and pressure to the two immiscible phases enables the catalyst to be in contact with the substrate to effect the catalytic reaction. Upon cooling the reactor, the reaction components separate into two distinct layers, allowing for the removal of the product from the reaction mixture, and recovery of the catalyst for recycling.

Several solvent combinations have been used for biphasic media in hydroformylation, and these include supercritical carbon dioxide/ionic liquids ($scCO_2$/IL), fluorous/organic, and aqueous/organic media.[38,44,45] These solvent combinations are viewed as greener opportunities for catalysis, and their suitability to Green Chemistry remains the drive for their continued application.[46,47]

1.3.1 Supercritical Carbon dioxide/Ionic liquids ($scCO_2$/IL) media

Ionic liquids can simple be defined as ionic organic compounds that are liquid at room temperature, with the upper melting temperature limit at 100 ºC.[42,48] The use of ionic liquids emanates from their good thermal stability, low volatility, as well as the ease in fine-tuning their chemical and physical properties by simply varying the structure of the cation or anion. Moreover, ionic liquids possess very powerful solvent properties, enabling the solvation of a wide range of organic molecules.[49–53] Most ionic liquids constitute organic cations and inorganic anions (Figure 1.1).[54] The solvation properties (polarity, hydrophilicity or hydrophobicity) of ionic liquids can be altered by using a suitable cation and anion constituent. A combination of ionic liquids with supercritical carbon dioxide has been widely studied as alternative solvents for homogeneously catalysed reactions, which include hydrogenation, carbon-carbon bond formation and hydroformylation.[55–58] Supercritical carbon dioxide offers reduced diffusion constraints to both the reactants/substrate and the reaction products, leading to effective product separation with negligible metal leaching.[41,59] The $scCO_2$/IL combination provides a good environment for improved reaction yields as well as facile product recovery and recyclability of the media without loss of ionic liquid functionality.[60] In a typical biphasic setup, the metal complex is dissolved in the ionic liquid, and the unit is charged with supercritical carbon dioxide, which acts as a carrier solvent for the substrate. This facilitates contact between the substrate and the metal complex in a biphasic media, and the subsequent solubilisation of the product into the supercritical carbon dioxide for extraction in a secondary vessel.

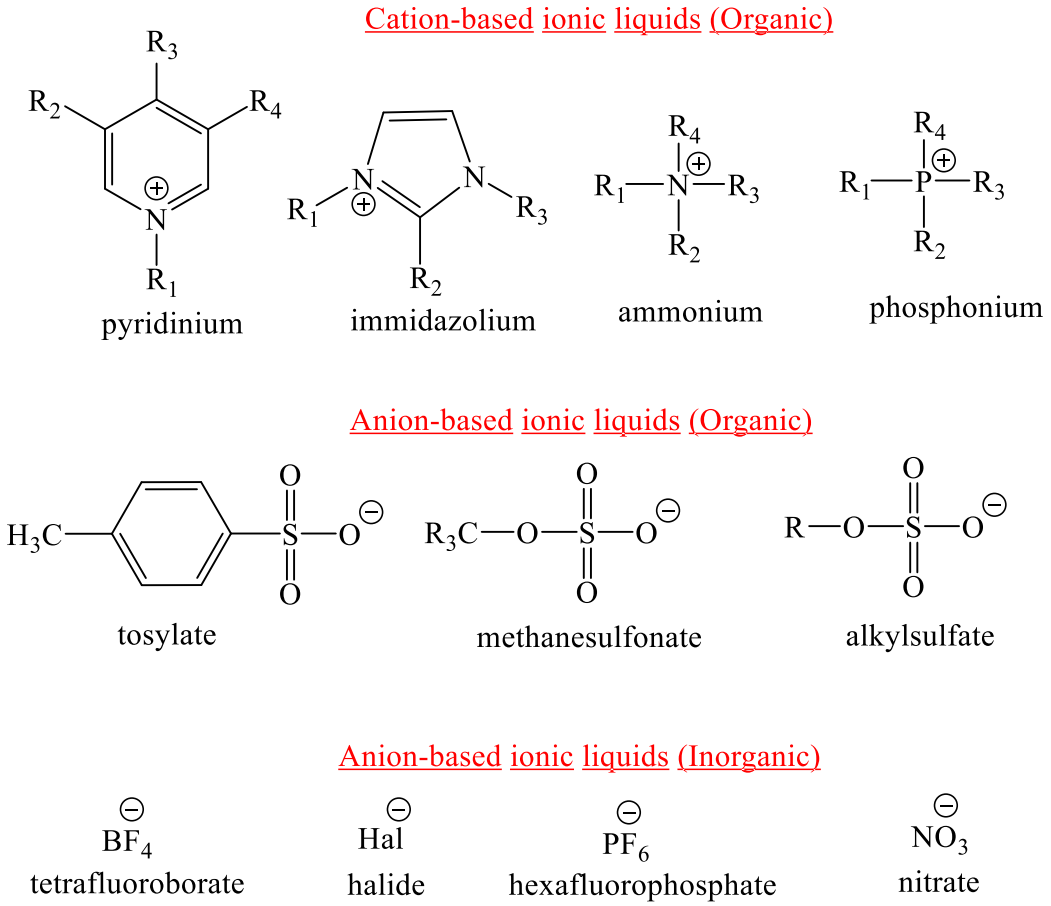

Figure 1.1 Illustrating examples of ionic liquid components.[54]

1.3.2 Fluorous/Organic biphasic media

The term fluorous was introduced by Horvath and Rabai [61] to mimic reactions occurring in aqueous/organic biphasic systems, emphasising that one of the phases in a two phase system is richer in fluorocarbons than the other. Such a two-phase system consists of a fluorous phase containing a preferentially fluorous-soluble catalyst and a second product phase (organic or inorganic solvent) with limited solubility in the fluorous phase (Figure 1.2). Fluorous biphasic systems have found applications in various catalytic chemical transformations, such as epoxidation, cross coupling, oxidation and hydroformylation of olefins through immobilisation of catalyst complexes in the fluorous phase.[62–65] Their low polarity and low miscibility with non-polar organic solvents at room temperature makes fluorous solvents ideal for application in biphasic media.[66,67] The solvents of choice for the fluorous phase are usually perfluoroalkanes, perfluorotrialkyl amines or perfluorodialkyl ethers, whereas toluene, acetone and tetrahydrofuran are the commonly used organic phase solvents. In the design of fluorous-soluble catalysts, the ligand is appended with fluorous-solubilising substituents comprising of

fluorocarbon moieties, also known as fluorous ponytails. It is necessary to insert spacer groups (often –CH_2–) before the fluorous ponytail, to decrease the strong electron-withdrawing effect of the fluorous substituents (complex **1.6**, Figure 1.2). Such modifications have an overall bearing on the electronic environment around the active metal centre, which may influence the catalytic performance of a catalyst towards the desirable product.[68]

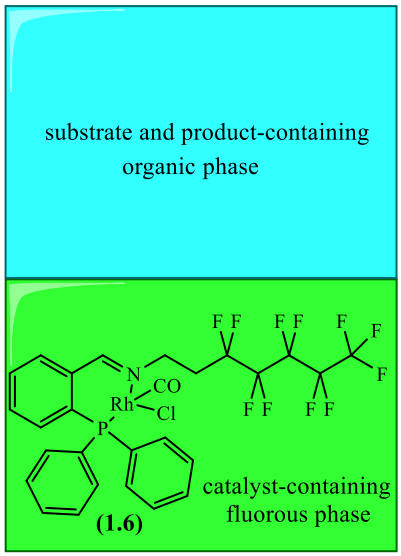

Figure 1.2 Illustrating the concept of fluorous biphasic catalysis.[68]

During the catalytic reaction, the fluoro-doped catalyst is brought into contact with the substrate either in the fluorous phase or at the interface of the two phases, effectively enabling the catalytic reaction to take place. It is desired that the catalyst possesses minimum to no solubility in the organic phase under the catalytic conditions, as this often results in loss of the active metal *via* leaching to the organic layer. Where the catalyst is effectively retained in the fluorous phase, successful repetitive use of the catalyst-containing layer can be achieved by allowing the two immiscible phases to separate at room temperature upon completion of the reaction. The organic products are then removed by decantation, leaving behind the heterogenized fluorous phase-catalyst readily available for use with fresh substrate in successive catalytic cycles.[69] Although considered too expensive for large-scale commercial processes, fluorous solvents tie in well with Green Chemistry principles owing to their properties as lowly toxic and inflammable solvents.[66,67] The concept of fluorous biphasic catalysis offers a promising catalyst separation step that could be attractive for future production of intermediates in the fine chemicals and pharmaceuticals industries.[68]

1.3.3 Aqueous/Organic biphasic media

The design of homogeneous catalysts bearing water-solubilising substituents has been the main basis for immobilisation of complexes aimed at efficient hydroformylation of long chain olefins. The substituents easily induce water-solubility to the complexes, creating an environment that allows for efficient contact of the substrate with the metal complex during the reaction, and facile product separation with negligible catalyst losses from the aqueous layer. The commonly explored polar substituents for the hydroformylation reaction are sulfonates, carboxylates, hydroxyl, phosphonates and quaternary ammonium groups.[70–76] Our research group has previously investigated catalyst precursors bearing these substituents in the aqueous biphasic hydroformylation of olefins (Figure 1.3).[77–80]

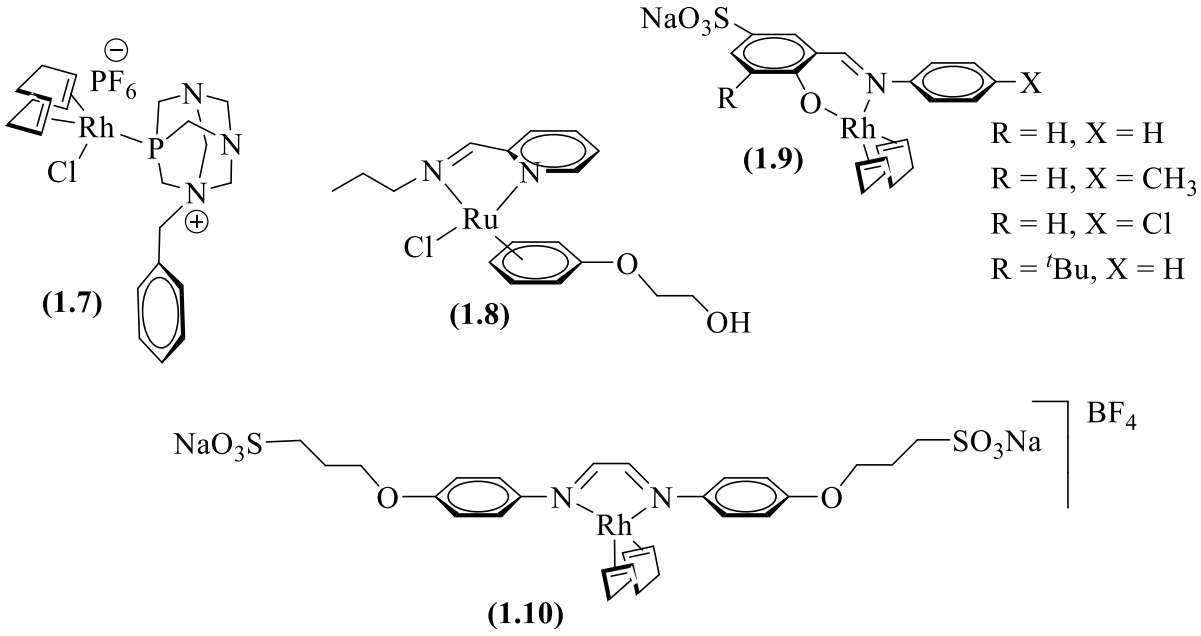

Figure 1.3 Selected examples of water-soluble complexes from our group, bearing commonly explored sulfonates, hydroxyl and quaternary ammonium water-solubilising substituents.[77–80]

The sulfonates are generally the widely preferred polar substituents owing to their good stability properties over a wide range of reaction conditions.[81,82] The first known sulfonated organometallic complex for hydroformylation ($[Rh(H)(CO)(TPPTS)_3]$, TPPTS (triphenylphosphinetrisulfonate) (Figure 1.4) was based on the modification of the conventional rhodium metal complex $[HRh(CO)(PPh_3)_3]$.[70,83] This highly water-soluble (1100 mg/mL at room temperature) complex was commercialised for the aqueous biphasic

hydroformylation of propene and butene as the Ruhrchemie/Rhône-Poulenc (RCH/RP) process.[83] Although this process is limited to short chain olefins owing to the difficulty in solubilising the longer chain olefins in the aqueous biphasic media, its discovery formed the basis for water-soluble sulfonated complexes being used for hydroformylation. This gave rise to more promising catalytic species with good activity and selectivity.[84–88] The aqueous biphasic recyclability concept follows the same principle as discussed for fluorous biphasic catalysis in Section 1.3.2 of this Chapter. The specifics regarding the separation of the water-soluble catalyst from the product are explained to greater detail in Section 5.2.3 of Chapter 5 of this document.

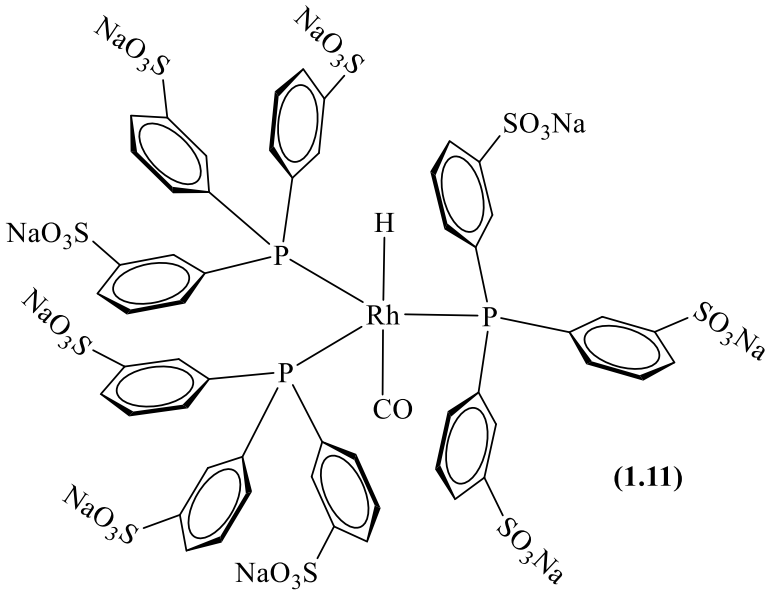

(1.11)

Figure 1.4 Water-soluble catalyst used in the Ruhrchemie/Rhône-Poulenc process.[70,83]

Several examples on the use of water-soluble catalysts in hydroformylation are reported in the literature. Barricelli and co-workers[89] reported the recoverable and recyclable aqueous biphasic systems of $[RhH(CO)(TPPTS)_3]$ and $[RhH(CO)(TPPMS)_3]$ for hydroformylation of C_6 alkenes and alkene mixtures. The catalyst precursors gave good catalytic activity, in addition to suppressing the competing isomerisation reaction under high but reasonable pressures (50 atm). Such advancements are quite important for designing catalyst precursors that can act as alternatives for the treatment of naphtha as well as for addressing related fuel upgrading issues.[90] However, owing to the known susceptibility of the phosphine-containing ligands to oxidation in the aqueous biphasic medium, attention has shifted to non-phosphine containing ligands for the preparation of water-soluble catalyst precursors.[91] Scrivanti and co-workers[92] reported the aqueous biphasic hydroformylation of styrene and 1-hexene using a water-soluble

catalyst prepared *in situ* from a combination of a water-soluble sulfonated pyridyl-triazolyl *N,N*-bidentate ligand (**1.12**) with the Rh(I) dimer $[RhCl(COD)]_2$ (COD = cyclooctadiene), (Figure 1.5). The catalyst posted good catalytic activity for both substrates, as well as excellent chemoselectivity for aldehydes. In addition, the catalyst could be recycled for at least four times with complete conversion of the substrate.

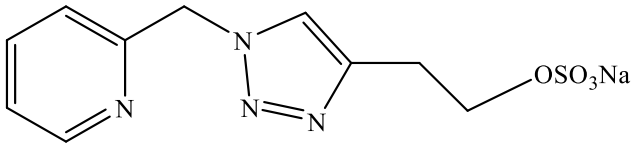

(1.12)

Figure 1.5 The water-soluble pyridyl-triazolyl *N,N*-bidentate ligand.[92]

Smith and co-workers[78–80] have extensively investigated non-phosphine containing complexes as catalyst precursors for aqueous biphasic hydroformylation of olefins. The group has prepared various bidentate sulfonated *N,N*- and *N,O*-ligands, which were subsequently reacted with a Rh precursor leading to water-soluble Rh(I) complexes (partly represented *vide supra*, Figure 1.3).[79,80,91] The sulfonated catalyst precursors have shown good solubility in water, a desirable characteristic to attaining tolerable catalyst immobilisation in the aqueous phase. Effectively the authors have shown good separation of the catalysts for recycling over several times (≥ 5 cycles) with good catalytic activity and moderate to good chemoselectivity for aldehydes.

It is worth mentioning that the main challenges facing aqueous biphasic hydroformylation systems are that of the catalyst leaching to the organic layer, and poor substrate solubility in water, resulting in low reaction rates and selectivity.[93] This is hugely undesirable from an economic and environmental view point. Various strategies have been implemented in efforts to achieve improved aqueous phase catalyst immobilisation in the hydroformylation of long chain olefins using aqueous biphasic media. These strategies include the use of cyclodextrins, surfactants and cosolvents.[94,95]

1.3.3.1 Cyclodextrins in aqueous biphasic hydroformylation

Cyclodextrins can be defined as cyclic oligosaccharides of D-glucopyranose units, constituting the α-cyclodextrins (six), β-cyclodextrins, (seven) and the γ-cyclodextrins (eight). Cyclodextrins are often used to improve mass transfer in aqueous-organic biphasic media through formation of inclusion complexes with a wide range of compounds (Scheme 1.3).[96] In a typical inclusion complex, the stability of the guest molecule being held within the cavity of the cyclodextrin host molecule is influenced by several forces. Depending on the temperature, pH of the system, guest and the type of cyclodextrin, these forces can be the van der Waals interactions, electrostatic interactions, hydrogen bonding, conformational strain reduction, charge transfer, and exclusion of cavity-bound high-energy water.[96] The β-cyclodextrins are mostly used because of ease of availability, relatively low price and the optimal cavity size compared to the α- and γ-cyclodextrins. The larger aperture of the γ-cyclodextrins, and the smaller aperture of the α-cyclodextrins often results in low catalytic conversions.[97,98]

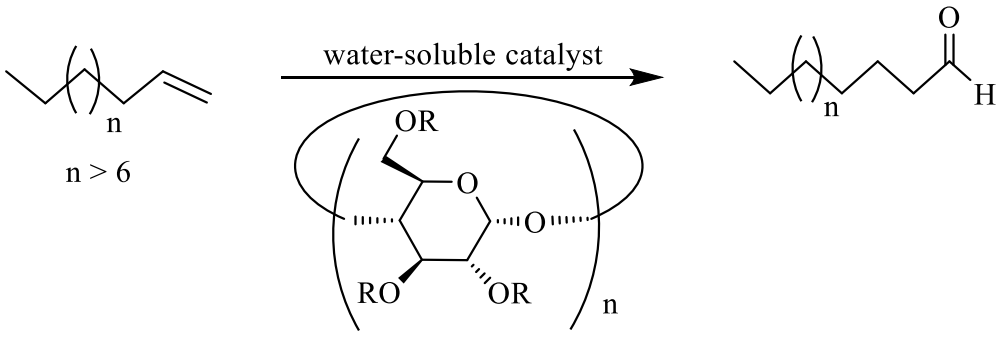

Scheme 1.3 Typical olefin hydroformylation reaction using cyclodextrins.[96]

When the inclusion of the guest molecule is successfully conducted, the physicochemical properties (solubility and stability) of the guest are affected. These properties are beneficial in aqueous biphasic hydroformylation, owing to the unique structure of the cyclodextrins, that is, the hydrophobic core (inner surface) for inclusion of the organic substrate and the hydrophilic exterior for interaction with water during the reaction. As a result, several potential benefits are realised and these include i) reduced catalyst leaching, ii) improved reaction rates and selectivity of reactions in water, iii) stable catalytic species in water, iv) exploitation of new avenues on the design of novel water-soluble catalysts, and vi) creating opportunities for improved understanding of cyclodextrin inclusion complex properties.[99–102]

In a typical reaction, the organometallic catalyst can be brought into contact with the substrate at the water/organic interface or contact can be in the aqueous phase through inclusion of the substrate in the hydrophobic core of the complex. Dauchy and co-workers[103] recently reported the application of salicylaldimine and salicylhydrazone ligands anchored on a β-CD scaffold for the Rh(I) aqueous biphasic hydroformylation of 1-decene (Figure 1.6). The complexes (**1.13**) showed good conversion of the substrate (> 80%) and moderate to good aldehyde chemoselectivity (40–72%) over a temperature of 60 and 80 ℃ (20 and 50 bar syngas pressure respectively). The Monflier group[104] has also reported the functionalisation of 1-decene in the rhodium catalysed aqueous biphasic hydroformylation using chemically modified β-cyclodextrins. The methylated-β-cyclodextrin gave excellent conversion (95%) and high reaction rates compared to non-modified β-cyclodextrin, as well as in the absence of the native β-cyclodextrin. The effectiveness of the chemically modified β-cyclodextrin was ascribed to the good solubility in both aqueous and organic phases, enabling the inclusion of the organic substrate and the facile release of the aldehyde undecanal product (for the cycle to go on).

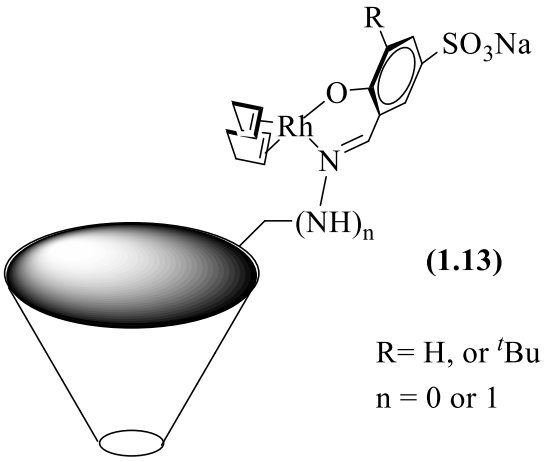

Figure 1.6 Illustrating salicylaldimine-based Rh(I) complexes grafted on a β-CD scaffold.[103]

In another related study, improved catalytic activity was reported in the presence of supramolecular interactions between β-cyclodextrins, a water-soluble phosphaadamantyl-based ligand, and a Rh precursor [Rh(acac)$(CO)_2$] (Figure 1.7).[105] An increase in activity was observed without altering the chemo- and regioselectivity of the catalytic system. The presence of the β-cyclodextrins was also reported to allow for the easy separation of the biphasic mixture. It is worth noting that this study was the first to demonstrate a successful cyclodextrin-mediated thermoregulation of the surface activity of an amphiphilic phosphane.

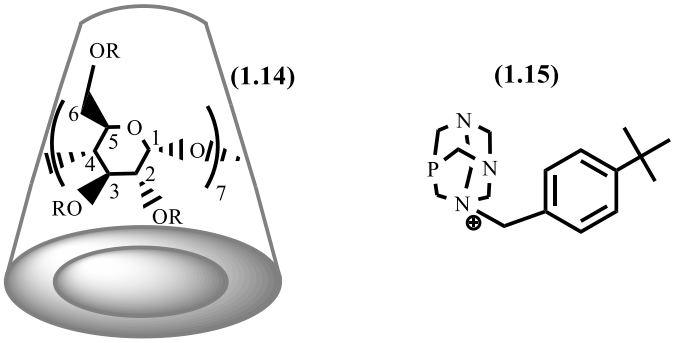

Figure 1.7 Illustrating a β-cyclodextrin and water-soluble phosphaadamantyl-based ligand.[105]

1.3.3.2 Surfactants in aqueous biphasic hydroformylation

The hydroformylation of long chain olefins in aqueous biphasic media has often been conducted successfully using surfactants as promoters, possessing both hydrophobic and hydrophilic characters (Figure 1.8).[94] The formation of micelles (normal or reverse) creates a system that minimises the transfer limitations associated with higher olefins in aqueous/organic biphasic systems.

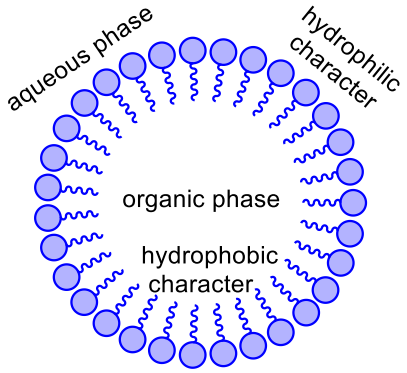

Figure 1.8 Illustration of a surfactant in biphasic media.[94]

Various anionic, cationic and non-ionic surfactants have been evaluated in biphasic media, with the cationic surfactants being the most widely applied.[106,107] Baricelli and co-workers[108] recently evaluated the effect of the cationic surfactant CTAB (cetyltrimethylammonium bromide ((**1.16**), Figure 1.9) on the hydroformylation rates of a rhodium-catalysed functionalisation of naturally occurring allylbenzenes, conducted in the presence of various water-soluble phosphines. The addition of small amounts of the cationic surfactant CTAB immensely improved the reaction rates, an indication of the effectiveness of the surfactant in breaking the phase transfer restriction. This observation was ascribed to an increase in the

number of micelles and the interfacial area, brought about by the increased concentration of the surfactant, and ultimately leading to the observed positive effect on the hydroformylation reaction. The mode of action could be explained through electrostatic interactions that exist between the positively charged moieties of CTAB (channelled towards the aqueous phase) and the anionic sulfonate group of the TPPTS ligand.[106] With these interactions at play, the aqueous/organic interface becomes enriched in the concentration of the active metal, leading to the observed accelerated reaction. However, reduced reaction rates were observed when the surfactant concentration was increased further above the critical micelle concentration. At this stage the system constitutes a surfactant-rich state (micro-emulsion) that possesses a characteristic solubility balance in both the aqueous and the organic phases. The structure of the micelles is altered from a spherical to a cylindrical shape with reduced superficial area, which disfavours the hydroformylation reaction rate. Moreover, the bromide ions of CTAB (Figure 1.9) were also reported to be competitively coordinating to the rhodium metal over the substrate, leading to detrimental effects on the reaction rate at high CTAB surfactant concentration.

More recently, Vieira and co-workers[109] reported the cetyltrimethylammonium chloride (CTAC)-mediated rhodium-catalysed aqueous biphasic hydroformylation (Rh/TPPTS) of natural bio-renewable acyclic terpenes ((**1.17**), Figure 1.9). The use of the cationic surfactant resulted in remarkable reaction rates and high yields of several fragrance compounds. The observed positive effect of the surfactant was reported to be *via* enhanced permeation of the substrate through the surfactant molecules, a phenomenon that facilitates the substrate to reach the catalyst that is embedded in the aqueous phase.

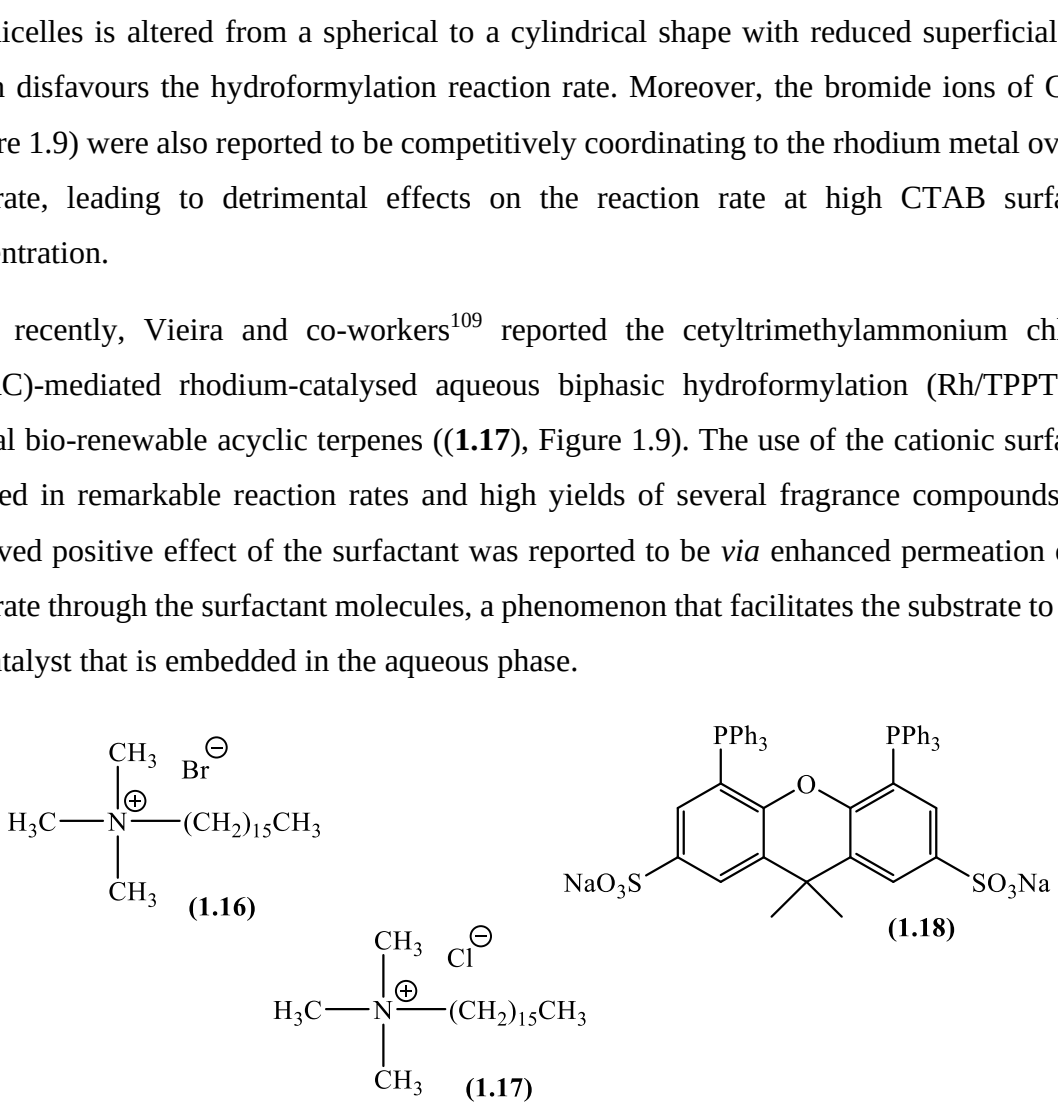

Figure 1.9 Illustrating structures of the surfactants CTAB and CTAC, and the water-soluble ligand SulfoXantPhos.[108–110]

Although anionic and non-ionic surfactants are rarely used due to their poor ability to encapsulate substrates, research on these surfactants is still pursued. Hamerla and co-workers[110] reported formulation of a multi-phase system comprising of water, 1-dodecene and a non-ionic surfactant for hydroformylation in the presence of an *in situ* prepared water-soluble rhodium-SulfoXantPhos catalyst (using ligand **1.18**, Figure 1.9). High reaction rates (TOF > 300 h^{-1}) and selectivities (*n/iso*, 98/2) were observed by varying the type of surfactant, ligand as well as the metal/ligand ratio. Efficient solubility of the surfactants in the multi-phase system was achieved by manipulating the reaction temperature, subsequently resulting in the formation of normal or reverse micelles which act as phase transfer agents. It is worth noting that minimum conversion was observed in reactions conducted in the absence of the surfactants, attesting to the effectiveness of the multi-phase system reported by the authors. The impact of related systems from an economic view point is demonstrated by Rost[111] and Müller[112] on their design of mini-plants for the hydroformylation of long chain olefins.

Nowothnick and co-workers[113] assessed the effects of temperature and amount of non-ionic surfactants on reaction rates, as well as on metal leaching in a system comprising of a combination of $Rh(acac)(CO)_2$ with the bidentate ligand SulfoXantPhos. An increase in the reaction rates was observed with increase in temperature, a phenomena that can be explained by the Gibbs "fish" prism at equal amounts of oil and water.[110,114] Formation of a water-in-oil microemulsion at high temperature enables catalyst encapsulation into micelles and subsequent catalyst transfer to the alkene, ultimately increasing the interaction of the substrate with the water-soluble catalyst. However, since high temperatures are known to promote isomerisation over hydroformylation, a notable decrease in selectivity was observed when the temperature was elevated to 110 °C. Overall, low catalyst losses were registered (< 0.5%), indicating the technical feasibility of the surfactants from an economical and environmentally friendly green chemistry standpoint.[45]

1.3.3.3 Cosolvents in aqueous biphasic hydroformylation

The conventional solvent of choice for the homogeneous hydroformylation reaction is usually toluene, a high boiling point solvent (111 °C) that possesses good dissolution properties of higher olefins as well as several organometallic complexes. Toluene is also the ideal solvent for aqueous biphasic hydroformylation owing to the good immiscibility properties with water at room temperature, in addition to good dissolution properties of syngas. Alternative use of

cosolvents in aqueous biphasic hydroformylation reactions has been investigated in the literature, aimed towards improving interactions of long chain olefins with water-soluble catalysts.[115–117]

Kalck and co-workers[118] investigated the use of cosolvents (ethanol, methanol, acetone and acetonitrile) in the aqueous biphasic hydroformylation of 1-octene using [$Rh_2(\mu\text{-}S^tBu)_2(CO)_2(TPPTS)_2$] and an excess of TPPTS. Improved reaction rates were observed in the presence of the cosolvents relative to the reaction conducted in the absence of cosolvents. However, a loss of aldehyde selectivity was reported in each case when using a cosolvent, exemplified by a 5–10% isomerisation. Furthermore, the regioselectivity for the linear aldehyde decreased from 96% to 83%. The overall influence of the cosolvents in the hydroformylation rates was determined to be in the following order:

Ethanol > Acetone >Acetonitrile > Methanol >> with no cosolvent

In another study, Wei and co-workers[119] reported the aqueous biphasic hydroformylation of higher alkenes using a rhodium catalyst derived from BISBIS (sodium salt of sulfonated 2,2'-bis(diphenylphosphinomethyl)-1,1'-biphenyl) (Figure 1.10), in the presence of a series of polar cosolvents.

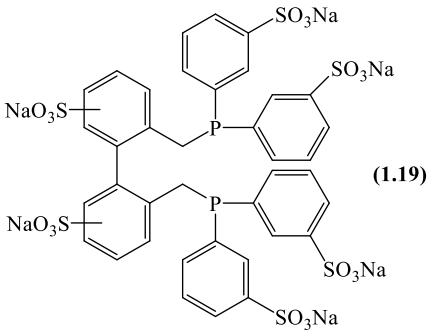

(1.19)

Figure 1.10 Illustrating the water-soluble ligand, BISBIS.[119]

As expected with a Rh-BISBIS catalyst, the linear aldehyde (> 95%) was favoured in the hydroformylation of higher alkenes (1-hexene, 1-octene, 1-decene and 1-dodecene). Good hydroformylation rates were observed in the order:

Acetonitrile ≈ Ethanol > Dimethyl ether ≥ Methanol > Tetrahydrofuran > no cosolvent

Good recyclability of up to 5 cycles without significant loss in activity (2095 h^{-1}) and linear aldehyde selectivity (> 95%) was observed using ethanol as the cosolvent, creating promising

prospects for future practical application of such a catalytic system. However, the strategy of using cosolvents is often hampered by undesired side reactions of the cosolvent with the aldehyde product, for example, formation of acetals in instances where alcoholic solvents such as ethanol and methanol have been used.[115,120] The use of cosolvents is also susceptible to leaching of the catalyst to the organic layer, as well as a decrease in aldehyde chemoselectivity. The overall drawbacks that are associated with aqueous biphasic hydroformylation have led to a more robust, energy efficient, non-destructive and eco-friendly catalyst recovery technology that utilises membranes.[121]

1.4 Organic solvent nanofiltration in hydroformylation

The use of membrane technology in catalysis is a relatively new and very attractive approach for the non-destructive selective retention of constituents of a homogeneous reaction (catalyst/unreacted substrate/impurity/product).[122–126] This approach is often used for the recovery of homogeneous catalysts for reuse without the need for application of stringent conditions, such as those employed in the recovery of hydroformylation catalysts by the conventional distillation process (high temperatures often deactivate the catalyst).[121] Membranes allow permeation by molecules upon application of a driving force based on pressure differences, concentration as well as electric potential between the different phases (the feed phase and the permeate phase, Figure 1.11). The application of pressure-driven and solvent-stable polymeric nanofiltration membranes, termed organic solvent nanofiltration (OSN) is a very attractive catalyst separation and recovery technique with the ability to recover molecules having as low molecular weight as 100 g mol^{-1}. This technique has proven to be a success for application in various sectors of industry, ranging from biological, oil, food and fine chemicals industries.[127]

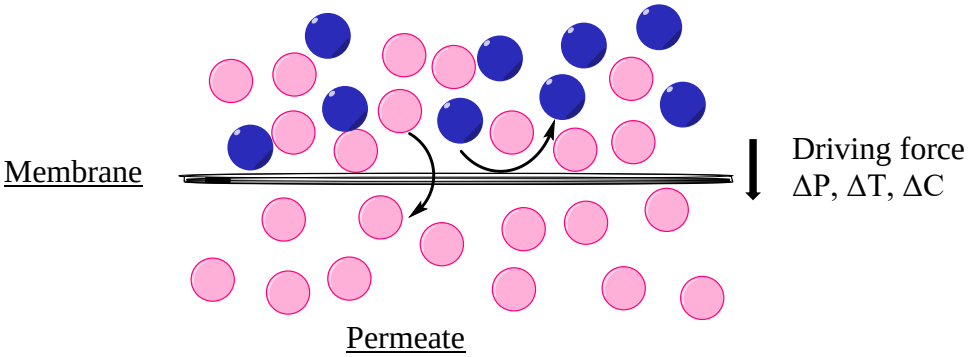

Figure 1.11 Illustration of a typical membrane process.[122]

The process of designing a suitable membrane is cumbersome as each membrane has to be tailored for a specific application (process-specific), putting into consideration temperature and pH limitations, and the membrane vulnerability to fouling and/ or concentration polarisation.[123] The choice of a membrane is usually based on the molecular weight of the catalyst relative to the other constituents of the feed. In a pioneering article in the field of membrane technology, Grosser and co-workers[128] reported the use of selectively permeable polyimide membranes in the separation of cobalt and rhodium complexes from hydroformylation products of 1-pentene. The membranes were highly effective, giving metal losses of less than 20% in the permeate. With more focus on the use of membranes for catalyst recovery, the technique slowly improved over the years towards the development of highly efficient membranes for hydroformylation. Subramaniam and co-workers[129] reported the effective retention of rhodium complexes in a homogeneous hydroformylation process by employing polymer bound bulky phosphite ligands in conjunction with polyimide membranes of appropriate molecular weight cut off (MWCO). The rhodium metal losses in the effluent were reported to be in the parts per billion range (less than 100 ppb) in both batch and continuous filtration of the solvent. These results are complimented by Priske and co-workers,[130] in their investigation of an integrated reaction and separation step for the rhodium catalysed hydroformylation of 1-octene and 1-dodecene, achieving a near perfect metal retention (over 99%).

More recently, Peddie and co-workers[131] reported the application of membrane technology in successfully recovering two commercially available homogeneous catalysts, the rhodium-based complex $HRh(CO)(PPh_3)_3$ and the cobalt-based complex $Co(C_5H_7O_2)_3$. The recovery of the catalysts was conducted in environments that are representative of the hydroformylation and hydrogenation reactions. Excellent recovery of the high molecular weight rhodium-based catalyst was achieved (> 98% recovery, MW ~ 920 g mol^{-1}), whereas the lower molecular weight cobalt-based catalyst gave good recovery of 88% (MW ~ 350 g mol^{-1}). The slightly reduced relative percentage recovery of the cobalt-based catalyst was ascribed to losses of the catalyst to the permeate as a result of the MWCO of the membrane used by the authors (400 g mol^{-1}). This means that the membrane can only achieve at least 90% retention of the catalyst for molecules possessing a molecular weight that is greater or equal to 400 g mol^{-1}.

Dreimann and co-workers[132] reported the separation of a homogeneously dissolved Rh catalyst complex combined with the ligands triphenylphosphine, Biphephos and Xantphos from different solvents and solvent mixtures originating from hydroformylation reactions (Figure 1.12). In this study, the separation of the catalyst-ligand mixture was conducted in a continuous

system, with the feed channelled directly from the reactor to the separation cell. During the recycling experiments, the catalytic system bearing the relatively low molecular weight monodentate triphenylphosphine (MW = 262 g mol^{-1}) gave low rejection of the ligand (66%) over two cycles, whereas the other two ligands Biphephos (787 g mol^{-1}) and Xantphos (579 g mol^{-1}) gave a rejection of 98% and 95% respectively. This is in line with the MWCO of the membrane (350 g mol^{-1}). A good rejection of the Rh-metal was achieved for all three reaction mixtures (94%, 97% and 97% respectively).

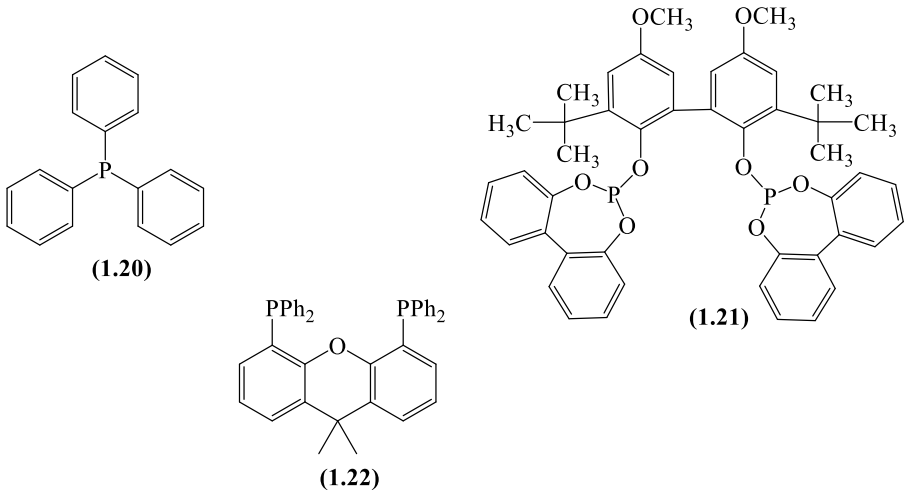

Figure 1.12 Illustrating the structures of Triphenylphosphine (**1.20**), Biphephos (**1.21**), and Xantphos (**1.22**).[132]

It is generally recognised that more focus is usually centred around strategies that lead to the effective recovery of a homogeneous catalyst for reuse. With this view, less destructive recovery techniques could be developed, which may result in minimum to no waste generated. This could be achieved *via* implementation of strategies that do not lead to the generation of large amounts of deactivated catalysts, which is often the case when using harsh catalyst separation techniques such as distillation. However, equally lucrative energy and waste minimisation opportunities also lie in the reduction of side product formation from isomerisation, as well as designing catalyst precursors that possess a precise bias for either linear or branched aldehydes. Dendrimers have often been evaluated for their influence on the activity and selectivity in the hydroformylation reaction.[133]

1.5 Metallodendrimers in hydroformylation

Dendrimers are defined as highly branched tree-like macromolecular structures with a well-defined, homogeneous, and monodisperse structure. When metals are incorporated into the dendritic arms that propagate from the core, the resultant dendritic structure is known as a metallodendrimer.[133] The motivation for such a design emanates from naturally occurring metalloenzymes, which often contain two or more active metal centres leading to enhanced catalytic activity.[134–136] The metals anchored onto the dendrimer surface act as multiple catalytically active sites, allowing for potentially enhanced catalytic activity over monometallic catalysts. The metal centres on these synthetic catalysts can act independently (taking advantage of the increase in nuclearity per molecule), or they can possess synergistic and cooperative effects between multiple active sites contained therein.[137] Moreover, the steric bulky nature of the dendrimer can impart the necessary properties to influence the regioselectivity of the catalyst towards linear aldehydes, reducing the need for a separation step of the branched aldehydes from the system. Various water-soluble multimetallic catalyst precursors have been reported in the literature, in the form of homobimetallic, heterobimetallic as well as metallodendritic species.[138–140] The ability to design catalysts that mimic metalloenzymes is a significant step towards improved reactivity for industrially important reactions such as hydroformylation. Although metallodendrimers are yet to make a profound breakthrough in hydroformylation, the prospects of improved catalytic efficiency are intriguing.

October and Mapolie [141] reported the application of a series of aryl ether iminopyridyl-based Rh(I) and Ru(II) metallodendrimers in the hydroformylation of 1-octene. The Rh(I) catalyst precursors (Figure 1.13) gave relatively high activities, and were superior to their Ru(II) counterparts which were prone to isomerisation of the olefin. As a result of the poor solubility of the higher generation complexes in the conventional solvent of choice for hydroformylation (toluene), the catalytic performance of the dendritic precatalysts was comparable to the mononuclear analogues, with no positive dendritic effect. However, such molecular weight enlarged (MWE) dendritic structures can be ideal candidates for catalyst recovery *via* organic solvent nanofiltration technique. The large molecular weight of a dendrimer is often associated with the necessary good structural stability, as well as the potential for efficient retention of the active catalytic species on the surface of a membrane.[127]

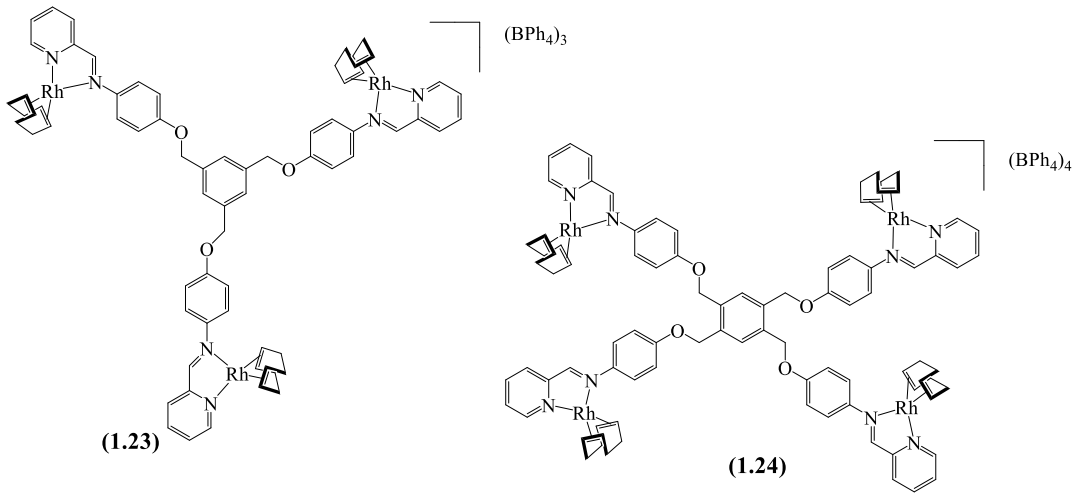

Figure 1.13 Illustrating the iminopyridyl-based trinuclear (**1.23**) and tetranuclear (**1.24**) complexes.[141]

Hager and co-workers[142] investigated the aqueous biphasic hydroformylation of 1-octene using catalyst precursors synthesised from a combination of $[RhCl(COD)]_2$ with the dendritic ligands tris-2-(5-sulfonato salicylaldimine ethyl)amine and DAB(5-sulfonato salicylaldimine), (Figure 1.14). The catalyst precursors showed good biphasic interaction with the long chain model substrate 1-octene, ascribed to a combination of the water-solubilising sulfonate groups, and the aliphatic dendritic arms. The catalyst precursors could be recycled up to five times with consistently good activities and selectivities, However, owing to the flexible nature on the core in both multinuclear structures, the regioselectivity for the linear aldehyde was comparable to that of the mononuclear analogues. This observation introduces the idea of future design of dendritic structures that possess a rigid core with the potential to better influence the regioselectivity towards the linear aldehyde.

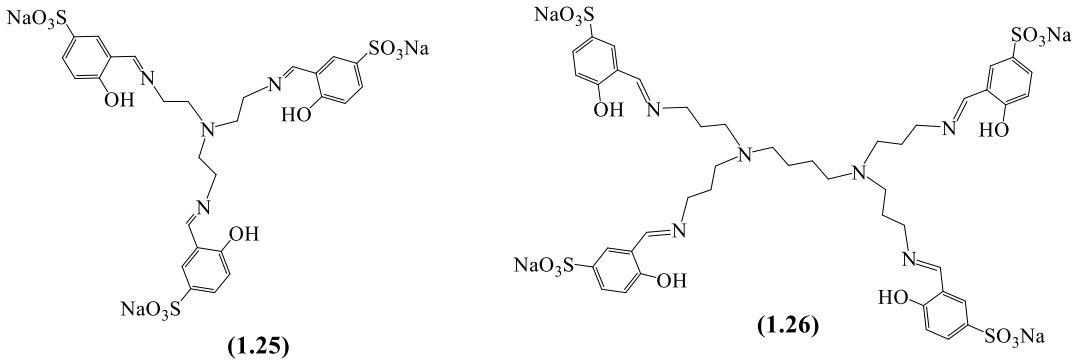

Figure 1.14 Illustrating the water-soluble salicylaldimine-based trimeric (**1.25**) and tetrameric (**1.26**) dendritic ligands.[142]

In two separate but related studies, Antonels[143] and Makhubela[144] (**1.27** and **1.28** respectively, Figure 1.15) investigated the catalytic potential of iminopyridyl and iminophosphine-based Rh(I) metallodendrimers in the hydroformylation of 1-octene. In both studies, the multinuclear dendritic structures were found to be effective catalyst precursors in the hydroformylation of 1-octene, giving higher conversions, faster reaction rates and slightly enhanced catalytic activity when compared with their mononuclear congeners. The activities and selectivities of these catalyst precursors could be fine-tuned and tailored towards specific product distribution by altering the temperature and pressure, with lower temperature and pressures yielding more of the iso-octene fractions. The metallodendrimers registered slightly enhanced regioselectivity for the linear aldehyde when compared to their mononuclear analogues, as well as to the unmodified sources of the rhodium metal. This opens promising avenues for the future design of catalyst precursors that can possess more improved control on regioselectivity. Moreover, the bulky nature of the metallodendrimers creates potential for future recovery using the OSN strategy.

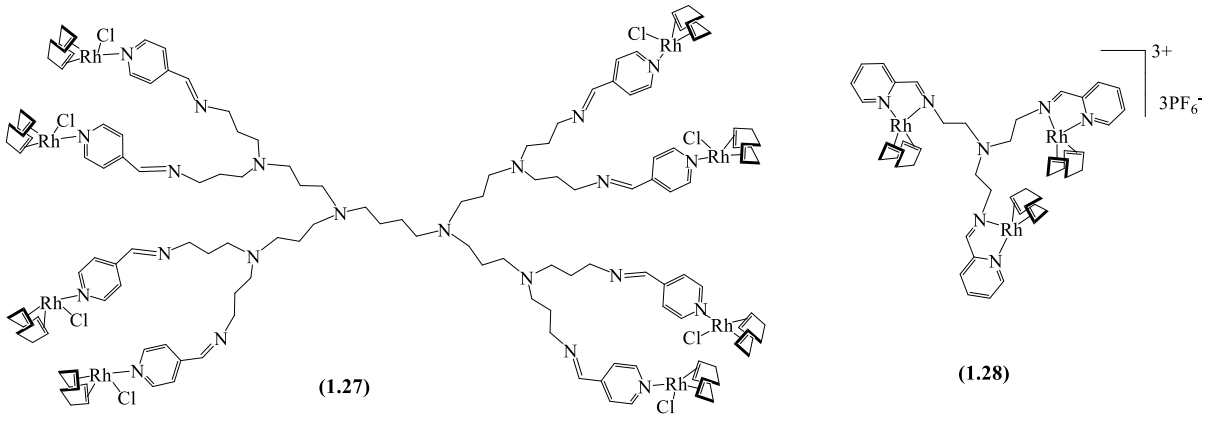

Figure 1.15 Selected examples of iminopyridyl-based metallodendrimers in hydroformylation, by Antonels and Makhubela.[143,144]

Ropartz and co-workers[145] reported the first ever positive dendritic effect in the homogeneous catalysed hydroformylation of 1-octene using Rh(I) metallodendrimers that are based on a polyhedral oligomeric silsesquioxanes (POSS) core. In this study, the dendrimers gave much higher linear selectivities (*l* : *b*, 14 : 1 for (**1.29**)) than their small molecule analogues (3–4 : 1 for (**1.30**, **1.31**, and **1.32**)) in the hydroformylation of 1-octene. The observed bias for the linear aldehyde was ascribed to the constraint in the 16 dendritic-arm-based structure of the higher generation dendrimer ((**1.29**), Figure 1.16). The generally high *l* : *b* ratios suggest that strong bidentate coordination occurs with the [Rh(acac)$(CO)_2$] (acac = acetylacetone) or that the high

local concentration of P atoms on the surface of the dendrimer increases the concentration of complexes for the necessary steric crowding. With enough steric crowding, it becomes possible to make eight-membered ring bidentate coordination favourable and these rings enhance the linear selectivity in hydroformylation reactions.

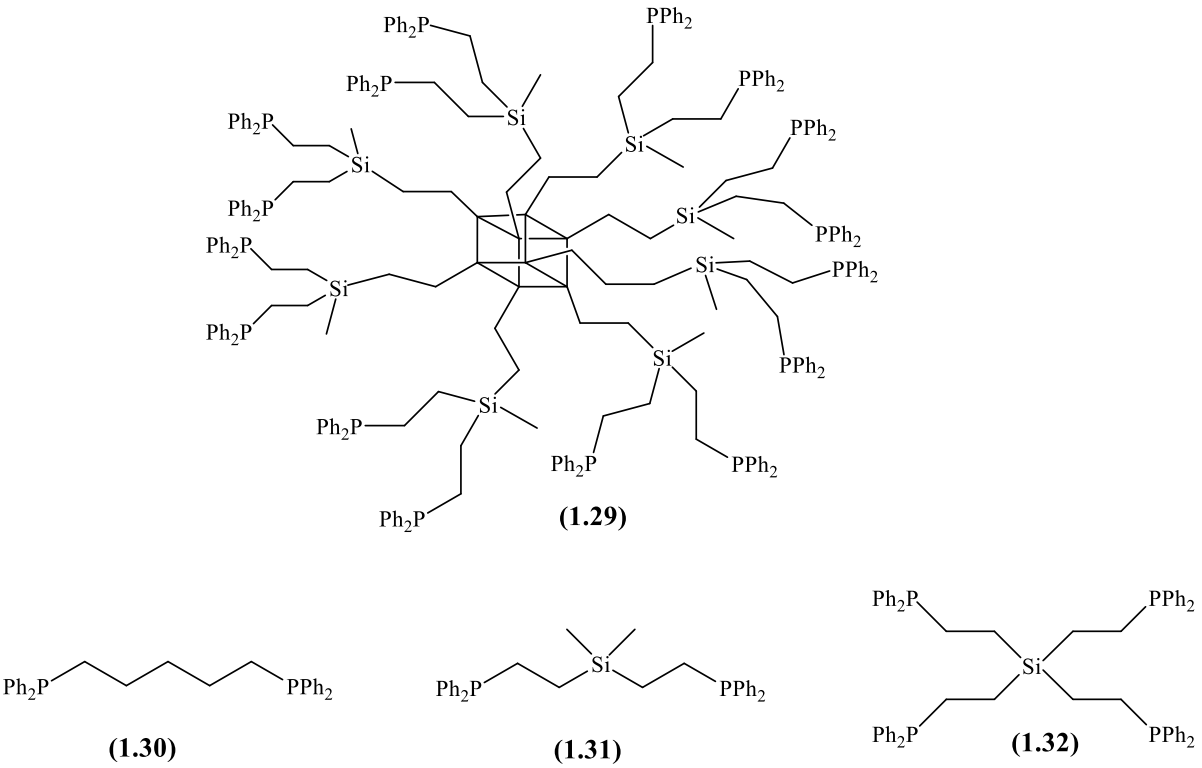

Figure 1.16 Illustrating the multimeric polyhedral oligomeric silsesquioxane (POSS)-based ligands for hydroformylation.[145]

In a recent study that focused on harnessing the electronic effects of the dendritic arms, Williams and co-workers[146] reported a series of aryl ether dendrons containing *N,O*-salicylaldimine entities at the focal point (Figure 1.17). The complexes were prepared by reacting the *N,O*-salicylaldimine-functionalised Fréchet dendrons (G_0, G_1 and G_2) with a $[RhCl(COD)]_2$ dimer. A slight positive dendritic effect was reported, evidenced by the slightly improved activities ((G_0) 550 h^{-1}, (G_1) 539 h^{-1} and (G_2) 576 h^{-1}) and reduced formation of isomers ((G_0) 11%, (G_1) 12% and (G_2) 7%). Although the change is not resoundingly pronounced with the generations, these results are indicative of a promising design strategy that can potentially influence the catalytic performance by appropriate tuning of the electronic environment around the metal centre.

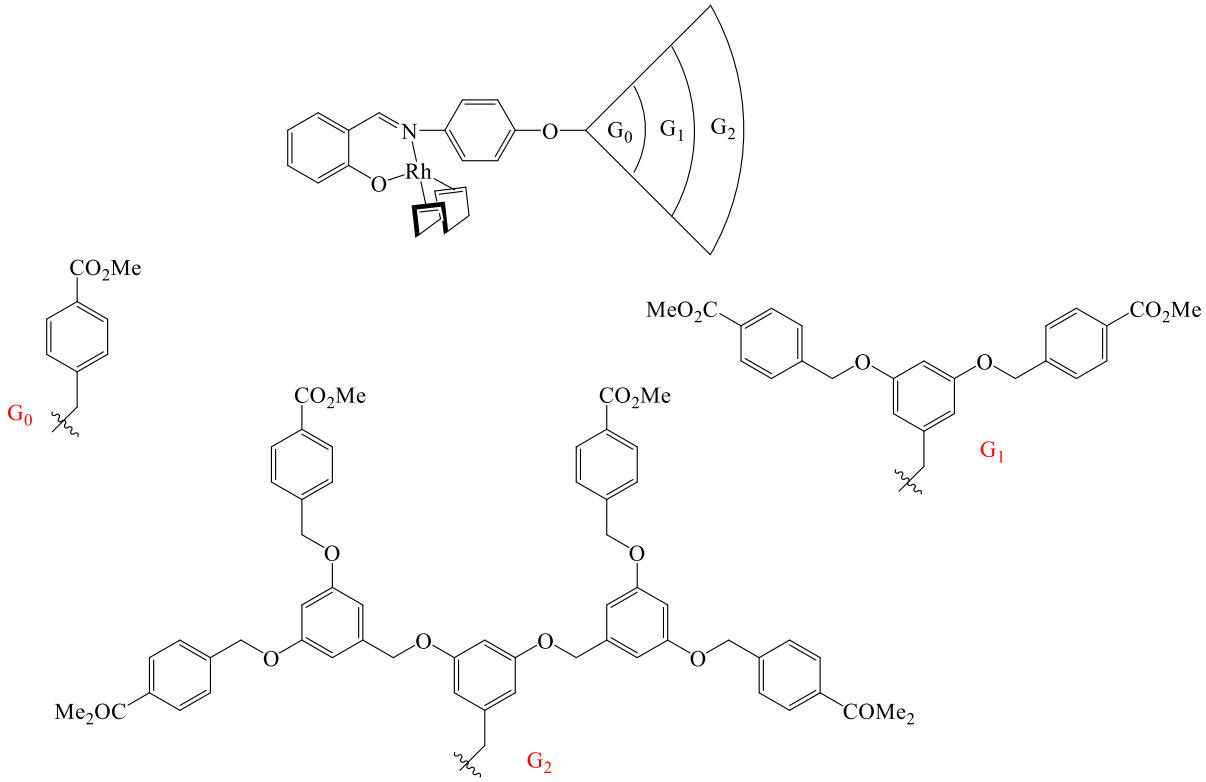

Figure 1.17 Illustrating the focal point salicylaldimine-based metallodendrimers for hydroformylation.[146]

While the use of metallodendrimers in hydroformylation is yet to make a significant catalytic breakthrough over using the monomeric analogues, attempts to fine-tune dendritic catalytic properties for better performing, highly selective, recoverable and reusable precatalysts remain of interest.

1.6 Summary/Closing remarks

Catalyst recovery and recyclability have been the challenge towards the development of highly efficient and economically viable industrial homogeneous catalytic processes. Designing easily recoverable and reusable catalyst precursors that possess remarkable catalytic activity and selectivity through multiple active sites is at the forefront of organometallic chemistry.[147] The application of such compounds in homogeneous catalysis with the aim of beneficiating the rare, expensive and fast depleting Platinum Group Metals (PGMs) is very intriguing. Moreover, if successfully conducted, the approach offers huge economic and environmental benefits *via* the application of greener technologies such as catalyst recovery through organic solvent

nanofiltration technique, as well as through aqueous biphasic approach. These recovery strategies are both in line with the Green Chemistry principles for sustainable development and can contribute immensely to waste reduction, energy efficiency, safer work spaces and the use non-toxic solvents (for example, water).[148] This project is premised on this basis and seeks to contribute to the strategies of homogeneous catalyst recovery that are focussed on hydroformylation.

1.7 Research Aims and Objectives

1.7.1 General Aims

The overall aim of this project is to synthesise and characterise novel mononuclear and multinuclear organometallic complexes of Rh(I), and to evaluate their catalytic effectiveness in the hydroformylation of higher olefins. The project seeks to conduct catalyst recoverability studies *via* the conventional aqueous-biphasic recovery technique, as well as the organic solvent nanofiltration strategy.

1.7.2 Specific Objectives

- To synthesise and characterise new aryl ether monomeric, trimeric and hexameric *N*,*O*-chelating salicylaldimine Schiff base ligands (Figure 1.18, overleaf).

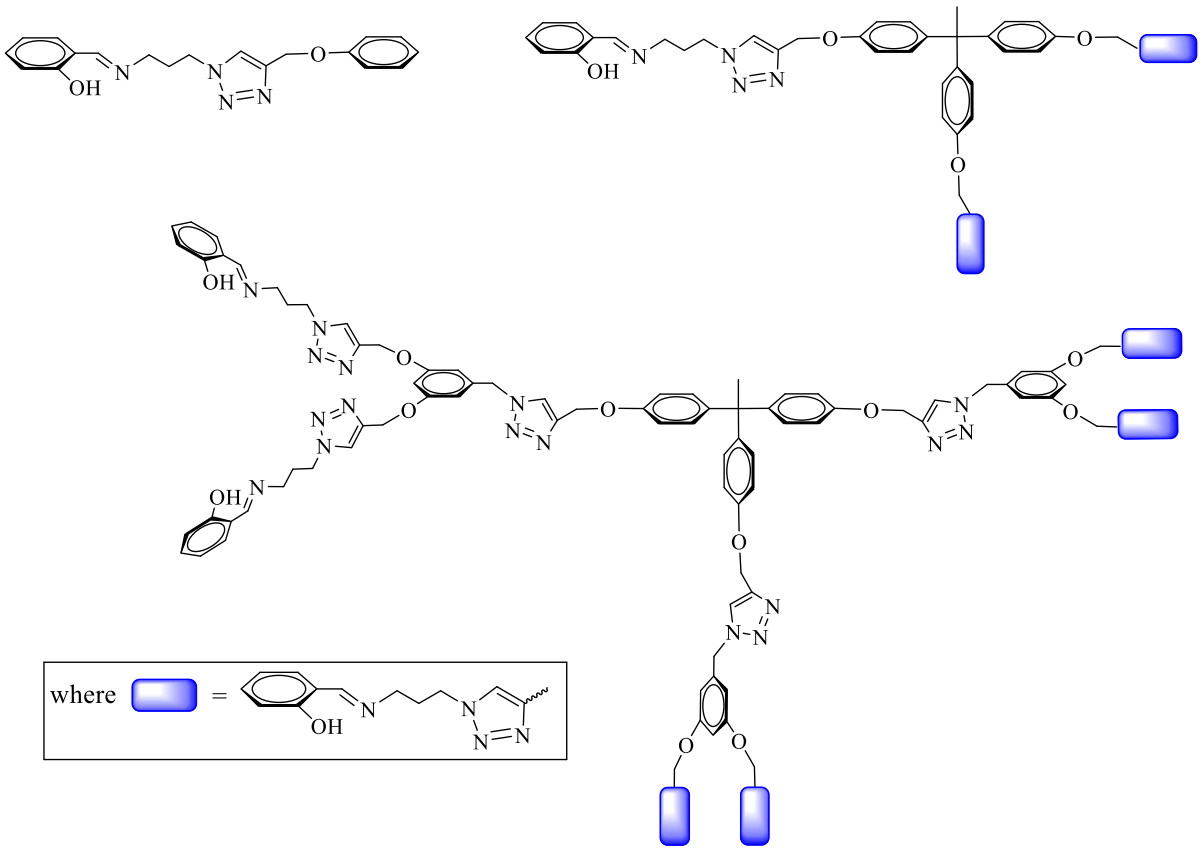

Figure 1.18 General structures of aryl ether monomeric, trimeric and hexameric *N,O*-chelating salicylaldimine Schiff base ligands.

- To synthesise and characterise new mononuclear, trinuclear and hexanuclear aryl ether salicylaldimine-based Rh(I) complexes (Figure 1.19, overleaf).

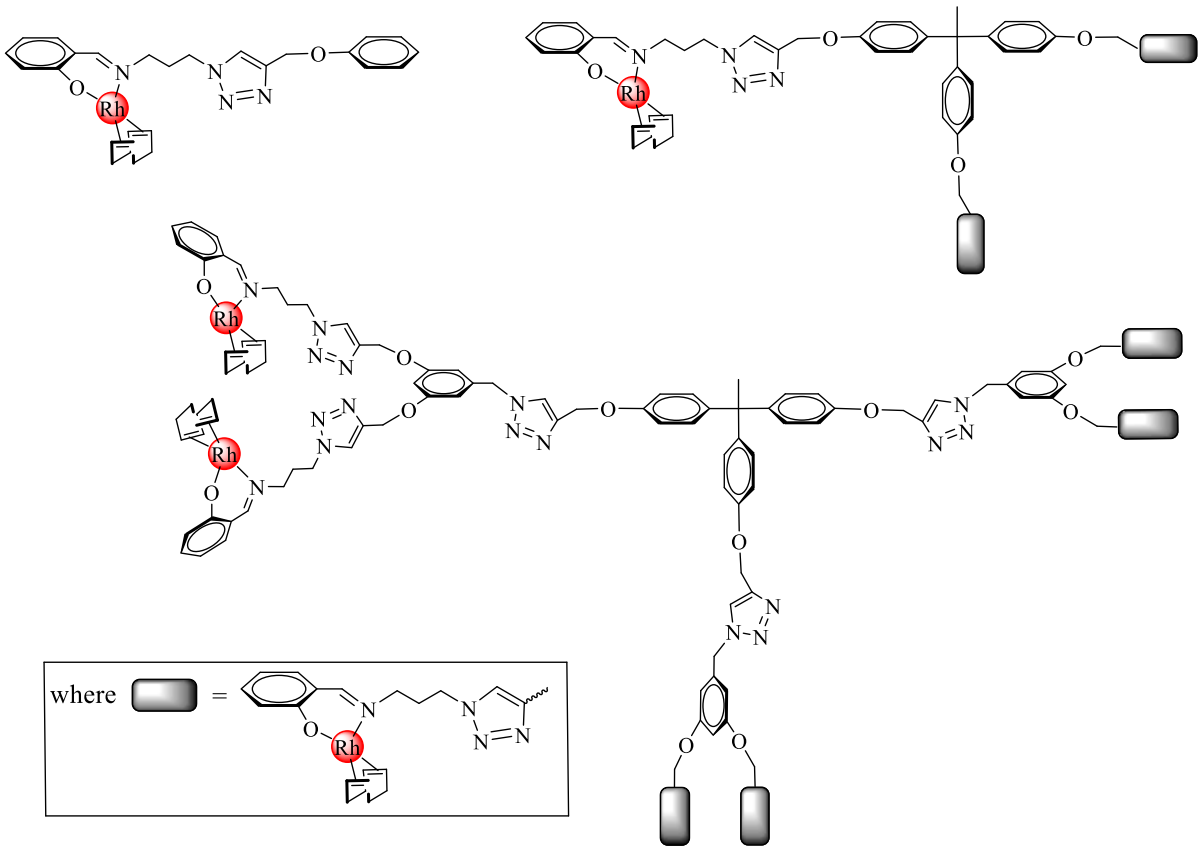

Figure 1.19 General structures of mononuclear, trinuclear and hexanuclear aryl ether salicylaldimine-based Rh(I) complexes.

- Application of the complexes in the hydroformylation of terminal (1-octene) and internal olefins (7-tetradecene and *trans*-4-octene), and evaluation in recyclability studies using organic solvent nanofiltration technique.

- To synthesise and characterise new water-soluble aryl ether salicylaldimine-based monomeric and trimeric Schiff base ligands (Figure 1.20, overleaf).

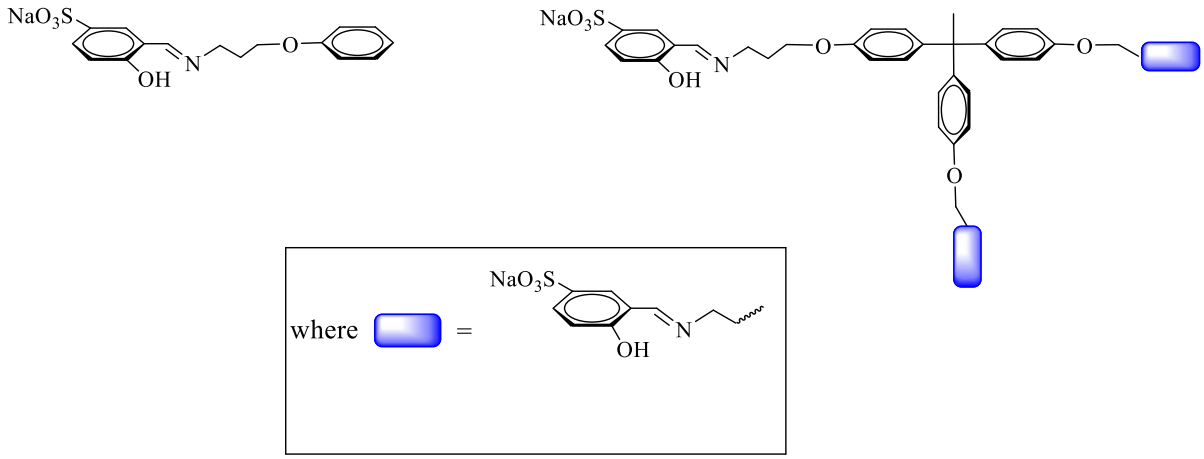

Figure 1.20 General structures of water-soluble aryl ether salicylaldimine-based monomeric and trimeric Schiff base ligands.

- To synthesise and characterise new mononuclear and trinuclear aryl ether salicylaldimine-based Rh(I) complexes (Figure 1.21).

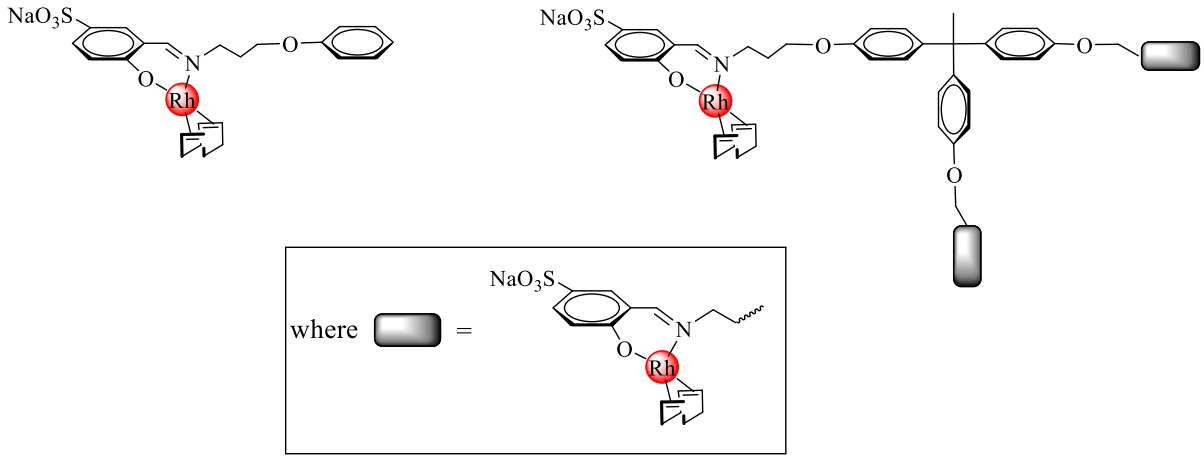

Figure 1.21 General structures of water-soluble aryl ether salicylaldimine-based mononuclear and trinuclear Rh(I) complexes.

- Application of the complexes in the hydroformylation of terminal (1-octene and styrene) and internal olefins (7-tetradecene), and evaluation in recyclability studies *via* aqueous biphasic approach.

1.8 References

1 A. J. B. Robertson, *Platin. Met. Rev.*, 1975, **19**, 64–69.

2 B. Lindström and L. J. Pettersson, *CatTech*, 2003, **7**, 130–138.

3 J. Wisniak, *Educ. quim.*, 2010, **21**, 60–69.

4 S. G. Brade-Birks, *Nature*, 1919, **104**, 94–95.

5 J. Hagen, in *Industrial Catalysis: A Practical Approach*, Wiley-VCH Verlag GmbH & Co. KGaA, 3rd edn., 2015, pp. 459–462.

6 R. M. Heck and R. J. Farrauto, *Appl. Catal. A Gen.*, 2001, **221**, 443–457.

7 Y. Nishihata, J. Mizuki, H. Tanaka, M. Uenishi and M. Kimura, *J. Phys. Chem. Solids*, 2005, **66**, 274–282.

8 H. U. Blaser and F. Spindler, *Top. Catal.*, 1997, **4**, 275–282.

9 H. U. Blaser and F. Spindler, *Chimia (Aarau).*, 1997, **51**, 297–299.

10 J. Crosby, *Pestic. Sci.*, 1996, **46**, 11–31.

11 H. Pellissier, *Tetrahedron*, 2013, **69**, 7171–7210.

12 J. M. Hawkins and T. J. N. Watson, *Angew. Chem. Int. Ed.*, 2004, **43**, 3224–3228.

13 A. Rahman, V. Uahengo and L. S. Daniel, *Glob. Drugs Ther.*, 2017, **2**, 1–6.

14 C. Li, C. Yang and H. Shan, *Ind. Eng. Chem. Res.*, 2007, **46**, 4914–4920.

15 J. M. Arandes, I. Abajo, D. López-Valerio, I. Fernández, M. J. Azkoiti, M. Olazar and J. Bilbao, *Ind. Eng. Chem. Res.*, 1997, **36**, 4523–4529.

16 H. M. Torres Galvis and K. P. de Jong, *ACS Catal.*, 2013, **3**, 2130–2149.

17 J. M. Thomas, *Nature*, 2015, **525**, 325–326.

18 K. Liu, A. Wang and T. Zhang, *ACS Catal.*, 2012, **2**, 1165–1178.

19 H. E. van Dam, L. J. Wisse and H. van Bekkum, *Appl. Catal.*, 1990, **61**, 187–197.

20 E. Farnetti, R. Di Monte and J. Kašpar, *Inorg. Bio-inorganic Chem.*, 1999, 2, 1–15.

21 C. E. Housecroft and A. G. Sharpe, in *Inorganic Chemistry*, Pearson Education Limited, Edinburgh, 2nd edn., 2005, pp. 786–807.

22 T. L. Church, Y. D. Y. L. Getzler, C. M. Byrne and G. W. Coates, *Chem. Commun.*, 2007, 657–674.

23 N. Yoneda, S. Kusano, M. Yasui, P. Pujado and S. Wilcher, *Appl. Catal. A Gen.*, 2001, **221**, 253–265.

24 G. J. Sunley and D. J. Watson, *Catal. Today*, 2000, **58**, 293–307.

25 P. W. N. M. van Leeuwen, in *Homogeneous Catalysis: Understanding the Art*, Kluwer Academic Publishers, Dordrecht, 1st edn., 2004, pp. 75–81.

26 C. O'Connor, G. Yagupsky, D. Evans and G. Wilkinson, *Chem. Commun.*, 1968, **38**, 420–421.

27 J. A. Osborn, F. H. Jardine, J. F. Young and G. Wilkinson, *J. Chem. Soc.*, 1966, 1711–1732.

28 R. E. Harmon, S. K. Gupta and J. Brown, *Chem. Rev.*, 1973, **73**, 21–52.

29 M. Beller, B. Cornils, C. D. Frohning and C. W. Kohlpaintner, *J. Mol. Catal. A Chem.*, 1995, **104**, 17–85.

30 R. L. Pruett, *J. Chem. Educ.*, 1986, **63**, 196–198.

31 S. M. Mercer, T. Robert, D. V. Dixon and P. G. Jessop, *Catal. Sci. Technol.*, 2012, **2**, 1315–1318.

32 R. Franke, D. Selent and A. Börner, *Chem. Rev.*, 2012, **112**, 5675–5732.

33 B. Cornils, W. A. Herrmann and M. Rasch, *Angew. Chem. Int. Ed.*, 1994, **33**, 2144–2163.

34 G. D. Frey, *J. Organomet. Chem.*, 2013, **754**, 5–7.

35 B. R. James, P. W. N. M. van Leeuwen and C. Claver, in *Rhodium Catalyzed Hydroformylation*, Kluwer Academic Publishers, New York, 1st edn., 2002, pp. 6–277.

36 S. Gladiali, J. Carles Bayón and C. Claver, *Tetrahedron: Asymmetry*, 1995, **6**, 1453–1474.

37 M. Vilches-Herrera, L. Domke and A. Börner, *ACS Catal.*, 2014, **4**, 1706–1724.

38 B. Cornils, W. A. Herrmann, I. T. Horvath, W. Leitner, S. Mecking, H. Olivier-Bourbigou and D. Vogt, in *Multiphase Homogeneous Catalysis*, Wiley-VCH Verlag GmbH & Co. KGaA, Weinheim, 2nd edn., 2005, pp. 3–21.

39 A. E. C. Collis and I. T. Horváth, *Catal. Sci. Technol.*, 2011, **1**, 912–919.

40 Â. C. B. Neves, M. J. F. Calvete, M. V. D. Pinho and M. M. Pereira, *Eur. J. Org. Chem.*, 2012, 6309–6320.

41 D. J. Cole-Hamilton, *Catalysis*, 2003, **299**, 1702–1707.

42 P. Tundo and A. Perosa, *Chem. Soc. Rev.*, 2007, **36**, 532–550.

43 P. J. Dyson, D. J. Ellis and T. Welton, *Platin. Met. Rev.*, 1998, **42**, 135–140.

44 E. A. Karakhanov and A. L. Maksimov, *Russ. J. Gen. Chem.*, 2009, **79**, 1370–1383.

45 M. Lombardo and C. Trombini, in *RSC Green Chemistry Series: Eco-Friendly Synthesis of Fine Chemicals*, Royal Society of Chemistry, 1st edn., 2009, pp. 1–79.

46 R. A. Sheldon, *Green Chem.*, 2005, **7**, 267–278.

47 R. A. Sheldon, *Curr. Opin. Green Sustain. Chem.*, 2019, **18**, 13–19.

48 K. N. Marsh, J. A. Boxall and R. Lichtenthaler, *Fluid Phase Equilib.*, 2004, **219**, 93–98.

49 Y. Xu, Y. Wang, Y. Zeng, J. Jiang and Z. Jin, *Catal. Letters*, 2012, **142**, 914–919.

50 Z. Yan, W. Yanhua, X. U. Yicheng, S. Ying, Z. Jiaqi, J. Jingyang and J. I. N. Zilin, *Chinese J. Catal.*, 2012, **33**, 402–406.

51 Q. Lin, W. Jiang, H. Fu, H. Chen and X. Li, *Appl. Catal. A Gen.*, 2007, **328**, 83–87.

52 P. J. Dyson, *Dalton Trans.*, 2003, 2964–2974.

53 J. M. Marinkovic, A. Riisager, R. Franke, P. Wasserscheid and M. Haumann, *Ind. Eng. Chem. Res.*, 2019, **58**, 2409–2420.

54 S. T. Handy, *Ionic Liquids - Classes and Properties*, InTech, Croatia, Rijeka, 1st edn., 2011.

55 M. Solinas, A. Pfaltz, P. G. Cozzi and W. Leitner, *J. Am. Chem. Soc.*, 2004, **126**, 16142–16147.

56 E. Ramsey, Q. Sun, Z. Zhang, C. Zhang and W. Gou, *J. Environ. Sci.*, 2009, **21**, 720–726.

57 D. Geier, P. Schmitz, J. Walkowiak, W. Leitner and G. Franciò, *ACS Catal.*, 2018, **8**, 3297–3303.

58 X. Jin, J. Feng, S. Li, H. Song, C. Yu, K. Zhao and F. Kong, *Mol. Catal.*, 2019, **475**, 110503.

59 S. L. Desset, U. Hintermair and D. J. Cole-Hamilton, *Top. Catal.*, 2010, **53**, 963–968.

60 E. Bogel-Łukasik, C. I. Melo and R. Bogel-Łukasik, *J. Supercrit. Fluids*, 2012, **61**, 191–198.

61 D. J. Adams, D. J. Cole-Hamilton, E. G. Hope, P. J. Pogorzelec and A. M. Stuart, *J. Organomet. Chem.*, 2004, **689**, 1413–1417.

62 W. Chen, L. Xu and J. Xiao, *Chem. Commun.*, 2000, 839–840.

63 M. S. Yu, D. P. Curran and T. Nagashima, *Org. Lett.*, 2005, **7**, 3677–80.

64 R. H. Fish, *Chem. Eur. J.*, 1999, **5**, 1677–1680.

65 L. P. Barthel-Rosa and J. A. Gladysz, *Coord. Chem. Rev.*, 1999, **190**–**192**, 587–605.

66 Y. Huang, E. Perperi, G. Manos and D. J. Cole-Hamilton, *J. Mol. Catal. A Chem.*, 2004, **210**, 17–21.

67 D. F. Foster, D. J. Adams, D. Gudmunsen, A. M. Stuart, E. G. Hope and D. J. Cole-

Hamilton, *Chem. Commun.*, 2002, 722–723.

68 J. Rábai, Z. Szlávik and I. T. Horváth, in *Handbook of Green Chemistry and Technology*, Blackwell Science Ltd, Oxford, 1st edn., 2002, pp. 502–523.

69 I. T. Horváth and J. Rábai, *Science*, 1994, **266**, 72–75.

70 B. Cornils and E. G. Kuntz, *J. Organomet. Chem.*, 1995, **502**, 177–186.

71 K. H. Shaughnessy, *Chem. Rev.*, 2009, **109**, 643–710.

72 B. E. Hanson, H. Ding and C. W. Kohlpaintner, *Catal. Today*, 1998, **42**, 421–429.

73 N. Pinault and D. W. Bruce, *Coord. Chem. Rev.*, 2003, **241**, 1–25.

74 G. Fremy, R. Grzybek, E. Monflier, A. Mortreux, A. M. Trzeciak and J. Ziolkowski, *J. Organomet. Chem.*, 1995, **505**, 11–16.

75 T. Borrmann, H. W. Roesky and U. Ritter, *J. Mol. Catal. A Chem.*, 2000, **153**, 31–48.

76 D. A. Aubry, N. N. Bridges, K. Ezell and G. G. Stanley, *J. Am. Chem. Soc.*, 2003, **125**, 11180–11181.

77 D. S. Ramarou, B. C. E. Makhubela and G. S. Smith, *J. Organomet. Chem.*, 2018, **870**, 23–31.

78 L. C. Matsinha, P. Malatji, A. T. Hutton, G. A. Venter, S. F. Mapolie and G. S. Smith, *Eur. J. Inorg. Chem.*, 2013, 4318–4328.

79 L. C. Matsinha, S. F. Mapolie and G. S. Smith, *Dalton Trans.*, 2015, **44**, 1240–1248.

80 N. N. Omosun and G. S. Smith, *Eur. J. Inorg. Chem.*, 2019, 2558–2564.

81 T. Bartik, B. Bartik, B. E. Hanson, K. H. Whitmire and I. Guo, *Inorg. Chem.*, 1993, **32**, 5833–5837.

82 D. U. Parmar, H. C. Bajaj, S. D. Bhatt and R. V Jasra, 2003, **2**, 34–39.

83 C. W. Kohlpaintner, R. W. Fischer and B. Cornils, *Appl. Catal. A Gen.*, 2001, **221**, 219–225.

84 K. Cousin, T. Vanbésien, E. Monflier and F. Hapiot, *Catal. Commun.*, 2019, **125**, 37–42.

85 O. L. Eliseev, T. N. Bondarenko, S. N. Britvin, P. P. Khodorchenko and A. L. Lapidus, *Mendeleev Commun.*, 2018, **28**, 264–266.

86 X. Zhang, J. Wei and X. Zhang, *New J. Chem.*, 2019, **43**, 14134–14138.

87 T. Pogrzeba, M. Illner, M. Schmidt, N. Milojevic, E. Esche, J. U. Repke and R. Schomäcker, *Ind. Eng. Chem. Res.*, 2019, **58**, 4443–4453.

88 M. Zábranský, I. Císařová, A. M. Trzeciak, W. Alsalahi and P. Štěpnička, *Organometallics*, 2019, **38**, 479–488.

89 P. J. Baricelli, E. Lujano, M. Modroño, A. C. Marrero, Y. M. García, A. Fuentes and R. A. Sánchez-Delgado, *J. Organomet. Chem.*, 2004, **689**, 3782–3792.

90 V. J. Guanipa, L. G. Melean, M. M. Alonzo, A. Gonzalez, M. Rosales, F. Lopez-Linares and P. J. Baricelli, *Appl. Catal. A Gen.*, 2009, **358**, 21–25.

91 L. C. Matsinha, S. Siangwata, G. S. Smith and B. C. E. Makhubela, *Catal. Rev. - Sci. Eng.*, 2019, **61**, 111–133.

92 A. Scrivanti, V. Beghetto, M. Alam, S. Paganelli, P. Canton, M. Bertoldini and E. Amadio, *Inorganica Chim. Acta*, 2017, **455**, 613–617.

93 O. Wachsen, K. Himmler and B. Cornils, *Catal. Today*, 1998, **42**, 373–379.

94 L. Obrecht, P. C. J. Kamer and W. Laan, *Catal. Sci. Technol.*, 2013, **3**, 541–551.

95 T. Rösler, T. A. Faßbach, M. Schrimpf, A. J. Vorholt and W. Leitner, *Ind. Eng. Chem. Res.*, 2019, **58**, 2421–2436.

96 F. Hapiot, S. Tilloy and E. Monflier, *Chem. Rev.*, 2006, **106**, 767–781.

97 E. M. M. Del Valle, *Process Biochem.*, 2004, **39**, 1033–1046.

98 L. Leclercq and A. R. Schmitzer, *Organometallics*, 2010, **29**, 3442–3449.

99 H. Bricout, F. Hapiot, A. Ponchel, S. Tilloy and E. Monflier, *Sustainability*, 2009, **1**,

924–945.

100 S. Tilloy, H. Bricout and E. Monflier, *Green Chem.*, 2002, **4**, 188–193.

101 F. Hapiot, H. Bricout, S. Tilloy and E. Monflier, *Eur. J. Inorg. Chem.*, 2012, 1571–1578.

102 E. Monflier, S. Tilloy, Y. Castanet and A. Mortreux, *Tetrahedron Lett.*, 1998, **39**, 2959–2960.

103 M. Dauchy, M. Ferreira, J. Leblond, H. Bricout, S. Tilloy, G. S. Smith and E. Monflier, *Pure Appl. Chem.*, 2018, **90**, 845–855.

104 T. Mathivet, C. Méliet, Y. Castanet, A. Mortreux, L. Caron, S. Tilloy and E. Monflier, *J. Mol. Catal. A Chem.*, 2001, **176**, 105–116.

105 N. Six, A. Guerriero, D. Landy, M. Peruzzini, L. Gonsalvi, F. Hapiot and E. Monflier, *Catal. Sci. Technol.*, 2011, **1**, 1347–1353.

106 L. Obrecht, P. C. J. Kamer and W. Laan, *Catal. Sci. Technol.*, 2013, **3**, 541–551.

107 S. K. Sharma and R. V. Jasra, *Catal. Today*, 2015, **247**, 70–81.

108 P. J. Baricelli, M. Rodriguez, L. G. Melean, M. Modro, M. Borusiak, M. Rosales, B. Gonzalez, K. C. B. de Oliveira, E. V. Gusevskaya and N. Eduardo, *Appl. Catal. A Gen.*, 2015, **490**, 163–169.

109 C. G. Vieira, M. C. de Freitas, K. C. B. de Oliveira, A. de C. Faria, E. N. dos Santos and E. V. Gusevskaya, *Catal. Sci. Technol.*, 2015, **5**, 960–966.

110 T. Hamerla, A. Rost, Y. Kasaka and R. Schomäcker, *ChemCatChem*, 2013, **5**, 1854–1862.

111 A. Rost, M. Müller, T. Hamerla, Y. Kasaka, G. Wozny and R. Schomäcker, *Chem. Eng. Process. Process Intensif.*, 2013, **67**, 130–135.

112 D. Müller, D. Hoang, V. Alejandro, H. Arellano-garcia, Y. Kasaka, M. Müller, R. Schomäcker and G. Wozny, *Chem. Eng. Sci.*, 2014, **115**, 127–138.

113 H. Nowothnick, A. Rost, T. Hamerla, R. Schomäcker, C. Müller and D. Vogt, *Catal.*

Sci. Technol., 2013, **3**, 600.

114 P. Schrader, C. Paasche and S. Enders, *Chem. Eng. Sci.*, 2014, **115**, 139–147.

115 R. M. Deshpande, Purwanto, H. Delmas and R. V. Chaudhari, *Ind. Eng. Chem. Res.*, 1996, **35**, 3927–3933.

116 J. Bianga, N. Herrmann, L. Schurm, T. Gaide, J. M. Dreimann, D. Vogt and T. Seidensticker, *Eur. J. Lipid Sci. Technol.*, 2020, **122**, 1900317.

117 I. Hablot, J. Jenck, G. Casamatta and H. Delmas, *Chem. Eng. Sci.*, 1992, **47**, 2689–2694.

118 F. Monteil, R. Queau and P. Kalck, *J. Organomet. Chem.*, 1994, **480**, 177–184.

119 J.-Z. Wei, J.-W. Lang, H.-Y. Fu, R.-X. Li, X.-L. Zheng, M.-L. Yuan and H. Chen, *Transit. Met. Chem.*, 2016, **41**, 599–603.

120 Y. Liu, J. Zhao, Y. Zhao, H.-M. Liu, H. Fu, X. Zheng, M. Yuan, R. Li and H. Chen, *RSC Adv.*, 2019, **9**, 7382–7387.

121 V. S. Shende, V. B. Saptal and B. M. Bhanage, *Chem. Rec.*, 2019, **19**, 2022–2043.

122 I. Vural Gürsel, T. Noel, Q. Wang and V. Hessel, *Green Chem.*, 2015, **17**, 2012–2026.

123 K. de Smet, S. Aerts, E. Ceulemans, I. F. J. Vankelecom and P. A. Jacobs, *Chem. Commun.*, 2001, 597–598.

124 W. E. Siew, C. Ates, A. Merschaert and A. G. Livingston, *Green Chem.*, 2013, **15**, 663–674.

125 D. Ormerod, B. Sledsens, G. Vercammen, D. van Gool, T. Linsen, A. Buekenhoudt and B. Bongers, *Sep. Purif. Technol.*, 2013, **115**, 158–162.

126 D. de Groot, E. B. Eggeling, J. C. de Wilde, H. Kooijman, R. J. van Haaren, A. W. van der Made, A. L. Spek, D. Vogt, J. N. H. Reek, C. J. Kamer and P. W. N. M. van Leeuwen, *Chem. Commun.*, 1999, 1623–1624.

127 H. P. Dijkstra, G. P. M. van Klink and G. van Koten, *Acc. Chem. Res.*, 2002, **35**, 798–810.

128 L. W. Gosser, W. H. Knoth and G. W. Parshall, *J. Mol. Catal.*, 1977, **2**, 253–263.

129 J. Fang, R. Jana, J. A. Tunge and B. Subramaniam, *Appl. Catal. A Gen.*, 2011, **393**, 294–301.

130 M. Priske, K. Wiese, A. Drews, M. Kraume and G. Baumgarten, *J. Memb. Sci.*, 2010, **360**, 77–83.

131 W. L. Peddie, J. N. van Rensburg, H. C. M. Vosloo and P. van der Gryp, *Chem. Eng. Res. Des.*, 2017, **121**, 219–232.

132 J. M. Dreimann, A. J. Vorholt, M. Skiborowski and A. Behr, *Chem. Eng. Trans.*, 2016, **47**, 343–348.

133 D. Astruc and F. Chardac, *Chem. Rev.*, 2001, **101**, 2991–3023.

134 P. J. Deuss, R. Denheeten, W. Laan and P. C. J. Kamer, *Chem. Eur. J.*, 2011, **17**, 4680–4698.

135 M. H. Pørez-Temprano, J. A. Casares and P. Espinet, *Chem. Eur. J.*, 2012, **18**, 1864–1884.

136 P. Govender, B. Therrien and G. S. Smith, *Eur. J. Inorg. Chem.*, 2012, 2853–2862.

137 J. Park and S. Hong, *Chem. Soc. Rev.*, 2012, **41**, 6931–6943.

138 S. Liu, A. Motta, M. Delferro and T. J. Marks, *J. Am. Chem. Soc.*, 2013, **135**, 8830–8833.

139 R. A. Krüger and T. Baumgartner, *Dalton Trans.*, 2010, **39**, 5759–67.

140 K. Nakao, G. Choi, Y. Konishi, H. Tsurugi and K. Mashima, *Eur. J. Inorg. Chem.*, 2012, **17**, 1469–1476.

141 J. October and S. F. Mapolie, *J. Organomet. Chem.*, 2017, **840**, 1–10.

142 E. B. Hager, B. C. E. Makhubela and G. S. Smith, *Dalton Trans.*, 2012, **41**, 13927–35.

143 N. C. Antonels, J. R. Moss and G. S. Smith, *J. Organomet. Chem.*, 2011, **696**, 2003–2007.

144 B. C. E. Makhubela, A. M. Jardine, G. Westman and G. S. Smith, *Dalton Trans.*, 2012, **41**, 10715–10723.

145 L. Ropartz, R. E. Morris, D. F. Foster and D. J. Cole-Hamilton, *Chem. Commun.*, 2001, 361–362.

146 C. Williams, M. Ferreira, E. Monflier, S. F. Mapolie and G. S. Smith, *Dalton Trans.*, 2018, **47**, 9418–9429.

147 H. U. Blaser, A. Indolese and A. Schnyder, *Curr. Sci.*, 2000, **78**, 1336–1344.

148 P. T. Anastas and J. C. Warner, *The 12 Principles of Green Chemistry*, Oxford University Press, New York, 1998.

Chapter 2

Synthesis and characterisation of aryl ether-based mono- and multinuclear salicylaldimine Rh(I) complexes

This Chapter forms part of a publication titled "*Olefin hydroformylation and kinetic studies using mono- and trinuclear N,O-chelate rhodium(I)-aryl ether precatalysts*", cited as:
S. Siangwata, N. C. C. Breckwoldt, N. J. Goosen and G. S. Smith, *Appl. Catal. A Gen.* 2019, **585**, 117179.

2.1 Introduction

The ease of design and synthesis of functional and/or ancillary ligands for catalysis plays a major role in the overall catalyst performance, stability as well as re-usability. Several efforts continue to be made towards the development of facile synthesis strategies for tailor-made homogeneous catalysts. Ugo Joseph Schiff's discovery of Schiff base ligands has created an attractive class of compounds that have found application in various homogeneous catalytic transformations, owing to the good stability and versatility of the resultant precursors to metallo-imines.[1–5] These imine-based precursor ligands are prepared *via* a condensation reaction between a primary amine and an aldehyde or ketone (Scheme 2.1).[6–9] In the first step of the mechanism, the amine acts as the nucleophile, attacking the carbonyl carbon and forming an unstable carbinolamine. This undergoes a double proton transfer, followed by the rate-determining water-elimination step for the generation of the azomethine product.

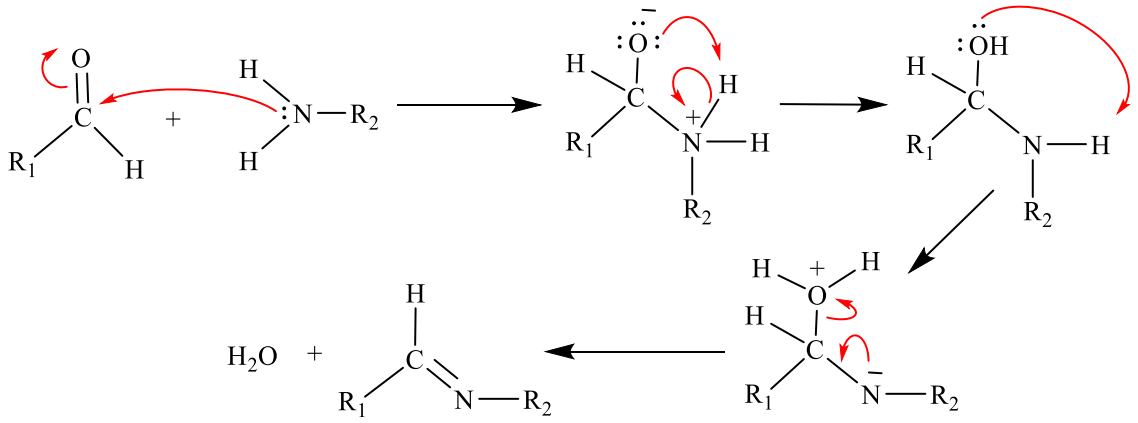

Scheme 2.1 Mechanism of a Schiff base condensation reaction.

Schiff base ligands impart improved physicochemical stability to metal complexes, for example, from the inherent chelating ability of *N,O*-bidentate ligand systems. Such potentially beneficial characteristics have led to our group extensively exploring the application of the *N,O*-bidentate chelating ligands in catalysis.[10–14] Anchoring these salicylaldimine-based ligands to dendritic supports under the premise of mimicking the naturally occurring metalloenzymes (bearing two or more active sites) has the potential of improving the catalytic performance of the resultant coordination compounds, due to the multiple catalytically active sites that propagate from the core.[15,16] These highly branched metallodendritic tree-like polymers possess a 3D structure that provides a high degree of surface functionality and versatility (Figure 2.1). In addition, the appropriate choice of a dendrimer scaffold may allow for facile catalyst recovery through filtration by gravity,[17] or by means of pressurised size exclusion-based membrane techniques.

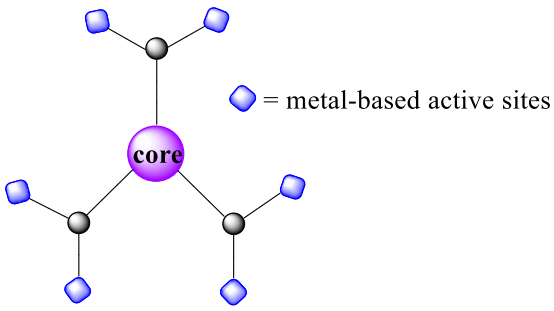

Figure 2.1 Metallodendrimer containing peripheral catalytic sites.

The construction of low to high generation aryl ether-based metallodendrimers has been reported in the literature, through Williamson ether syntheses with dendritic wedges bearing benzyl halide functional groups.[12,18–21] The mechanism proceeds *via* the generation of the alkoxide-ion intermediate, which functions as the nucleophile and attacks the electrophilic carbon of the alkyl halide to create a new C–O bond (Scheme 2.2). Subsequently, as in a typical S_N2 fashion, the halide ion is displaced as the leaving group leading to the aryl-ether product. The Williamson ether reaction remains the most popular method for preparing ethers, and the reaction is very attractive owing to the facile in-situ generation of the alkoxide, tolerance to a wide range of solvents as well as the application of less harsh reaction temperatures (50 – 100 °C).

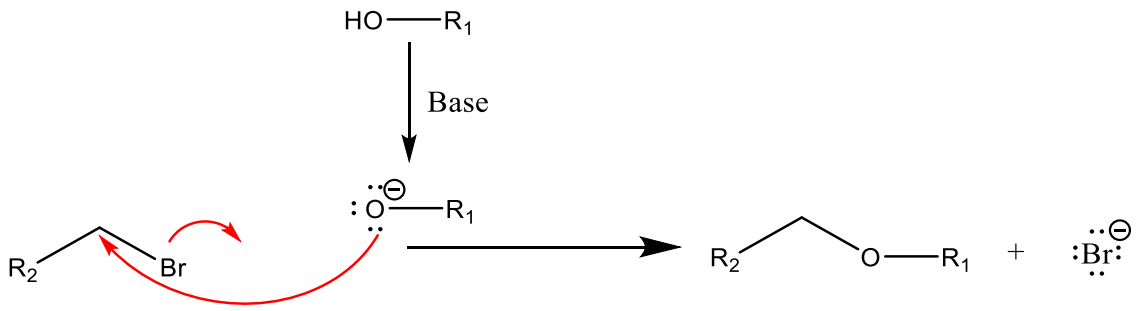

Scheme 2.2 General mechanism of the Williamson ether synthesis.

To the best of our knowledge, no Rh(I) salicylaldimine-based benzyl halide dendritic wedges have been anchored to 1,1,1-tris(4′-hydroxyphenyl)ethane core for potential application as hydroformylation pre-catalysts. The dendrimer-based molecular weight enlargement of precatalyst provides an avenue to be explored towards the design and synthesis of highly active, recoverable and reusable catalyst precursors for the hydroformylation of longer chain olefins. In this chapter we report on the synthesis and characterisation of potentially recoverable molecular-weight-enlarged Rh(I) salicylaldimine-based aryl ether mono- and multinuclear complexes.

For the development of our salicylaldimine aryl-ether-based metallodendritic structures, we first prepared the mononuclear congeners to our multinuclear Rh(I)-complexes, as presented in the following sections.

2.2 Synthesis and characterisation of Rh(I)-propylsalicylaldimine complex (2.2)

The synthesis of the mononuclear complex **2.2** was conducted by first carrying out a Schiff base condensation reaction of salicylaldehyde with propylamine in dry methanol, leading to the monomeric propylsalicylaldimine ligand **2.1** (Scheme 2.3 overleaf). The imine-based ligand **2.1** was isolated as a yellow oil in near quantitative yields and characterised by elemental analysis (C, H, N), FT-IR, ^{1}H NMR and ^{13}C{^{1}H} spectroscopy as well as mass spectrometry.

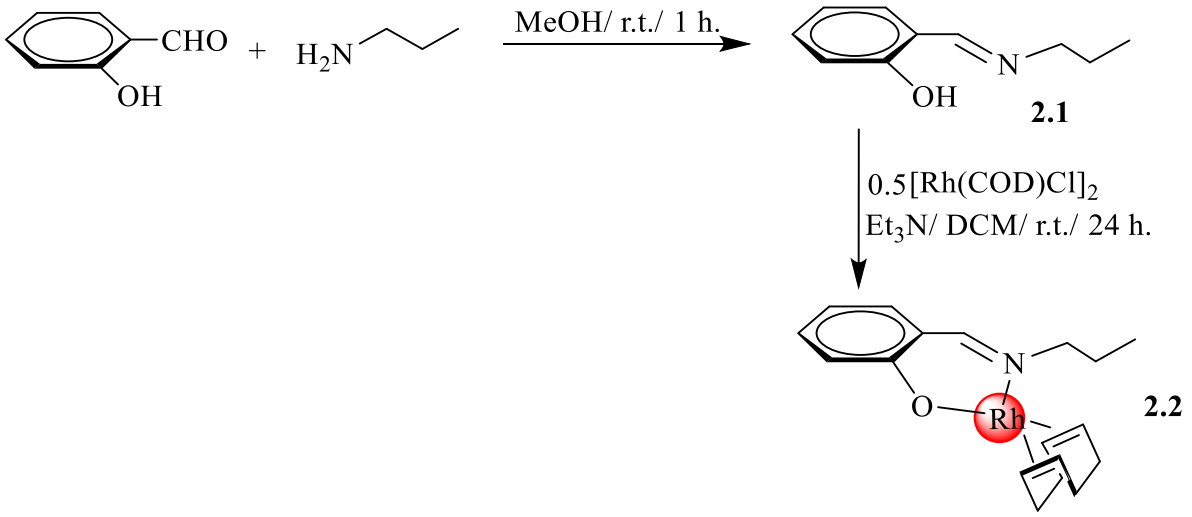

Scheme 2.3 Synthesis of Rh(I)-propylsalicylaldimine complex **2.2**.

The ^{1}H NMR spectrum of **2.1** (Figure 2.2) correlates with literature[22] and accounts for all the expected protons in the structure of **2.1**. The signals for the hydroxyl and imine protons in Figure 2.2 are observed as singlets in their characteristic regions (δ = 13.66 (H_1) and 8.54 (H_8) respectively). The methylene protons of the propyl moiety are observed upfield as a triplet (H_9) and a sextet (H_{10}) due to coupling to neighbouring protons. The methyl protons (H_{11}) occur as a triplet further upfield and integrate for the expected number of protons. The infrared spectrum shows the presence of a characteristic strong imine ν(C=N) absorption band at 1635 cm^{-1}, and an absorption band at 2970 cm^{-1} corresponding to the ν(O–H) stretching frequency.

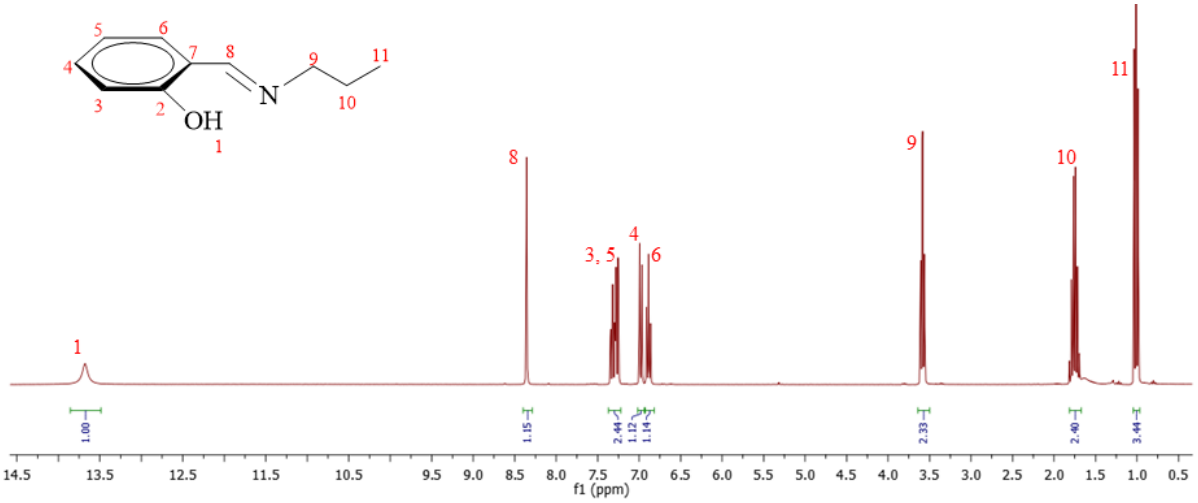

Figure 2.2 ^{1}H NMR ($CDCl_3$) spectrum for propylsalicylaldimine ligand **2.1**.

After ascertaining the structural integrity of **2.1**, deprotonation of this monomeric ligand with triethylamine and subsequent complexation with half molar equivalent of the Rh(I) dimer $[RhCl(COD)]_2$, (COD = 1,5-cyclooctadiene) led to the new Rh(I)-based propylsalicylaldimine mononuclear complex **2.2**, as presented in Scheme 2.3 *vide supra*. The complex was isolated in quantitative yields as a brown solid, and the structural integrity was determined using ^{1}H NMR, 2D NMR (HSQC and COSY) and $^{13}C\{^1H\}$ NMR spectroscopy, as well as elemental analysis and infrared spectroscopy. Notable differences in signals from the ^{1}H NMR spectrum of **2.1** to the spectrum of **2.2** (Figure 2.3 overleaf) are the upfield shift of the imine signal (from δ = 8.54 in **2.1**, to δ = 8.18 in **2.2**), as well as the observation of the hydroxyl-proton-signal only in the spectrum of the ligand and not in the spectrum of the complex. This provides evidence of successful deprotonation for subsequent chelation to form **2.2**. The upfield shift of the imine signal is attributed to increased electron density around the imine functionality arising from the back-donation of electrons by the rhodium-metal centre upon coordination. Also observed in the ^{1}H NMR spectrum are signals characteristic of the olefinic protons of the cyclooctadiene moiety (H_{11} and $H_{11'}$), as well as the methylene protons (H_{12} and $H_{12'}$). Appearance of the methylene protons as two separate multiplets emanates from the *trans*-effects on proton resonances due to the coordinating *N,O*-bidentate ligand, as explained to detail for similar Rh(I)-salicylaldimine complexes by Enamullah and co-workers.[23] All the other protons (aromatic and propyl chain) are accounted for in their expected regions in the ^{1}H NMR spectrum of **2.2**. In the $^{13}C\{^1H\}$ NMR spectrum, the olefinic carbon atoms of the cyclooctadiene moiety are observed as doublets, attributed to coupling to the rhodium metal centre (*trans* to N: $^1J_{Rh-C}$ = 12 Hz, and *trans* to O: $^1J_{Rh-C}$ = 14 Hz). These ^{103}Rh–^{13}C spin-spin coupling constants correlate well with those in literature for related (η^2:η^2–COD)-Rh–Schiff base complexes.[11,23] The infrared spectrum of **2.2** shows a shift of the imine absorption band to a lower wavenumber (ν(C=N) = 1602 cm^{-1}), from that of **2.1** (ν(C=N) = 1635 cm^{-1}). This is attributed to the weakening of the double-bond character of the imine functionality as a result of back-donation of electrons from the rhodium metal centre through synergic effects. This has been reported for similar compounds in the literature.[10,11,13,24] Successful deprotonation of the hydroxyl proton for chelation is also validated in the infrared spectrum of **2.2**, which does not show the ν(O–H) stretching frequency.

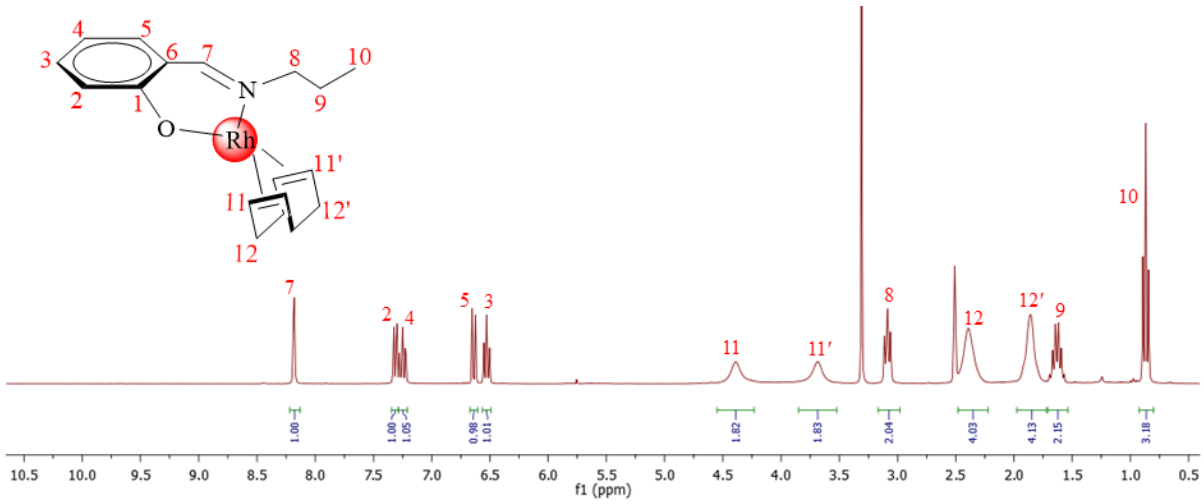

Figure 2.3 ^{1}H NMR (DMSO-d_6) spectrum for Rh(I)-propylsalicylaldimine complex **2.2**.

The favourable preparation of the mononuclear analogue **2.2** laid the groundwork for the synthesis of analogous Rh(I) salicylaldimine-based multinuclear complexes. The approach to the synthetic strategy for the multinuclear dendritic structures was based on the aryl ether functionality, as this can be readily controlled, and the reaction conditions and solvents often used in literature are tolerant to the iminium functionality. A convergent dendrimer synthesis approach was conducted through preparation of a Rh(I)-based metalloligand, which was then anchored to the trimeric core, as well as to a bis-hydroxy benzyl alcohol wedge *via* Williamson ether synthesis, as discussed in the following sections.

2.3 Synthesis and characterisation of Rh(I)-bromopropylsalicylaldimine complex (2.4)

The monomeric precursor ligand *N*-3-bromopropylsalicylaldimine (**2.3**) was prepared according to a previously reported literature procedure,[25] through a Schiff base condensation reaction of salicylaldehyde with 3-bromopropylamine hydrobromide salt in ethanol–water mixture (Scheme 2.4 overleaf). The iminium-based product (**2.3**) was isolated as a viscous yellow oil in good yield (90%), and characterised by FT-IR, ^{1}H NMR and ^{13}C{^{1}H} NMR spectroscopy as well as mass spectrometry.

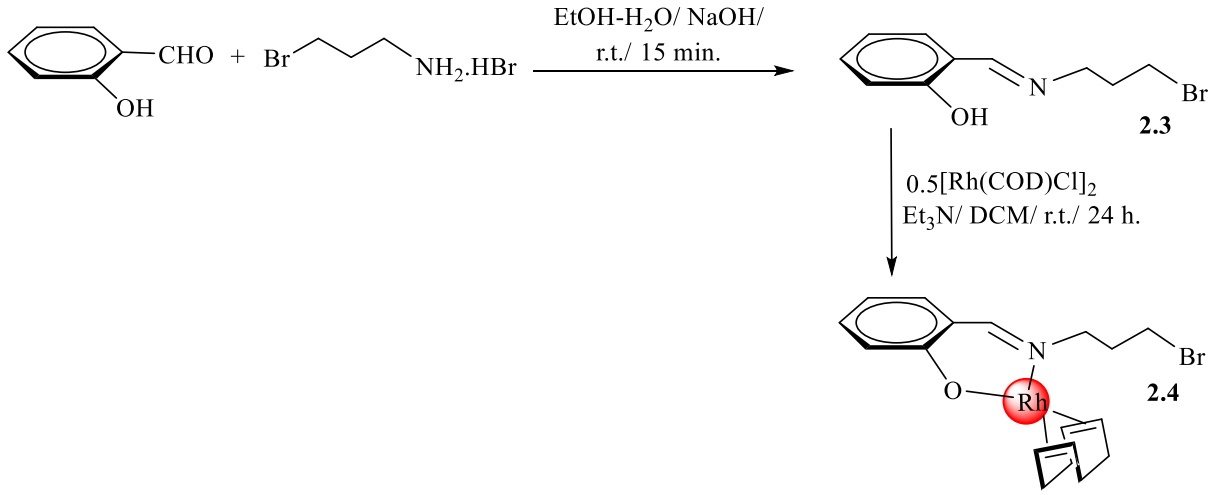

Scheme 2.4 Synthesis of Rh(I)-bromopropylsalicylaldimine complex **2.4**.

The signals for the hydroxyl and imine protons are observed as singlets in their characteristic regions (at δ = 13.31 and 8.58 respectively) in the ^{1}H NMR spectrum of **2.3** (Figure 2.4), and these are in good agreement with literature.[25] The methylene protons of the propyl moiety are observed upfield as triplets (H_9 and H_{11}) and a quintet (H_{10}) due to coupling to neighbouring protons (H_9, ^{3}J = 6.6 Hz; H_{11} and H_{10}, ^{3}J = 6.3 Hz). The mass spectrum data shows a base peak for $[M]^{+}$ at *m/z* = 242.86, corresponding to the molecular weight of **2.3**. The infrared spectrum shows a characteristic strong imine ν(C=N) absorption band at 1629 cm^{-1}, as well as an absorption band at 2937 cm^{-1} corresponding to the ν(O–H) stretching frequency. All the data agrees with the expected structure of **2.3** and this is in line with the data reported in literature.[25]

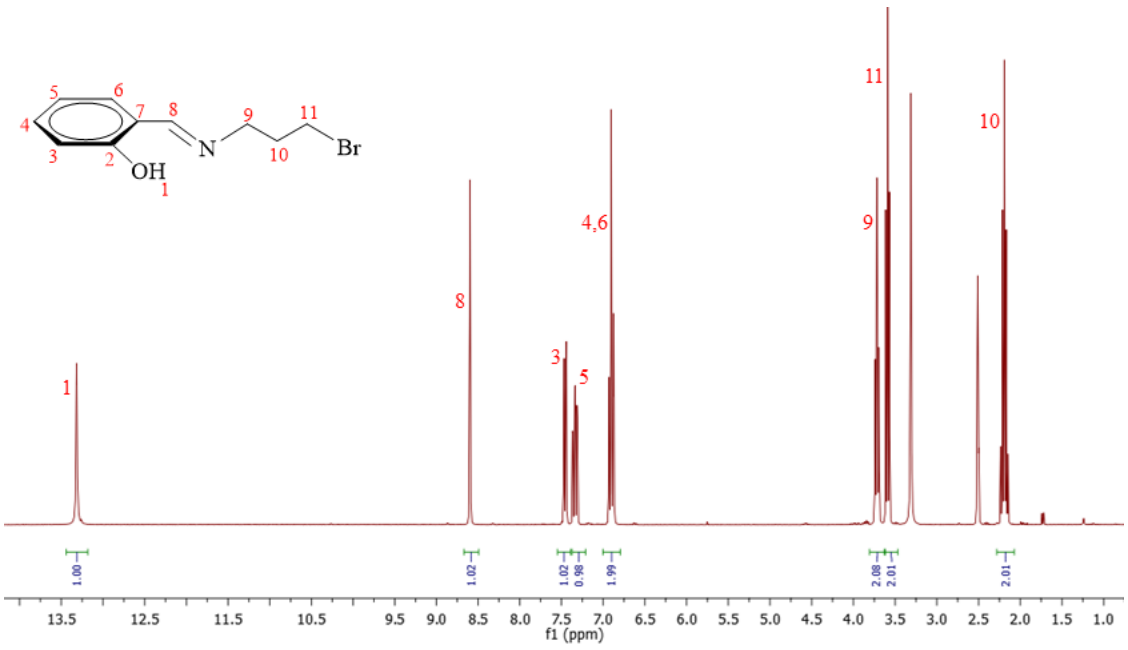

Figure 2.4 ^{1}H NMR (DMSO-d$_6$) spectrum for *N*-3-bromopropylsalicylaldimine **2.3**.

The salicylaldimine-based ligand **2.3** was then deprotonated using triethylamine, after which complexation was conducted with half molar equivalent of the Rh(I) dimer $[RhCl(COD)]_2$, (COD = 1,5-cyclooctadiene) to give the metalloligand product **2.4** as a yellow solid in good yield (76%). A close resemblance of the ^{1}H NMR spectrum of **2.4** (Figure 2.5) to that of **2.2** is noticeable, with only differences in the splitting pattern of the methylene protons (H_9 and H_{10} in **2.2**) which are observed in the spectrum of **2.4** as a quintet (H_9) and a triplet (H_{10}). All the other proton and carbon signals are observed in their characteristic regions and their splitting patterns are as explained for **2.2**. Infrared spectroscopy data also substantiates formation of complex **2.4**, with the spectrum showing a shift of the imine absorption band to lower frequency upon coordination of the ligand to the metal, from ν(C=N) = 1629 cm^{-1} (**2.3**) to ν(C=N) = 1600 cm^{-1} (**2.4**). The observed shift is due to similar reasoning to the shifts reported for **2.2**. The EI-MS spectrum shows a peak for $[M]^+$ in the positive ion-mode at *m/z* = 452.95, where M is the molecular ion peak.

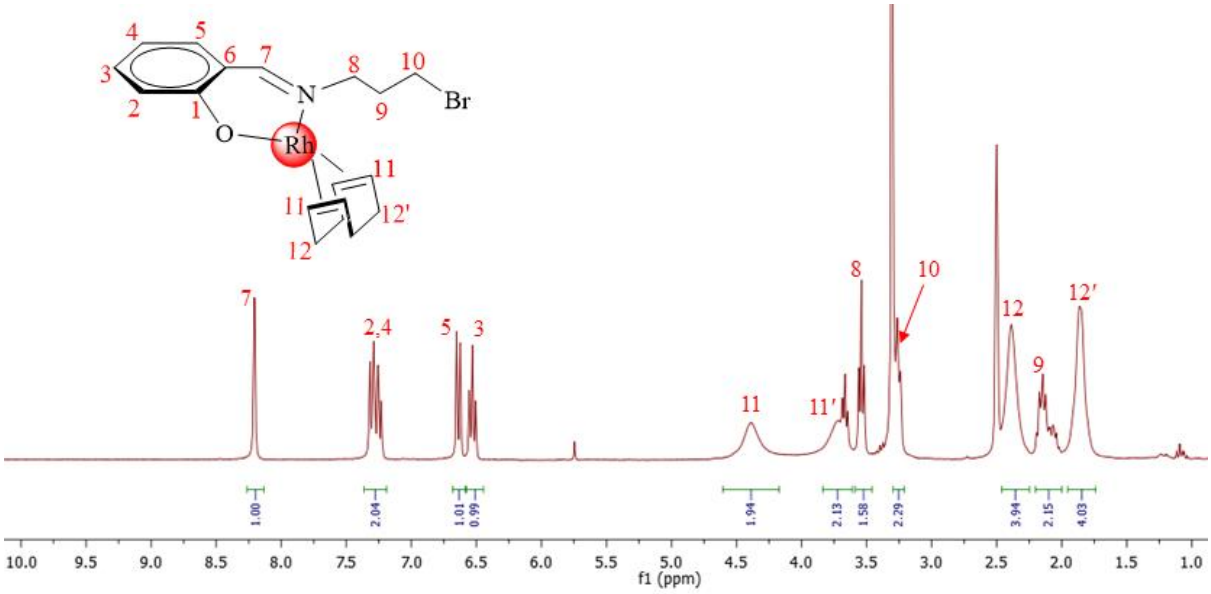

Figure 2.5 ^{1}H NMR (DMSO-d_6) spectrum for Rh(I)-bromopropylsalicylaldimine complex **2.4**.

The halide-bearing metalloligand **2.4** forms the building block for the dendritic structures of this work. The multinuclear structures are very attractive owing to the possibility of improved reactivity in areas such as catalysis, as often-observed with the naturally occurring metallobiomolecules (iron-containing hemoglobin, zinc-containing carboxypeptidase and the copper-containing hemocyanin).[15] Anchoring of **2.4** to a phenolic-based core and wedge *via* Williamson ether synthesis of the metallodendritic structures is discussed in the following sections.

2.4 Synthesis and characterisation of Rh(I)-aryl ether low generation dendritic complex (2.5)

The new aryl ether dendritic complex **2.5** was synthesised *via* a Williamson ether reaction of the metalloprecursor Rh(I)-bromopropylsalicylaldimine **2.4** with the trifunctional core 1,1,1-tris(4-hydroxyphenyl)ethane (THPE) in acetone (Scheme 2.5), and the product was isolated as a brown solid in low yield (22%). Several attempts to improve the yield of **2.5** were not successful, owing to the losses of the product during purification *via* trituration, with periodic decanting of the impurities with petroleum ether.

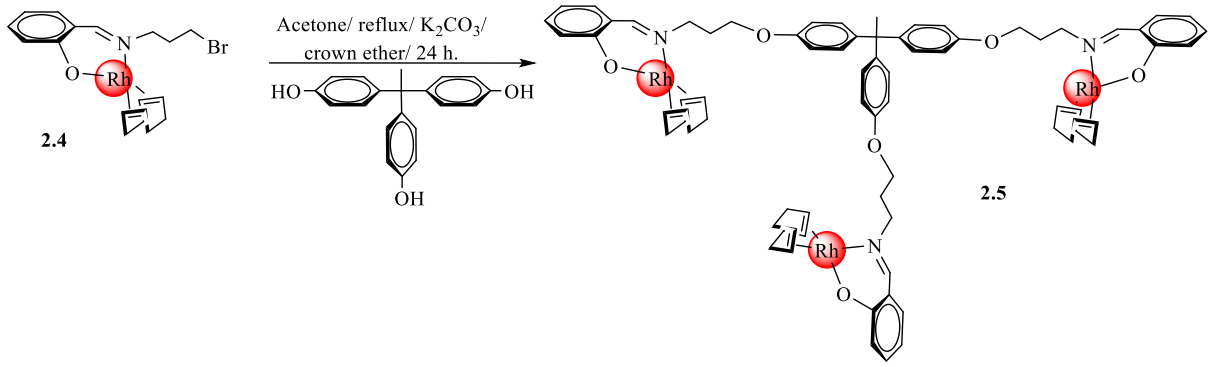

Scheme 2.5 Synthesis of the THPE-anchored trinuclear complex **2.5**.

Successful anchoring of **2.4** to the core is shown in Figure 2.6 by the presence of the diagnostic signal for the methyl protons of the THPE core (H_{16}), observed as overlapping signals with the methylene protons of the propyl chain (H_9) at *ca.* δ = 2.0. The signal for the imine proton is observed in the characteristic region (δ = 8.20), accounting for 3 protons as proposed in the structure of **2.5**. Infrared spectroscopy data shows the imine absorption band at ν(C=N) = 1604 cm^{-1}, further corroborating the successful functionalisation of the trimeric core.

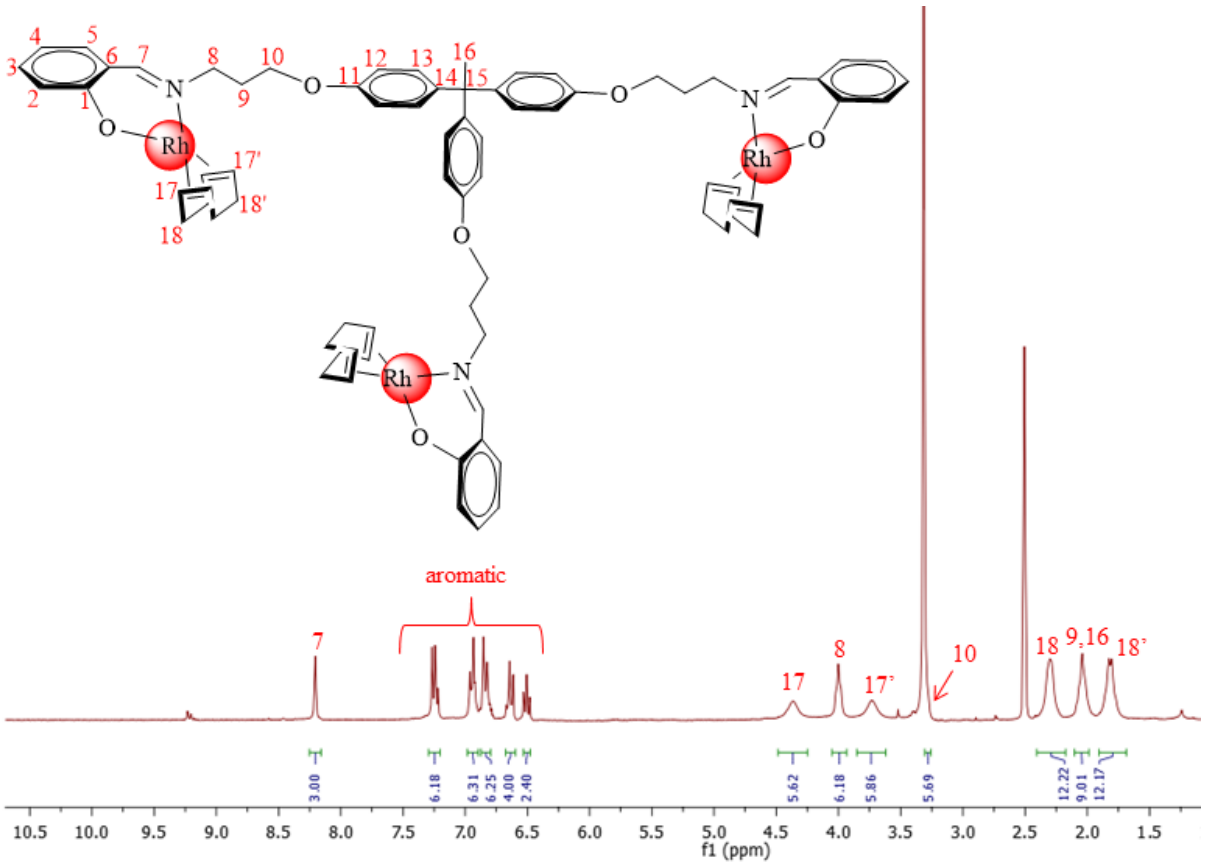

Figure 2.6 ^{1}H NMR (DMSO-d_6) spectrum for Rh(I) aryl ether dendritic complex **2.5**.

The successful synthesis of the trinuclear complex **2.5**, although isolated in unexpectedly low yields, forms a good representation of a low generation dendritic structure for our system. The spectroscopic characterisation data was in good agreement with the proposed structure of **2.5**. To further increase our dendrimer generation to a larger macromolecular structure, we again utilised the convergent approach in preparing a binuclear salicylaldimine aryl ether-based wedge, with the aim of ultimately anchoring the wedge to a trimeric core as discussed below.

2.5 Synthesis and characterisation of Rh(I)-aryl ether first-generation benzyl alcohol complex (2.6)

The first-generation benzyl alcohol dendritic wedge **2.6** was prepared *via* a Williamson ether reaction of the metalloprecursor **2.4** with 3,5-dihydroxybenzyl alcohol in acetone (Scheme 2.6), and the product was isolated as a brown solid in low yield (34%).

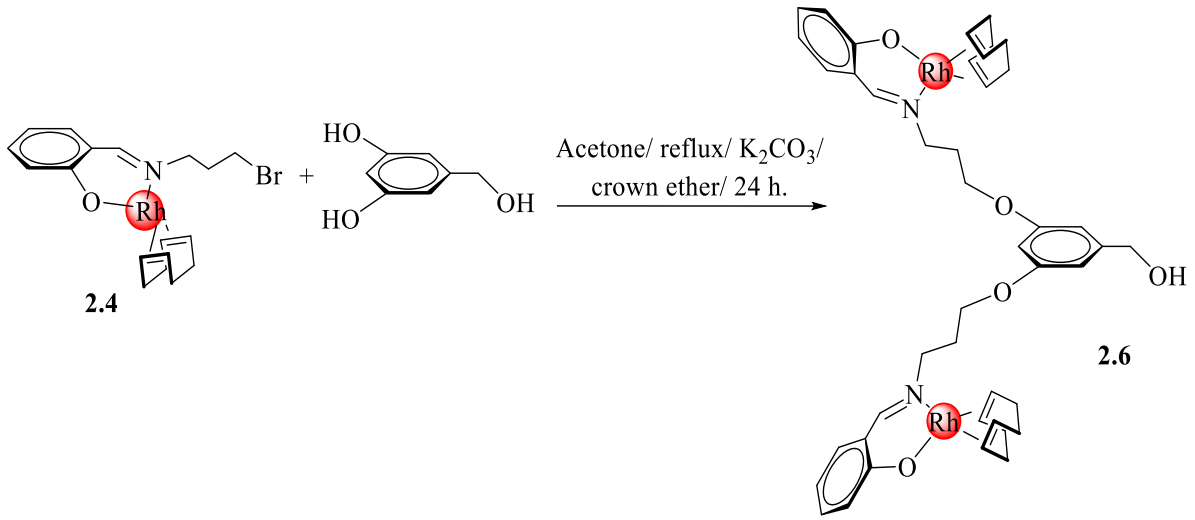

Scheme 2.6 Synthesis of the first-generation benzyl alcohol binuclear dendritic wedge **2.6**.

Successful anchoring of **2.4** to 3,5-dihydroxybenzyl alcohol in a bifunctional manner is represented in the ^{1}H NMR spectrum of **2.6** (Figure 2.7), which does not show the signal for the hydroxyl protons of the 3,5-dihydroxybenzyl alcohol starting material. In addition, the signal for the imine protons is observed as a singlet integrating for two protons at δ = 8.22, further corroborating successful bifunctionalisation to form **2.6**. All the aromatic protons of the salicylaldimine and the benzyl alcohol moieties are accounted for in their characteristic regions. The methylene protons of the benzyl alcohol moiety (H_{17}) are observed as an overlapping signal with the olefinic protons of the cyclooctadiene moiety (H_{11}) at *ca*. δ = 4.40. The hydroxyl proton of the benzyl alcohol moiety (H_{18}) appears at *ca*. δ = 5.20 as a triplet due to coupling with the neighbouring methylene protons (H_{17}). All the other protons of the cyclooctadiene moiety are observed in their expected regions and account for the expected number of protons in the structure of **2.6**.

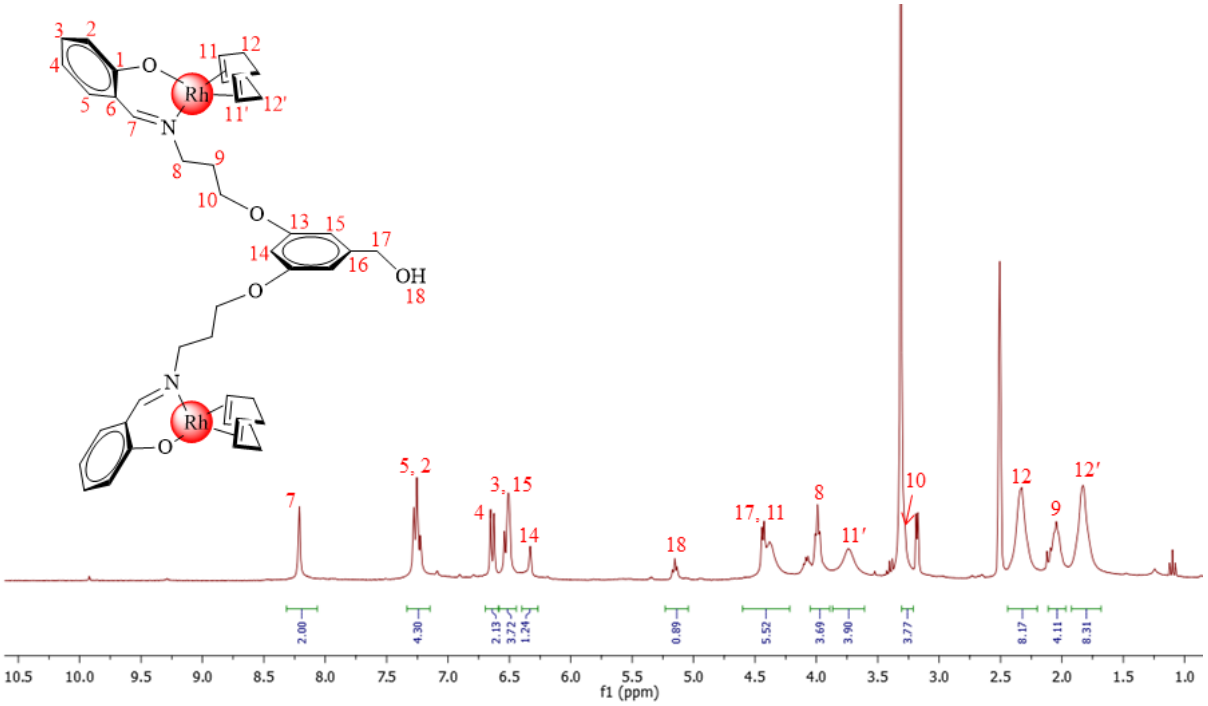

Figure 2.7 ^{1}H NMR (DMSO-d_6) spectrum for the binuclear benzyl alcohol wedge **2.6**.

In order to anchor complex **2.6** to the THPE core, several attempts to activate the alcohol functionality (–$\underline{OH}_{18}$) to a better leaving group were carried out. The Appel reaction was conducted several times under known standard conditions and solvents used in the literature, but the desired product could not be attained. With the view of the tedious purification of the complexes **2.5** and **2.6** which lead to very low yields, it was prudent to investigate the synthesis of related multinuclear structures using a high yielding synthesis procedure such as Click chemistry, which would subsequently compliment the beneficiation of the rhodium metal as one of the rare, expensive and fast depleting Platinum Group Metals.

2.6 Synthesis and characterisation of 4-(phenoxymethyl)-1*H*-1,2,3-triazol-1-yl-propylsalicylaldimine ligand (2.9)

The application of Click chemistry, a newer approach that is known for the high yielding reactions and the ease of availability of starting materials was then conducted, as presented in the following sections. Click chemistry is attractive due to the excellent functional group tolerance and the adherence to the 12 Principles of Green Chemistry through generation of only harmless products that can be removed by non-chromatographic methods.[26,27]

The Cu(I)-catalysed azide-alkyne cycloaddition click reaction (CuAAC) provides an excellent route for ligand design as the reaction is regioselective only to 1,4-disubstituted 1,2,3-triazoles, and can be effectively conducted at room temperature.[28–30] When copper salts are used as catalysts for the click reaction, the active species are often generated in situ owing to the known instability of copper(I) species.[31] For example, the active species can be generated either from a copper(II) salt such as Cu_2SO_4 using sodium ascorbate as a reducing agent,[32–34] or from a polymeric copper(I) salt such as CuI using diisopropylethylamine as a promoter.[35] The general mechanism involves the initial formation of a copper-acetylide complex, which is then followed by the coordination of the organic azide *via* the substituted nitrogen (Scheme 2.7). Cycloaddition of this copper-azide-alkyne intermediate leads to a 6-membered ring which undergoes ring contraction to form a copper triazolide intermediate. Protonation results in the elimination of the 1,4-disubstituted 1,2,3-triazole product.[36–38]

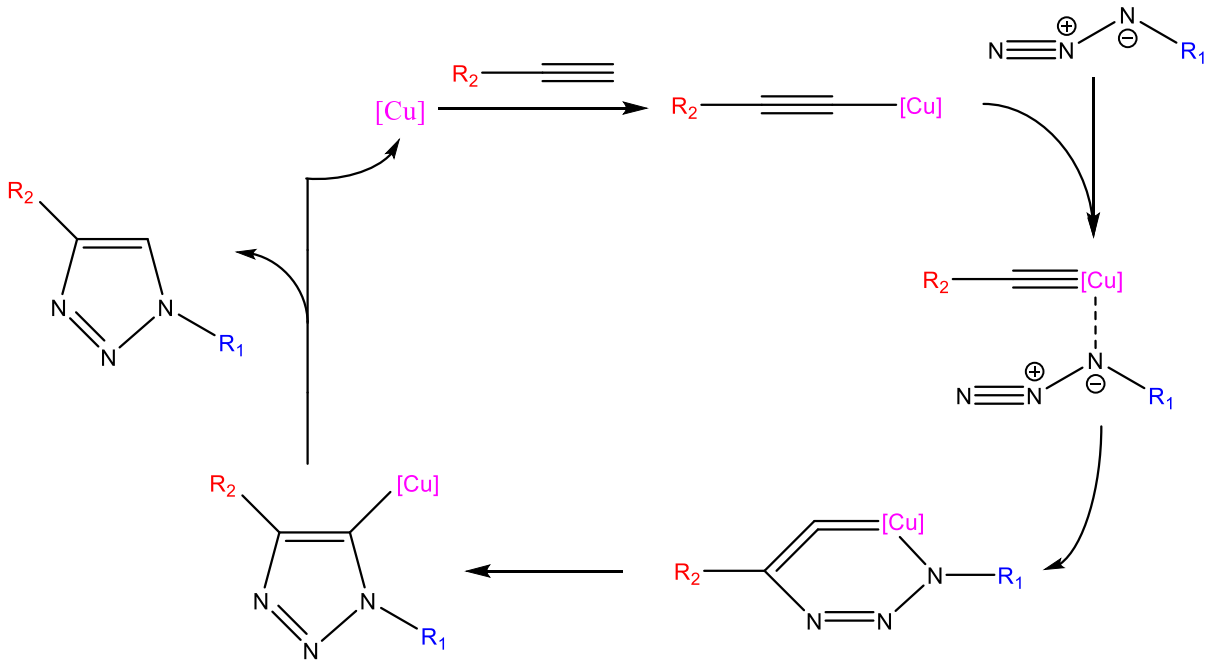

Scheme 2.7 Catalytic mechanism for the CuAAC to form 1,4-disubstituted 1,2,3-triazoles.[36–38]

In the preparation of the monomeric triazole-based ligand (**2.9**), we first synthesised the azide (**2.7**) and the alkyne (**2.8**) *via* azidation and Williamson ether synthesis respectively, illustrated in Scheme 2.8 overleaf. The compounds were characterised using various spectroscopic and analytical techniques.

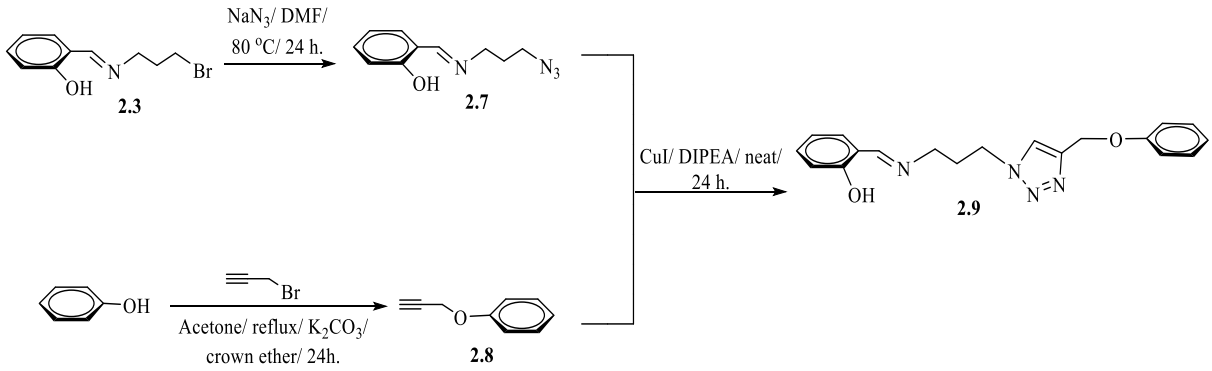

Scheme 2.8 Synthesis of 4-(phenoxymethyl)-1*H*-1,2,3-triazol-1-yl-propylsalicylaldimine ligand **2.9**.

The azide (**2.7**) was prepared by the reaction of **2.3** with sodium azide in dimethylformamide (Scheme 2.8) to obtain the product as a yellow oil in good yield (89%). In the characterisation of **2.7**, a notable observation is the upfield shift of the signals assigned to the methylene protons in the ^{1}H NMR spectrum of **2.7** compared to the spectrum of **2.3**, which is indicative of the shielding effect by the more electron-donating azido group. Furthermore, the infrared spectrum substantiates formation of **2.7** by showing absorption bands at 3056 cm^{-1} corresponding to the ν(O–H) stretching frequency, 2103 cm^{-1} characteristic of the ν(–N_3) stretching frequency, as well as a characteristic strong imine ν(C=N) stretching frequency at 1635 cm^{-1}. LC-MS (ESI-detector) data shows a protonated molecular ion for $[M + H]^+$ at *m/z* = 205.1.

On the other hand, the alkyne phenyl propargyl ether (**2.8**) was prepared according to a previously reported literature procedure,[39] *via* a Williamson ether reaction of propargyl bromide and phenol in acetone (Scheme 2.8). The product was isolated as a yellow oil in good yield (86%). The ^{1}H NMR spectrum of **2.8** shows the methylene protons (H_3) appear as a doublet at δ = 4.78 due to long range coupling with the alkyne proton (H_1) which appears as a triplet at δ = 3.52. The infrared spectrum shows absorption bands at 3266 cm^{-1} and 2119 cm^{-1} corresponding to ν(≡C–H) and ν(C≡C) alkyne stretching frequencies respectively.

Finally, the new triazole-based monomeric ligand **2.9** was prepared through a diisopropylethylamine-promoted CuI-catalysed azide-alkyne cycloaddition reaction of azidopropyl salicylaldimine **2.7** with the phenyl propargyl ether **2.8** (Scheme 2.8).[35] The product was isolated in good yield (85%) as a dull yellow solid. Successful synthesis of **2.9** is shown by the presence of a characteristic triazole signal at δ = 8.27 (H_{12}) in the ^{1}H NMR

spectrum (Figure 2.8). Furthermore, the $^{13}C\{^1H\}$ NMR spectrum substantiates formation of **2.9** by showing diagnostic signals at δ = 143.4 and δ = 124.9 assigned to the triazole carbons C_{13} and C_{12} respectively. This correlates with similar data available in the literature for 1,4-substituted 1,2,3-triazoles.[40] The infrared spectrum confirms formation of **2.9** by showing an absorption band at 3087 cm^{-1} assigned to the (C–H) stretching frequency of the 1,2,3-triazole, and does not show the absorption bands previously reported for the azido $\nu(-N_3)$ (2103 cm^{-1}) and alkyne (3266 cm^{-1} and 2119 cm^{-1}) stretching frequencies of **2.7** and **2.8** respectively. This is in line with data reported in the literature for Cu(I)-catalysed azide-alkyne "Click" cycloaddition reactions.[41] A characteristic strong imine ν(C=N) stretching frequency is also observed at 1627 cm^{-1}, as well as the ν(O–H) stretching frequency at 3060 cm^{-1}. The ESI-MS data shows a protonated molecular ion peak for $[M + H]^+$ in the positive ion-mode at *m/z* = 337.1747.

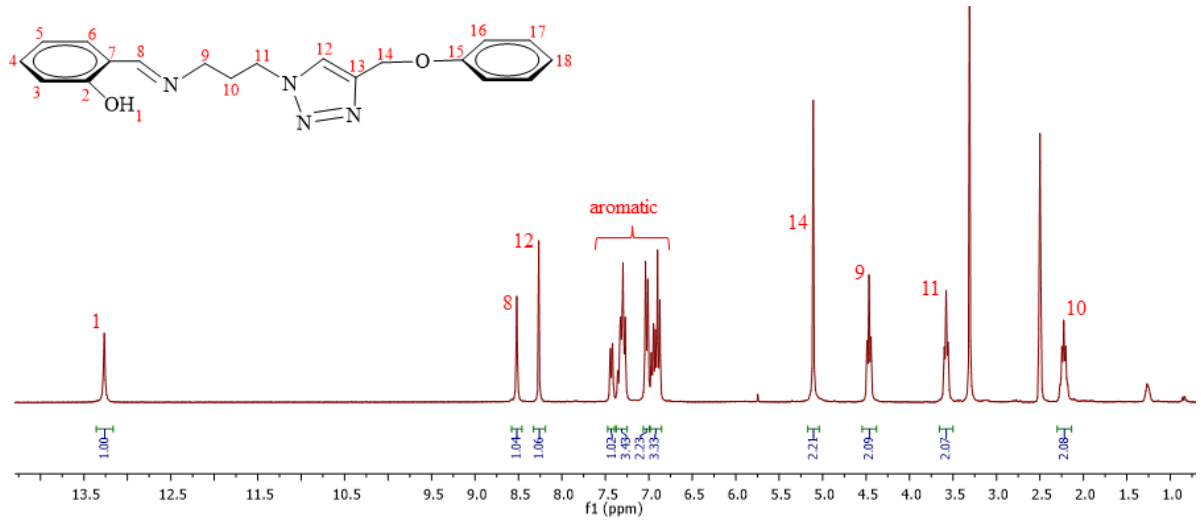

Figure 2.8 ^1H NMR (DMSO-d_6) spectrum for 4-(phenoxymethyl)-1*H*-1,2,3-triazol-1-yl-propylsalicylaldimine ligand **2.9**.

2.7 Synthesis and characterisation of 4-(phenoxymethyl)-1*H*-1,2,3-triazol-1-yl-propylsalicylaldimine-based Rh(I) complex (2.10)

The Rh(I)-triazole-based complex was synthesised by deprotonation of **2.9** with triethylamine, and subsequent complexation with half molar equivalent of the Rh(I) dimer $[RhCl(COD)]_2$, (COD = 1,5-cyclooctadiene), Scheme 2.9. The mononuclear product was isolated as a yellow solid in good yield (83%).

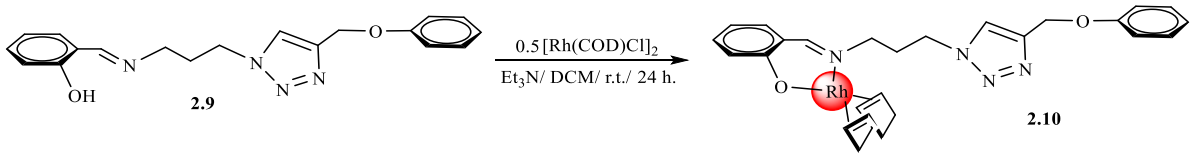

Scheme 2.9 Synthesis of 4-(phenoxymethyl)-1*H*-1,2,3-triazol-1-yl-propylsalicylaldimine-based Rh(I) complex **2.10**.

The ^{1}H NMR spectrum (Figure 2.9) shows an upfield shift of the signal for the imine proton, from δ = 8.52 in **2.9** to δ = 8.18 in **2.10**. This is due to increased electron density around the imine functionality as a result of back-donation by the rhodium-metal centre. Moreover, the spectrum does not show the signal for the hydroxyl proton previously reported in **2.9**, indicative of successful deprotonation for coordination of the ligand in a bidentate manner. Also observed in the ^{1}H NMR spectrum are signals characteristic of the olefinic protons of the cyclooctadiene moiety (H_{18} and H_{18}'), as well as the methylene protons (H_{19} and H_{19}'). The infrared spectrum shows a shift of the imine absorption band to lower frequency upon coordination of the ligand to the metal, from ν(C=N) = 1627 cm^{-1} (**2.9**) to ν(C=N) = 1602 cm^{-1} (**2.10**). The observed shift is due to the weakening of the double-bond character of the imine functionality as a result of back-donation of electrons from the rhodium metal centre through synergic effects. This has been reported for similar compounds in the literature.[10,11,13,24] Successful deprotonation of the hydroxyl proton for chelation is also validated in the infrared spectrum of **2.10**, which does not show the ν(O–H) stretching frequency. The ESI-MS data shows a protonated molecular ion peak for [M + H]$^{+}$ in the positive ion-mode at *m/z* = 547.1712.

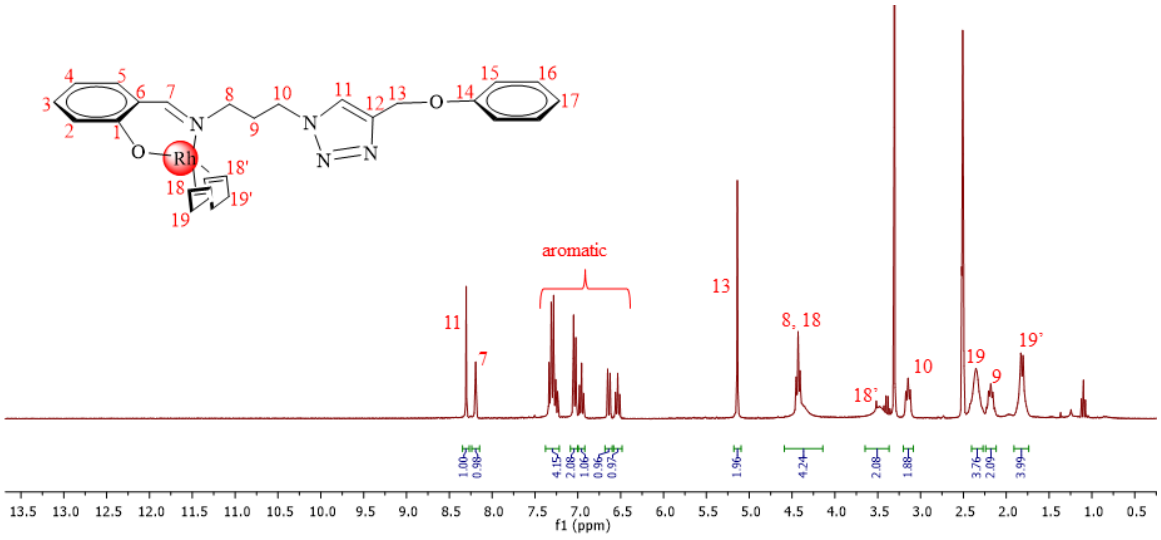

Figure 2.9 ^{1}H NMR (DMSO-d$_6$) spectrum for 4-(phenoxymethyl)-1*H*-1,2,3-triazol-1-yl-propylsalicylaldimine-based Rh(I) complex **2.10**.

After successful synthesis of the mononuclear triazolyl complex (**2.10**), we then followed a similar approach in the preparation of the low generation trinuclear Rh(I) complex, starting from the preparation of the THPE-based trimeric core **2.11**, as shown in the following section.

2.8 Synthesis and characterisation of 1,1,1-tris(4-propargyl ether phenyl)ethane (2.11)

The rigid THPE-based trialkynyl core was synthesised *via* the Williamson ether reaction of THPE with propargyl bromide in acetone (Scheme 2.10), and the product was isolated in good yield (94%) as a light-brown oil which solidifies into a dirty-white solid when dried *in vacuo*.

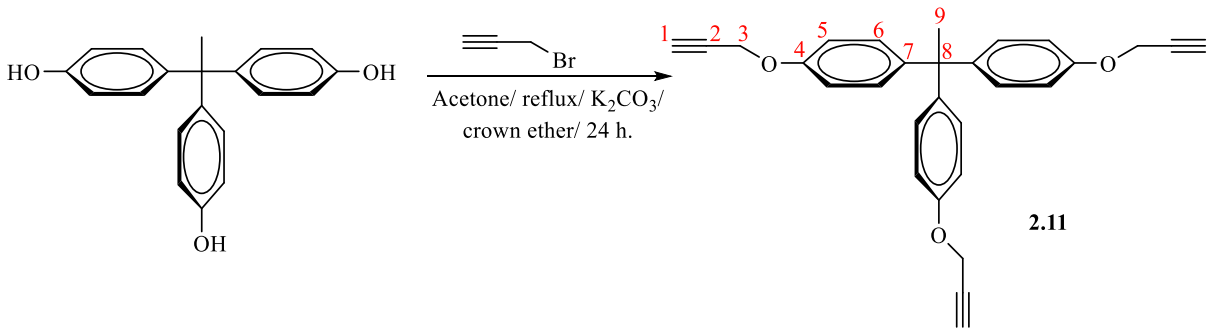

Scheme 2.10 Synthesis of 1,1,1-tris(4-propargyl ether phenyl)ethane **2.11**.

The diagnostic signal (H_9) of the core is observed upfield in the ^{1}H NMR spectrum, integrating for 3 protons at δ = 2.05. The methylene protons (H_3) appear as a doublet at δ = 4.75 due to long range coupling with the alkyne proton (H_1) which appears as a triplet at δ = 3.52. The aromatic protons are all accounted for in their characteristic region (δ = 6.97–6.87). The infrared spectrum shows two absorption bands at 3282 cm^{-1} and 3266 cm^{-1} corresponding to ν(≡C–H), as well as two absorption bands at 2131 cm^{-1} and 2119 cm^{-1} corresponding to ν(C≡C) stretching frequencies of the alkyne.

2.9 Synthesis and characterisation of 1,1,1-tris(4-phenoxymethyl)ethane-1*H*-1,2,3-triazol-1-yl-propylsalicylaldimine ligand (2.12)

The low generation dendritic aryl ether triazole-based tris-ligand **2.12** was then prepared by anchoring the azidopropyl salicylaldimine (**2.7**) to the trialkynyl core 1,1,1-tris(4-propargyl ether phenyl)ethane (**2.11**). The reaction was successfully conducted *via* a diisopropylethylamine-promoted CuI-catalysed azide-alkyne cycloaddition reaction (Scheme

2.11).[35] The trimeric product **2.12** was isolated as a dull yellow solid in good yield (90%) by trituration in petroleum ether.

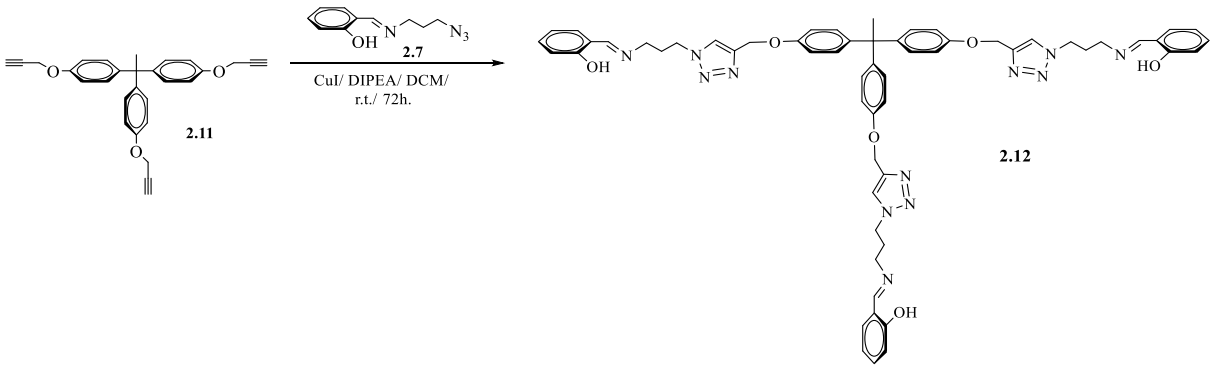

Scheme 2.11 Synthesis of 1,1,1-tris(4-phenoxymethyl)ethane-1*H*-1,2,3-triazol-1-yl-propylsalicylaldimine ligand **2.12**.

Structural elucidation of the new trimeric low generation ligand (**2.12**) was done using various spectroscopic and analytical techniques. Successful anchoring of **2.7** to the trimeric core **2.11** is evidenced in the ^{1}H NMR spectrum of **2.12** (Figure 2.10), which shows the diagnostic signals for the triazole and imine protons at δ = 8.26 (H_{12}) and δ = 8.51 (H_8) respectively. In addition, the presence of the signal for the methyl protons of the THPE core upfield at δ = 2.04 further attests to the structure of **2.12**. All the other protons are observed in their expected regions in the proposed structure of **2.12**, with the signal for the hydroxyl protons of the salicylaldimine moiety appearing at δ = 13.37 (H_1). More conclusive results were seen through the ^{13}C{^{1}H} NMR spectrum, wherein the signals for the triazole carbons are observed in their characteristic regions for a 1,4-substituted triazole (δ = 143.5 (C_{13}) and δ = 124.8 (C_{12})). Further to that, the infrared spectrum of **2.12** does not show the previously reported absorption bands of the alkyne (**2.11**) and the azide (**2.7**), thus corroborating formation of the trimeric ligand by showing a characteristic imine absorption band ν(C=N) at 1629 cm^{-1} as an intense band with a shoulder at 1611 cm^{-1}. The ESI-MS data further established the integrity of the trimeric dendrimer through revealing a sodium adduct molecular ion peak for [M + Na]$^{+}$ in the positive ion-mode at *m/z* = 1055.4918.

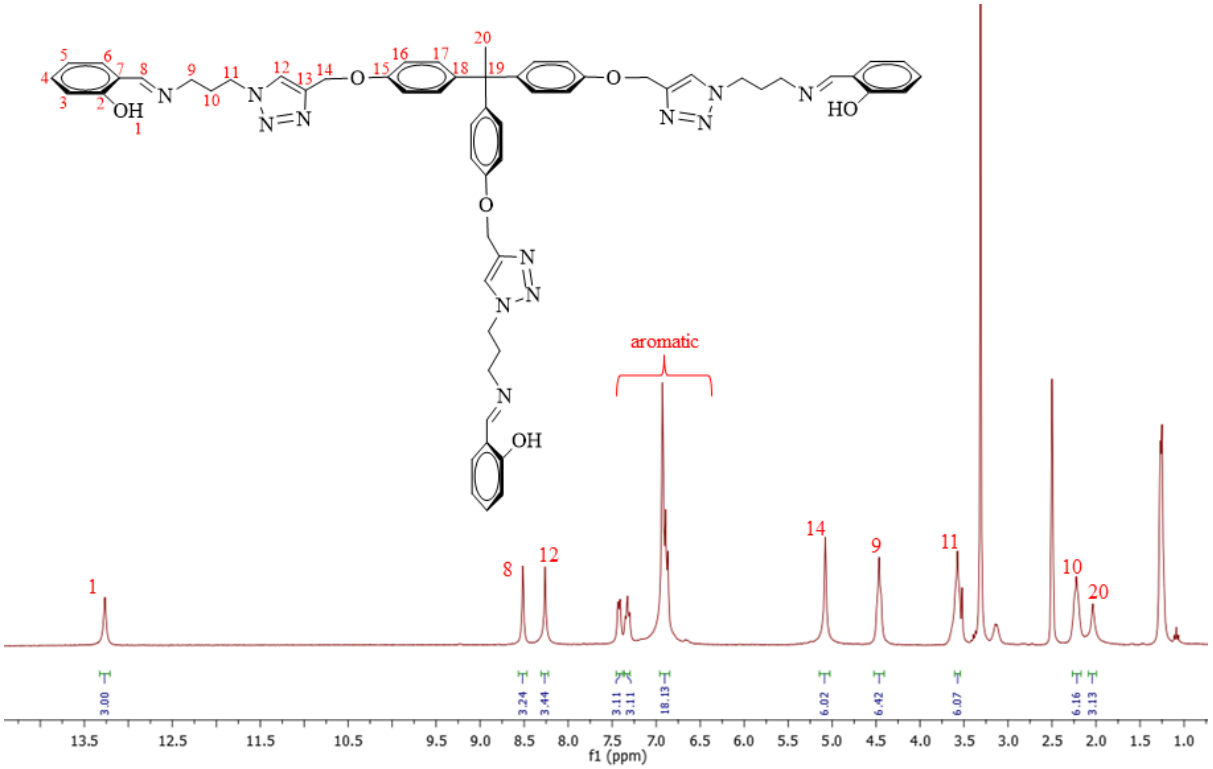

Figure 2.10 ^{1}H NMR (DMSO-d_6) spectrum for 1,1,1-tris(4-phenoxymethyl)ethane-1*H*-1,2,3-triazol-1-yl-propylsalicylaldimine ligand **2.12**.

2.10 Synthesis and characterisation of 1,1,1-tris(4-phenoxymethyl)ethane-1*H*-1,2,3-triazol-1-yl-propylsalicylaldimine-based Rh(I) complex (2.13)

The new trinuclear Rh(I)-triazole-based complex was synthesised by treating the dendritic ligand **2.12** with triethylamine, and subsequent complexation with one and a half molar equivalent of the dimeric $[RhCl(COD)]_2$, (COD = 1,5-cyclooctadiene) (Scheme 2.12). The Rh(I) metallodendrimer was isolated as a yellow solid in near quantitative yield (99%).

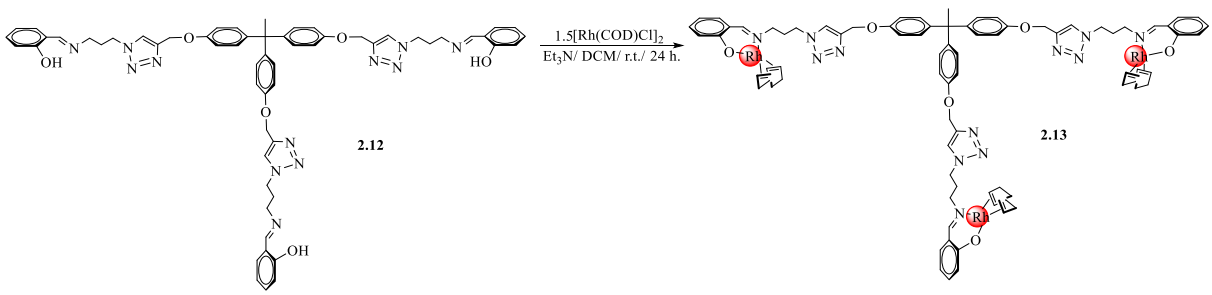

Scheme 2.12 Synthesis of 1,1,1-tris(4-phenoxymethyl)ethane-1*H*-1,2,3-triazol-1-yl-propylsalicylaldimine-based Rh(I) complex **2.13**.

The high yields obtained in the preparation of both the low generation trimeric ligand (**2.12**) and the Rh(I) trinuclear complex (**2.13**) attests to a characteristic of the Click chemistry synthetic route. This satisfies the objective of beneficiating the rhodium metal through high yielding reactions that lead to facile product isolation, as opposed to the cumbersome purification steps which led to the isolation of the initially proposed trinuclear complex **2.5** in poor yields.

In the characterisation of the new trinuclear low generation metallodendrimer **2.13**, successful complexation of **2.12** is shown in the ^{1}H NMR spectrum (Figure 2.11) through an upfield shift of the imine signal (from δ = 8.51 in **2.12**, to δ = 8.18 in **2.13**). In addition, the spectrum of **2.13** does not show the hydroxyl signal previously observed in **2.12**, which confirms coordination is through a bidentate manner. The signals for the 1,5-cyclooctadiene protons are observed in their characteristic region, and the integration agrees with the proposed trinuclear structure of **2.13**. All the other protons in the proposed structure of **2.13** are also accounted for in their expected regions. Evidence for the coordination on the Rh centre was further confirmed through the infrared spectrum, which shows a shift of the imine absorption band to lower frequency upon coordination of the ligand to the metal, from an intense band at ν(C=N) 1629 cm^{-1} (**2.12**) to an intense band at ν(C=N) 1603 cm^{-1} (**2.13**). The observed shift is due to similar reasoning to the shifts for **2.12**. Mass spectrometry (ESI-MS) gave evidence for the formation of the proposed metallodendrimer by displaying a peak corresponding to the $[M + H + Na]^{2+}$ ion in the positive ion-mode at *m/z* = 736.4466. The trinuclear metallodendrimer (**2.13**) is soluble in ethanol, dichloromethane, dimethylsulfoxide and sparingly in toluene at room temperature. Notably, the metallodendrimer is fairly thermally stable showing decomposition without melting at the onset temperature of 185 °C, while the mononuclear complex (**2.10)** decomposes at the onset of 98 °C.

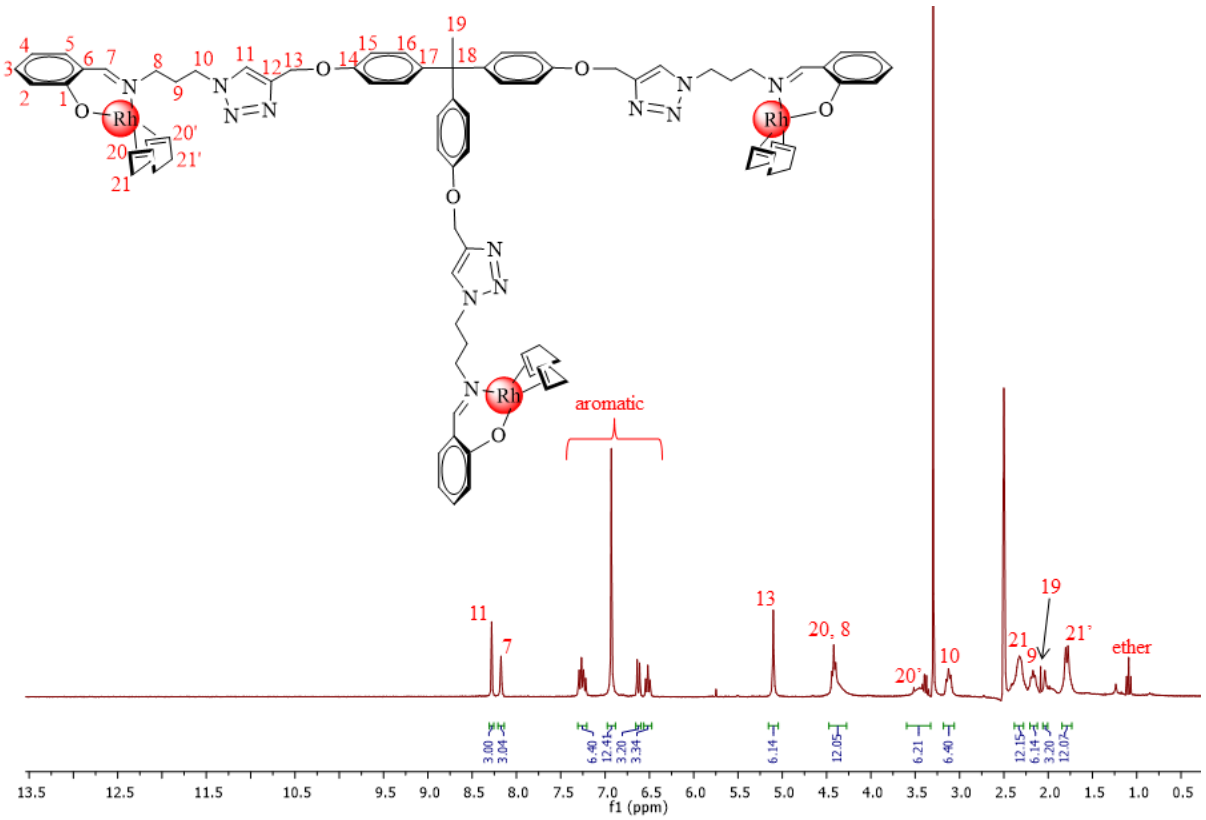

Figure 2.11 ^{1}H NMR (DMSO-d_6) spectrum for 1,1,1-tris(4-phenoxymethyl)ethane-1*H*-1,2,3-triazol-1-yl-propylsalicylaldimine-based Rh(I) complex **2.13**.

The extension of a metallodendrimer to higher generations is a very attractive approach owing to the potential of enhanced stability and improved reactivity due to the multiple active sites that propagate from the core.[32,42] Inspired by the high yielding and facile isolation of the low generation trimeric (**2.12**) and trinuclear (**2.13**) dendrimers, we were motivated to construct a higher generation hexameric ligand with potential to lead to the corresponding high generation hexanuclear metallodendritic congener. The building blocks to the hexameric dendrimer were synthesised *via* the convergent approach of preparing dendrimers, and this is discussed in the following sections.

2.11 Synthesis and characterisation of 3,5-bis(oxymethylene-1*H*-1,2,3-triazol-1-yl-propylsalicylaldimine) benzyl azide (2.17)

The azide dimeric wedge (**2.17**) to the hexameric ligand was prepared *via* a series of reactions following the Williamson ether synthesis, alcohol activation, Click chemistry and finally azidation procedures (Scheme 2.13).

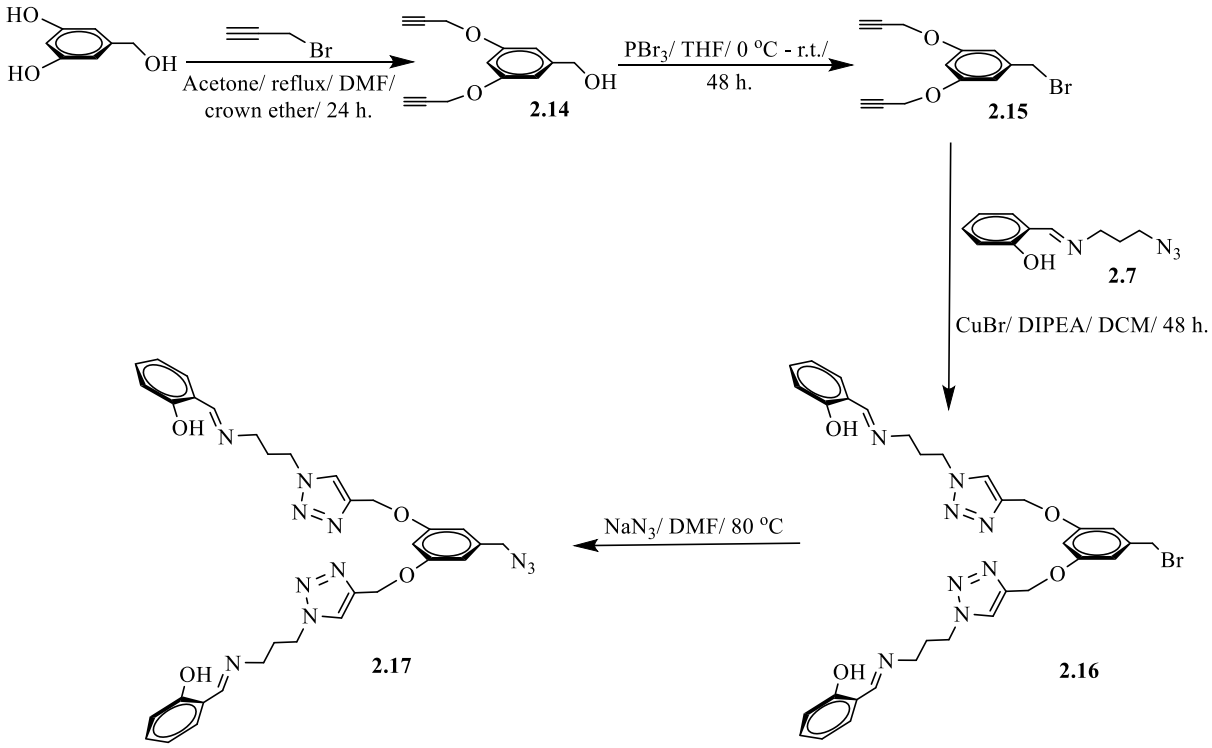

Scheme 2.13 Illustrating the synthetic route to the dimeric dendritic wedge **2.17**.

In the first step, 3,5-bis(propargyl ether)benzyl alcohol **2.14** was synthesised *via* a Williamson ether reaction of propargyl bromide and 3,5-dihydroxybenzyl alcohol in DMF, and the product (**2.14**) was isolated as a brown oil. Subsequent activation of the alcohol was then conducted in the second step using PBr_3 in dry THF. The resultant product 3,5-bis(propargyl ether)benzyl bromide (**2.15**) was isolated as a light-yellow viscous oil in good yield (94%).

Evidence of successful synthesis of the bis-alkyne **2.15** is shown through the ^{1}H NMR spectra (Figure 2.12) which accounts for all the expected protons in the structure of **2.15**. Notably, the spectrum of **2.15** does not show the signal for the alcohol proton previously observed in **2.14**, indicating successful activation of the alcohol. Moreover, a downfield shift of the signals (from **2.14** to **2.15)** is observed owing to the more electron withdrawing halide compared to the

hydroxyl functionality, substantiating the successful activation of the alcohol. Additionally, the infrared spectrum of **2.15** further substantiates activation of the alcohol by not showing the typical (O–H) absorption band, which was previously observed in the infrared spectrum of **2.14**. The infrared spectrum of **2.15** also shows two absorption bands at 3286 cm^{-1} and 3258 cm^{-1} corresponding to ν(≡C–H), as well as an absorption band at 2119 cm^{-1} corresponding to ν(C≡C) stretching frequencies of the alkyne.

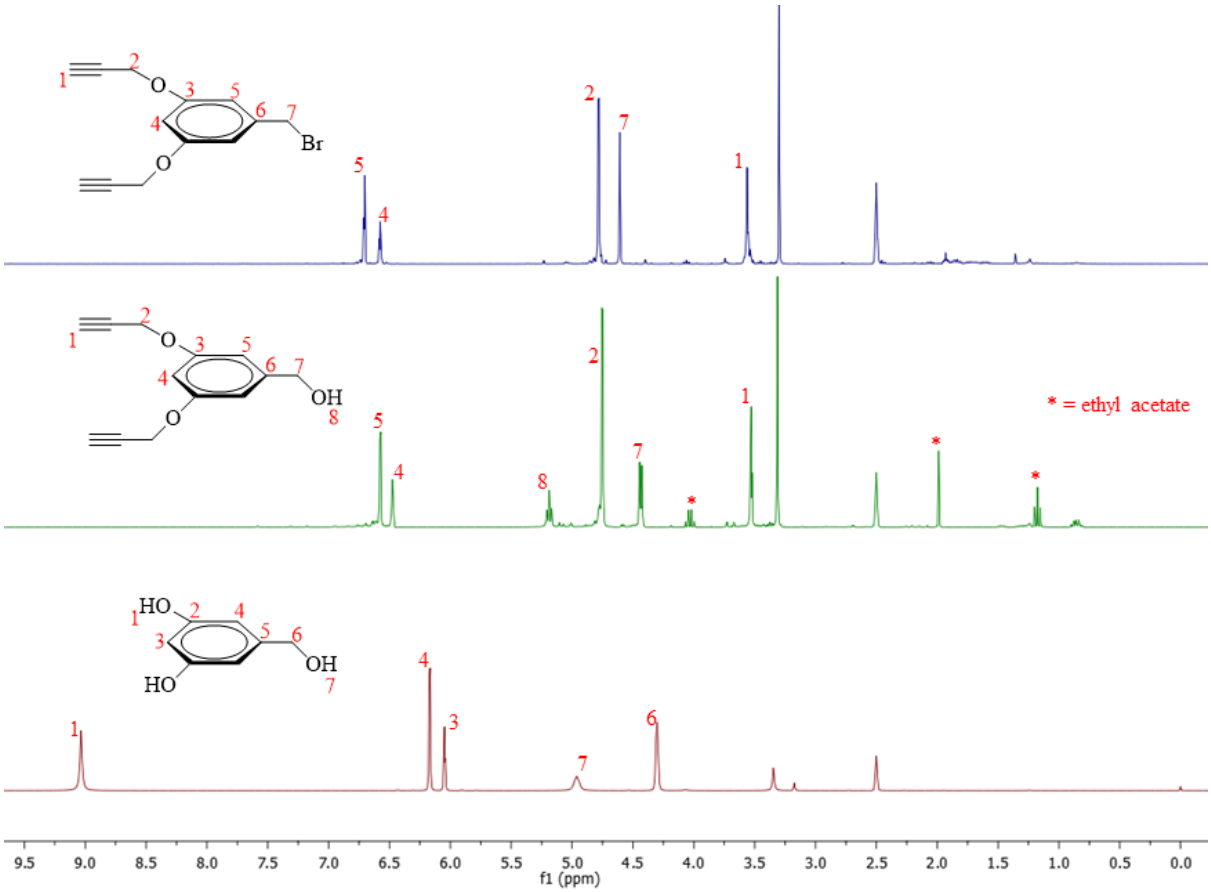

Figure 2.12 Stacked ^{1}H NMR (DMSO-d_6) spectra for 3,5-bis(propargyl ether)benzyl bromide **2.15**.

In the third step towards the synthesis of the azide functionalised bis-propylsalicylaldimine ligand **2.17**, the bis-functionalised bromo-precursor **2.16** was prepared through a diisopropylethylamine-promoted CuBr-catalysed azide-alkyne cycloaddition reaction of azidopropyl salicylaldimine **2.7** with 3,5-bis(propargyl ether)benzyl bromide **2.15** (Scheme 2.13).[35] The product **2.16** was isolated by trituration in petroleum ether as a dull yellow solid in moderate yield (61%), and characterised by various spectroscopic and analytical techniques. Subsequently, the halide-bearing bis-propylsalicylaldimine ligand **2.16** was treated with

sodium azide to obtain the product as a dull yellow solid which was characterised by FT-IR, ^{1}H NMR, 2D NMR spectroscopy (HSQC and COSY) and ^{13}C{^{1}H} spectroscopy.

In the ^{1}H NMR spectrum of **2.17** (Figure 2.13), the diagnostic triazole and imine signals are observed in their characteristic regions at δ = 8.25 (H_{12}) and δ = 8.51 (H_{8}) respectively, both integrating for two protons as expected in the proposed structure of **2.17**. Characteristic imine absorption bands ν(C=N) are observed at 1620 cm^{-1} and 1597 cm^{-1} in the infrared spectrum of **2.17**. Most importantly, the infrared spectrum gives more conclusive results of successful azidation by showing a characteristic azide stretching frequency at 2127 cm^{-1}. Additionally, the spectrum does not show the absorption bands previously reported for the azido and the alkyne stretching frequencies of **2.7** and **2.15** respectively, further substantiating the successful bi-functionalisation through the click chemistry reaction.

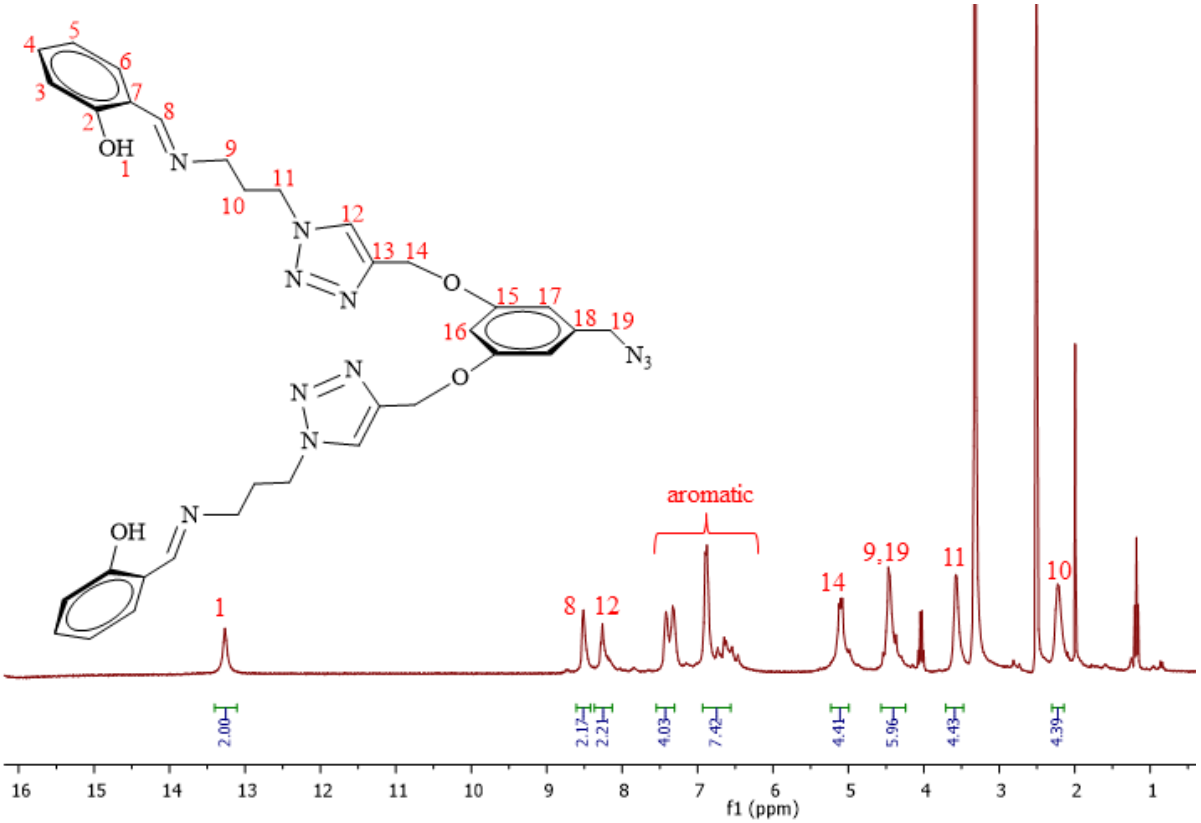

Figure 2.13 ^{1}H NMR (DMSO-d_6) spectrum for 3,5-bis(oxymethylene-1*H*-1,2,3-triazol-1-yl-propylsalicylaldimine) benzyl azide **2.17**.

The dimeric propylsalicylaldimine-based ligand **2.17** was then anchored to the tris-alkynyl core **2.11** in the preparation of the hexameric ligand, and this is discussed in the following section.

2.12 Synthesis and characterisation of the hexameric ligand (2.18)

The hexameric THPE anchored aryl ether propylsalicylaldimine-based triazolyl ligand was prepared through a diisopropylethylamine-promoted CuI-catalysed azide-alkyne cycloaddition reaction of the azide wedge **2.17** with the tris-alkyne core **2.11** (Scheme 2.14).[35] The new hexameric product **2.18** was successfully isolated by trituration in petroleum ether as a dull yellow solid which was characterised using ^{1}H NMR spectroscopy. Several attempts were made to purify **2.18**. However, the product could only be dissolved in dimethylsulfoxide at elevated temperatures to acquire the ^{1}H NMR spectrum, and dissolution in all the other available solvents could not be achieved once the product was isolated from the reaction. Purification by sublimation could not be achieved as well, as the compound decomposed under sublimation temperatures. The difficulty in the dissolution of higher dendrimer generations such as **2.18** is often reported in the literature and poses a challenge towards purification strategies for typically high molecular weight dendritic structures.[21,43]

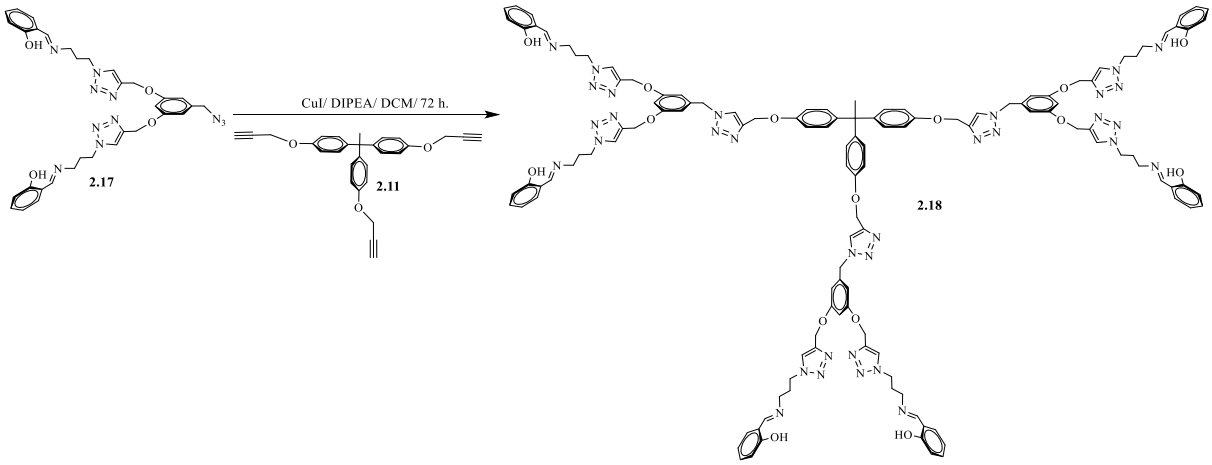

Scheme 2.14 Synthesis of the hexameric ligand **2.18**.

We report in Figure 2.14, the ^{1}H NMR spectrum of **2.18**, which despite reflecting the need for further purification, convincingly shows successful synthesis of the hexameric ligand through depicting all the desired signals for the expected protons in the proposed structure of **2.18**. The successful click chemistry reaction of the azide **2.17** and the tris-alkynyl core **2.11** is evidenced by the presence of a broad signal at δ = 9.33 integrating for 3 protons and assigned to the new triazole protons (H_{20}). This assignment for the new set of triazole protons is plausible as it is within the range typical of the signals for triazolyl protons.[40] On the other hand, the signals for the hydroxyl, imine and triazole protons of the propylsalicylaldimine triazolyl moiety are observed at δ = 13.27 (H_1), 8.53 (H_8) and 8.27 (H_{12}) respectively. These signals correlate well

with the previous assignment on the propylsalicylaldimine triazolyl moiety of **2.17**, assigned at δ = 13.27 (H_1), 8.51 (H_8) and 8.25 (H_{12}) for similar protons. The presence of the trifunctional core as part of the proposed structure of **2.18** is evidenced by the signal for the methyl protons of the core (H_{28}), assigned as overlapping signals with the methylene protons (H_{10}) in the region δ = 2.31–2.16. However, although clearly represented in the aromatic region, the signals for the aromatic protons integrate for more than the expected number of protons. The excess aromatic protons are presumed to be from the presence of unreacted trifunctional core, and this is corroborated by the unassigned signal at *ca*. 4.75 ppm corresponding to the methylene protons of the trifunctional core of **2.11** as observed prior to the click reaction. Alternative purification procedures may need to be investigated further in future.

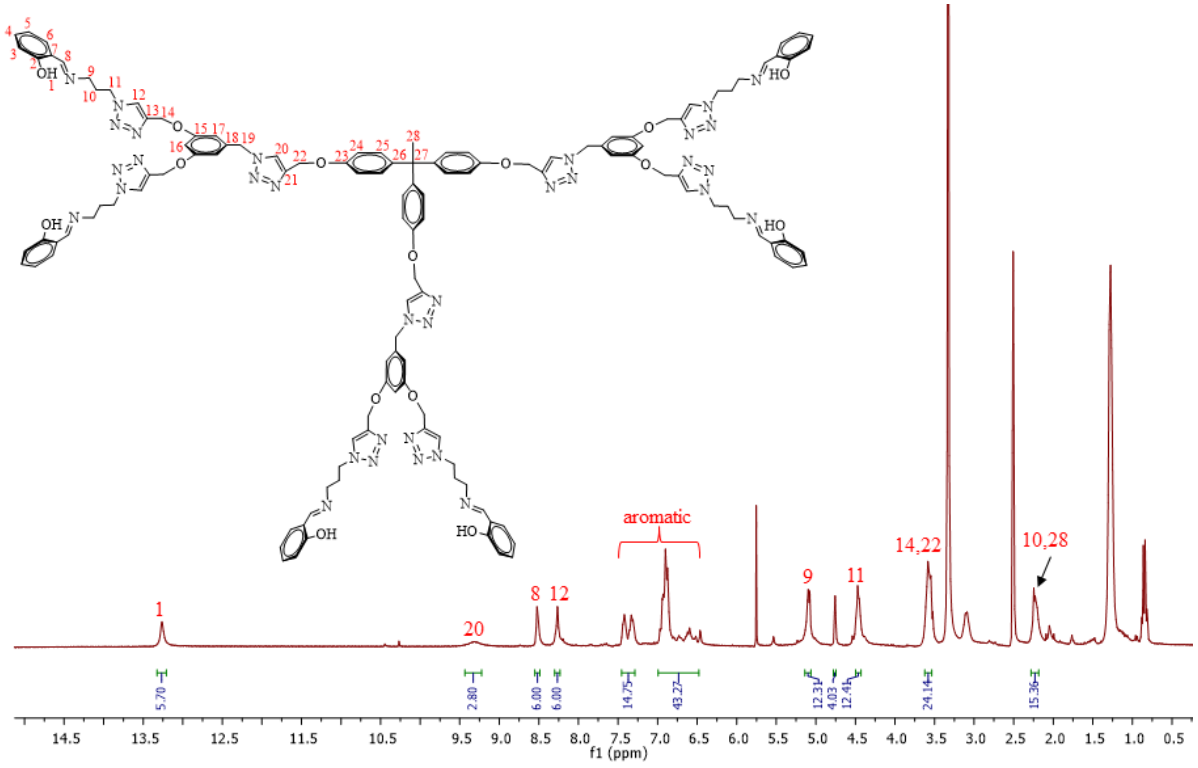

Figure 2.14 ^{1}H NMR (DMSO-d_6) spectrum for the hexameric ligand **2.18**.

2.13 Summary

A series of new aryl-ether salicylaldimine-based Rh(I) mononuclear complex (**2.2**) and a trinuclear complex (**2.5**) were successfully prepared following a Schiff base condensation protocol, followed by complexation with the appropriate quantity of the dimeric $[RhCl(COD)]_2$, and then Williamson ether synthesis. Using these strategies, a dinuclear aryl ether salicylaldimine wedge (**2.6**) was prepared. These compounds were characterised using various spectroscopic and analytical techniques. However, owing to the tedious purification demands for the isolation of **2.5** and **2.6**, these compounds were obtained in very low yields (22% and 34% respectively). This necessitated development of a new synthetic strategy that is high yielding with less cumbersome product isolation steps, such as the Click chemistry approach. This very attractive strategy was implemented in the preparation of a monomeric ligand (**2.9**) and a trimeric ligand (**2.12**) which were obtained in good yields (85% and 90% respectively). Complexation of the ligands **2.9** and **2.12** with the appropriate quantity of the Rh(I) dimer gave the corresponding mononuclear complex (**2.10**) and the low generation metallodendrimer (**2.13**) in good yields (83% and 99% respectively). The complexes showed fairly good thermal stability, with the onset for decomposition occurring at 185 °C for the trinuclear metallodendrimer complex (**2.13**), and at 98 °C for the mononuclear complex (**2.10**). The complexes were characterised using various spectroscopic and analytical techniques which include; ^{1}H NMR and $^{13}C\{^{1}H\}$ NMR spectroscopy, FT-IR spectroscopy, as well as mass spectrometry. The high yields obtained for the mono and trimeric ligands, as well as for the corresponding mononuclear and low generation trinuclear triazolyl Rh(I) complexes led to the extension of the synthetic strategy to a hexameric analogue. This was conducted *via* preparation of a bimeric propylsalicylaldimine triazolyl-based aryl ether ligand (**2.17**). However, the resultant high generation hexameric ligand (**2.18**) was obtained in slightly impure quality, though evidently present and could not be purified further due to insolubility constraints. The higher generation dendritic structures are often confounded by solubility challenges once isolated from the reaction mixtures. This has been the major drawback for synthesis of high molecular weight globular structures. However, the potential benefits of successfully synthesising and isolating such well-defined structures are very intriguing.[42,44,45]

2.14 References

1 T. T. Tidwell, *Angew. Chem. Int. Ed.*, 2008, **47**, 1016–1020.

2 A. M. Abu-dief and I. M. A. Mohamed, *Beni-Suef Univ. J. Basic Appl. Sci.*, 2015, **4**, 119–133.

3 W. Qin, S. Long, M. Panunzio and S. Biondi, *Molecules*, 2013, **18**, 12264–12289.

4 A. S. A. Dena, *Russ. J. Appl. Chem.*, 2014, **87**, 383–396.

5 K. C. Gupta and A. K. Sutar, *Coord. Chem. Rev.*, 2008, **252**, 1420–1450.

6 A. Xavier and N. Srividhya, *IOSR J. Appl. Chem.*, 2014, **7**, 6–15.

7 V. K. Rao, S. S. Reddy, B. S. Krishna and K. R. Mohan, *Green Chem. Lett. Rev.*, 2010, **3**, 217–223.

8 M. Abirami and V. Nadaraj, *Int. J. ChemTech Res.*, 2014, **6**, 2534–2538.

9 B. N. Ghose, *Rev. Port. Quim.*, 1983, **25**, 147–150.

10 S. Siangwata, N. Baartzes, B. C. E. Makhubela and G. S. Smith, *J. Organomet. Chem.*, 2015, **796**, 26–32.

11 E. B. Hager, B. C. E. Makhubela and G. S. Smith, *Dalton Trans.*, 2012, **41**, 13927–35.

12 C. Williams, M. Ferreira, E. Monflier, S. F. Mapolie and G. S. Smith, *Dalton Trans.*, 2018, **47**, 9418–9429.

13 L. C. Matsinha, S. F. Mapolie and G. S. Smith, *Dalton Trans.*, 2015, **44**, 1240–1248.

14 S. Siangwata, S. Chulu, C. L. Oliver and G. S. Smith, *Appl. Organomet. Chem.*, 2017, **31**, e3593.

15 P. J. Deuss, R. Denheeten, W. Laan and P. C. J. Kamer, *Chem. Eur. J.*, 2011, **17**, 4680–4698.

16 M. H. Pørez-Temprano, J. A. Casares and P. Espinet, *Chem. Eur. J.*, 2012, **18**, 1864–1884.

17 B. C. E. Makhubela, A. Jardine and G. S. Smith, *Green Chem.*, 2012, **14**, 338–347.

18 Y. Liao and J. R. Moss, *Organometallics*, 2003, **15**, 4307–4316.

19 I. J. Mavunkal, J. R. Moss and J. Bacsa, *J. Organomet. Chem.*, 2000, **594**, 361–368.

20 J. October and S. F. Mapolie, *J. Organomet. Chem.*, 2017, **840**, 1–10.

21 A.-M. Caminade, R. Laurent, B. Delavaux-Nicot and J.-P. Majoral, *New J. Chem.*, 2012, **36**, 217–226.

22 H. Oie, A. Sudo and T. Endo, *J. Polym. Sci. Part A Polym. Chem.*, 2011, **49**, 3174–3183.

23 C. Janiak, A.-C. Chamayou, A. K. M. R. Uddin, M. Uddin, S. K. Hagen and M. Enamullah, *Dalton Trans.*, 2009, **19**, 3698–3709.

24 L. Maqeda, B. C. E. Makhubela and G. S. Smith, *Polyhedron*, 2015, **91**, 128–135.

25 R. W. Kluiber and G. Sasso, *Inorg. Chim. Acta.*, 1970, **4**, 226–230.

26 D. Astruc, R. Ciganda, C. Deraedt, S. Gatard, L. Liang, N. Li, C. Ornelas, A. Rapakousiou, J. Ruiz, D. Wang, Y. Wang and P. Zhao, *Synlett*, 2015, **26**, 1437–1449.

27 H. C. Kolb, M. G. Finn and K. B. Sharpless, *Angew. Chem. Int. Ed.*, 2001, **40**, 2004–2021.

28 M. Meldal and C. W. Tornøe, *Chem. Rev.*, 2008, **108**, 2952–3015.

29 P. Wu, A. K. Feldman, A. K. Nugent, C. J. Hawker, A. Scheel, B. Voit, J. Pyun, J. M. J. Fréchet, K. B. Sharpless and V. V. Fokin, *Angew. Chem. Int. Ed.*, 2004, **43**, 3928–3932.

30 J. E. Hein and V. V. Fokin, *Chem. Soc. Rev.*, 2010, **39**, 1302.

31 V. D. Bock, H. Hiemstra and J. H. Van Maarseveen, *Eur. J. Org. Chem.*, 2006, 51–68.

32 L. Zhao, Q. Ling, X. Liu, C. Hang, Q. Zhao, F. Liu and H. Gu, *Appl. Organomet. Chem.*, 2018, **32**, 1–12.

33 E. H. Ryu and Y. Zhao, *Org. Lett.*, 2005, **7**, 1035–1037.

34 F. Yakushiji, H. Tanaka, K. Muguruma, T. Iwahashi, Y. Yamazaki and Y. Hayashi,

Chem. Eur. J., 2011, **17**, 12587–12590.

35 C. Shao, X. Wang, Q. Zhang, S. Luo, J. Zhao and Y. Hu, *J. Org. Chem.*, 2011, **76**, 6832–6836.

36 V. Castro, H. Rodríguez and F. Albericio, *ACS Comb. Sci.*, 2016, **18**, 1–14.

37 V. O. Rodionov, V. V. Fokin and M. G. Finn, *Angew. Chem. Int. Ed.*, 2005, **44**, 2210–2215.

38 L. Liang and D. Astruc, *Coord. Chem. Rev.*, 2011, **255**, 2933–2945.

39 P. K. Biswas, S. Saha, T. Paululat and M. Schmittel, *J. Am. Chem. Soc.*, 2018, **140**, 9038–9041.

40 X. Creary, A. Anderson, C. Brophy, F. Crowell and Z. Funk, *J. Org. Chem.*, 2012, **77**, 8756–8761.

41 S. Sun and P. Wu, *J. Phys. Chem. A*, 2010, **114**, 8331–8336.

42 L. Ropartz, R. E. Morris, D. F. Foster and D. J. Cole-Hamilton, *Chem. Commun.*, 2001, 361–362.

43 D. Astruc and F. Chardac, *Chem. Rev.*, 2001, **101**, 2991–3023.

44 J. Palomero, J. A. Mata, F. González and E. Peris, *New J. Chem.*, 2002, **26**, 291–297.

45 D. de Groot, P. G. Emmerink, C. Coucke, J. N. H. Reek, P. C. J. Kamer and P. W. N. M. van Leeuwen, *Inorg. Chem. Commun.*, 2000, **3**, 711–713.

Chapter 3

Mono- and trinuclear *N,O*-chelate Rh(I)-aryl ether complexes: Olefin hydroformylation and kinetic studies

This Chapter forms part of a publication titled "*Olefin hydroformylation and kinetic studies using mono- and trinuclear N,O-chelate rhodium(I)-aryl ether precatalysts*", cited as:
S. Siangwata, N. C. C. Breckwoldt, N. J. Goosen and G. S. Smith., *Appl. Catal. A Gen.* 2019, **585**, 117179.

3.1 Introduction

The design and synthesis of highly efficient, selective and reusable catalysts have over the years gained momentum. The main drive towards the continued efforts to improving the well-known and industrially important catalytic reactions can be viewed, to a greater extent, from a Green Chemistry perspective.[1–6] The need for catalyst recovery and recyclability poses a challenge towards the sustainable development of highly efficient and economically viable industrial catalytic processes. There are huge environmental and economic gains through a catalytic system that can offer excellent efficiency with facile catalyst recovery for multiple reuses.[7–9] The availability of base and performance chemical feedstocks such as alkanes and alkenes from the Fischer-Tropsch Process at Sasol necessitates the need for the design and synthesis of new, more efficient and selective catalysts which will allow for the conversion into more useful products and add value to hydrocarbon products. Moreover, the Merensky and UG2 Reefs provide South Africa with access to a range of transition metals, especially the Platinum Group Metals (PGMs), essential in the field of catalysis. Beneficiation of these expensive, rare and fast depleting metals under the guise of elemental sustainability through greener recovery systems is of global importance. Organometallic complexes based on the PGMs have found a steady application as catalysts in a range of large scale reactions for valorisation of hydrocarbons, such as in carbonylation (for example, the Monsanto process),[8,10–12] hydrogenation (for example, Wilkinson catalyst),[13–15] and hydroformylation reactions.[16–18]

The hydroformylation reaction (Scheme 3.1) involves the addition of carbon monoxide and hydrogen to olefins, leading to the formation of aldehydes as the major products, and often isomers, alcohols as well as hydrogenates as by-products. This atom-economic reaction is the success story of homogeneous catalysis, and stands as the largest homogeneous transition metal complex-catalysed reaction in industry.[19–21]

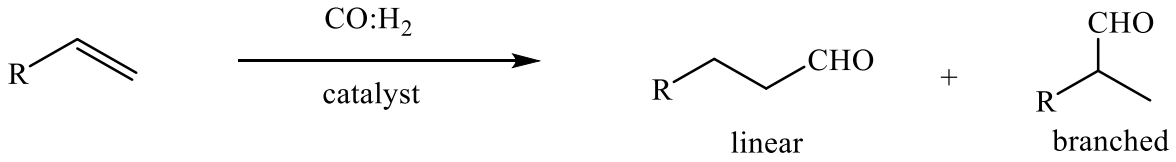

Scheme 3.1 The hydroformylation reaction.

The principal metal used in the design of catalysts for hydroformylation is rhodium because of its remarkable catalytic activity and selectivity for aldehydes under mild reaction conditions (typically, 80 – 100 °C and 10 – 25 bar).[19,22] However, like most homogeneous catalytic systems, this reaction is hampered by difficulties in the separation of the catalyst from the products. Achieving a good, efficient and sustainable isolation of the catalyst is of paramount importance as the presence of residual metal in the product stream often comes with huge financial implications that impacts on several fields. Where the substrate is of low boiling point, for example, the short chain alkenes, separation and recovery of the catalyst is effectively carried out *via* the conventional distillation method. Conversely, this method is only limited to low molecular weight olefins, since the high temperatures that are required for high boiling point long chain olefins often lead to catalyst decomposition and subsequently low catalyst activity.[23]

To that effect, several strategies have been used to facilitate the recovery of homogeneous catalysts in the hydroformylation of medium-to-long chain olefins, while maintaining the high activity and selectivity of the rhodium-based catalyst precursors. These strategies mainly involve the immobilisation of a catalyst on a solid support (polymers), as well as heterogenization of a catalyst in a different phase to that of the reactants and products (biphasic catalysis).[24–33,34] A less explored, though highly attractive recovery technique is the use of membrane technology which allows permeation through the membrane by selected molecules upon application of a driving force. This technique is easily tuneable by manipulating the various physicochemical properties of both the membrane (pore size, material, thickness and

diameter) and the constituents of the feed (molecular weight, polarity, geometry, viscosity and surface tension).[35–40]

A noteworthy strategy in membrane technology is the organic solvent nanofiltration technique (OSN), which entails the use of nanofiltration membranes to separate molecules present in organic solvents without the need for processes that are catalyst-destructive or that require high-energy.[9,41–47] This is considered a greener approach towards homogeneous catalyst recovery because of its relatively low energy requirements and facile catalyst separation without the need for biphasic media. These membranes are also deemed user-friendly and the whole process can be readily scaled up. Moreover, the OSN recovery technique is highly successful when the catalyst is of high molecular weight relative to the other constituents of the feed. This allows for the determination of the molecular weight cut-off (MWCO), which is the molecular weight at which the membrane will achieve 90% rejection/retention.[48] Since homogeneous catalysts (such as those used for hydroformylation) are usually of the same molecular weight as the reagents and products, molecular weight enlargement (MWE) of the catalyst can facilitate efficient membrane filtration. Various soluble supports have been used for molecular weight enlargement of homogeneous catalysts, and these include polyhedral oligomeric silsesquioxanes (POSS), polymers and dendrimers.[49–51] When metals are incorporated into dendritic arms of the support, the resulting metallodendrimers often possess enhanced catalytic activity due to the multiple catalytic sites that propagate from the core.[52–54] These mimic naturally occurring metalloenzymes, which often possess improved catalytic efficiency over their mononuclear analogues owing to multiple active sites. In view of such potentially beneficial catalytic properties, we discuss in this chapter, the application of a mononuclear and a low generation metallodendritic complex of Rh(I) as catalyst precursors in the hydroformylation of a linear α-olefin and internal olefins. The recovery of these complexes using the OSN technique, as well as their kinetic studies in the hydroformylation of 1-octene are also evaluated.

3.2 Results and discussion

3.2.1 Preliminary hydroformylation screening using precatalyst 2.10

Preliminary hydroformylation experiments were performed using the model mononuclear catalyst precursor **2.10** (Figure 3.1), and 1-octene as the model substrate. This substrate is a good representation of the medium to long chain olefins, which form high boiling point

aldehyde products that require harsh separation conditions from the catalyst, often resulting in catalyst decomposition and subsequent loss in catalyst activity. Therefore, successful transformation of 1-octene would be beneficial towards efforts of efficient hydroformylation of medium to long chain olefins.

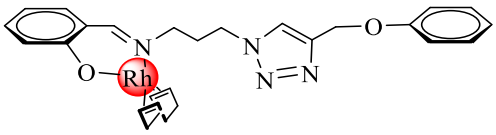

Figure 3.1 Aryl-ether Rh(I)-mononuclear complex **2.10**.

The conditions of the study (temperature and syngas pressure) were based on our previously reported work on the hydroformylation of 1-octene using analogous Rh(I) catalyst precursors bearing *N*,*O*-bidentate ligands.[55–58] In a typical experiment, the reactor was charged with toluene (7.5 mL), 1-octene (1.21 g, 10.7 mmol), dodecane as the internal standard (100 µL) and precatalyst **2.10** (2.87×10^{-3} mmol, substrate : Rh ratio 2500 : 1). The reactor was heated to the desired temperature (75 °C, 85 °C, or 95 °C) and then flushed with syngas (CO : H_2), and pressurised to the appropriate syngas pressure (20 bar, 30 bar, or 40 bar). Samples were analysed after 4 hours using gas chromatography (GC). Authentic iso-octenes and aldehydes, alcohols and *n*-octane were used to confirm the products.

3.2.1.1 The Effect of Temperature and Pressure on Conversion

The temperature and pressure were varied at a fixed time of 4 hours to determine the effect of heat (75–95 °C) and total syngas pressure (1:1, CO:H_2, 20–40 bar) on the conversion of 1-octene. Moderate conversion of 1-octene (79%) is observed at the lowest temperature and pressure (75 °C and 20 bar syngas pressure) of this study (Figure 3.2). Increasing the temperature (to 85 °C and 95 °C) at a constant pressure of 20 bar results in near-quantitative conversion of 1-octene (> 97%), indicative of the energy required for the activation of the olefin, a phenomenon that is anticipated as the rate of a catalytic reaction generally increases with an increase in temperature.[59] A further increase in temperature and pressure has no significant effect on the conversion of 1-octene. A slight decline in conversion is observed when the conditions are raised from 30 bar (75 °C and 85 °C) to 40 bar (75 °C and 85 °C). A more detailed understanding of how the various conditions of this study affect the composition

of the products that emanate from the conversion of 1-octene using precatalyst **2.10** is discussed further in terms of chemoselectivity and regioselectivity.

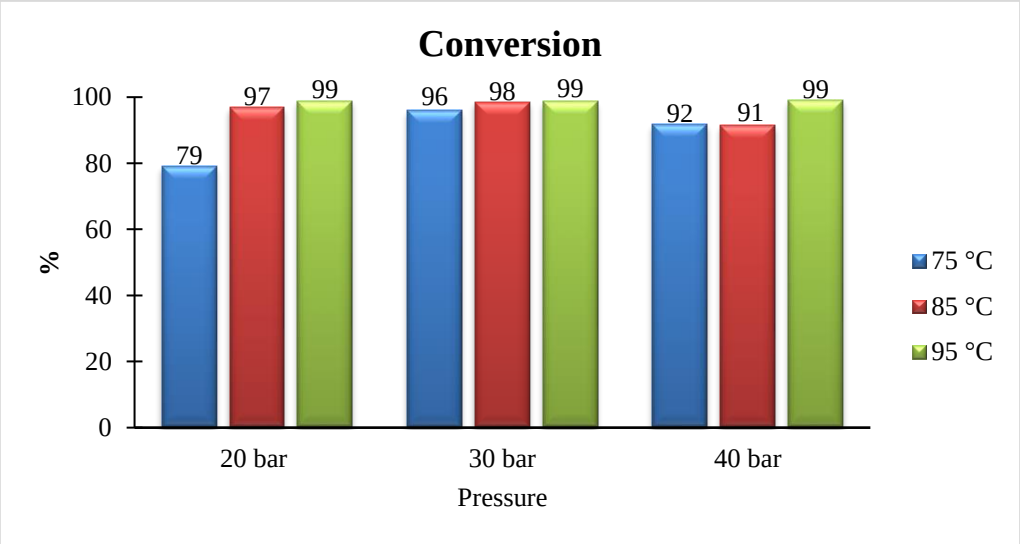

Figure 3.2 Conversion of 1-octene with temperature and pressure, at constant time (4 h) for complex **2.10**.

3.2.1.2 The Effect of Temperature and Pressure on Chemoselectivity

The chemoselectivity of a hydroformylation catalyst is often described as the selective preference of the desired formation of aldehydes over formation of isomeric, alcohols and/or hydrogenation products. In this study, no alcohols or hydrogenation products were observed under the different conditions in the hydroformylation of 1-octene, and as such, the calculated chemoselectivity for precatalyst **2.10** represents the bias towards aldehydes over isomeric products (Figure 3.3). In assessing the effect of temperature and pressure, a gradual increase in chemoselectivity for aldehydes is observed at constant pressure (20 bar) with increase in temperature, from 31% aldehydes (75 °C) to 49% aldehydes (95 °C). A further increase in pressure with an increase in temperature results in improved chemoselectivity towards aldehydes of up to 96%. The observed bias towards aldehydes with an increase in syngas pressure and temperature can be ascribed to the improved hydroformylation of the iso-octenes to aldehydes due to an increase in the concentration of CO in the system, which limits isomerisation and accelerates the CO migration step.[60] Generally, a high CO concentration interferes with the metal-hydride addition-elimination promoted isomerisation through an improved rate of CO-migratory insertion, and in the presence of hydrogen leads to the formation of aldehydes over isomers.[61] However, a slight decrease in total aldehydes is

observed when temperature is increased from 85 °C (96%) to 95 °C (89%) at constant pressure of 40 bar, as there exists a competition between hydroformylation and isomerisation, and high temperatures are generally known to favour isomerisation of the olefin prior to hydroformylation to aldehydes.[61] This is further supported through the aldehyde regiochemistry, as described in the following section.

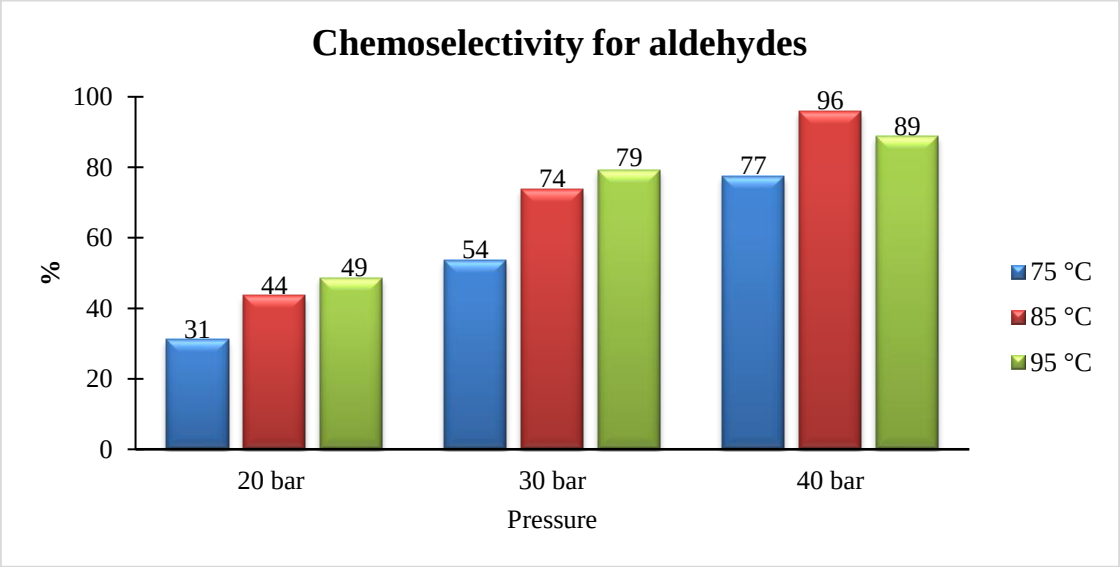

Figure 3.3 Chemoselectivity for aldehydes with temperature and pressure, at constant time (4 h) for complex **2.10**.

3.2.1.3 The Effect of Temperature and Pressure on Regioselectivity

The regioselectivity of a catalyst is an important consideration to assess in hydroformylation, described as the bias towards either linear or branched aldehydes. Transformation of these aldehydes leads to important intermediates known as the oxo intermediates (specialty esters, carboxylic acids, polyols, alcohols and amines). These have found various applications in the detergents, pharmaceuticals, plasticisers, agrochemicals as well as the fragrance industries, all of which utilise over 10 million tonnes of aldehydes per annum.[19] In this study (Figure 3.4), a higher degree of linear aldehydes (73%) is observed at low temperature and pressure (75 °C/ 20 bar). These are formed *via* the anti-Markovnikov addition of the olefin to the metal-alkyl bond during the hydroformylation cycle. Increasing the temperature at constant pressure (75 °C – 95 °C/ 20 bar) results in a decrease in linear aldehydes, as there exists a temperature-promoted isomerisation of the terminal olefin. This leads to iso-octenes which gradually undergo hydroformylation in an isomerisation-hydroformylation tandem process that

culminates in the formation of branched aldehydes. The observed shift to branched aldehydes can also be explained by the direct hydroformylation of the substrate *via* the Markovnikov addition to the metal-alkyl bond. A further increase of syngas pressure (30 – 40 bar) with temperature gives more of branched aldehydes, as the rate of *β*-hydride elimination becomes slower than CO-migratory insertion at increased CO concentrations, shifting the two competitive processes in favour of hydroformylation over formation of isomers. This observation is further depicted by the *n:iso* ratios in Table 3.1, which decrease as the temperature is raised from 75 °C to 95 °C. It can be postulated that the tetracarbonyl rhodium species $[Rh(CO)_4]^+$ may form at higher pressure, and can influence the selectivity of the catalyst.

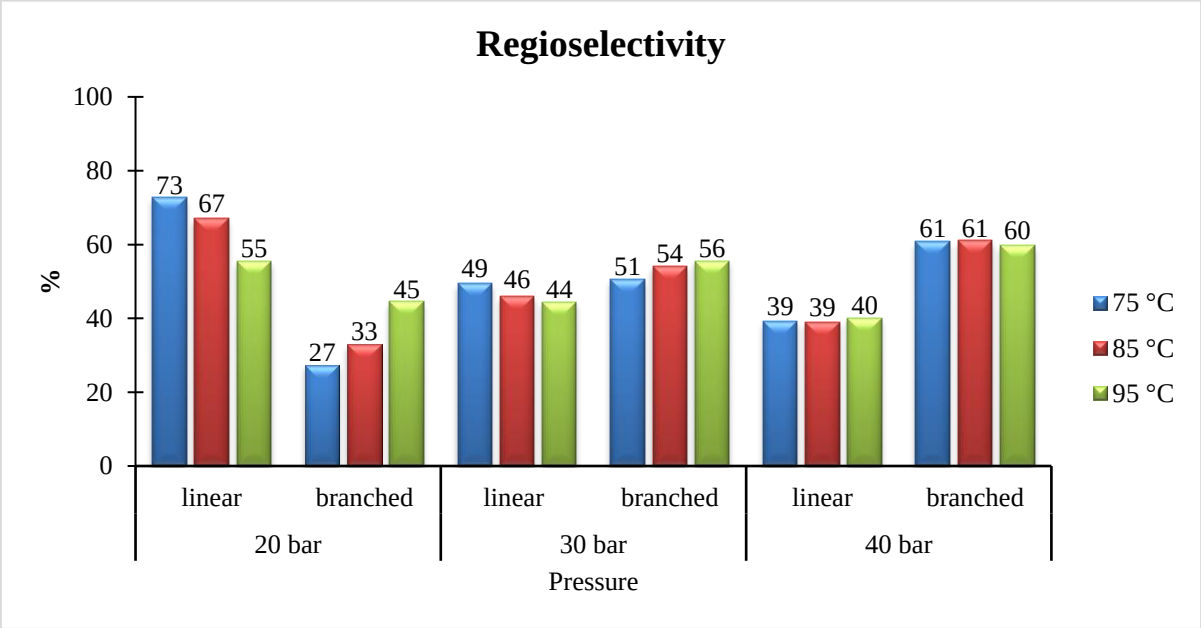

Figure 3.4 Regioselectivity with temperature and pressure, at constant time (4 h) for complex **2.10**.

3.2.1.4 The Effect of Temperature and Pressure on Activity

The key consideration for the overall performance of a hydroformylation catalyst is often best described using the catalyst activity, which is defined as the molar ratio of the aldehyde products to the metal catalyst loading per unit time. This gives a better indication of the efficiency of the catalyst in improving the rate of a reaction. In the transformation of 1-octene, precatalyst **2.10** shows a steady increase in activity when pressure is increased at constant temperature, from 154 h^{-1} (75 °C/ 20 bar) to 444 (75 °C/ 40 bar), (Table 3.1). This is due to the

increase in the concentration of syngas in the system, resulting in improvement of the rates of the reaction. This trend also corresponds well with the observed increase in conversion and total aldehydes at constant temperature, which further supports the observed hydroformylation rates. A gradual increase in activity is observed when temperature is increased at constant pressure, from 323 h^{-1} (75 °C/ 30 bar), 454 h^{-1} (85 °C/ 30 bar) to 489 h^{-1} (95 °C/ 30 bar), indicative of the energy required to improve the rate of the reaction using precatalyst **2.10**. The best activity is observed when syngas pressure and reactor temperature are increased to 40 bar and 85 °C respectively (554 h^{-1}, entry 6).

Table 3.1 Hydroformylation of 1-octene using catalyst precursor **2.10** for 4 h[a].

Entry	Temp. (°C)	Pressure (bar)	Conv. (%)	Aldehydes (%)[b]	Isoalkenes (%)	*n/iso*[c]	TOF (h^{-1})[d]
1	75	20	79	31	69	73:27	154
2	75	30	96	54	46	67:33	323
3	75	40	92	77	23	55:45	444
4	85	20	97	44	56	49:51	264
5	85	30	98	74	26	46:54	454
6	85	40	99	90	10	44:56	554
7[e]	85	40	93	56	44	63:37	329
8	95	20	99	49	51	39:61	301
9	95	30	99	79	21	39:61	489
10	95	40	99	89	11	40:60	549

[a]Reactions carried out with syngas (1:1) in toluene (7.5 ml) with 7.175 mmol of 1-octene and 2.87×10^{-3} mmol of Rh catalyst. The reactor was purged with syngas. GC conversions obtained using dodecane as an internal standard in relation to authentic standard iso-octenes and aldehydes. [b]Total aldehydes formed (from octene and iso-alkenes converted) which includes the primary aldehyde product, nonanal, and isoaldehydes. [c]The molar ratio of primary linear aldehyde product (*n*) and isoaldehydes (*iso*) formed. [d]TOF = (mmol of aldehydes per mmol of Rh)/time. [e]Entry 7 was conducted in the presence of mercury. Average error estimate = ± 0.68.

3.2.1.5 Mercury poisoning experiment

The mercury drop test was carried out to determine if the reaction was entirely homogeneous or may have taken place in the presence of nanoparticles (*vide supra*, entry 7, Table 3.1). A drop of mercury was added to the reaction components to amalgamate any nanoparticles that

may be present, rendering them unavailable for catalysis. A negligible decrease in conversion is observed {from 99% (entry 6) to 93% (entry 7)}, though notably the quantity of total aldehydes decreases from 90% (entry 6) to 56% (entry 7). This suggests, as has been observed in previous studies with analogous Rh(I) catalyst precursors,[56,58] that the nanoparticles mediate the hydroformylation reaction. Interesting to note is the improved regioselectivity for the linear aldehyde in the presence of mercury, indicative of the good stabilisation of the resultant isomers from their possible transformation to branched aldehydes. A closer look at identifying the nanoparticles could be beneficial in designing specifically tailor-made isomerisation catalyst precursors. The regioselectivity of a catalyst towards linear aldehydes could also be potentially improved *via* bulkier macromolecular structures, which may provide the necessary steric influence. Furthermore, it can be envisaged that bulky dendritic catalysts may possess improved stability and catalytic activities due to the multiple catalytically active sites. It is on this premise that we evaluated the low generation trinuclear metallodendrimer **2.13** in the hydroformylation of 1-octene.

3.2.2 Catalytic evaluation using precatalyst 2.13

Optimum conditions for the experiments conducted using catalyst precursor **2.10** were established at 85 °C and 40 bar, based on the good chemoselectivity for aldehydes (90%), near-quantitative conversion of the substrate (99%) and the high activity (554 h^{-1}). As a consequence of the near-complete conversion and to delineate more meaningful results, it was decided to evaluate the trinuclear precatalyst at a reduced syngas pressure. The trinuclear complex **2.13** (Figure 3.5) was successfully tested in the hydroformylation of 1-octene under milder reaction conditions of 85 °C and 20 bar. Under these conditions of study, the dendritic complex **2.13** shows similar catalyst performance as the mononuclear analogue **2.10** (Table 3.2). It is worth noting that the trinuclear complex is less soluble in toluene than the mononuclear complex under the tested conditions, suggesting a less favourable interaction between the substrate and the catalyst precursor. Previous literature studies report that the poorer solubility of dendritic catalyst precursors in the conventional solvent of choice for hydroformylation (toluene), often leads to less evident dendritic effects.[55,62]

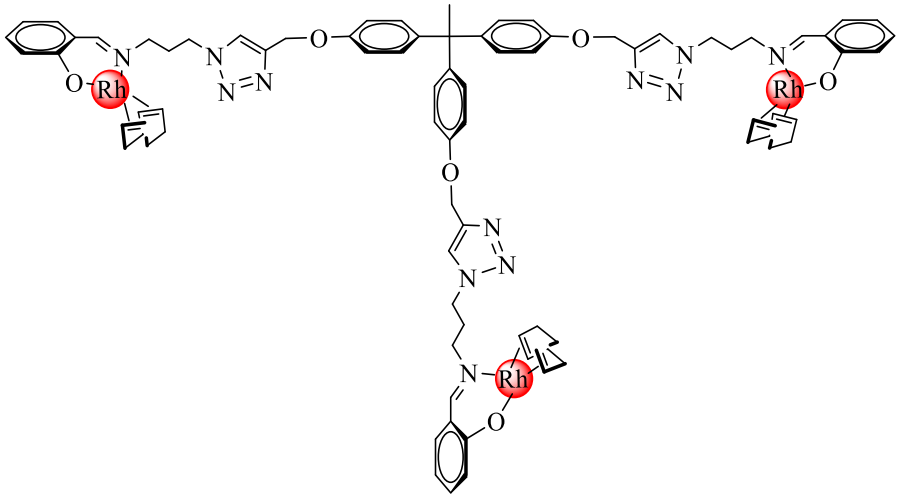

Figure 3.5 Aryl-ether Rh(I)-trinuclear complex **2.13**.

Table 3.2 Hydroformylation of 1-octene with catalyst precursors **2.10** and **2.13** for 4 h[a].

Complex	Temp. (°C)	Pressure (bar)	Conv. (%)	Aldehydes (%)[b]	Isoalkenes (%)	*n/iso*[c]	TOF (h^{-1})[d]
2.10	85	20	97	44	56	49:51	264
2.13	85	20	98	43	57	49:51	265

[a]Reactions carried out with syngas (1:1) in toluene (7.5 ml) with 7.175 mmol of 1-octene and 2.87×10^{-3} mmol of Rh catalyst for **2.10**, and 9.57×10^{-4} mmol of Rh catalyst for **2.13**. GC conversions obtained using dodecane as an internal standard in relation to authentic standard iso-octenes and aldehydes. [b]Total aldehydes formed (from octene and iso-olefins converted) which includes the primary aldehyde product, nonanal, and isoaldehydes. [c]The molar ratio of primary linear aldehyde product (*n*) and isoaldehydes (*iso*) formed. [d]TOF = (mmol of aldehydes per mmol of Rh)/time. Average error estimate = ± 0.76.

3.2.3 Substrate variation

The versatility of rhodium-based catalysts is a desirable characteristic that can help cement the financial gap between the often expensive PGM-based catalyst precursors and the relatively abundant and cheaper first row transition metal-based catalysts (Fe, Co, Ni, Cu-based). If carried out successfully, this may open new avenues towards repositioning of known PGM-based catalyst precursors. In light of the potential economic incentive of successfully repositioning a catalyst, the substrate scope was extended to the internal olefins 7-tetradecene and *trans*-4-octene, which are highly important substrates in the surfactant industry. Hydroformylation of such substrates is generally carried out at high temperatures (> 100 °C) owing to the high thermodynamic stability of internal olefins over their terminal

counterparts.[61,63–65] In this study, the experiments were carried out at 120 °C and 40 bar for 4 h using the mononuclear complex **2.10** (Table 3.3).

Good conversions of both substrates were observed (> 80%) under the chosen conditions of study, with catalyst precursor **2.10** showing good chemoselectivity towards aldehydes (90%) for 7-tetradecene. The relatively shorter carbon chain internal olefin *trans*-4-octene gave a higher percentage of iso-octenes to aldehydes (82% : 18%, respectively), which could be explained by the relative ease of isomerisation of *trans*-4-octene compared to 7-tetradecene, which is highly thermodynamically stable. Moreover, minute quantities of 1-octene and nonanal were observed in the hydroformylation of *trans*-4-octene, indicative of the highly preferential isomerisation of *trans*-4-octene over hydroformylation. This is further evidenced by the lower activity of *trans*-4-octene (102 h^{-1}) to that of 7-tetradecene (841 h^{-1}). Overall, catalyst precursor **2.10** shows attractive hydroformylation adaptability to different substrates, from the linear α-olefin (1-octene) to internal olefins (7-tetradecene and *trans*-4-octene), which is critical from a Green Chemistry perspective. Moreover, the ability to recover and reuse the versatile catalyst can further add value to a fast-depleting-resource-based catalyst through circularity, as presented in the following section.

Table 3.3 Hydroformylation of internal olefins with catalyst precursor **2.10** for 4 h[a].

Substrate	Temp. (°C)	Pressure (bar)	Conv. (%)	Aldehydes (%)[b]	Isoalkenes (%)	TOF (h^{-1})[c]
7-tetradecene	120	40	85	90	10	841
Trans-4-octene	120	40	92	18	82	102

[a]Reactions carried out with syngas (1:1) in toluene (7.5 ml) with 7.175 mmol of 1-octene and 2.87 × 10^{-3} mmol of Rh catalyst for **2.10**. GC conversions obtained using dodecane as an internal standard in relation to authentic standard iso-octenes and aldehydes. [b]Total aldehydes formed (from substrate and iso-olefins converted) which includes the primary branched aldehyde product and iso-aldehydes. [c]TOF = (mmol of aldehydes per mmol of Rh)/time. Average error estimate = ± 0.51.

3.2.4 Reusability of the catalysts: Organic Solvent Nanofiltration (OSN)

Designing a tailor-made catalyst that is not only fit-for-purpose but maintains activity after recovery is very attractive from a circular economy viewpoint. Moreover, using catalyst recovery techniques that are cleaner, harmless and less energy-intensive is a much sought-after approach towards reducing waste, minimising potential work hazards and conducting reactions at ambient temperature and pressure. Organic solvent nanofiltration membrane technique is one such approach that is usually operated at ambient temperature and mild pressure to achieve good separation of constituents of a reaction. This technique mostly takes advantage of the differences in the molecular weight and size of the components of a feed. In this work, catalyst recyclability experiments were carried out for 2 h at 85 °C and 40 bar, after which the organic solvent nanofiltration membrane technique was conducted to recover the catalyst for reuse. The separation of the catalyst from the products was achieved by using a stainless-steel dead-end separation cell mounted with a pre-conditioned Duramem® 200 membrane. The choice of the membrane was mainly influenced by the molecular weight cut-off of the membrane (MWCO = 200 g mol^{-1}), in-line with the molecular weight of the catalysts under study (complex **2.10** = 546.48 g mol^{-1}; complex **2.13** = 1447.35 g mol^{-1}). The membrane would only allow part of the feed to permeate through, in this case the substrate (1-octene, MW 112 $gmol^{-1}$), products (aldehydes, iso-octenes and isomers), and toluene would be collected as the permeate, while the catalyst is retained as the retentate (Figure 3.6). The recovered post-reaction catalyst-containing retentate is then decanted from the cell and reintroduced into the catalytic reactor bearing fresh substrate and toluene, and the reaction repeated for 2 h, with the OSN membrane separation carried out thereafter. The catalyst performance throughout these cycles is reported in the following sections.

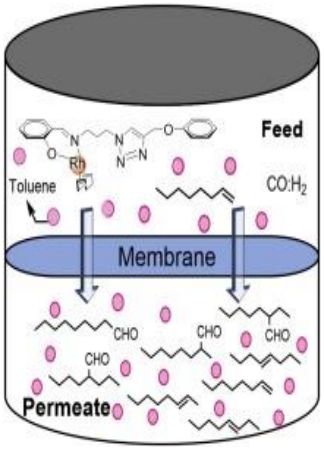

Figure 3.6 Illustration of Organic Solvent Nanofiltration membrane technique.

3.2.4.1 The Effect of catalyst recycling on Conversion

The catalyst precursors **2.10** and **2.13** maintain good conversion of 1-octene after OSN recovery with each cycle (Figure 3.7), with catalyst precursor **2.10** showing only a slight decline in conversion (to 91%) after the 4th cycle. This is indicative of the effectiveness of the OSN membrane in retaining the active species of both catalyst precursors after each successive cycle. Such good catalyst and membrane performance are further corroborated by inductively coupled plasma optical emission spectroscopy (ICP-OES), which revealed no detectable levels of rhodium present in the permeate (99% rejection). This is attractive and renders this approach a highly efficient and greener recovery technique.

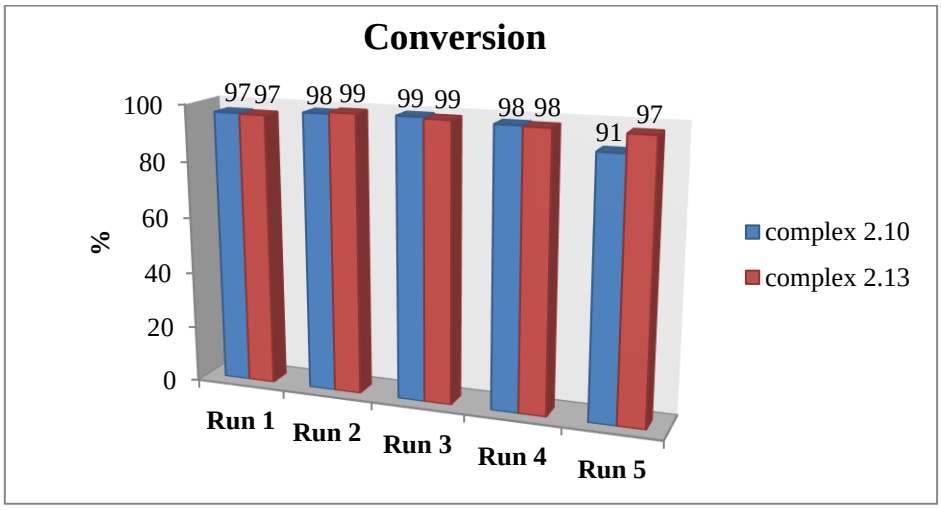

Figure 3.7 Percentage conversion of 1-octene during OSN recyclability studies in the hydroformylation of 1-octene.

3.2.4.2 The Effect of catalyst recycling on Activity

A closer look at the catalytic performance in terms of activity is shown in Figure 3.8 overleaf. Both catalyst precursors show remarkably good catalytic activity with each cycle. An increase in activity from the 1st cycle to the 2nd cycle is observed for both catalysts **2.10** (from 882 h^{-1} to 960 h^{-1}) and **2.13** (from 929 h^{-1} to 957 h^{-1}). This could be due to the already present catalytically active tetracarbonyl rhodium species $[Rh(CO)_4]^+$ that is formed during the 1st cycle, allowing for a faster reaction rate in the 2nd cycle. At this stage no catalyst induction period can be expected to exist as the active catalytic species has been generated during the 1st cycle. However, a gradual decrease in activity is observed from the 2nd cycle to the 5th cycle, a phenomenon that can be attributed to a gradual partial degradation of the active species from

cycle 2, as the catalyst periodically gets exposed to air upon transfer from the reactor to the membrane cell in-between each cycle. This trend is observed with respect to the chemoselectivity for aldehydes, as discussed in the section overleaf.

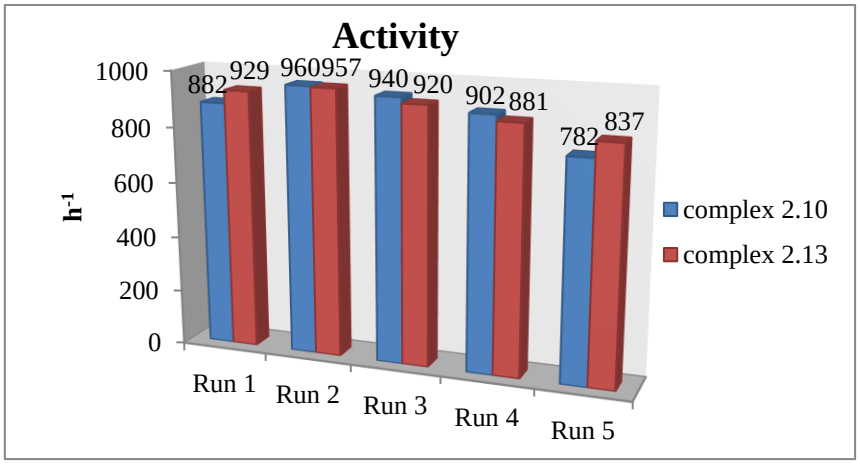

Figure 3.8 Activity of the complexes during OSN recyclability studies in the hydroformylation of 1-octene.

3.2.4.3 The Effect of catalyst recycling on Chemoselectivity for aldehydes

The catalyst precursors **2.10** and **2.13** show appreciably good to moderate chemoselectivity for aldehydes with each successive cycle (Figure 3.9). In a generic trend, the preference for aldehydes is comparable for both catalyst precursors with each cycle, with the best aldehyde chemoselectivity at 78% (Run 2 for both complexes). Beyond the 2nd cycle, the chemoselectivity for aldehydes is observed to decline slowly, ascribed to the formation of iso-octenes being favoured at this stage. This suggests that the active species remains the same with each recycle and some degradation may occur, leading to the slight decline in aldehyde chemoselectivity. It should be noted that no alcohols were observed at any instance during the recycling of the catalysts, indicating that the active species maintained the selectivity between the aldehydes and iso-octenes only.

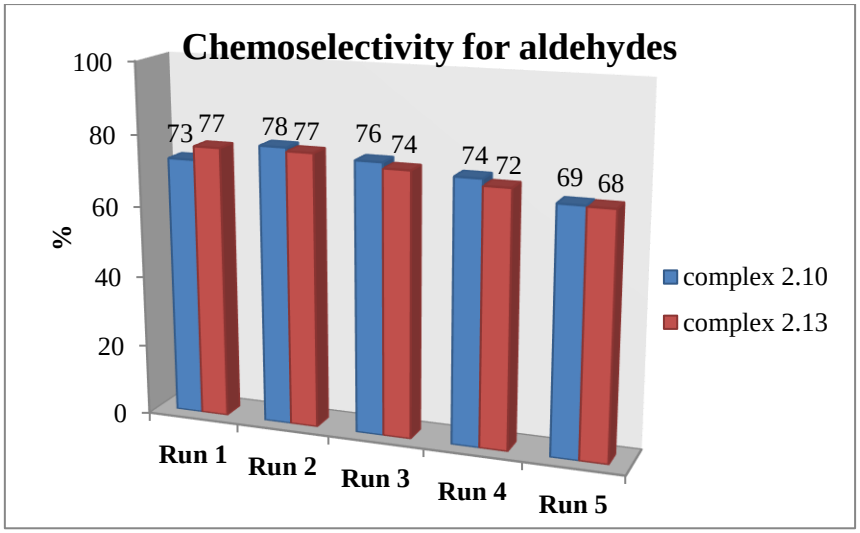

Figure 3.9 Chemoselectivity for aldehydes during OSN recyclability studies in the hydroformylation of 1-octene.

To further gain understanding of the rates of 1-octene transformation beyond the activity {TOF = (mmol of aldehydes per mmol of Rh)/time} described *vide supra*, kinetic experiments were conducted using precatalysts **2.10** and **2.13** in the hydroformylation of 1-octene. This allows for the prediction of how the speed of the reaction will change under certain reaction conditions.

3.2.5 Kinetic Experiments on hydroformylation of 1-octene

A complete kinetic study was conducted using the mononuclear catalyst precursor **2.10** through varying the temperature, time, catalyst loading and partial pressure of CO and H_2 gases. The reactions were carried out over a maximum period of 4 h, and the reported values for 1-octene represent the number of moles of substrate that are remaining at each respective time interval.

*3.2.5.1 Product-distribution-time studies using **2.10**: influence of temperature*

The influence of temperature on the product distribution over time was investigated during the hydroformylation of 1-octene at constant pressure of 40 bar using catalyst precursor **2.10** (Figure 3.10). At the lowest temperature of this study (75 ℃), the number of moles of the substrate decrease steadily over time, Figure 3.10a. Increasing the temperature to 85 ℃ shows a substantial decline of 1-octene in the system over time, with a further increase in temperature to 95 ℃ resulting in near-perfect depletion of the substrate. Moreover, at a lower temperature

of 75 °C, a steady build-up of iso-octenes is observed between 1 h and 3 h of the reaction, Figure 3.10c. This would be expected as the rate of isomerisation is generally slower at lower temperatures.[57,66] However, as these iso-octenes build-up in the system at 75 °C, an optimum level is reached at 3 h, beyond which a driving force towards conversion of the isomers to branched aldehydes comes into effect, resulting in the observed rapid decline in iso-octenes, from 29.51 mol% to 20.70 mol% at 3 and 4 h respectively (Figure 3.10c). This observation is further supported by the sharp increase in branched aldehydes between 3 and 4 h of the reaction at 75 °C, from 11.57 mol% to 31.64 mol% respectively, Figure 3.10d. At higher temperatures of 85 °C and 95 °C, the rate of isomerisation is greater immediately from the 1 h interval (Figure 3.10c), a phenomenon that is expected at high temperatures. These iso-octenes decline rapidly as they are immediately converted to branched aldehydes, further substantiating the observed trend depicted in Figure 3.10d at the same temperatures of 85 °C and 95 °C. Moreover, the formation of the linear aldehyde (nonanal) with increase in temperature occurs slowly with time (Figure 3.10b), as the dominance of the branched aldehydes becomes pronounced due to the high temperatures favouring the double-bond isomerisation of the substrate prior to hydroformylation.

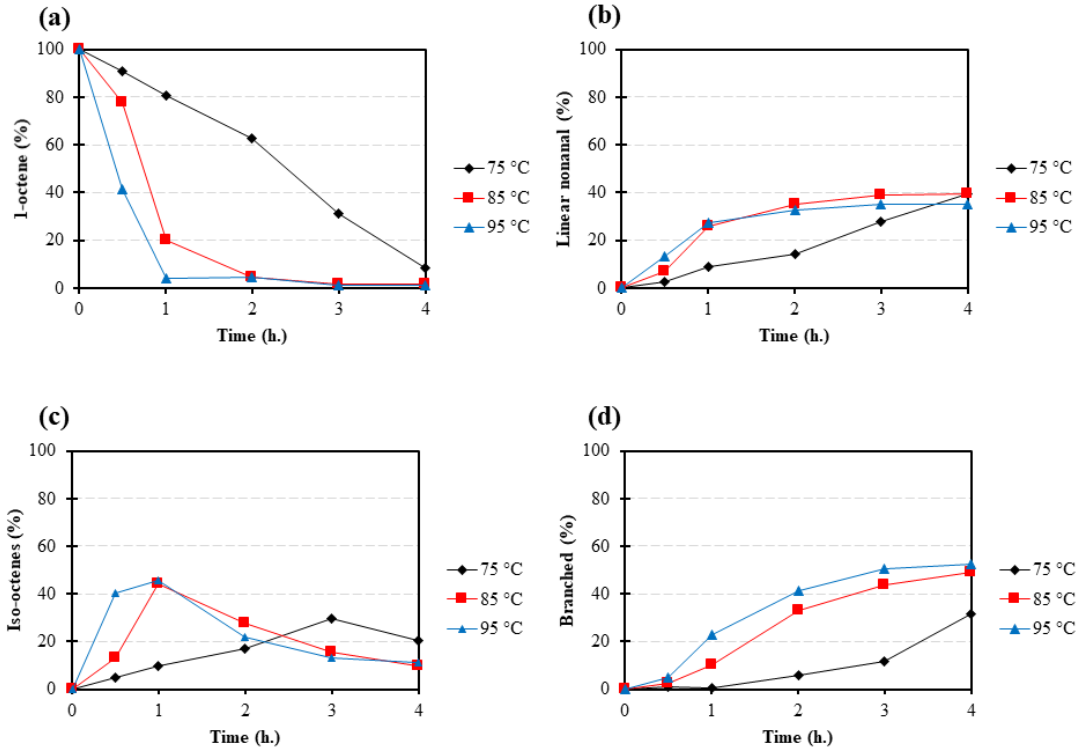

Figure 3.10 Product-distribution-time profiles for the hydroformylation of 1-octene at various temperatures and constant pressure (40 bar) over time using precatalyst **2.10**.

*3.2.5.2 Product-distribution-time studies using **2.10**: influence of pressure*

The influence of pressure on the product distribution over time was investigated during the hydroformylation of 1-octene at constant temperature of 85 °C using catalyst precursor **2.10** (Figure 3.11). It should be mentioned that there was no notable influence on performance of the catalyst when the partial pressure of the CO and H_2 were varied at 85 °C. Hence the data reported herein represents that obtained at equimolar ratio of CO:H_2. The lower syngas pressure of 20 bar favours greater accumulation of iso-octenes with time (over two hours) before these can build-up sufficiently enough to create a driving force for their hydroformylation into aldehydes (after 2 h, Figure 3.11c). This driving force is reached earlier at higher pressures (at 1 h, for 30 and 40 bar, Figure 3.11c), allowing for a more improved transformation of these iso-octenes to branched aldehydes between 1 and 4 h of reaction time. This corresponds well with the observed sudden increase of branched aldehydes from 1 h of reaction time (Figure 3.11d) at the same syngas pressure of 30 and 40 bar.

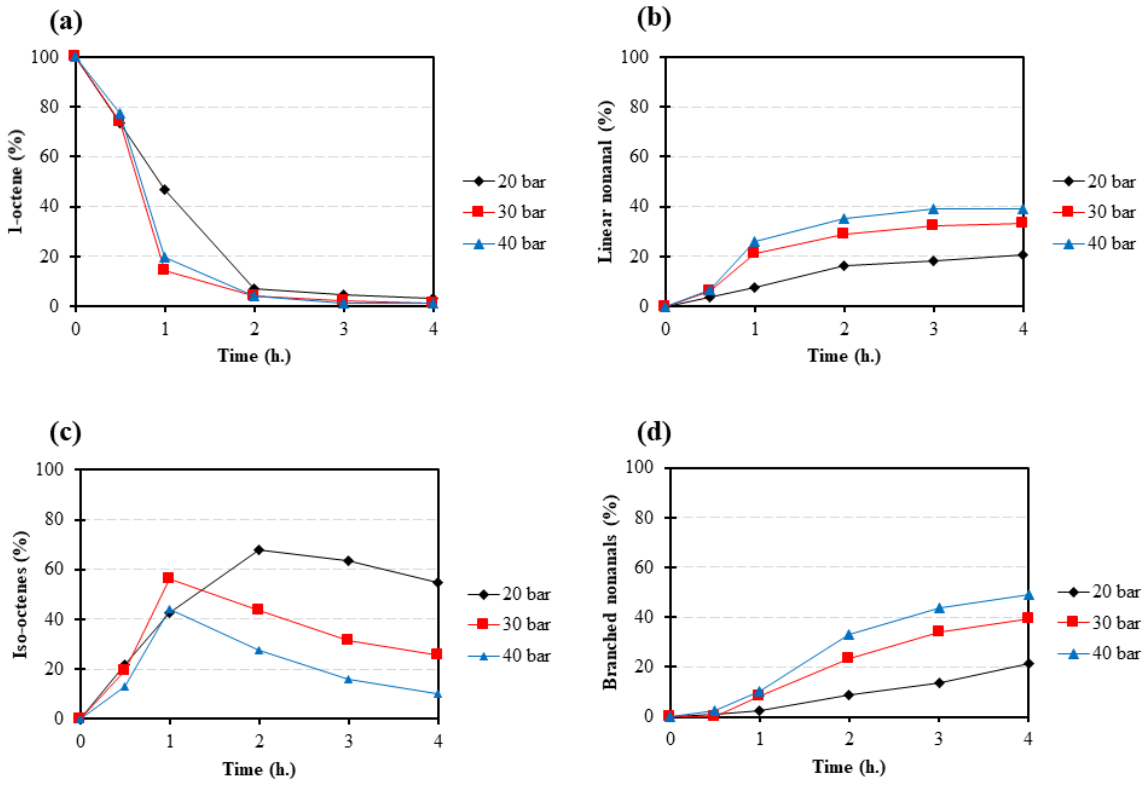

Figure 3.11 Product-distribution-time profiles for the hydroformylation of 1-octene at various pressures and constant temperature (85 °C) over time using precatalyst **2.10**.

*3.2.5.3 Product-distribution-time studies using **2.10**: influence of catalyst loading*

The influence of catalyst loading on the product distribution over time was investigated during the hydroformylation of 1-octene at the optimum temperature (85 °C) and pressure (40 bar) using catalyst precursor **2.10** (Figure 3.12). The quantity of 1-octene in the system is observed at comparable levels to the normal and double catalyst loading between 2 h and 4 h time intervals (Figure 3.12a), which is indicative of a system that has reached the optimum point of influence with respect to the catalyst loading. Interesting to note is the increase in iso-octenes from 1 h (18.27 mol%) to 2 h (37.87 mol%) at half catalyst loading (Figure 3.12c), indicative of the influence of low catalyst concentration on lowering the rate of isomerisation. This leads to a slower build-up of iso-octenes, before finally being overcome at a longer reaction time (2–4 h) *via* conversion thereof to the branched aldehydes, which is evident later than that at higher catalyst concentrations, an observation further supported by the profile depicted in Figure 3.12d.

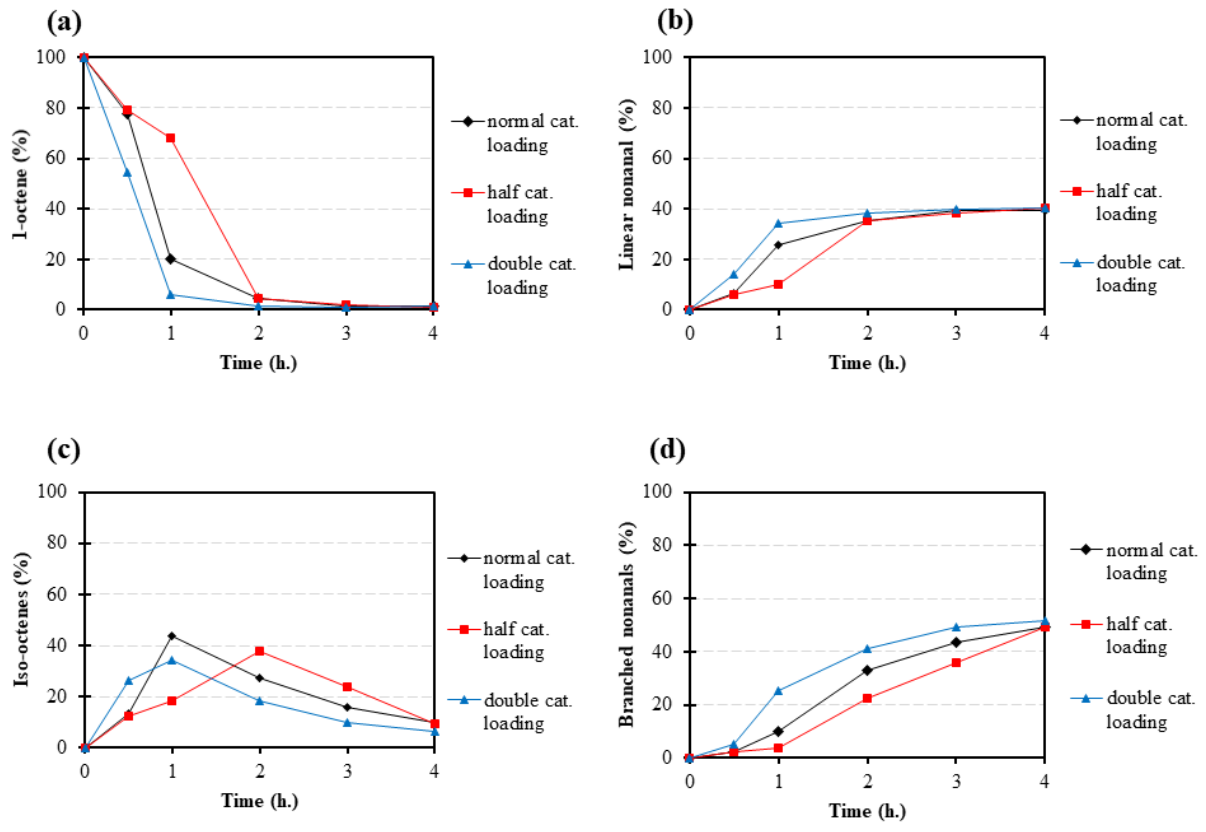

Figure 3.12 Product-distribution-time profiles for the hydroformylation of 1-octene over time, at constant temperature (85 °C) and pressure (40 bar) with varying catalyst loading, using precatalyst **2.10**.

A closer look at the chemo- and regioselectivity product distribution profiles using the normal catalyst loading under optimum conditions (85 °C and 40 bar) is shown in Figure. 3.13. The iso-octenes accumulate during the first hour of reaction, beyond which hydroformylation occurs rapidly, leading to formation of more branched aldehydes.

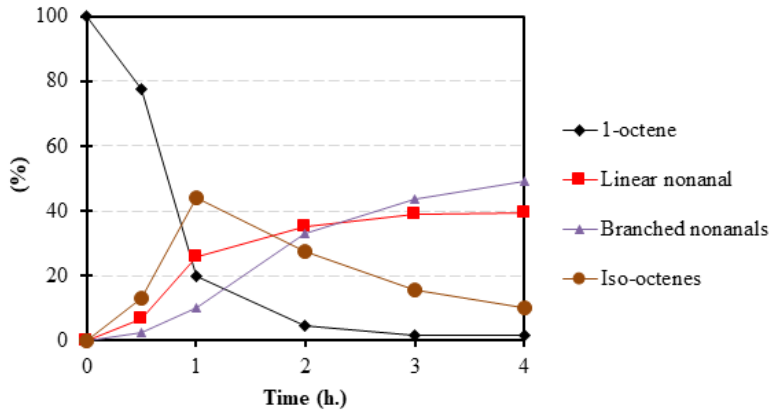

Figure 3.13 Substrate and product-distribution-time profile at normal catalyst loading (2.87 × 10^{-3} mmol of Rh catalyst) and optimum conditions (85 °C / 40 bar) with mononuclear complex **2.10**.

*3.2.5.4 Product-distribution-time studies using **2.13***

The product-distribution-time profile using catalyst precursor **2.13** for the hydroformylation of 1-octene were evaluated and compared against that of the mononuclear complex **2.10** at a temperature of 85 °C and a syngas pressure of 20 bar. The kinetics of the trinuclear complex are similar to that of the mononuclear complex (Figure 3.14). This behaviour suggests that the metal centres of the trinuclear complex are behaving as a mononuclear entity in the system, which correlates with the catalytic data obtained (*vide supra*). It is generally accepted that similar reaction kinetics translate to similar rate constants, necessitating the determination of the rate constants of the pre-catalysts based on the data obtained for the mononuclear complex **2.13**.

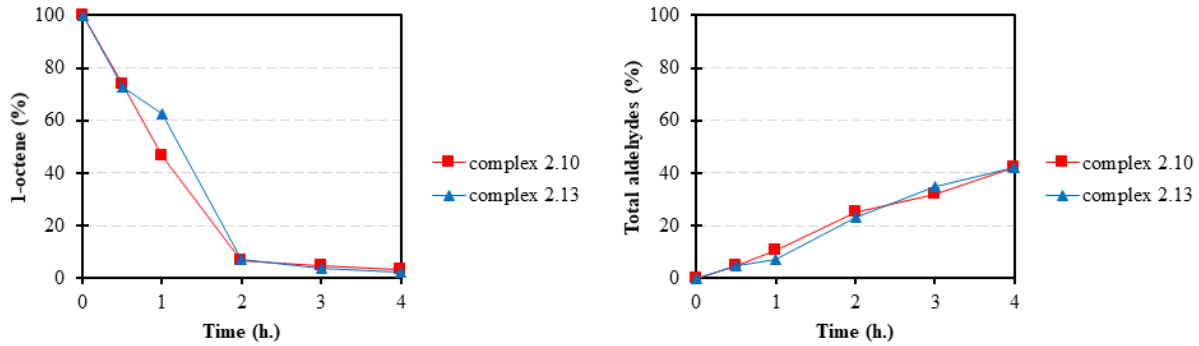

Figure 3.14 Substrate and product-distribution-time profiles with the mono- (**2.10**) and trinuclear (**2.13**) precatalysts over time.

3.2.5.5 Determination of the reaction rate constants and calculation of activation energy

From the product distribution profiles of the catalyst precursor **2.10** (based on total aldehydes formed), the observed reaction rate constants (k_{obs}) were then estimated from Eq. 1 using the least square regression analysis, with first-order dependence in the olefin, shown in Table 3.4 below.

$$\frac{d(C_{octenes})}{dt} = -k_{obs}C_{octenes} \quad \ldots\ldots\ldots eq.(1)$$

Table 3.4 Reaction rate constants of catalyst precursor **2.10**.

Entry	Temp. (°C)	P_{Total} (bar)	Catalyst load	k_{obs} (h^{-1})
1	75	40	normal	0.19
2	85	40	normal	0.49
3	95	40	normal	0.60
4	85	30	normal	0.33
5	85	20	normal	0.13
6	85	40	half	0.39
7	85	40	double	0.71

The rate constants agree with the general expectation of the rate of a catalytic reaction increasing with increase in temperature at constant pressure (40 bar, entries 1 to 3). Moreover, at constant temperature (85 °C), varying the pressure results in an increase in the rate constants, indicative of the effect of increased concentration of syngas in the system, from 0.13 h^{-1}

(20 bar, entry 5) to 0.49 h^{-1} (40 bar, entry 2). The effect of the catalyst loading is also evident on the rate constants at a constant temperature and pressure of 85 °C and 40 bar respectively, increasing from 0.39 h^{-1} (entry 6, half catalyst loading) to 0.49 h^{-1} (entry 2, normal catalyst loading) and 0.71 h^{-1} (entry 7, double catalyst loading). As expected, the influence of temperature on the rate constant is consistent with the Arrhenius Equation (Eq. 2).

$$k_{obs} = k_0 e^{\left(-\frac{E}{RT}\right)} \quad \ldots\ldots\ldots\ldots\ldots eq.(2)$$

From this equation, the activation energy was calculated to be 62 kJ mol^{-1}. This value is comparable to the ranges obtained using similar rhodium(I) catalysts for the hydroformylation of medium-chain alpha-olefins in a homogeneous solution.[67,68,69]

To further describe the observed rate constants (k_{obs}) in terms of catalyst and syngas pressure effects of Table 3.4, a fundamental mechanism-based rate law model was applied, as proposed by Dutta and co-workers, and shown in Eq. 3.[69]

$$\frac{dC_{octenes}}{dt} = -\frac{kC_{Rh}(P_{CO})(P_{H2})C_8}{1 + K(P_{CO})} \quad \ldots\ldots\ldots\ldots\ldots eq.(3)$$

However, the rate model did not satisfactorily describe the observed rate constants. This might be due to simplifications of the mechanistic steps used to derive the rate model equation. To obtain a better fit of the observed rate data necessitated modifying the rate model with respect to the catalyst loading, as given in Equation 4.

$$\frac{dC_{octenes}}{dt} = -\frac{kC_{Rh}^{\alpha}(P_{CO})(P_{H2})C_8}{1 + K(P_{CO})} \quad \ldots\ldots\ldots\ldots\ldots eq.(4)$$

A summary of the kinetic parameters obtained from Equation 4 are shown in Table 3.5.

Table 3.5 Summary of the rate model parameters.

Parameter	Value
k_0 ($L^{\alpha}\,mol^{-\alpha}\,bar^2\,h^{-1}$)	5.64 x 10^8
E_A ($kJ.mol^{-1}$)	62
K (bar^{-1})	0.12
α	0.7

A parity plot of the observed and predicted rate constants was then generated and is shown in Figure 3.15.

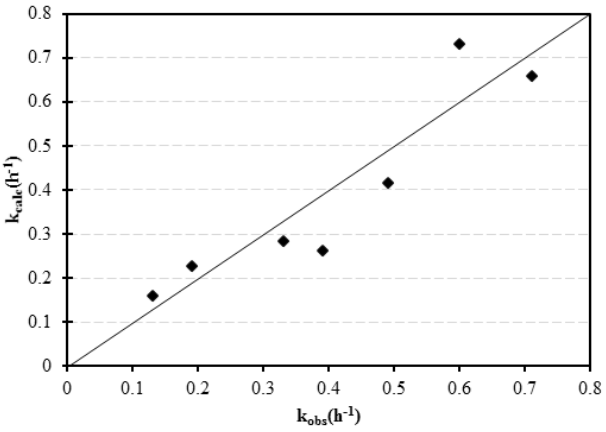

Figure 3.15 Parity plot of predicted (k_{calc}) and experimental (k_{obs}) reaction rate constants**.**

The parity plot shows that the observed rate constants satisfactorily compare to the calculated mechanism-based model rate constants, in support of the experimental kinetics obtained for the mononuclear complex **2.10** in the hydroformylation of 1-octene. To the best of our knowledge, there are no reports of kinetic studies on 1-octene using salicylaldimine-based Rh(I) complexes. However, several kinetics on hydroformylation of olefins have been reported in the literature, for both homogeneous and biphasic systems.[70–77]

3.3 Summary

The ability to successfully evaluate precatalysts that lead to appreciably good overall catalyst performance is a noteworthy step in the hydroformylation of the often-strenuous medium to long chain terminal and internal olefins. The mild optimum reaction conditions (85 °C, 40 bar for 4 h) obtained in the hydroformylation of 1-octene using the mononuclear complex **2.10** are very attractive, since 1-octene forms the simplest representation of the substrates that lead to highly desirable medium to long chain aldehyde products. In addition, these conditions compare well with our previously reported conditions of study using similar Rh(I) catalyst precursors.[55–58] The observed regioselectivity towards branched aldehydes at high temperatures of this study can be ascribed to a generally accepted tandem isomerisation-hydroformylation process, in conjunction with Markovnikov addition of the olefin. This is accelerated by an increase in total syngas pressure, which results in further improved conversion of the resultant iso-octenes. Mercury poisoning experiments using catalyst precursor **2.10** reveal a nanoparticle assisted transformation of 1-octene, with improved bias towards linear aldehydes. This experiment shows that the reaction does not occur in its entirety as a homogeneous transformation when using our catalytic system, as has also been observed in our previous studies with analogous Rh(I) catalyst precursors.[56,58] Large macromolecular structures such as the dendritic complex **2.13** are often confounded with poor solubility in the solvent of choice for hydroformylation, as often reported in the literature.[55,62] The low generation metallodendrimer **2.13** gave comparable catalytic conversion and activity to its mononuclear counterpart **2.10**, ascribed to the poor solubility of **2.13** in toluene, which limits the interaction of the precatalyst with the substrate. Moreover, the three metal centres in precatalyst **2.13** can be viewed, in this case, to be acting as a single mononuclear entity, and not independently enough to positively influence the catalytic performance through the inherent multiple active sites. To increase the substrate scope and assess the versatility of our catalytic system, precatalyst **2.10** was evaluated in the hydroformylation of the equally important internal olefins, 7-tetradecene and *trans*-4-octene. These are intriguing intermediates for the surfactant industry, leading to a wide array of products such as shampoos, bubble baths, liquid hand soap, light and heavy-duty liquid and powder detergents. In this study, precatalyst **2.10** gave good conversions of both internal olefins (> 80 %), with the relatively shorter *trans*-4-octene giving higher quantities of isomers owing to the relative ease of isomerisation compared to the more thermodynamically stable 7-tetradecene. The successful recovery and reuse of both catalysts **2.10** and **2.13** in their active states is synonymous with the United Nations Sustainable

Development Goals, through the use of a greener recovery technique such as organic solvent nanofiltration membrane technology (OSN) in the beneficiation of expensive, rare and fast depleting metals such as rhodium. Moreover, this aligns the homogeneous hydroformylation process with Green Chemistry through effective elemental sustainability that is aimed towards a circular economy. Evaluation of the complexes **2.10** and **2.13** for their recoverability in the hydroformylation of 1-octene using the OSN membrane technique gave good recyclability for at least 5 times, with appreciably consistent catalyst performance throughout the cycles. This is significant towards addressing one of the major challenges of designing recoverable and reusable homogeneous hydroformylation catalysts. Moreover, the membrane recovery efficiency of the metal could be attested to, by using the ICP-OES analysis, which revealed a near-perfect (99%) rejection of the rhodium metal. Such prevention of metal loss is vital for downstream agrochemicals as well as pharmaceutical end-products, which undergo strict product composition analysis. To further gain understanding of the driving forces for the hydroformylation process using our catalytic system, kinetic studies were carried out using precatalysts **2.10** and **2.13**, leading to the determination of the rate constants in the hydroformylation of 1-octene. Subsequently, the activation energy was then calculated to be 62 kJ mol^{-1}, which compares well with similar Rh(I) catalysts reported in the literature. Moreover, the observed reaction rate constants correlate well with a modified fundamental mechanistic-based rate model, validating the experimental kinetic data obtained in this study. This provides additional information to better infer on how the reaction proceeds at a molecular level.

3.4 References

1 B. Lindström and L. J. Pettersson, *CatTech*, 2003, **7**, 130–138.

2 B. Cornils, in *Topics in Current Chemistry*, Springer-Verlag Berlin Heidelberg, Berlin, Germany, 1999, vol. 206, pp. 133–149.

3 R. A. Sheldon, I. Arends and U. Hanefeld, in *Green Chemistry and Catalysis*, Wiley-VCH Verlag GmbH & Co. KGaA, Weinheim, 1st edn., 2007, pp. 1–2.

4 J. Wisniak, *Educ. quim.*, 2010, **21**, 60–69.

5 B. Cornils and W. A. Herrmann, in *Applied Homogeneous Catalysis with Organometallic Compounds*, Wiley-VCH Verlag GmbH & Co. KGaA, Weinheim, 2nd

edn., 2002, pp. 601–625.

6 P. T. Anastas and J. C. Warner, *The 12 Principles of Green Chemistry*, Oxford University Press, New York, 1998.

7 H. Nowothnick, A. Rost, T. Hamerla, R. Schomäcker, C. Müller and D. Vogt, *Catal. Sci. Technol.*, 2013, **3**, 600.

8 N. Yoneda, S. Kusano, M. Yasui, P. Pujado and S. Wilcher, *Appl. Catal. A Gen.*, 2001, **221**, 253–265.

9 W. E. Siew, C. Ates, A. Merschaert and A. G. Livingston, *Green Chem.*, 2013, **15**, 663–674.

10 T. L. Church, Y. D. Y. L. Getzler, C. M. Byrne and G. W. Coates, *Chem. Commun.*, 2007, 657–674.

11 G. J. Sunley and D. J. Watson, *Catal. Today*, 2000, **58**, 293–307.

12 P. W. N. M. van Leeuwen, in *Homogeneous Catalysis: Understanding the Art*, Kluwer Academic Publishers, Dordrecht, 1st edn., 2004, pp. 75–81.

13 C. O'Connor, G. Yagupsky, D. Evans and G. Wilkinson, *Chem. Commun.*, 1968, **38**, 420–421.

14 J. A. Osborn, F. H. Jardine, J. F. Young and G. Wilkinson, *J. Chem. Soc.*, 1966, 1711–1732.

15 R. E. Harmon, S. K. Gupta and J. Brown, *Chem. Rev.*, 1973, **73**, 21–52.

16 M. Beller, B. Cornils, C. D. Frohning and C. W. Kohlpaintner, *J. Mol. Catal. A Chem.*, 1995, **104**, 17–85.

17 R. L. Pruett, *J. Chem. Educ.*, 1986, **63**, 196–198.

18 S. M. Mercer, T. Robert, D. V. Dixon and P. G. Jessop, *Catal. Sci. Technol.*, 2012, **2**, 1315–1318.

19 R. Franke, D. Selent and A. Börner, *Chem. Rev.*, 2012, **112**, 5675–5732.

20 J. Halpern, *Pure Appl. Chem.*, 2001, **73**, 209–220.

21 T. Vanbesien, F. Hapiot and E. Monflier, *Lipid Technol.*, 2013, **25**, 175–178.

22 B. R. James, P. W. N. M. van Leeuwen and C. Claver, in *Rhodium Catalyzed Hydroformylation*, Kluwer Academic Publishers, New York, 1st edn., 2002, pp. 6–277.

23 D. J. Cole-Hamilton and R. P. Tooze, in *Catayst Separation, Recovery, and Recycling*, Springer, Dordrecht, 1st edn., 2006, vol. 30, pp. 4–35.

24 D. Sharma, V. Ganesh and A. Sakthivel, *Appl. Catal. A Gen.*, 2018, **555**, 155–160.

25 B. Cornils, *Org. Process Res. Dev.*, 1998, **2**, 121–127.

26 W. Keim, *Green Chem.*, 2003, **5**, 105–111.

27 M. Benaglia, in *Recoverable and Recyclable Catalysts*, John Wiley & Sons, Ltd., Chichester, 1st edn., 2009, pp. 1-458.

28 A. E. C. Collis and I. T. Horváth, *Catal. Sci. Technol.*, 2011, **1**, 912–919.

29 C. De, R. Saha, S. K. Ghosh, A. Ghosh, K. Mukherjee, S. S. Bhattacharyya and B. Saha, *Res. Chem. Intermed.*, 2013, **39**, 3463–3474.

30 M. Janssen, J. Wilting, C. Müller and D. Vogt, *Angew. Chem. Int. Ed.*, 2010, **49**, 7738–41.

31 Â. C. B. Neves, M. J. F. Calvete, M. V. D. Pinho and M. M. Pereira, *Eur. J. Org. Chem.*, 2012, 6309–6320.

32 C. Li, W. Wang, L. Yan and Y. Ding, *Front. Chem. Sci. Eng.*, 2018, **12**, 113–123.

33 E. Vunain, P. Ncube, K. Jalama and R. Meijboom, *J. Porous Mater.*, 2018, **25**, 303–320.

34 T. Van Vu, H. Kosslick, A. Schulz, J. Harloff, E. Paetzold, M. Schneider, J. Radnik, N. Steinfeldt, G. Fulda and U. Kragl, *Appl. Catal. A Gen.*, 2013, **468**, 410–417.

35 I. Vural Gürsel, T. Noel, Q. Wang and V. Hessel, *Green Chem.*, 2015, **17**, 2012–2026.

36 M. Christian and D. Vogt, *Green Chem.*, 2011, **13**, 2247–2257.

37 M. Rabiller-Baudry, G. Nasser, T. Renouard, D. Delaunay and M. Camus, *Sep. Purif. Technol.*, 2013, **116**, 46–60.

38 E. L. V Goetheer, A. W. Verkerk, L. J. P. van den Broeke, E. de Wolf, B. Deelman, G. van Koten and J. T. F. Keurentjes, *J. Catal.*, 2003, **219**, 126–133.

39 N. S. A. Razak, M. S. Shaharun, H. Mukhtar and M. F. Taha, *Sains Malays.*, 2013, **42**,

515–520.

40 L. W. Gosser, W. H. Knoth and G. W. Parshall, *J. Mol. Catal.*, 1977, **2**, 253–263.

41 P. Marchetti, M. F. J. Solomon, G. Szekely and A. G. Livingston, *Chem. Rev.*, 2014, **114**, 10735–10806.

42 P. van der Gryp, A. Barnard, J. Cronje, D. de Vlieger, S. Marx and H. C. M. Vosloo, *J. Memb. Sci.*, 2010, **353**, 70–77.

43 J. T. Scarpello, D. Nair, L. M. Freitas dos Santos, L. S. White and A. G. Livingston, *J. Memb. Sci.*, 2002, **203**, 71–85.

44 A. Keraani, T. Renouard, C. Fischmeister and C. Bruneau, *ChemSusChem*, 2008, **1**, 927–933.

45 K. de Smet, S. Aerts, E. Ceulemans, I. F. J. Vankelecom and P. A. Jacobs, *Chem. Commun.*, 2001, 597–598.

46 M. Priske, K. Wiese, A. Drews, M. Kraume and G. Baumgarten, *J. Memb. Sci.*, 2010, **360**, 77–83.

47 A. Lejeune, M. Rabiller-Baudry and T. Renouard, *Sep. Purif. Technol.*, 2018, **195**, 339–357.

48 P. Schmidt, E. Laura, P. Lutze and A. Górak, *Chem. Eng. Sci.*, 2014, **115**, 115–126.

49 G. Giffels, J. Beliczey, M. Felder and U. Kragl, *Tetrahedron: Asymmetry*, 1998, **9**, 691–696.

50 N. Brinkmann, D. Giebel, G. Lohmer, M. T. Reetz and U. Kragl, *J. Catal.*, 1999, **168**, 163–168.

51 J. Fang, R. Jana, J. A. Tunge and B. Subramaniam, *Appl. Catal. A Gen.*, 2011, **393**, 294–301.

52 P. J. Deuss, R. Denheeten, W. Laan and P. C. J. Kamer, *Chem. Eur. J.*, 2011, **17**, 4680–4698.

53 M. H. Pørez-Temprano, J. A. Casares and P. Espinet, *Chem. Eur. J.*, 2012, **18**, 1864–1884.

54 D. Astruc and F. Chardac, *Chem. Rev.*, 2001, **101**, 2991–3023.

55 E. B. Hager, B. C. E. Makhubela and G. S. Smith, *Dalton Trans.*, 2012, **41**, 13927–35.

56 S. Siangwata, S. Chulu, C. L. Oliver and G. S. Smith, *Appl. Organomet. Chem.*, 2017, **31**, e3593.

57 S. Siangwata, N. Baartzes, B. C. E. Makhubela and G. S. Smith, *J. Organomet. Chem.*, 2015, **796**, 26–32.

58 L. C. Matsinha, S. F. Mapolie and G. S. Smith, *Dalton Trans.*, 2015, **44**, 1240–1248.

59 R. M. Deshpande, Purwanto, H. Delmas and R. V. Chaudhari, *Ind. Eng. Chem. Res.*, 1996, **35**, 3927–3933.

60 C. Williams, M. Ferreira, E. Monflier, S. F. Mapolie and G. S. Smith, *Dalton Trans.*, 2018, **47**, 9418–9429.

61 M. Vilches-Herrera, L. Domke and A. Börner, *ACS Catal.*, 2014, **4**, 1706–1724.

62 J. October and S. F. Mapolie, *J. Organomet. Chem.*, 2017, **840**, 1–10.

63 L. Le Goanvic, J. Couturier, J. Dubois and J. Carpentier, *Catalysts*, 2018, **8**, 1–22.

64 Y. Yan, X. Zhang and X. Zhang, *J. Am. Chem. Soc.*, 2006, **128**, 16058–16061.

65 M. Haumann, H. Koch, P. Hugo and R. Schomäcker, *Appl. Catal. A Gen.*, 2002, **236**, 173–178.

66 N. C. Antonels, J. R. Moss and G. S. Smith, *J. Organomet. Chem.*, 2011, **696**, 2003–2007.

67 M. M. Diwakar, R. M. Deshpande and R. V. Chaudhari, *J. Mol. Catal. A Chem.*, 2005, **232**, 179–186.

68 B. M. Bhanage, S. S. Divekar, R. M. Deshpande and R. V. Chaudhari, *J. Mol. Catal. A Chem.*, 1997, **115**, 247–257.

69 M. S. Shaharun, B. K. Dutta, H. Mukhtar and S. Maitra, *Chem. Eng. Sci.*, 2010, **65**, 273–281.

70 R. M. Deshpande, Purwanto, H. Delmas and R. V. Chaudhari, *Ind. Eng. Chem. Res.*, 1996, **35**, 3927–3933.

71 R. M. Deshpande, A. A. Kelkar, A. Sharma, C. Julcour-Lebigue and H. Delmas, *Chem.*

Eng. Sci., 2011, **66**, 1631–1639.

72 A. C. J. Koeken, L. J. P. van den Broeke, B. J. Deelman and J. T. F. Keurentjes, *J. Mol. Catal. A Chem.*, 2011, **346**, 1–11.

73 V. K. Srivastava, S. K. Sharma, R. S. Shukla, N. Subrahmanyam and R. V. Jasra, *Ind. Eng. Chem. Res.*, 2005, **44**, 1764–1771.

74 M. Rosales, O. Soto, B. González, I. Pacheco and P. J. Baricelli, *Transit. Met. Chem.*, 2018, **43**, 451–461.

75 N. C. C. Breckwoldt, N. J. Goosen, H. C. M. Vosloo and P. van der Gryp, *React. Chem. Eng.*, 2019, **4**, 695–704.

76 S. Güven, B. Hamers, R. Franke, M. Priske, M. Becker and D. Vogt, *Catal. Sci. Technol.*, 2014, **4**, 524–530.

77 R. V. Chaudhari, A. Seayad and S. Jayasree, *Catal. Today*, 2001, **66**, 371–380.

Chapter 4

Synthesis and characterisation of water-soluble aryl ether-based mononuclear and trinuclear salicylaldimine Rh(I)-complexes

This Chapter forms part of a publication titled "*Aqueous olefin hydroformylation using water-soluble mono- and trinuclear N,O-chelate rhodium(I)-aryl ether precatalysts*", cited as:
S. Siangwata, N. J. Goosen and G. S. Smith., *Appl. Catal. A Gen*. 2020, **603**, 117736.

4.1 Introduction

The successful synthesis of water-soluble ligands forms an attractive approach towards the drive to effectively conduct reactions in non-hazardous solvents (for example, water), a part of the values outlined in the Green Chemistry Principles.[1] Such an approach underscores the importance of designing tailor-made structures that are fit-for-purpose and will be able to sustain subsequent reaction conditions, such as when intended for catalysis using various reaction conditions of temperature, pressure, and often a non-conventional choice of solvent.[2]

Schiff-base ligands have proven to be versatile structures that have been used for the synthesis of coordination compounds designed for catalytic applications.[3–8] Our group has in the past reported good catalytic properties from catalyst precursors bearing Schiff base ligands, partly ascribed to the good stability of the ligands in the solvents of choice under the reported reaction conditions (Scheme 4.1 overleaf).[9–15] Modification of Schiff-base bearing structures with hydrophilic substituents enables solubilisation of the ligands and consequently complexes in aqueous media, enabling the retention of the catalyst precursors in the eco-friendly aqueous media.[16–22] However, appending water-soluble substituents such as the sulfonate group is confounded with sensitivity of other functional groups to the often-harsh conditions required to successfully conduct the reaction, necessitating protection of the sensitive functionalities prior to sulfonation. When successfully carried out, the water-soluble structures can be extended to large macromolecular structures such as dendrimers.[17,23–25]

Creating a balance between the water-solubilising groups and the hydrophobic component of a dendrimer is the most underlying factor towards the design and synthesis of large

macromolecular structures that can be effectively retained in aqueous media. This can be achieved by systematically increasing the number of water-solubilising moieties, for example from monomeric to trimeric structures. This approach is attractive in applications such as catalysis, owing to the dual benefits realised from such systems through alignment with the Green Chemistry Principles,[26,27] as well as through the often-improved bio-inspired overall reactivity of the resultant multinuclear structures.[28–32]

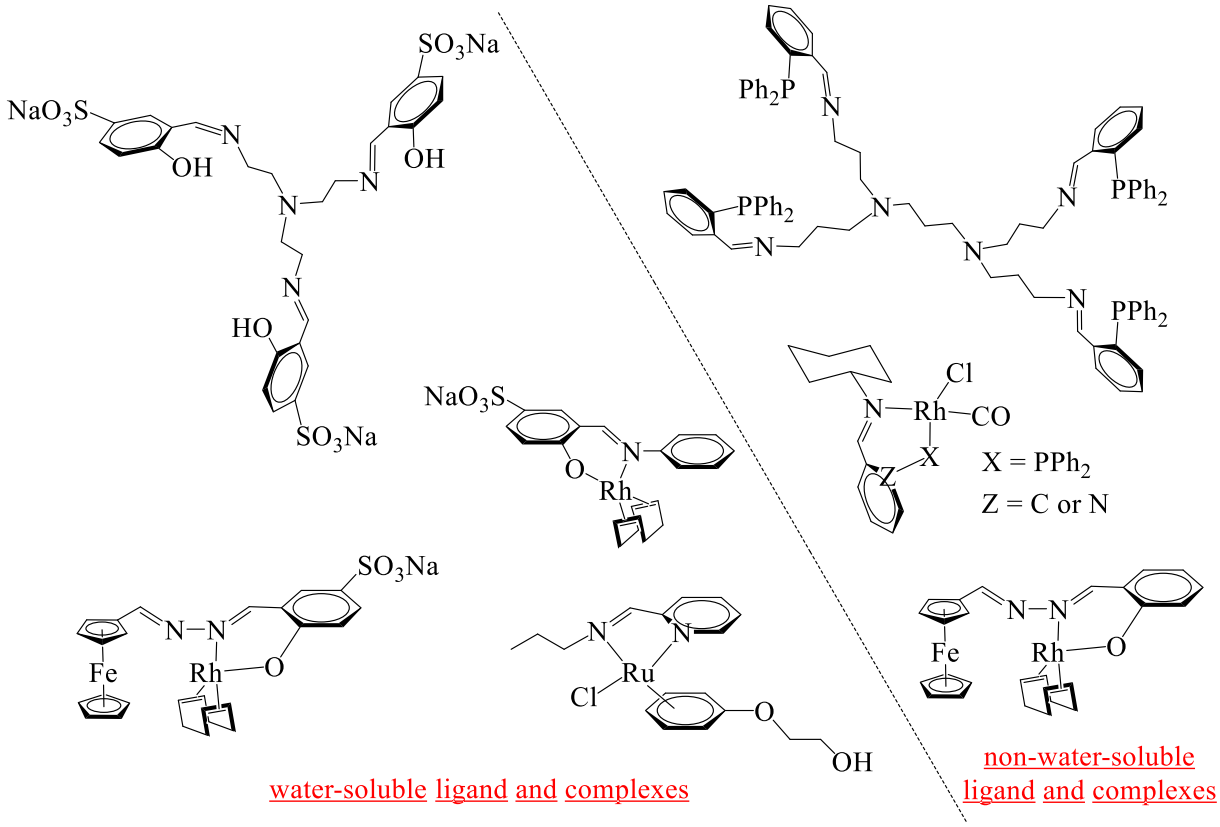

Scheme 4.1 Selected examples of water-soluble and non-water-soluble Schiff base ligands and complexes from our group.[9,12,14,17,19–21]

The flexibility or rigidity of the supporting core in multinuclear dendritic structures forms a critical component in the design of dendritic structures. A rigid core can impart stability in the general architecture of the dendrimer, with the possibility of influencing the product distribution of catalytic transformations. Aryl ether scaffolds bearing a rigid core of 1,1,1-tris(4-hydroxyphenyl)ethane (THPE) have been reported in the literature, synthesised *via* both convergent and divergent dendrimer synthesis approach, and etherification through the Williamson ether synthetic route.[33–36] The potential benefit that comes with the successful preparation and application of water-soluble multinuclear structures which follow similar facile

synthetic strategies cannot be overemphasised.[37] Therefore, in this chapter, we report on the preparation of water-soluble Schiff base ligands and the mono- and trinuclear aryl ether-based complexes of rhodium anchored to a rigid THPE core. To the best of our knowledge, there is no available literature on the synthesis of water-soluble salicylaldimine aryl ether-bearing ligands and their rhodium complexes.

4.2 Synthesis and characterisation of monosodium 5-sulfonato salicylaldehyde (4.1)

To prepare the water-soluble sulfonated component of the aryl ether based monomeric and trimeric ligands, we followed a literature procedure based on our previous work (Scheme 4.2),[17] which follows the same mechanism as described in Section 2.1 of Chapter 2. The precursor ligand **4.1** was synthesised following a series of aldehyde group protection, sulfonation and acid-catalysed imine hydrolysis reactions. In the first step (Scheme 4.2), salicylaldehyde was reacted with aniline through a Schiff base condensation reaction, affording *N*-phenyl-salicylaldimine as a yellow crystalline solid, with subsequent sulfonation leading to the water-soluble *N*-phenyl-salicylaldimine. The protection of the aldehyde with aniline prior to sulfonation is necessary as the aldehyde group readily gets protonated in the presence of sulfuric acid to form the undesired oxocarbenium ion. In the sulfonation of the protected aldehyde, the 5-position of the aromatic ring is favoured due to the hydroxyl group directing the sulfonate substituent to the *para* position, which is complemented by the imine group, directing the sulfonate substituent to the *meta* position. Addition of a base to the sulfonated *N*-phenyl-salicylaldimine precursor, followed by acid-catalysed imine hydrolysis affords the sulfonated salicylaldehyde **4.1** in good yield (64%) as a yellow solid.

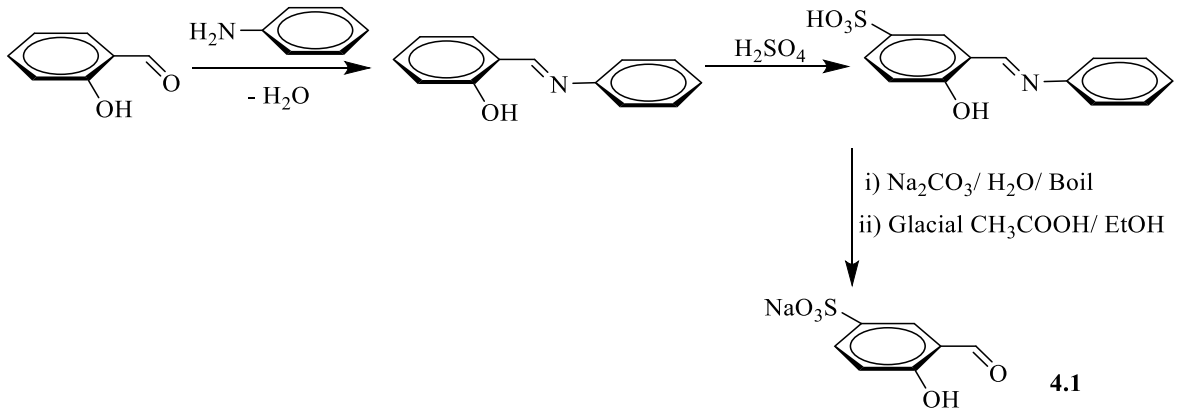

4.1

Scheme 4.2 Preparation of monosodium 5-sulfonato salicylaldehyde **4.1**.

The characterisation data of **4.1** is in good agreement with literature,[17] as observed in the ^{1}H NMR spectrum which displays the signals for the aldehyde and hydroxyl protons at δ = 9.97 and δ = 11.62 respectively, as well as the signals for the aromatic protons appearing in the region δ = 8.20–7.13. The ^{13}C{^{1}H} NMR spectrum shows the carbonyl carbon signal in the characteristic region at δ = 197.20. The infrared (IR) spectrum further corroborates formation of **4.1** with absorption bands at 1659 cm^{-1} and 3432 cm^{-1}, assigned to the ν(C=O) and ν(O–H) stretching frequencies respectively.

Following the successful synthesis of the water-soluble aldehyde, we then set out to prepare the amines for the monomeric and trimeric ligands *via* a series of ^{t}butyloxycarbonyl protection and deprotection steps in the presence of a base (triethylamine, TEA) and acid (trifluoroacetic acid, TFA) respectively.

4.3 Synthesis and characterisation of ^{t}butyl(3-bromopropyl)carbamate (4.2)

Amine protection forms an integral part of synthetic organic chemistry, with the ideal protecting groups being those that can be easily added and removed from the compound of interest. Common protecting groups include fluorenylmethyloxycarbonyl (Fmoc), *p*-nitrophenyl and butyl dicarbonate (Boc) moieties. In the case where Boc moiety is used as the protecting group, the protection mechanism (Scheme 4.3) involves a nucleophilic attack of a carbonyl of the di-^{t}butyl dicarbonate (Boc_2O) site by the amine, producing the ^{t}butyl carbonate as the leaving group. This is followed by triethylamine base (TEA) abstracting a proton from the resultant quaternary ammonium cation to give the protected amine, while the ^{t}butyl carbonate breaks down into carbon dioxide and the relatively more basic ^{t}butoxide, which abstracts a proton from the less basic protonated triethylamine to form ^{t}butanol.

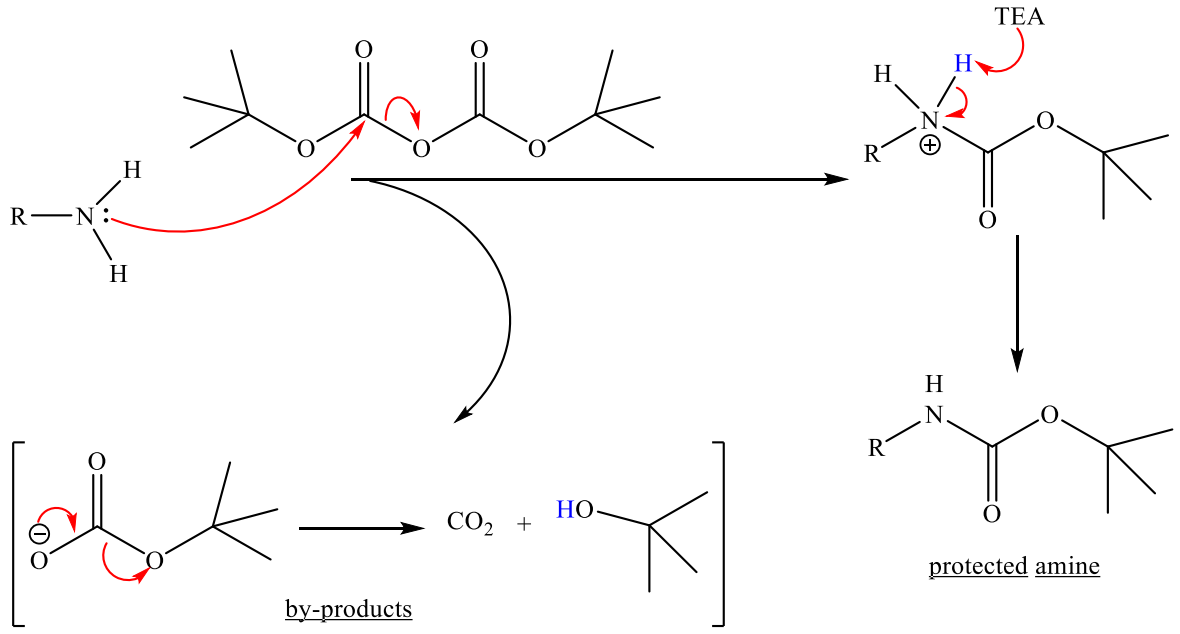

Scheme 4.3 Mechanism for Boc protection of amines.

In this work, the protected amine **4.2** was prepared following available literature procedures,[38] from the reaction of 3-bromopropylamine hydrobromide salt with the base triethylamine, and the subsequent reaction of the free secondary amine with the protecting group di-^{t}butyl dicarbamate $(Boc)_2O$ (Scheme 4.4). The product was isolated in good yield (96%) as a colourless oil from excess unreacted di-^{t}butyl dicarbamate using azeotropic distillation with methanol.

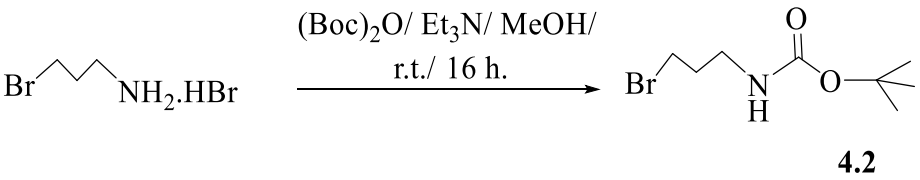

Scheme 4.4 Synthesis of ^{t}butyl(3-bromopropyl)carbamate (**4.2**).

The spectroscopic characterisation data is in good agreement with literature,[38] showing a broad signal integrating for one proton at δ = 4.65, assigned to the 2^o amine proton (H_4) in the ^{1}H NMR spectrum of **4.2** (Figure 4.1). The diagnostic signal for the Boc moiety is observed upfield as a singlet at δ = 1.44 (H_1) integrating for the appropriate number of protons. The signals for the methylene protons (H_7, H_6, H_5) are observed with the expected multiplicity (triplet, quintet and quartet respectively) and integrate for the appropriate number of protons. The $^{13}C\{^1H\}$

NMR spectrum shows the diagnostic carbon signal (C=O) in the characteristic region at δ = 156.1. The infrared (IR) spectrum further substantiates protection of the 1° amine to the 2° amine in **4.2** through the absorption bands at 3378 cm^{-1} and 1684 cm^{-1} assigned to the ν(N–H) and ν(C=O) stretching frequencies.

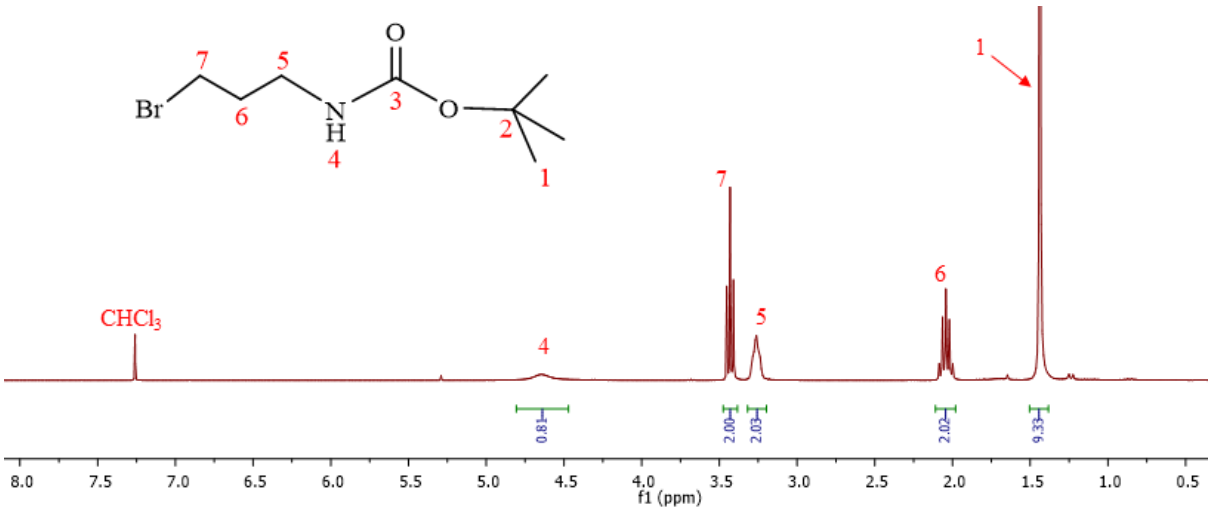

Figure 4.1 ^{1}H NMR ($CDCl_3$**)** spectrum for ^{t}butyl(3-bromopropyl)carbamate (**4.2**).

The 2° amine **4.2** forms the building block for our monomeric and trimeric ligands, through etherification with the respective aryl alcohols and subsequent deprotection to regenerate the 1° amine in **4.5** and **4.6**, as described in the following section.

4.4 Synthesis and characterisation of 3-phenoxypropylamine (4.5) and 1,1,1-tris(4-phenoxymethyl)ethane-propylamine (4.6)

To synthesise the amines **4.5** and **4.6**, we first prepared the aryl ether precursors **4.3** and **4.4** bearing the protected amine, and the reactions were conducted *via* Williamson ether synthesis of ^{t}butyl(3-bromopropyl)carbamate **4.2** with either phenol or 1,1,1-tris(4-hydroxyphenyl)ethane respectively (Scheme 4.5). The products were isolated as white solids in good yields (82 % (**4.3**), 84% (**4.4**)).

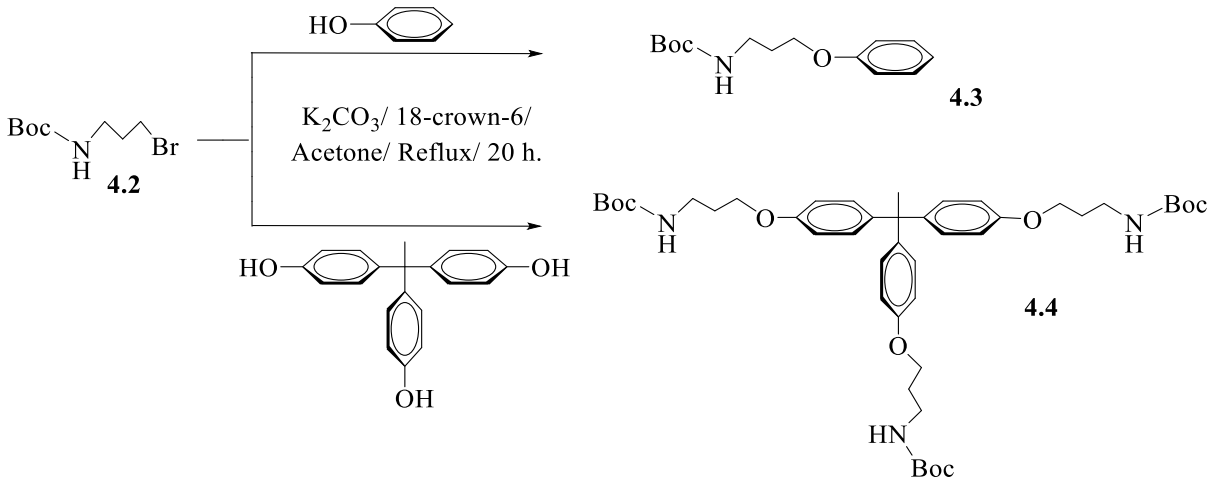

Scheme 4.5 Synthesis of the aryl ether protected amines **4.3** and **4.4**.

The stacked ^{1}H NMR spectra (Figure 4.2 overleaf) accounts for all the expected signals in the structures of **4.3** and **4.4**, with the signals for the aromatic protons observed in their characteristic regions (δ = 7.35–6.75) and integrate for the appropriate number of protons for both compounds. The signals for the amine protons (H_4) are observed as broad signals at ca. 4.70 ppm, and the ^{t}butyl protons (H_1) appear as the expected singlets at δ = 1.47 (**4.3**) and δ = 1.44 (**4.4**) integrating for 9 and 27 protons respectively. Two additional signals are observed in the $^{13}C\{^{1}H\}$ NMR spectrum of **4.4** compared to that of **4.3**, appearing at δ = 50.77 and δ = 30.94 assigned to C_{12} and C_{13} of **4.4** respectively.

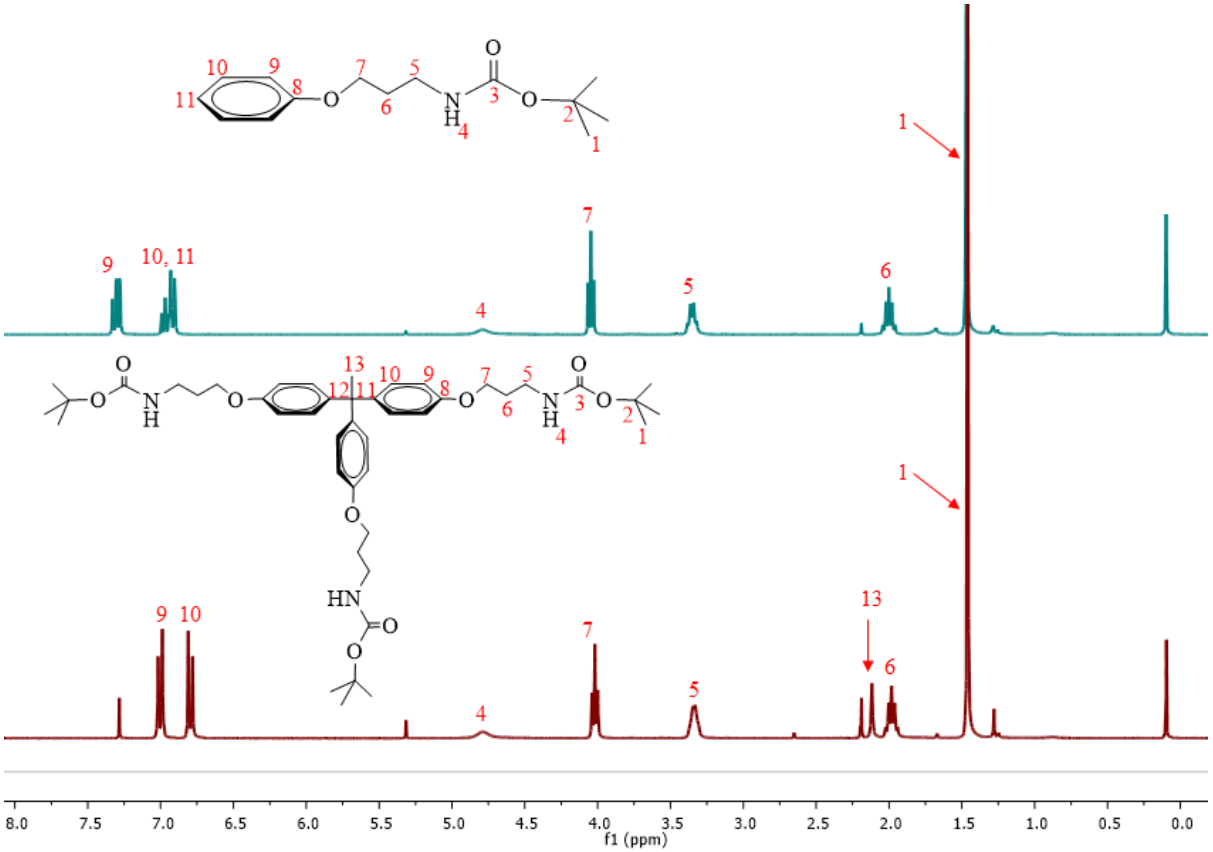

Figure 4.2 Stacked ^{1}H NMR ($CDCl_3$) spectra of **4.3** and **4.4**.

The infrared (IR) spectra further substantiates formation of **4.3** and **4.4** with absorption bands at 3302 cm^{-1} and 1679 cm^{-1}, assigned to the ν(N–H) and ν(C=O) stretching frequencies of **4.3** respectively, and shoulder-bearing broad absorption bands at 3353 cm^{-1} and 1687 cm^{-1} assigned to ν(N–H) and ν(C=O) stretching frequencies of **4.4** respectively. The deprotection of **4.3** and **4.4** was then conducted using TFA in dichloromethane to regenerate the 1^{o} amine in **4.5** and **4.6** respectively (Scheme 4.6).

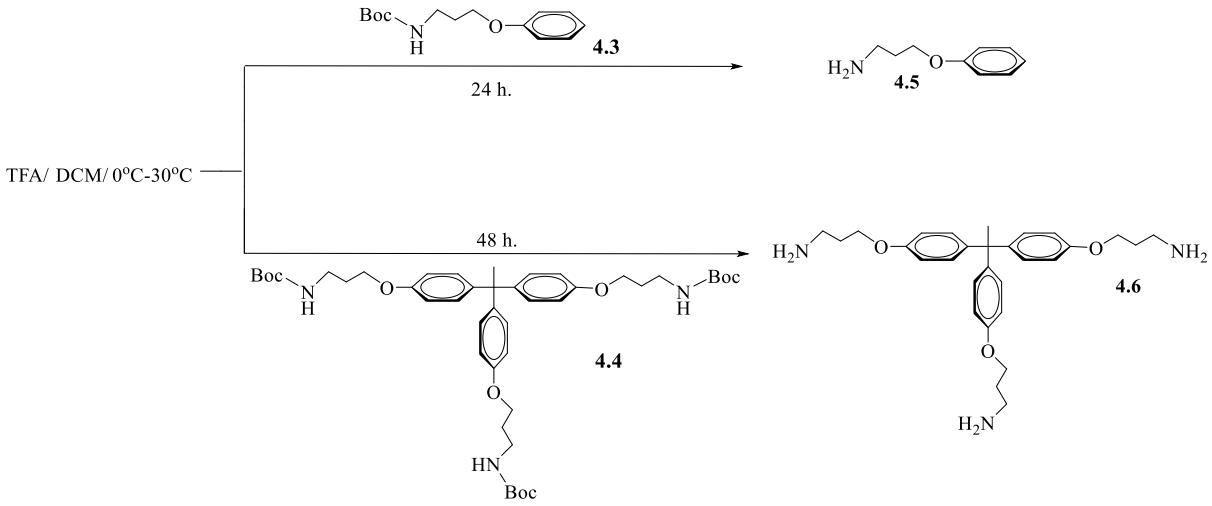

Scheme 4.6 Synthesis of the deprotected aryl ether propylamines **4.5** and **4.6**.

The deprotection mechanism (Scheme 4.7) takes place *via* protonation of the ^{t}butyl carbamate moiety by TFA, and subsequent loss of the ^{t}butyl cation to form carbamic acid. Decarboxylation of the carbamic acid by the TFA anion leads to the free, deprotected amine product.

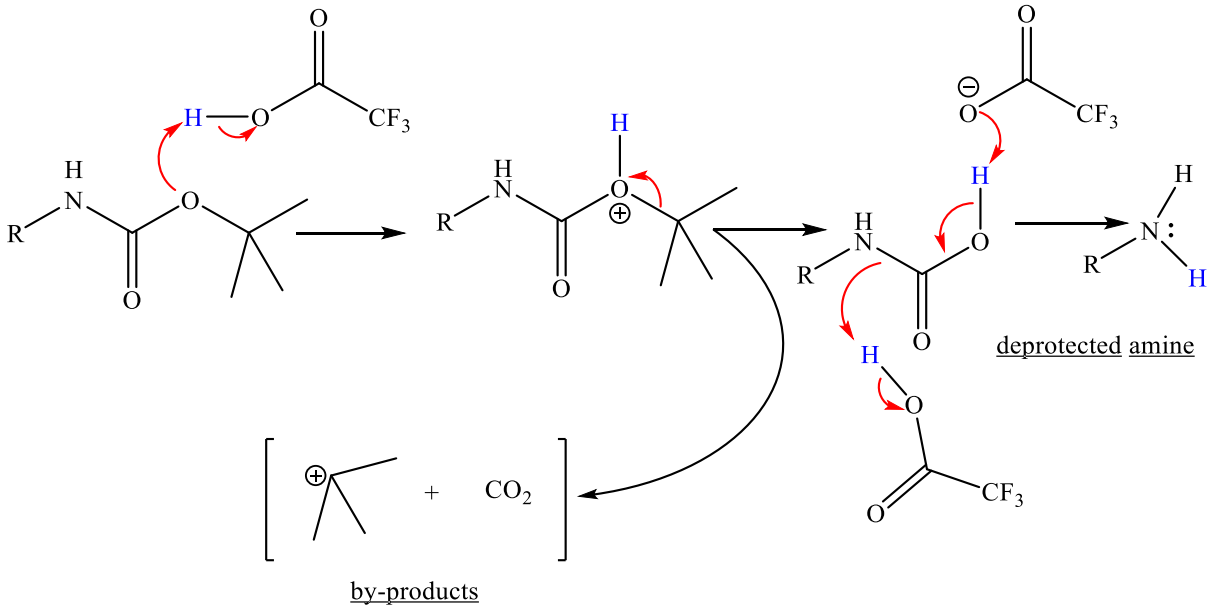

Scheme 4.7 Mechanism for TFA-mediated Boc deprotection of amines.

In this study, the deprotected compounds **4.5** and **4.6** were isolated in moderate yields (71% (**4.5**), 74% (**4.6**)) as yellow and clear oils respectively. Successful regeneration of the 1° amine is evidenced in the stacked ^{1}H NMR spectra (Figure 4.3 overleaf) of **4.5** and **4.6**, which show

the signals for the amine protons (H_1) at δ = 1.55 (**4.5**) and δ = 1.60 (**4.6**) both integrating for the appropriate number of protons. All aromatic protons and carbons appear in their characteristic region in the ^{1}H NMR and $^{13}C\{^{1}H\}$ NMR spectra of both **4.5** and **4.6**. Both ^{1}H NMR and $^{13}C\{^{1}H\}$ NMR sets of spectra do not show the previously observed Boc moiety signals of **4.3** and **4.4**, further corroborating successful deprotection of the amine to form **4.5** and **4.6**. In addition, the infrared (IR) spectra of **4.5** and **4.6** do not show the previously observed absorption bands for the Boc moiety of **4.3** and **4.4**. The spectra show absorption bands at 3319 cm^{-1} and 3038 cm^{-1} for the ν(N–H) stretching frequencies of **4.5**, and 3361 cm^{-1} and 3282 cm^{-1} for the ν(N–H) stretching frequencies of **4.6**.

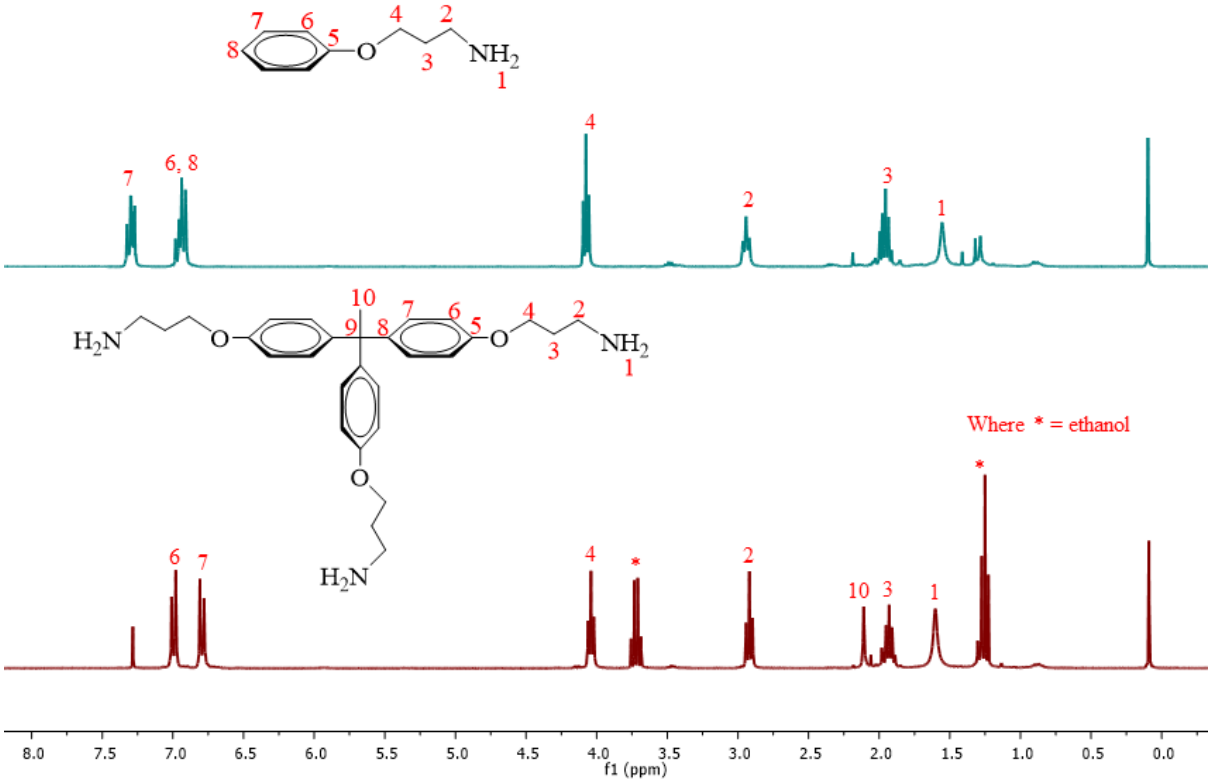

Figure 4.3 Stacked ^{1}H NMR ($CDCl_3$) spectra of deprotected aryl ether propylamines **4.5** and **4.6**.

The amines **4.5** and **4.6** were then reacted with the water-soluble, 5-sulfonato salicylaldehyde (**4.1**) through Schiff base condensation reactions, leading to the water-soluble monomeric and trimeric *N,O*-Schiff base ligands **4.7** and **4.8** respectively, as described in the following section.

4.5 Synthesis and characterisation of water-soluble 5-sulfonato phenoxypropylsalicylaldimine ligand (4.7) and 1,1,1-tris(4-phenoxymethyl)ethane-propyl-5-sulfonato salicylaldimine ligand (4.8)

The new water-soluble monomeric and trimeric ligands were synthesised *via* Schiff base condensation reactions of the respective amines **4.5** and **4.6** with the water-soluble, 5-sulfonato salicylaldehyde (**4.1**) (Scheme 4.8). The ligands were isolated as yellow solids in moderate yields (67% (**4.7**), 72% (**4.8**)) and possess good solubility in water at room temperature (21.4 mg/mL (**4.7**), 19.6 mg/mL (**4.8**)). The moderate yields (> 65%) were ascribed to the reactions not going to completion as evidenced by the presence of unreacted aldehyde and amine when monitored by ^{1}H NMR spectroscopy over long reaction periods of up to 72 hours. The reactions were then optimised at 20 h and the products were isolated after a series of recrystallisation and trituration procedures were conducted.

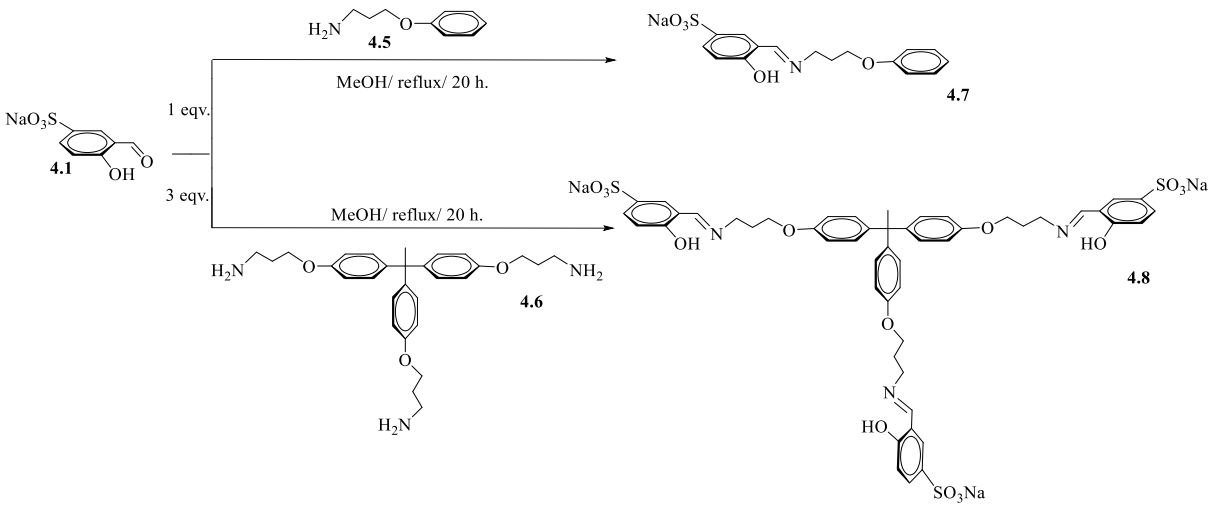

Scheme 4.8 Synthesis of the water-soluble aryl ether mono- and trimeric salicylaldimine ligands **4.7** and **4.8**.

Successful preparation of the Schiff base ligands is observed in the stacked ^{1}H NMR spectra (Figure 4.4), which show the diagnostic signals for the imine protons (H_8) appearing at δ = 8.64 in both **4.7** and **4.8**, and the signals for the hydroxyl protons (H_1) at δ = 13.70 (**4.7**) and δ = 13.64 (**4.8**). The signals for the aromatic protons are observed in their characteristic regions, between δ = 7.73–6.77 for both ligands, and the methylene protons (H_9, H_{10}, H_{11}) are observed with the appropriate multiplicity. Additionally, the ^{1}H NMR spectrum of **4.8** shows the signal for the methyl protons (H_{17}) of the core overlapping with the methylene protons (H_{10}), both integrating for the expected number of protons. All the carbon atoms are accounted for in the

$^{13}C\{^{1}H\}$ NMR spectra, which also show the signals for the imine carbons at the characteristic region for both ligands, appearing at δ = 166.5 (**4.7**) and δ = 166.4 (**4.8**) as further evidence to formation of the imine-based ligands. The infrared (IR) spectra of **4.7** and **4.8** do not show the previously observed absorption bands for the carbonyl stretching frequency of **4.1**, as well as the absorption bands for the amine stretching frequencies of the 1° amines **4.5** and **4.6**. However, the spectra show absorption bands characteristic of the imine stretching frequencies ν(C=N) at 1649 cm^{-1} (**4.7**) and 1637 cm^{-1} (**4.8**) with a shoulder at 1609 cm^{-1} (**4.8**), further corroborating formation of the imine-based ligands. Also observed are absorption bands at 3286 cm^{-1} (**4.7**) and 3337 cm^{-1} (**4.8**) characteristic of the ν(O–H) stretching frequencies. The ESI–MS spectra show peaks associated with the anionic ligands in the absence of the Na ion(s), for $[M]^-$ (**4.7**) in the negative ion-mode at *m/z* = 334.0746 (calcd 334.0749), and $[M + Cl]^-$ observed in the negative ion-mode at *m/z* = 1084.2738 (calcd 1084.6675) for **4.8**.

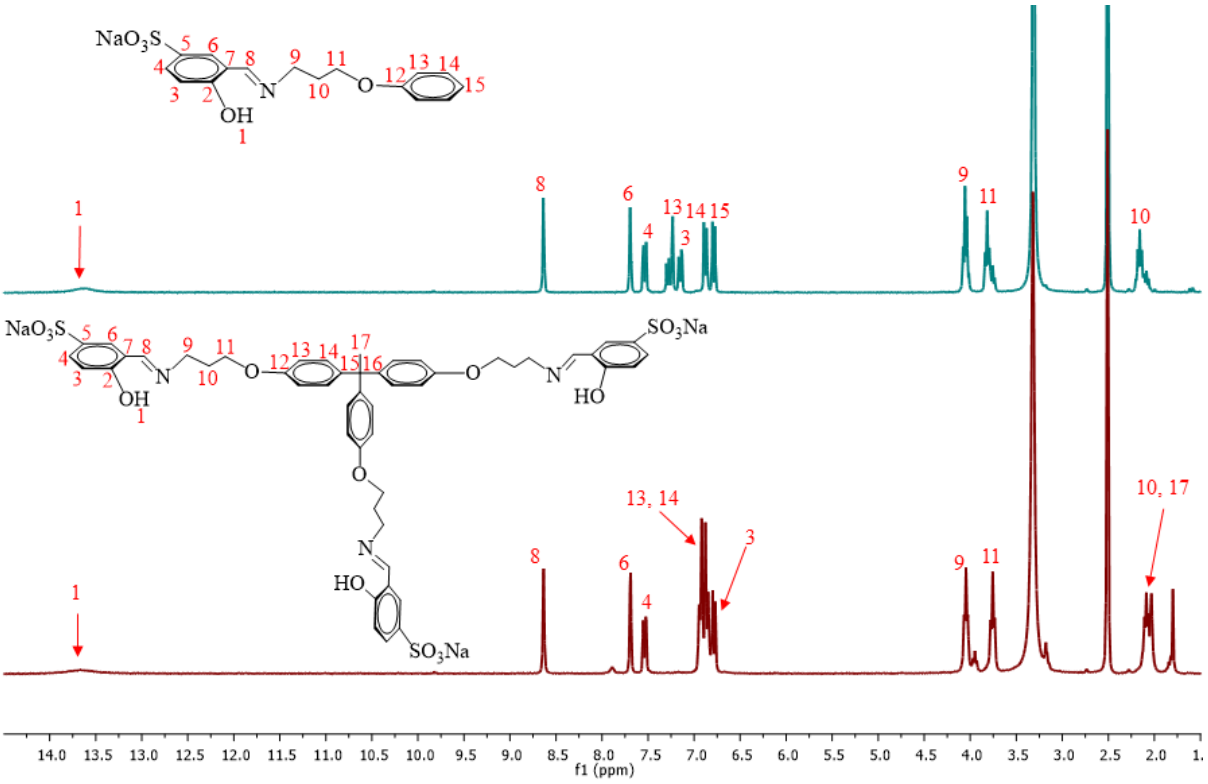

Figure 5.4 Stacked ^{1}H NMR (DMSO-d_6) spectra of water-soluble aryl ether mono- and trimeric salicylaldimine ligands **4.7** and **4.8**.

The good aqueous solubility of both the monomeric (**4.7**) and trimeric (**4.8**) ligands is very attractive for further applications. This ultimately means the ligands can potentially lead to water-soluble coordination compounds, which is attractive from a Green Chemistry viewpoint.

This phenomenon was evaluated in the following section, wherein the preparation and characterisation of the mononuclear and trinuclear complexes is reported.

4.6 Synthesis and characterisation of water-soluble 5-sulfonato phenoxypropylsalicylaldimine Rh(I) complex (4.9) and 1,1,1-tris(4-phenoxymethyl)ethane-propyl-5-sulfonato salicylaldimine Rh(I) complex (4.10)

The new mononuclear (**4.9**) and trinuclear (**4.10**) rhodium(I) complexes were prepared *via* deprotonation of the ligands **4.7** and **4.8** respectively, using NaH as the base, and subsequent complexation with the appropriate molar equivalence of the Rh(I) dimer $[RhCl(COD)]_2$, (COD = 1,5-cyclooctadiene), (Scheme 4.9). Both complexes were isolated as yellow solids in good yields (94% (**4.9**), 98% (**4.10**)) and show appreciably good solubility in water at room temperature (15.7 mg/mL (**4.9**), 8.6 mg/mL (**4.10**)). The reduced aqueous solubility upon complexation is also observed in literature for related compounds,[17,19] and this can be ascribed to the increased hydrophobicity as a result of the cyclooctadiene entity.

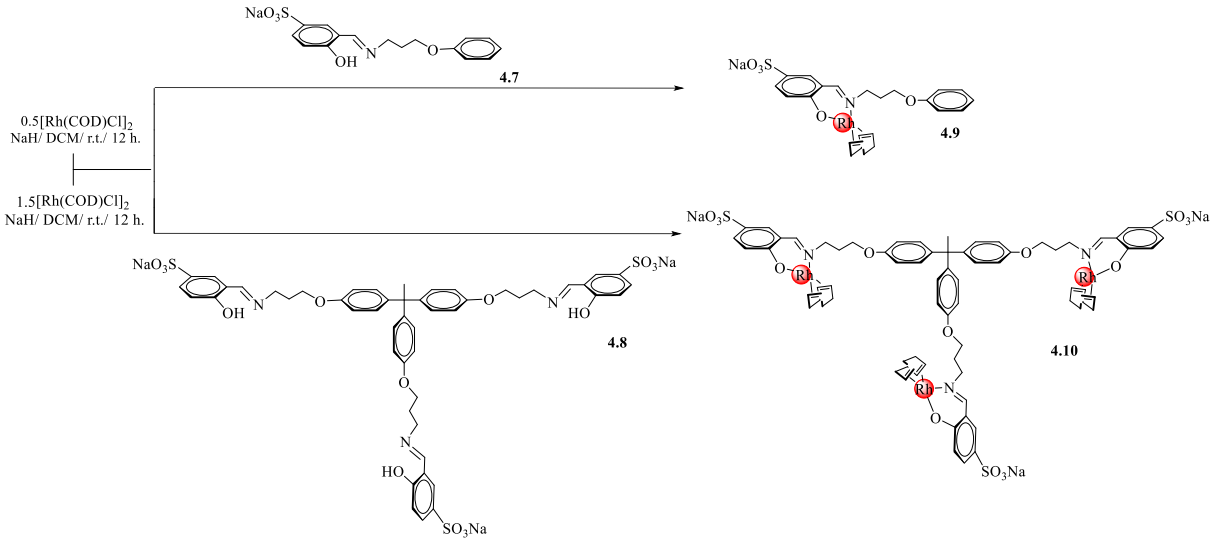

Scheme 4.9 Synthesis of water-soluble aryl ether mono- and trinuclear salicylaldimine-based Rh(I) complexes **4.9** and **4.10**.

Evidence of successful coordination of the ligands (**4.7** and **4.8**) to the Rh-metal centre is given by the upfield shift of the signal for the imine protons, from δ = 8.64 (**4.7** and **4.8**) to δ = 8.28 (**4.9**) and δ = 8.29 (**4.10**) in the ^{1}H NMR spectra of both complexes (Figures 4.5 and 4.6)

characteristic of the synergistic effect involving M-to-L pi-donation and L-to-M sigma donation. Both spectra do not show the signal for the hydroxyl protons previously observed in **4.7** and **4.8**, indicative of successful deprotonation of the ligands and subsequent ligand coordination to the metal centre in a bidentate manner. The signals for the protons of the cyclooctadiene moiety appear as broadened signals and integrate for the appropriate number of protons in both the mononuclear (**4.9**) and trinuclear (**4.10**) complexes. The $^{13}C\{^{1}H\}$ NMR spectra show the olefinic carbon atoms of the cyclooctadiene moiety as doublets, attributed to coupling to the rhodium metal centre (*trans* to N: $^{1}J_{Rh-C}$ = 12 Hz, and *trans* to O: $^{1}J_{Rh-C}$ = 14 Hz) and correlate well with those in literature for related (η^2:η^2–COD)-Rh–Schiff base complexes.[17,39] Successful deprotonation of the hydroxyl proton for chelation is also shown in the infrared spectra of both complexes, which do not show the ν(O–H) stretching frequencies previously observed in the ligands. The infrared spectra of both complexes also show shifts of the imine absorption bands, from 1649 cm^{-1} in the monomeric ligand (**4.7**), to 1606 cm^{-1} in the mononuclear complex (**4.9**). On the other hand, the shifts for the tris-analogues are from 1637 cm^{-1} (shoulder:1609 cm^{-1}) to 1605 cm^{-1} (shoulder: 1586 cm^{-1}) for **4.8** and **4.10** respectively. The observed shifts to lower wave numbers upon coordination of the ligands to the metal substantiates the coordination of the imine nitrogen, as has been reported for similar compounds in the literature.[10,17,19,21] The ESI–MS spectra of the complexes show a peak for $[M + Cl]^-$ in the negative ion-mode at *m/z* = 578.9556 (calcd 579.5195) for **4.9**, while a peak for $[M + 2H]^{2+}$ is observed in the positive ion-mode at *m/z* = 863.5983 (calcd 863.5079) for **4.10**.

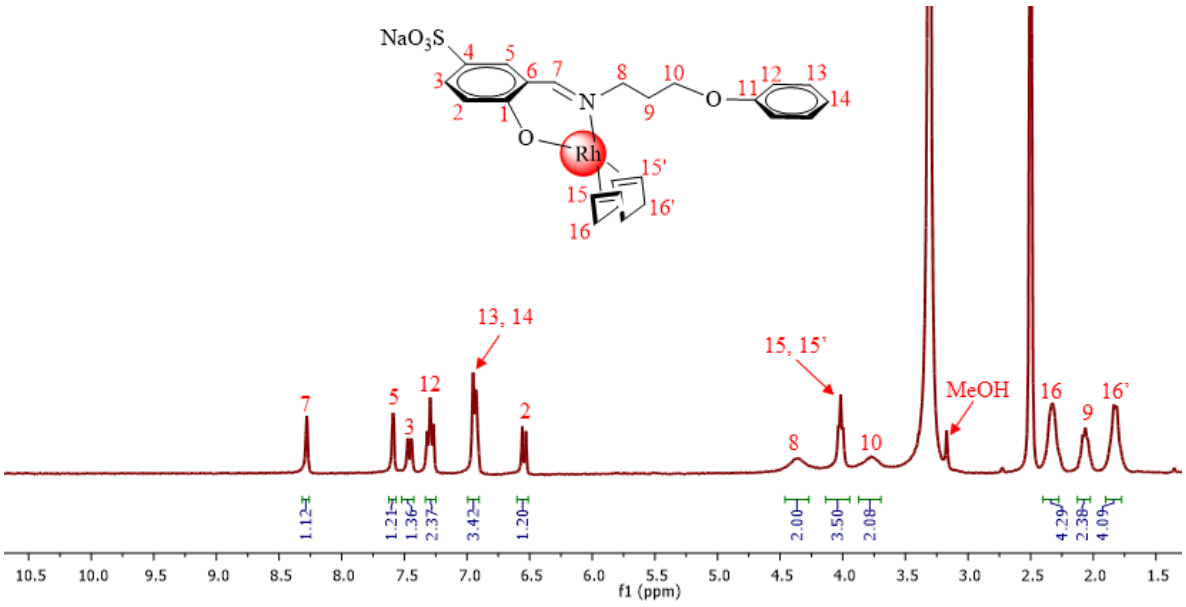

Figure 4.5 ^{1}H NMR (DMSO-d_6) spectrum of the water-soluble mononuclear complex **4.9**.

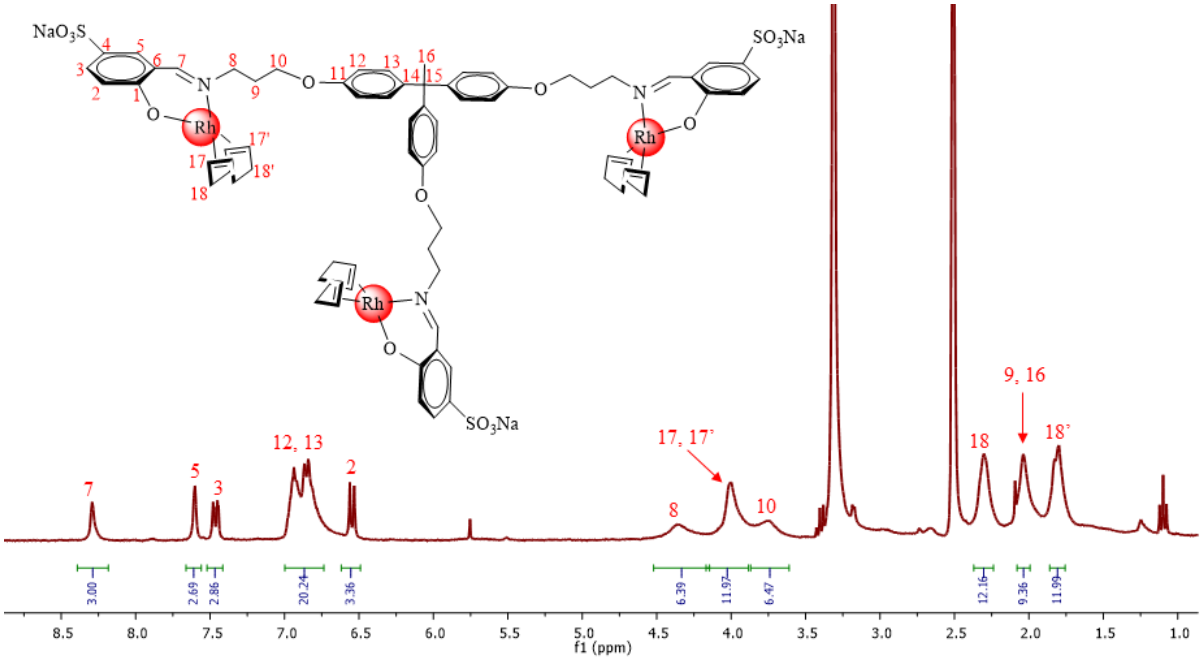

Figure 4.6 ^{1}H NMR (DMSO-d_6) spectrum of the water-soluble trinuclear complex **4.10**.

The successful synthesis of the water-soluble mononuclear complex **4.9** and the trinuclear congener **4.10** opens avenues to be explored through increasing the nuclearity of the dendrimers with a systematic increase in the water-solubilising substituents, leading to the potential application of such structures in aqueous catalysis.

4.7 Summary

In this work, we have reported on the synthesis of two new water-soluble salicylaldimine aryl ether Rh(I) mononuclear and trinuclear complexes. To successfully append the water-solubilising substituent to the ligand precursors, it was prudent to first protect the aldehyde prior to sulfonation. This was achieved by the reaction of salicylaldehyde with aniline through a Schiff base condensation reaction to afford the imine intermediate which then underwent sulfonation with concentrated sulfuric acid. The sodium salt of the resultant sulfonated intermediate was then prepared, followed by the acid-catalysed imine hydrolyses (deprotection) to regenerate the aldehyde as the water-soluble precursor **4.1**. The amines for the monomeric and trimeric ligand synthesis were prepared *via* a series of Boc-protection, etherification and Boc-deprotection synthetic strategies. The choice of Boc as the protecting group was ideal owing to the ease of addition to the amines at ambient temperatures, as well as the facile removal thereafter, with less complicated end-product purification steps. All three

procedures (Boc-protection, Williamson ether synthesis and Boc-deprotection) were conducted successfully and afforded the monomeric (**4.5**) and trimeric amines (**4.6**) in appreciably good yields (> 70%). The synthesis of the rigid trimeric amine-bearing core (**4.6**) was necessary to provide a platform to systematically anchor the water-solubilising component of the coordination compound possessing increased multinuclearity. The water-soluble precursor **4.1** was then anchored on **4.5** and **4.6** *via* Schiff base condensation reactions to afford the water-soluble monomeric (21.4 mg/mL) and trimeric (19.6 mg/mL) salicylaldimine-based aryl ether ligands **4.7** and **4.8** respectively. The trimeric ligand **4.8** shows slightly reduced solubility to the monomeric congener owing to the hydrophobicity imparted by the triaryl core of **4.8**. The ligands were then reacted with the appropriate molar equivalence of the Rh(I) dimer $[RhCl(COD)]_2$ in the presence of NaH to afford the products as yellow solids after recrystallisation in methanol. The complexes were obtained in good yields (> 95%) and show appreciably good solubility in water at room temperature (15.7 mg/mL (**4.9**), 8.6 mg/mL (**4.10**)).

4.8 References

1 P. T. Anastas and J. C. Warner, *The 12 Principles of Green Chemistry*, Oxford University Press, New York, 1998.

2 M.-O. Simon and C.-J. Li, *Chem. Soc. Rev.*, 2012, **41**, 1415–1427.

3 V. K. Rao, S. S. Reddy, B. S. Krishna and K. R. Mohan, *Green Chem. Lett. Rev.*, 2010, **3**, 217–223.

4 K. C. Gupta and A. K. Sutar, *Coord. Chem. Rev.*, 2008, **252**, 1420–1450.

5 O. S. Taskin, S. Dadashi-Silab, B. Kiskan, J. Weber and Y. Yagci, *Macromol. Chem. Phys.*, 2015, **216**, 1746–1753.

6 S. M. Wilkinson, T. M. Sheedy and E. J. New, *J. Chem. Educ.*, 2016, **93**, 351–354.

7 W. Qin, S. Long, M. Panunzio and S. Biondi, *Molecules*, 2013, **18**, 12264–12289.

8 A. M. Abu-dief and I. M. A. Mohamed, *Beni-Suef Univ. J. Basic Appl. Sci.*, 2015, **4**, 119–133.

9 S. Siangwata, S. Chulu, C. L. Oliver and G. S. Smith, *Appl. Organomet. Chem.*, 2017, **31**, e3593.

10 L. Maqeda, B. C. E. Makhubela and G. S. Smith, *Polyhedron*, 2015, **91**, 128–135.

11 N. C. Antonels, J. R. Moss and G. S. Smith, *J. Organomet. Chem.*, 2011, **696**, 2003–2007.

12 N. C. Antonels, B. Therrien, J. R. Moss and G. S. Smith, *Inorg. Chem. Commun.*, 2009, **12**, 716–719.

13 B. C. E. Makhubela, A. M. Jardine, G. Westman and G. S. Smith, *Dalton Trans.*, 2012, **41**, 10715–10723.

14 N. C. C. Breckwoldt, N. J. Goosen, P. Van der Gryp and G. S. Smith, *Appl. Catal. A Gen.*, 2019, **573**, 49–55.

15 B. C. E. Makhubela, A. Jardine and G. S. Smith, *Green Chem.*, 2012, **14**, 338–347.

16 P. J. Dyson, D. J. Ellis and T. Welton, *Platin. Met. Rev.*, 1998, **42**, 135–140.

17 E. B. Hager, B. C. E. Makhubela and G. S. Smith, *Dalton Trans.*, 2012, **41**, 13927–35.

18 M. Dauchy, M. Ferreira, J. Leblond, H. Bricout, S. Tilloy, G. S. Smith and E. Monflier, *Pure Appl. Chem.*, 2018, **90**, 845–855.

19 S. Siangwata, N. Baartzes, B. C. E. Makhubela and G. S. Smith, *J. Organomet. Chem.*, 2015, **796**, 26–32.

20 L. C. Matsinha, P. Malatji, A. T. Hutton, G. A. Venter, S. F. Mapolie and G. S. Smith, *Eur. J. Inorg. Chem.*, 2013, 4318–4328.

21 L. C. Matsinha, S. F. Mapolie and G. S. Smith, *Dalton Trans.*, 2015, **44**, 1240–1248.

22 N. N. Omosun and G. S. Smith, *Eur. J. Inorg. Chem.*, 2019, 2558–2564.

23 E. R. de Jong, Eric Manoury, J.-C. Daran, C.-O. Turrin, J. Chiffre, A. Sournia-Saquet, W. Knoll, J.-P. Majoral and A.-M. Caminade, *J. Organomet. Chem.*, 2012, **718**, 22–30.

24 A. Gong, Q. Fan, Y. Chen, H. Liu, C. Chen and F. Xi, *J. Mol. Catal. A Chem.*, 2000,

159, 225–232.

25 N. Pinault and D. W. Bruce, *Coord. Chem. Rev.*, 2003, **241**, 1–25.

26 P. T. Anastas and J. B. Zimmerman, *Environ. Sci. Technol.*, 2003, **37**, 95–101.

27 R. A. Sheldon, I. Arends and U. Hanefeld, in *Green Chemistry and Catalysis*, Wiley-VCH Verlag GmbH & Co. KGaA, Weinheim, 1st edn., 2007, pp. 1–2.

28 P. Govender, A. K. Renfrew, C. M. Clavel, P. J. Dyson, B. Therrien and G. S. Smith, *Dalton Trans.*, 2011, **40**, 1158–1167.

29 P. Govender, B. Therrien and G. S. Smith, *Eur. J. Inorg. Chem.*, 2012, 2853–2862.

30 R. Payne, P. Govender, B. Therrien, C. M. Clavel, P. J. Dyson and G. S. Smith, *J. Organomet. Chem.*, 2013, **729**, 20–27.

31 I. Bratko and M. Gómez, *Dalton Trans.*, 2013, **42**, 10664–81.

32 P. J. Deuss, R. Denheeten, W. Laan and P. C. J. Kamer, *Chem. Eur. J.*, 2011, **17**, 4680–4698.

33 P. Antoni, D. Nyström, C. J. Hawker, A. Hult and M. Malkoch, *Chem. Commun.*, 2007, 2249–2251.

34 C. J. Hawker and J. M. J. Fréchet, *J. Am. Chem. Soc.*, 1990, **112**, 7638–7647.

35 Y. Liao and J. R. Moss, *Organometallics*, 2003, **15**, 4307–4316.

36 I. J. Mavunkal, J. R. Moss and J. Bacsa, *J. Organomet. Chem.*, 2000, **594**, 361–368.

37 C. J. Hawker, K. L. Wooley and J. M. J. Fréchet, *J. Chem. Soc. Perkin Trans.*, 1993, 1287–1297.

38 H. Li, M. A. Hao, L. Wang, W. Liang and K. Chen, *Org. Prep. Proced. Int.*, 2009, **41**, 301–307.

39 C. Janiak, A.-C. Chamayou, A. K. M. R. Uddin, M. Uddin, S. K. Hagen and M. Enamullah, *Dalton Trans.*, 2009, **19**, 3698–3709.

Chapter 5

Water-soluble mono- and trinuclear *N,O*-chelate Rh(I)-aryl ether complexes for olefin hydroformylation

This Chapter forms part of a publication titled "*Aqueous olefin hydroformylation using water-soluble mono- and trinuclear N,O-chelate rhodium(I)-aryl ether precatalysts*", cited as:
S. Siangwata, N. J. Goosen and G. S. Smith., *Appl. Catal. A Gen*. 2020, **603**, 117736.

5.1 Introduction

The discovery of hydroformylation by Otto Roelen in 1938 marked a turning point in the history of homogeneous catalysis.[1,2] The olefin-to-aldehydes homogeneous transformation (Scheme 5.1) has developed to become the largest homogeneous transition metal complex-catalysed reaction in industry, initially producing only 10 000 tonnes of aldehydes per annum in the 1950s, to a current approximate of 10 million tonnes of aldehydes per annum.[3–7] The significance of this reaction cannot be over emphasised, being the backbone to the supply of a wide range of products such as plasticisers, fragrance, agrochemicals, pharmaceuticals and detergents.[8,9]

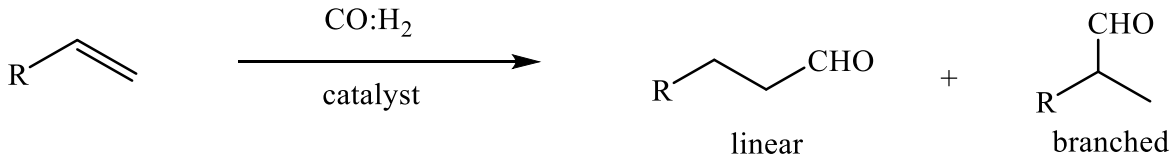

Scheme 5.1 The hydroformylation reaction.

In view of the wide product range that emanates from the downstream transformation of the aldehydes, it is prudent to conduct the hydroformylation reaction in a sustainable and a circular economy-based environment. Such an approach stems from the need to beneficiate the principal metal of choice for hydroformylation (rhodium), which is part of the rare, fast-depleting and relatively expensive Platinum Group Metals (PGMs).[10] Investigating value-adding strategies may help circumvent the major drawback of homogeneous catalysis, mainly being complications in catalyst separation from the substrate for reuse.[11–17] The recovery of homogeneous catalysts through biphasic means has been explored, in efforts to bridge the

properties of homogeneous catalysis (good selectivity and moderate working temperature) with heterogeneous catalysis (high reaction rates and the ease of product separation from the reactants).[18–21] Various media have been explored as supports for catalyst immobilisation in biphasic systems, such as fluorous – organic,[22–29] supercritical carbon dioxide – ionic liquids,[30–37] and the predominantly applied aqueous – organic biphasic approach.[38–41]

Aqueous biphasic catalysis is a very attractive strategy, mainly due to the use of water which is non-immiscible with most organic solvents, as well as its outstanding properties as an eco-friendly solvent.[42–44] Moreover, water is relatively cheap, readily accessible, odourless, non-flammable and non-toxic, highly polar and a good solvent for many gases. The pioneering example of water being used at an industrial scale as a reaction medium for biphasic catalysis is exemplified by Ruhrchemie/Rhône-Poulenc in the hydroformylation of propylene to butanal using the sulfonated water-soluble Rh(I)-organometallic complex $[Rh(H)(CO)(TPPTS)_3]$.[45–47] Using this approach, the catalyst is immobilised in the aqueous phase due to the sulfonated ligands, whereas the substrate is in the organic phase (Figure 5.1). The technique allows for efficient heterogenization of the catalyst with respect to the reactants and products. However, since the reaction takes place at the interface of the two phases, this approach has been limited to short chain olefins, owing to the poor solubility of longer chain olefins (> C5) in water.[48–51] As a result, mass transfer limitations pose an economic threat due to low reaction rates. Moreover, catalyst leaching from the aqueous layer to the organic layer has been a major challenge in designing catalysts that can fully remain immobilised throughout repetitive usage of the aqueous phase.[52–55] The prevention of metal leaching to the product is vital for the downstream products, especially agrochemicals as well as pharmaceutical end-products, which undergo strict product composition analysis. Therefore, the strategic design of highly active, versatile, robust and reusable catalysts is of paramount importance in homogeneous catalysis.

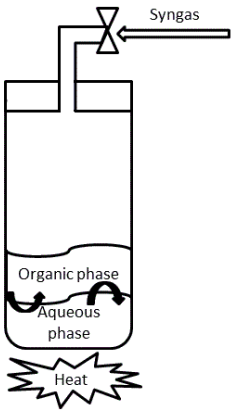

Figure 5.1 Illustrating aqueous biphasic catalysis

The application of highly water-soluble structures that are anchored to rigid supports and possessing multiple active sites may open avenues aimed at curbing the unwanted major catalyst loss *via* leaching, while beneficiating the metal through good catalytic performance over multiple usages. In this chapter, we discuss the evaluation of a water-soluble mononuclear and a low generation metallodendritic complex of Rh(I) as catalyst precursors in the hydroformylation of a linear α-olefin (1-octene), and an aryl substituted olefin (styrene).

5.2 Results and discussion

5.2.1 Preliminary hydroformylation screening using precatalyst 4.9

Preliminary hydroformylation experiments were performed using the model water-soluble mononuclear catalyst precursor **4.9** (Figure 5.2), and 1-octene as the model substrate. This substrate is a good representation of medium to long chain olefins, which show poor interaction with the catalyst at the aqueous – organic interface, often resulting in poor to moderate transformation. Therefore, the successful transformation of 1-octene would be beneficial towards efforts aimed at efficient hydroformylation of medium-to-long chain olefins.

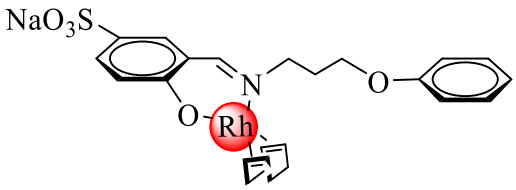

Figure 5.2 Water-soluble salicylaldimine aryl-ether Rh(I)-mononuclear complex **4.9**.

The catalytic reactions were carried out in a 90 ml stainless steel pipe reactor. The conditions of the study (temperature and syngas pressure) were based on our previously reported work on the hydroformylation of 1-octene using analogous Rh(I) catalyst precursors bearing *N*,*O*-bidentate ligands.[55–57] In a typical experiment, the water-soluble catalyst precursor **4.9** (1.63 mg) ($H_2O_{solubility/25°C}$ = 15.7 mg/mL) was dissolved in distilled water (5 mL) at a metal loading of 2.87×10^{-3} mmol and metal-to-substrate ratio (Rh : 1-octene) of 1 : 2500. This was charged into 90 mL stainless steel pipe reactors, followed by 1-octene (805 mg, 7.175 mmol) and the internal standard *n*-decane (204 mg, 1.435 mmol) in toluene (5 mL). The reactor was heated to the desired temperature (75 °C, 85 °C, 95 °C, or 105 °C) and then flushed with syngas (CO : H_2, 1:1), and pressurised to the appropriate syngas pressure (30 bar, 40 bar, or 50 bar). Samples

were analysed after 4 h using gas chromatography (GC). Authentic iso-octenes and aldehydes, alcohols and *n*-octane were used to confirm the products.

5.2.1.1 The Effect of Temperature and Pressure on Conversion

The water-soluble catalyst precursor **4.9** was evaluated in the hydroformylation of 1-octene using aqueous-organic biphasic media, by varying the temperature and syngas pressure (75–105 °C, and 30–50 bar respectively) at a fixed time of 4 h (Figure 5.3). Under these conditions, near-quantitative conversion of the substrate was attained, indicative of the presence of good interfacial interaction between the catalytic active species and the substrate.

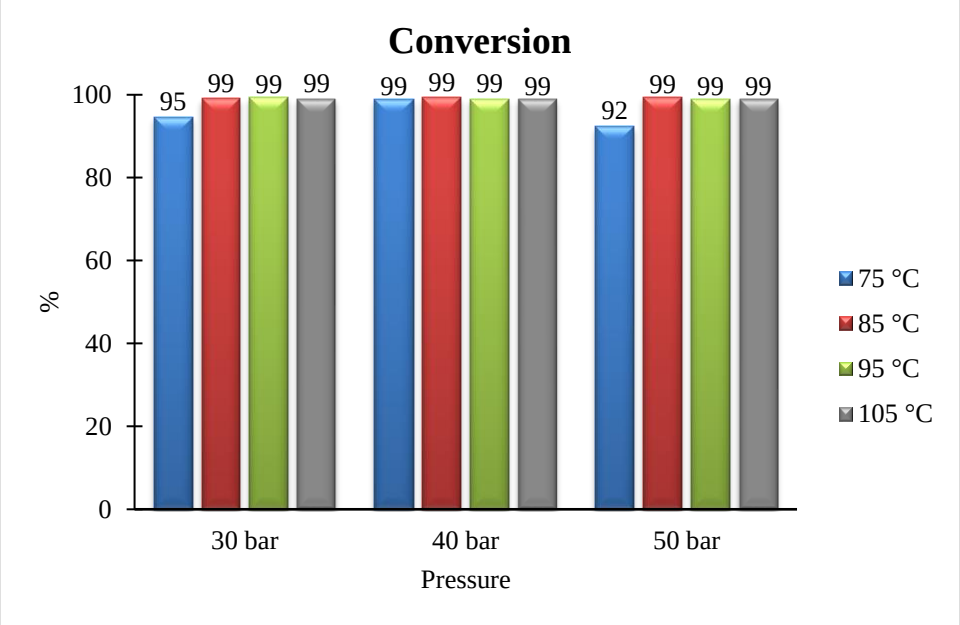

Figure 5.3 Conversion of 1-octene with temperature and pressure, at constant time (4 h.) for complex **4.9**.

A more detailed understanding of the composition of the products emanating from the observed conversions is described in the following sections, in terms of chemoselectivity and regioselectivity of catalyst precursor **4.9**.

5.2.1.2 The Effect of Temperature and Pressure on Chemoselectivity

The preferential formation of aldehydes is an important aspect of a hydroformylation catalyst, as this has a huge economic significance where absolute aldehyde chemoselectivity can be achieved, eliminating any costs associated with the separation of side products. In assessing the effect of temperature and pressure on the chemoselectivity of catalyst precursor **4.9**, varying the syngas pressure (from 30–50 bar) at a constant temperature (75 °C) results in a slight improvement in the selectivity for aldehydes (Figure 5.4). A considerable increase in the total aldehydes is observed when the pressure is varied at a constant temperature of 85 °C, from 63% (30 bar) to 90% (50 bar) and this could be attributed to the increased CO concentration in the system, limiting the isomerisation of the olefin while accelerating the CO migration step of the hydroformylation cycle (Section 1.2, Chapter 1). A further increase in temperature and pressure (105 °C / 50 bar), has no significant effect in the chemoselectivity for aldehydes. At this high temperature and pressure (105 °C / 50 bar), there exists a strong competition between thermally promoted isomerisation and excess-CO promoted hydroformylation. However, with excess CO present in the system, each isomerisation cycle can be interrupted by the formation of the corresponding metal-acyl complex through insertion of CO into the metal-alkyl bond, and irreversibly converting the intermediates to aldehydes.[58] Interesting to note, no alcohols or hydrogenation products were observed even at high temperatures of this study (105 °C), attesting to the consistently good hydroformylation selectivity of this catalyst.

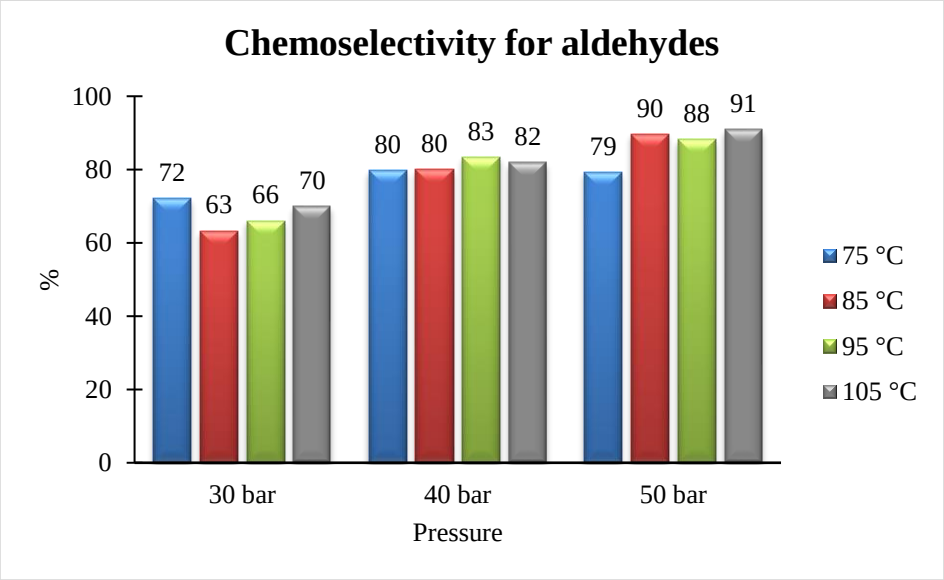

Figure 5.4 Chemoselectivity for aldehydes with temperature and pressure, at constant time (4 h.) for complex **4.9**.

5.2.1.3 The Effect of Temperature and Pressure on Regioselectivity

The regioselectivity of catalyst precursor **4.9** was studied at different temperature and pressure in the hydroformylation of 1-octene (Figure 5.5). The catalyst precursor **4.9** shows good regioselectivity for the linear aldehyde, nonanal (70%) at the lowest conditions of this study (75 °C and 30 bar). An increase in temperature at a constant pressure (75–105 °C / 30 bar) results in a gradual decrease in the linear aldehyde, and subsequent increase in the branched aldehydes. In addition to the generally accepted primary route leading to the formation of branched aldehydes *via* the Markovnikov addition of the olefin to the metal-alkyl bond, the increase in branched aldehydes can also be ascribed to the subsequent hydroformylation of the iso-octenes that form as a result of temperature-promoted preferential double bond isomerisation of the olefin. Moreover, although reported as a rare occurrence by Brookhart and Lenges,[59] the observed shift in the ratio of the linear aldehyde to branched aldehydes with increase in temperature at constant syngas pressure can partly be due to a combination of a hydroformylation-decarbonylation-hydroformylation sequence. The linear aldehyde is reported to undergo a temperature-driven formyl group migration to an internal position, consequently leading to an increase of the branched aldehydes with a decrease in the linear aldehyde. It should be noted that this sequence is also dependant on the catalyst in use, and therefore this presumption may not necessarily be the contributing factor to the observed regioselectivity shifts in our study. Surprising to note, increasing the pressure to 50 bar has no further significant effect on the regioselectivity of precatalyst **4.9**. This can be ascribed to a system that has see-sawed between the rate of β-hydride elimination and the rate of CO-migratory insertion, leading to no overall net change in the branched and linear aldehydes which are formed mainly *via* the Markovnikov and *anti*-Markovnikov addition respectively.

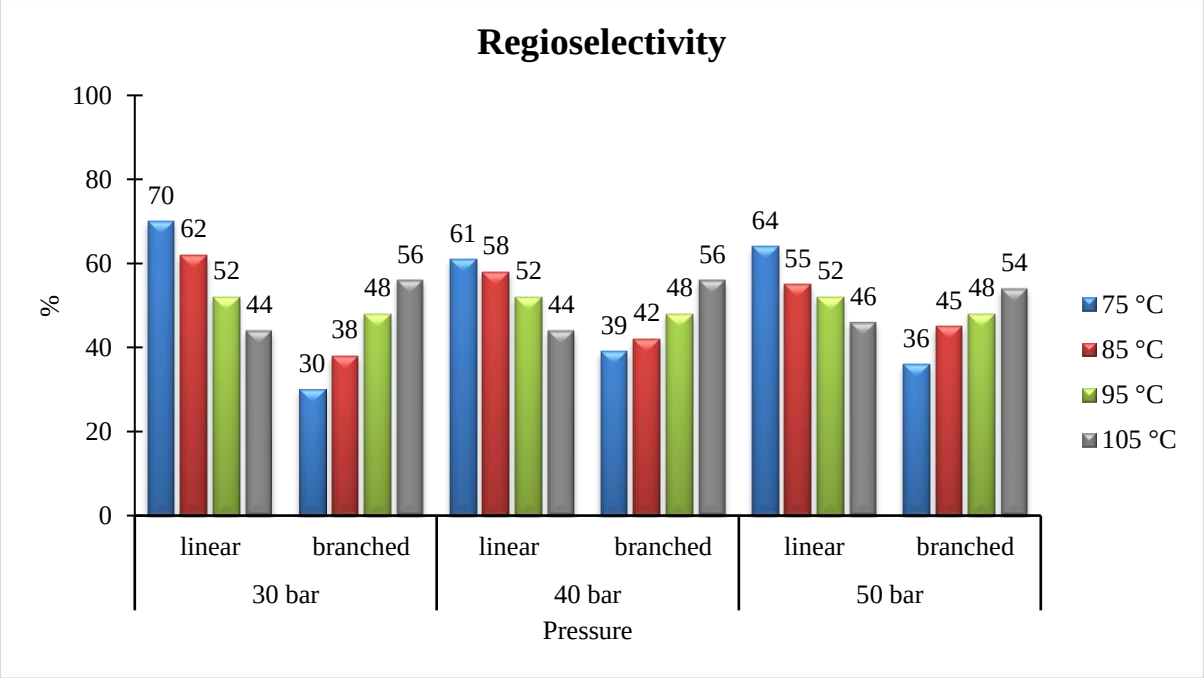

Figure 5.5 Regioselectivity with temperature and pressure, at constant time (4 h.) for complex **4.9**.

5.2.1.4 The Effect of Temperature and Pressure on Activity

The activity of a catalyst ((mmol of aldehydes per mmol of Rh)/time) in a biphasic media is often confounded with mass transfer limitations of the catalyst and the substrate. Designing a catalyst that demonstrates good and appreciable activity under biphasic environments is a very challenging but equally intriguing strategy towards value-addition of the PGM-based metal catalysts. In the transformation of 1-octene, the catalyst precursor **4.9** generally shows a gradual increase in activity when pressure is increased at constant temperature, for example, from 426 h^{-1} (75 °C / 30 bar) to 458 h^{-1} (75 °C / 50 bar) (Table 5.1). The increased syngas concentration in the system potentially results in predominantly the tetracarbonyl rhodium species $[Rh(CO)_4]^+$.[60–62] Weakening of the Rh–CO bond facilitates the dissociation of CO and subsequent insertion into the metal-alkyl bond, accelerating the formation of the acyl-complex intermediate, and consequently resulting in improved hydroformylation rates. This trend is also observed at slightly higher temperatures of this study (85 °C–105 °C) when pressure is varied from 30 bar to 50 bar. Overall, the optimum conditions were established at 85 °C / 50 bar, based on the good activity (557 h^{-1}), chemoselectivity for aldehydes (90%) and conversion of the substrate (99%), entry 6.

Table 5.1 Hydroformylation of 1-octene using catalyst precursor **4.9** for 4 h[a].

Entry	Temp. (°C)	Pressure (bar)	Conv. (%)	Aldehydes (%)[b]	Iso-octenes (%)	*n/iso*[c]	TOF (h^{-1})[d]
1	75	30	95	72	28	70:30	426
2	75	40	99	80	20	61:39	493
3	75	50	92	79	21	64:36	458
4	85	30	99	63	37	62:38	392
5	85	40	99	80	20	58:42	496
6	85	50	99	90	10	55:45	557
7	95	30	99	66	34	52:48	410
8	95	40	100	83	17	52:48	518
9	95	50	100	88	12	52:48	550
10	105	30	100	70	30	44:56	433
11	105	40	100	82	18	44:56	508
12	105	50	100	91	9	46:54	569

[a]Reactions carried out with ($CO–H_2$) (1:1) in H_2O:Toluene (5:5 mL) with 7.175 mmol of 1-octene and 2.87×10^{-3} mmol of Rh catalyst. The reactor was purged with syngas. GC conversions obtained using n-decane as an internal standard in relation to authentic standard iso-octenes and aldehydes. [b]Total aldehydes formed (from octene and iso-octenes converted), which includes the primary aldehyde product, nonanal, and branched aldehydes. [c]The molar ratio of primary linear aldehyde product nonanal (*n*) and branched aldehydes (*iso*) formed. [d]TOF = (mmol of aldehydes per mmol of Rh)/time. Average error estimate = ± 0.45.

5.2.2 Catalytic evaluation using precatalyst 4.10 and Mercury poisoning experiments

The application of metallodendritic structures in catalysis is very intriguing, owing to the potential of improved catalytic performance of metallodendrimers over their mononuclear congeners.[63–65] However, the dendritic structures tend to have reduced solubility in the solvent of choice for catalysis than the mononuclear analogues, often having an impact on the catalytic performance of the metallodendrimer. In this study, the water-soluble trinuclear complex **4.10** (Figure 5.6) ($H_2O_{solubility/25°C}$ = 8.6 mg/mL) was successfully evaluated in the hydroformylation of 1-octene under the optimum conditions of temperature and pressure (85 °C / 50 bar) (Table 5.2). The trinuclear precatalyst shows good conversion (99%, entry 2) of 1-octene at 4 h of the catalytic transformation, as well as comparable aldehyde selectivity (88%, entry 2) to that of the mononuclear complex (90%, entry 1). Comparable regioselectivities and activities are also

observed at 4 h with both catalyst precursors (*n/iso* = 55:45 (**4.9** and **4.10**); TOF = 557 h^{-1} (**4.9**) and 555 h^{-1} (**4.10**) respectively).

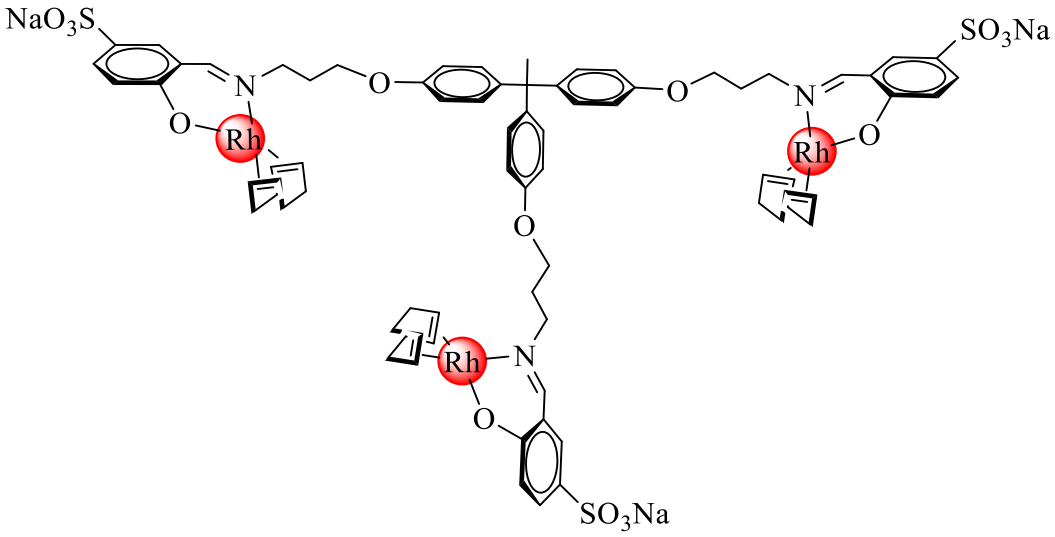

Figure 5.6 Water-soluble salicylaldimine aryl-ether Rh(I)-trinuclear complex **4.10**.

Table 5.2 Hydroformylation of 1-octene using catalyst precursors **4.9** and **4.10** for 4 h[a].

entry	Complex	Temp. (°C)	Pressure (bar)	Conv. (%)	Aldehydes (%)[b]	Iso-octenes (%)	*n/iso*[c]	TOF (h^{-1})[d]
1	**4.9**	85	50	99	90	10	55:45	557
2	**4.10**	85	50	99	88	12	55:45	555
3	**4.9**[e]	85	50	73	67	33	71:29	305
4	**4.10**[e]	85	50	78	66	34	70:30	323

[a]Reactions carried out with ($CO–H_2$) (1:1) in H_2O:Toluene (5:5 mL) with 7.175 mmol of 1-octene and 2.87×10^{-3} mmol of Rh catalyst for **4.9**, and 9.57×10^{-4} mmol of Rh catalyst for **4.10**. The reactor was purged with syngas. GC conversions obtained using n-decane as an internal standard in relation to authentic standard iso-octenes and aldehydes. [b]Total aldehydes formed (from octene and iso-octenes converted), which includes the primary aldehyde product, nonanal, and branched aldehydes. [c]The molar ratio of primary linear aldehyde product nonanal (*n*) and branched aldehydes (*iso*) formed. [d]TOF = (mmol of aldehydes per mmol of Rh)/time. [e]Mercury poisoning experiments. Average error estimate = ± 0.58.

A more detailed understanding of the observed catalytic performance is depicted in the substrate and product-distribution-time profiles of the two catalyst precursors **4.9** (Figure 5.7a) and **4.10** (Figure 5.7b), conducted over time at optimum conditions (85 °C / 50 bar). In a generic trend, the two catalyst precursors show appreciably good transformation of the substrate over time. A closer look at the profiles indicate that the trinuclear complex shows superior

performance over the mononuclear complex within the 1st hour of the reaction, showing 2.19 mol% (**4.10**, Figure 5.7b) of 1-octene present in the system compared to 27.22 mol% (**4.9**, Figure 5.6a). The mononuclear complex reaches closely similar quantities only at the 2 h interval (1.66 mol%). Such catalytic performance alludes to a positive dendritic effect of the trinuclear complex **4.10** over the mononuclear complex **4.9**, owing to the inherent multiple active sites of **4.10**. This observation is further complimented by the higher ratio of the linear aldehyde nonanal at the 1 h interval, when using the trinuclear complex **4.10** (47.16 mol%, Figure 5.7b) compared to the mononuclear complex **4.9** (34.68 mol%, Figure 5.7a). At this stage, the bulky nature of the trinuclear complex can be viewed as responsible for the observed ratios of linear to branched aldehydes of **4.10** over the ratio depicted by the less bulky precatalyst **4.9**. Despite the seemingly complete transformation of 1-octene by the 1 h and 2 h intervals for precursors **4.10** and **4.9** respectively, branched aldehydes are observed to increase in the system with time. This is ascribed to the ease of hydroformylation of the iso-octenes to branched aldehydes, wherein at this stage, there exists no competition for the catalytic active sites between the substrate (now depleted) and the iso-octenes present in the system.

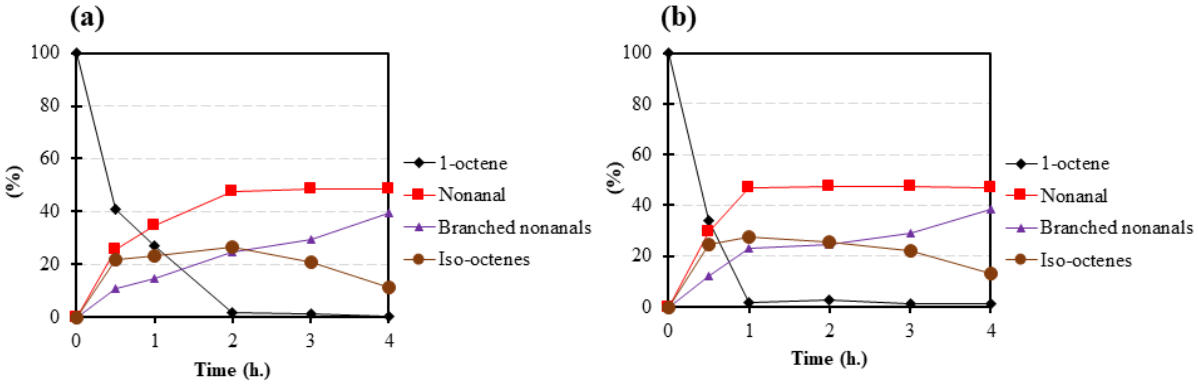

Figure 5.7 Substrate and product-distribution-time profiles with the mono- **4.9** (a) and trinuclear precatalysts **4.10** (b) at optimum conditions (85 ℃ / 50 bar).

Further to this, mercury poisoning experiments were conducted to add insight to the homogeneity of the catalytic reactions. This would suppress any contribution to the catalytic performance arising from the presence of nanoparticles. When a drop of mercury was added to the reaction mixture, a decline in the catalytic performance of both precatalysts was observed, indicative of a nanoparticle-mediated transformation for both precatalysts **4.9** and **4.10** (Table 2, entries 3 and 4 *vide supra*). Such results show that the catalytic reaction is proceeding *via* a combination of both homogeneous and heterogeneous species. Interesting to

note is the improved regioselectivity for the linear aldehyde upon amalgamation of the nanoparticles with mercury. This occurs with an increase in the total iso-octenes, indicative of a system that stabilises against the possible transformation of these iso-octenes to branched aldehydes. A closer look at the nanoparticles could open avenues to potentially robust and tailor-specific catalyst precursors. The observed behaviour of precatalysts **4.9** and **4.10** upon addition of mercury is similar to our previously reported studies on analogous water-soluble salicylaldimine Rh(I)-complexes.[53,55–57] It is worth noting that despite the nanoparticle enhanced catalytic performance stated in the literature, our previously reported analogous catalyst precursors maintained good catalytic performance over several cycles in the hydroformylation of 1-octene.[53,55,57] Considering that motivation, our assessment of the "recovery-for-reusability" of precatalysts **4.9** and **4.10** is discussed in the following sections.

5.2.3 Reusability of the catalysts: Aqueous biphasic hydroformylation

The reusability of the water-soluble catalyst precursors **4.9** and **4.10** was evaluated in the aqueous biphasic hydroformylation of 1-octene. This approach is a green technique owing to the use of water, a non-toxic and relatively abundant solvent, in addition to being immiscible with a wide range of organic solvents.[66] The technique imparts the ability to separate the catalyst-containing phase from the product-bearing phase, providing a very attractive way of recovering the catalyst for potential recurring use. This is attractive to industry, where strategies on effective and sustainable catalyst recovery and reuse have a huge impact on the economics of an industrial scale setup. In our recyclability assessments, a typical recycling study (Figure 5.8) first proceeded *via* immobilising the catalyst in the aqueous phase following a similar manner and optimum conditions (85 °C / 50 bar) as described in Section 5.2.1 of this Chapter. During the course of the reaction, vigorous stirring allows for the interfacial interaction between the aqueous phase and the organic phase, bringing the catalyst and the substrate into contact and effectively enabling the catalytic transformation to occur. After the desired reaction time has been reached, cooling of the reactor allows for the two immiscible phases to effectively separate. The product-containing organic layer can then be decanted, and a fresh sample of the substrate can be added to the same catalyst-containing aqueous phase. This aqueous phase can be taken through repetitive cycles with assessment of the catalytic performance at each cycle. In this study, interpretation of the results obtained from the gas chromatography analysis of each cycle is discussed in the following sections.

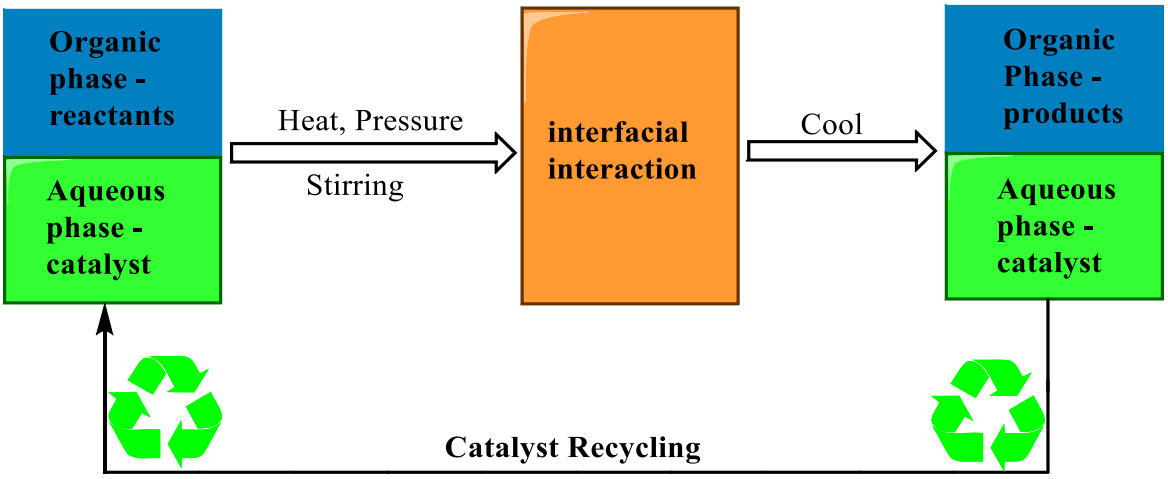

Figure 5.8 Illustrating the principle of catalyst recycling in aqueous biphasic catalysis.

5.2.3.1 The effect of catalyst recycling on conversion

The catalyst precursors **4.9** and **4.10** were successfully recycled for at least 5 times in the hydroformylation of 1-octene, with a gradual decline in conversion with each cycle (Figure 5.9). The ability to maintain appreciably moderate to good conversions over 5 cycles is attractive from a circular economy viewpoint, with future potential of improving on the findings. The observed decrease in conversion with recycling of the catalyst could be attributed to low concentration of the active metal species in the aqueous layer after the first cycle, possibly as a result of leaching of the metal catalyst to the organic phase. This has been observed in the literature for analogous water-soluble salicylaldimine Rh(I) complexes.[53,55,57] Inductively coupled plasma optical emission spectroscopy (ICP-OES) analysis referenced to the initial metal loading shows an overall rhodium metal loss of 41% (**4.9**) and 57% (**4.10**) from the aqueous layer, supporting the observed steady decrease in 1-octene conversions for both catalyst precursors **4.9** and **4.10**. However, this does not rule out the possibility of a gradual metal degradation-promoted decrease in conversion, often associated with repetitive use of the same catalyst containing phase.

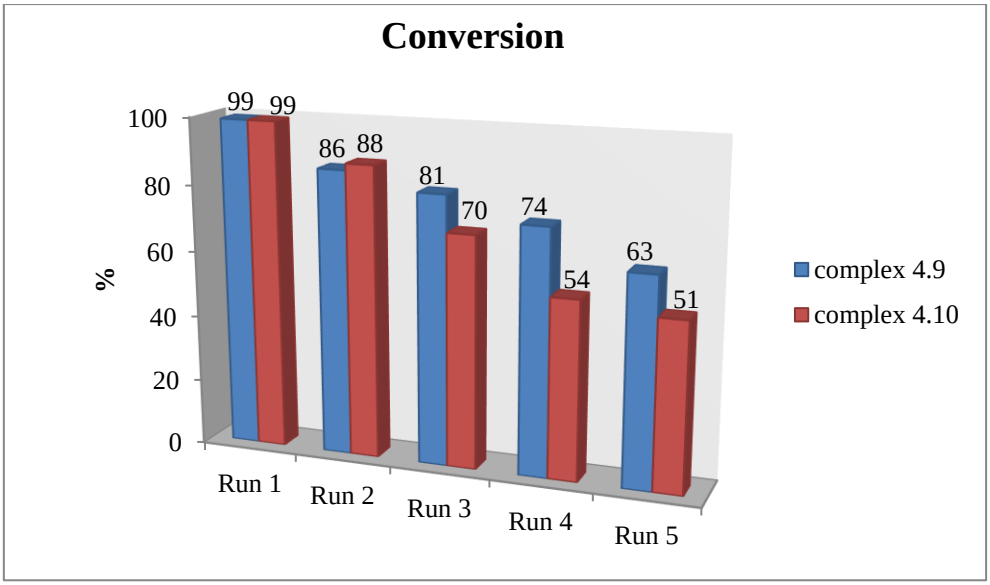

Figure 5.9 Percentage conversion of 1-octene during aqueous biphasic recyclability studies in the hydroformylation of 1-octene.

5.2.3.2 The effect of catalyst recycling on chemoselectivity

The catalyst precursors **4.9** and **4.10** show appreciably good to moderate chemoselectivity for aldehydes over the 5 cycles conducted in this study (Figure 5.10). A decrease in chemoselectivity for aldehydes is observed from the 1st cycle to the 2nd cycle for both catalyst precursors **4.9** (from 90% to 71%) and **4.10** (from 88% to 66%). Thereafter, a more consistent but steady decrease is observed from the 2nd cycle to the 5th cycle. This suggests that despite the loss of active metal from the aqueous layer through leaching as proven by ICP-OES analysis, the remaining aqueous-immobilised active metal species maintain a good bias towards aldehydes. It should be noted that no hydrogenation products (alkanes or alcohols) were observed at any instance during the recycling of the catalysts, further indication of a consistent preservation of selectivity between the aldehydes and iso-octenes only. Consistency of a catalyst in the selectivity for the target product (aldehydes) is a very attractive and desirable trait in a catalyst, more-so when evaluating the relatively expensive PGM-based catalysts such as precatalysts **4.9** and **4.10** over several cycles.

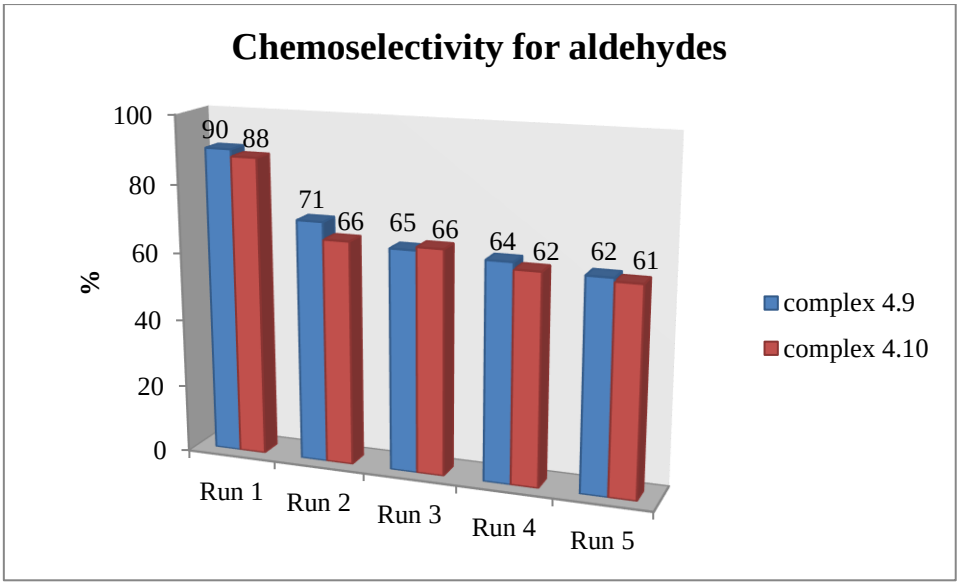

Figure 5.10 Chemoselectivity for aldehydes during aqueous biphasic recyclability studies in the hydroformylation of 1-octene.

5.2.3.3 The effect of catalyst recycling on activity

A closer inspection of the catalytic performance in terms of activity ((mmol of aldehydes per mmol of Rh)/time) is shown in Figure 5.11. It should be noted that the activities reported in the recyclability studies were calculated in reference to the initial Rh-metal loading. The catalyst precursors **4.9** and **4.10** display a decrease in the activity from the 1st cycle to the 2nd cycle (557 h^{-1} to 384 h^{-1} (**4.9**); and 555 h^{-1} to 367 h^{-1} (**4.10**)) (Figure 5.11). This is consistent with the observed chemoselectivity and conversion of both catalysts, since activity is a bi-function of the "chemoselectivity for aldehydes" that are calculated against the "registered conversion" of the substrate. A gradual decrease in activity from the 3rd cycle (ca. 300 h^{-1}) is observed for both catalysts **4.9** and **4.10**, possibly due to a combination of active metal degradation with constant reuse, as well as active metal leaching to the product-containing organic phase, as attested to by the ICP-OES experiments reported in Section 5.2.3.1 of this Chapter.

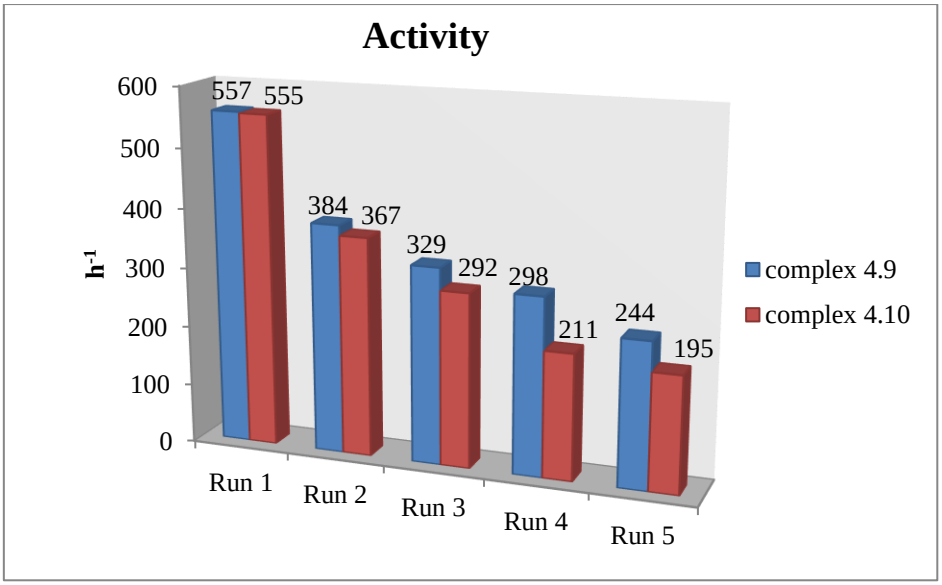

Figure 5.11 Activity of the complexes during aqueous biphasic recyclability studies in the hydroformylation of 1-octene.

In attempts to circumvent catalyst leaching from the aqueous phase to the organic phase under hydroformylation conditions, the experiments for the hydroformylation of 1-octene were conducted with excess added water-soluble trimeric ligand at various quantities under optimum conditions (85 °C / 50 bar / 4 h.). The premise of this study was in view of the excellent solubility of the ligands in water compared to the water-solubility of the complexes, which could possibly be advantageous in stabilising the metal complex from leaching to the organic layer under the conditions of study.

5.2.4 Excess ligand addition studies

In the assessment of the effect of additional trimeric ligand ($H_2O_{solubility/25°C}$ = 19.6 mg/mL) on recyclability studies, the trinuclear precatalyst **4.10** ($H_2O_{solubility/25°C}$ = 8.6 mg/mL) was chosen as it displayed a higher proportion of metal loss to the organic phase than the mononuclear precatalyst **4.9** during the aqueous biphasic recyclability studies, as evidenced by the ICP-OES experiments. The ligand-to-metal complex ratio was varied in multiples of 3 (from 0 to 12 equivalents) and the reactions were conducted with the same metal loading, (Table 5.3). Excellent conversion of 1-octene was maintained (99%) throughout the ligand addition studies under optimum conditions. The complex displays a slight decrease in chemoselectivity for

aldehydes on addition of 3 equivalents of the ligand, from 88% to 72%, and subsequent increase in iso-octenes from 12% to 28%. This can be ascribed to the steric hindrance of the active metal centres of the complex by the additional bulky ligand, consequently reducing access of the metal by the substrate. The uncoordinated free substrate becomes susceptible to temperature-promoted isomerisation, leading to the observed rise in the iso-octenes and reduced chemoselectivity for aldehydes. However, the additional steric bulk around the active metal centres provide improved regioselectivity for the linear aldehyde nonanal, from 55% (0 equiv.) to 66% (3 equiv.). The general steric influence on regioselectivity of hydroformylation catalysts has been reported in literature, with the most prominent examples involving the bulkier triphenylphosphine ligands.[67] Continued addition of the ligand in this study (up to 12 equiv.) did not give a pronounced change in the overall catalytic performance of catalyst **4.10**, as observed for example, from the activities that are maintained below the initial 555 h^{-1}.

Table 5.3 Excess ligand addition studies using catalyst precursor **4.10** for 4 h[a].

Ligand eqv.	Temp. (°C)	Pressure (bar)	Conv. (%)	Aldehydes (%)[b]	Iso-octenes (%)	*n/iso*[c]	TOF (h^{-1})[d]
0	85	50	99	88	12	55:45	555
3	85	50	99	72	28	66:34	443
6	85	50	99	72	28	66:34	446
9	85	50	99	77	23	64:36	474
12	85	50	99	76	24	66:34	470

[a]Reactions carried out with ($CO–H_2$) (1:1) in H_2O:Toluene (5:5 mL) with 7.175 mmol of 1-octene and 9.57×10^{-4} mmol of Rh catalyst (**4.10**). The reactor was purged with syngas. GC conversions obtained using n-decane as an internal standard in relation to authentic standard iso-octenes and aldehydes. [b]Total aldehydes formed (from octene and iso-octenes converted), which includes the primary aldehyde product, nonanal, and branched aldehydes. [c]The molar ratio of primary linear aldehyde product nonanal (*n*) and branched aldehydes (*iso*) formed. [d]TOF = (mmol of aldehydes per mmol of Rh)/time. Average error estimate = ± 0.33.

Since the attempts to improve the catalytic performance of our system through additional ligand lowered the overall catalytic activity and aldehyde selectivity of catalyst **4.10**, this strategy was not pursued further in recycling studies. However, in view of our previously reported data on good recyclability of water-soluble Rh(I) complexes conducted in the absence of the organic solvent toluene,[68] we discuss in the following sections, the "neat" hydroformylation of 1-octene in water.

5.2.5 Reusability of the catalysts: Neat (in water only) hydroformylation

The exclusion of the organic solvent (toluene) provides the potential to hedge the catalyst from leaching, and possibly improve on the recyclability of the PGM-based water-soluble catalysts. In such a study, the substrate (1-octene) and internal standard (*n*-decane) can be viewed to a lesser extent as the organic phase, although the entire system could be considered "neat", for ease of distinguishing from the toluene-present aqueous biphasic approach reported in Section 5.2.4 of this Chapter. In a typical "neat" recycling study, the catalyst is immobilised in the aqueous phase by dissolution in water, followed with the addition of the substrate and internal standard only, (toluene excluded). The reaction is then conducted for 4 h following a similar manner and optimum conditions (85 °C / 50 bar) as described in Section 5.2.1 of this Chapter, after which the reactor is cooled to room temperature, and the contents transferred to a vial. The organic products are then extracted with toluene and immediately decanted from the catalyst-containing aqueous-phase and analysed by gas chromatography. A fresh sample of the substrate and internal standard is added to the same catalyst-containing aqueous layer, and this can be taken through repetitive cycles with assessment of the catalytic performance at each cycle. Interpretation of the results obtained from the gas chromatography analysis is discussed in the following sections.

5.2.5.1 The effect of catalyst recycling on conversion

The catalyst precursors **4.9** and **4.10** were successfully evaluated in the "neat" (in water only) hydroformylation of 1-octene under the optimum conditions (85 °C / 50 bar / 4 h.). Both catalysts could be recycled at least 5 times (Figure 5.12 overleaf), as with the studies reported *vide supra* on hydroformylation using the water-toluene biphasic strategy. Interesting to note in this assessment is the consistently good conversion of 1-octene (over 70%) displayed by the trinuclear complex **4.10** throughout the 5 cycles. The gradual decline in conversion after the 1st cycle can be ascribed to slight active metal degradation with constant heating of the catalyst, as the absence of the organic solvent rules out any excessive leaching of the catalyst to the organic products. However, the mononuclear complex **4.9** shows a drastic decline in conversion of the substrate, from 83% (1st cycle) to 32% (5th cycle). This can be attributed to increased susceptibility to metal degradation of **4.9** in the absence of toluene, as evidenced by the formation of a visually quantifiable black particulate matter of the initial complex with each cycle. Interesting to note, the black mass is hardly observed with **4.10**, indicative of good stability that is possibly induced by the larger macromolecular structure.

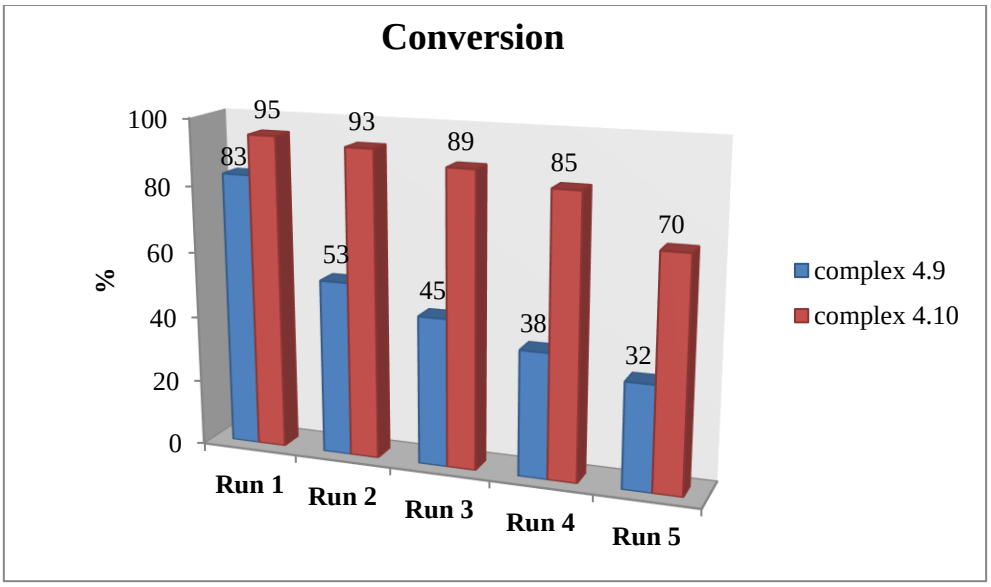

Figure 5.12 Conversion of the complexes during the "in-water only" recyclability studies in the hydroformylation of 1-octene.

5.2.5.2 The effect of catalyst recycling on chemoselectivity

The two catalysts maintain good to moderate chemoselectivity for aldehydes (> 65%) throughout the cycles (Figure 5.13 overleaf). These values are comparable to the data obtained in the hydroformylation experiments carried out in the presence of toluene (Figure 5.13 vs Figure 5.10). This shows that both catalysts **4.9** and **4.10** retain consistency in aldehyde selectivity over isomerisation throughout the cycles, despite the evident degradation of **4.9** with constant reuse.

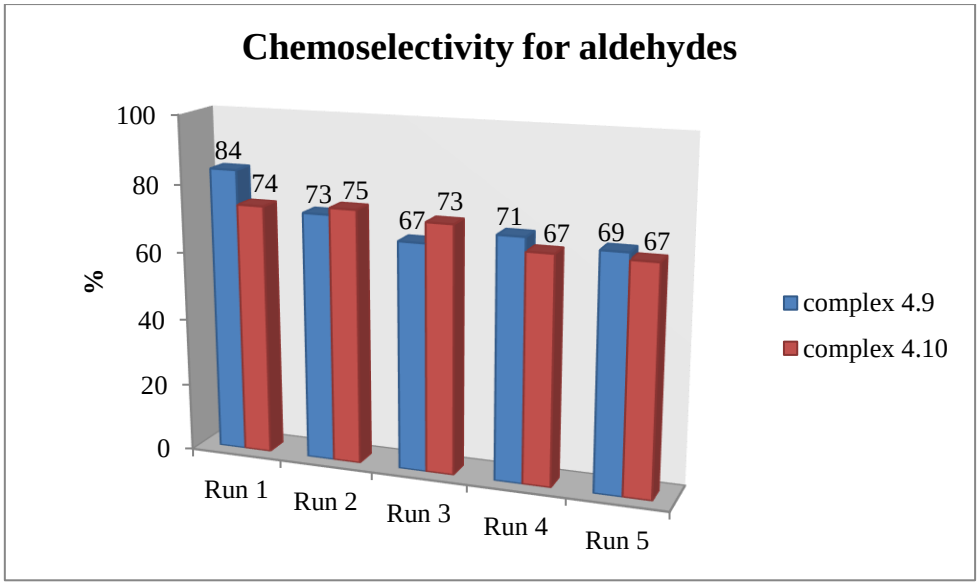

Figure 5.13 Chemoselectivity of the complexes during the "in-water only" recyclability studies in the hydroformylation of 1-octene.

5.2.5.3 The effect of catalyst recycling on activity

The catalyst precursors **4.9** and **4.10** show moderate activity throughout the "neat" recyclability studies (Figure 5.14 overleaf). A considerable decline in the activity of **4.9** is observed with each cycle, from 437 h^{-1} in the 1st cycle to 139 h^{-1} in the 5th cycle. This would be expected since the activity is dependent on the total aldehydes produced from the determined conversion, and as such the aldehydes formed from precatalyst **4.9** are a culmination of a considerable decline in conversion, as reported *vide supra*. On the other hand, the trinuclear complex **4.10** displays appreciably good activity throughout the cycles when compared to the experiments conducted in the presence of toluene (Figure 5.14 vs Figure 5.11). This corroborates that leaching may have been the primary contributor to the observed decline in activity with the water-toluene biphasic approach depicted in Figure 5.11, whereas active metal degradation is a secondary contributor. In the "neat" studies, inductively coupled plasma optical emission spectroscopy (ICP-OES) analysis referenced to the initial metal loading shows an overall rhodium metal loss of 69% (**4.9**) and 38% (**4.10**), indicative of the high degree of active metal degradation of **4.9** compared to the dendrimer-stabilised **4.10**. The affinity of precatalyst **4.10** for the organic phase (leaching) that is observed in studies involving toluene could be attributed to the slightly reduced water-solubility of **4.10** ($H_2O_{solubility/25°C}$ = 8.6 mg/mL) compared to **4.9** ($H_2O_{solubility/25°C}$

= 15.7 mg/mL), resulting from a combination of the hydrophobic tris(hydroxyphenyl)ethane (THPE) core with the cyclooctadiene moieties on each metal centre of **4.10**.

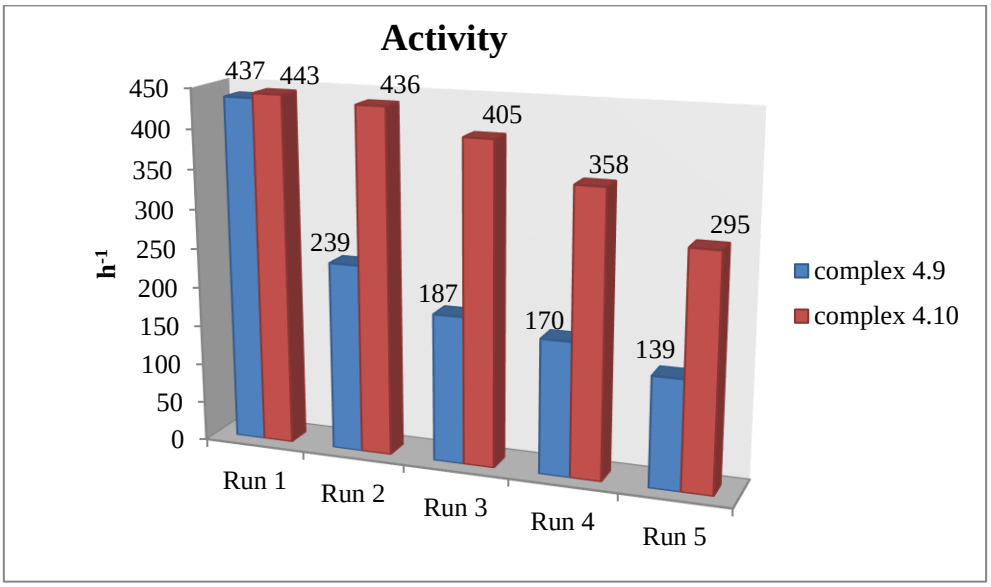

Figure 5.14 Activity of the complexes during the "in-water only" recyclability studies in the hydroformylation of 1-octene.

With the view of the potentially beneficial catalyst stabilisation properties by large macromolecular structures, we sought to evaluate our water-soluble trinuclear complex **4.10** against our group's previously reported water-soluble trinuclear complex. [53]

5.2.6 Aqueous biphasic comparative study

The comparative assessment was carried out using the trinuclear complex **4.10**, bearing the rigid THPE core, against the tris-2-(aminoethyl)amine flexible core-bound salicylaldimine water-soluble complex **4.11** (Figure 5.15 overleaf). It should be noted that complex **4.11** is reported to have been generated *in situ* owing to difficulties in isolating the preformed complex. The reactions using **4.10** were conducted following the conditions reported in the literature for the hydroformylation of 1-octene (6.37 mmol) with **4.11**, and a similar metal loading (9.57×10^{-4} mmol of Rh-metal).[53] At the lowest conditions of the comparative study (75 °C / 30 bar) good conversions are observed for both complexes **4.10** (99%) and **4.11** (79%) (Table 5.4). At these conditions, catalyst precursor **4.10** also displays greater aldehyde chemoselectivity (77%) when compared to catalyst precursor **4.11** (52%). The higher

proportion of iso-octenes in **4.11** can be explained by the possibility of restricted access of the active metal centre by the substrate owing to the flexible core, which may assume an unfavourable conformation in solution. A restriction of access to the catalytic centre of **4.11** consequently leads to a temperature-promoted isomerisation of the substrate, as observed previously in this study when excess ligand is added to the trinuclear complex **4.10**. In general, the trinuclear complex **4.10** shows superior catalytic performance over complex **4.11** when compared under similar conditions of temperature and pressure, showing the benefits of a rigid supporting core over a flexible one.

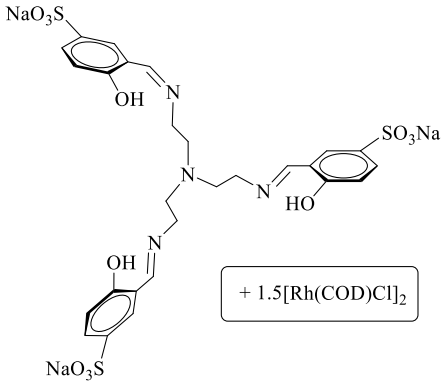

Figure 5.15 *In situ* prepared water-soluble salicylaldimine Rh(I) catalyst precursor **4.11**.[53]

Table 5.4 Aqueous biphasic hydroformylation of 1-octene comparative study with **4.10** and **4.11**[53] for 8 h[a].

Entry	Catalyst	Temp. (°C)	Pressure (bar)	Conv. (%)	Aldehydes (%)[b]	Iso-octenes (%)	TOF (h^{-1})[d]
1	**4.10**	75	30	99	77	23	239
2	**4.11**	75	30	79	52	48	189
3	**4.10**	95	30	99	85	15	266
4	**4.11**	95	40	89	64	36	233
5	**4.10**	75	40	99	90	10	279
6	**4.11**	75	40	94	81	19	294
7	**4.10**	75	50	99	94	6	293
8	**4.11**	75	50	82	46	54	167

[a]Reactions carried out with ($CO–H_2$) (1:1) in H_2O:Toluene (5:5 mL) with 6.37 mmol of 1-octene and 9.57×10^{-4} mmol of Rh catalyst (**4.10** and **4.11**). The reactor was purged with syngas. GC conversions obtained using n-decane as an internal standard in relation to authentic standard iso-octenes and aldehydes. [b]Total aldehydes formed (from octene and iso-octenes converted), which includes the primary aldehyde product, nonanal, and branched aldehydes. [c]The molar ratio of primary linear aldehyde product nonanal (*n*) and branched aldehydes (*iso*) formed. [d]TOF = (mmol of aldehydes per mmol of Rh)/time. Average error estimate = ± 0.19.

5.2.7 Substrate scope

The versatility of the mononuclear (**4.9**) and trinuclear (**4.10**) complexes was evaluated in the hydroformylation of styrene (Scheme 5.2). The hydroformylation of styrene is a very attractive model in the transformation of vinylarenes, owing to the usually absolute chemoselectivity for aldehydes, as well as the wide potential applications of the resultant branched and linear aldehydes.[7,69] In the assessment of the versatility of our precatalysts **4.9** and **4.10**, the aqueous biphasic experiments were conducted under the optimised conditions obtained in the hydroformylation of 1-octene using **4.9** (85 ℃ / 50 bar / 4 h.), at a substrate-to-catalyst molar ratio of 2500:1.

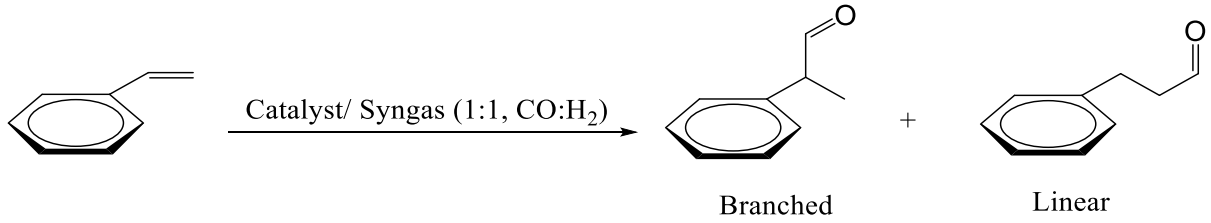

Scheme 5.2 Illustration of hydroformylation of styrene.

The hydroformylation of styrene predominantly leads to the branched, chiral oxo-aldehyde. Generally, the hydroformylation cycle would account for the formation of the aldehydes *via* the migratory insertion of the olefin into the Rh-H bond, leading to a 4-coordinate Rh-primary alkyl complex (for linear aldehydes) and a Rh-secondary alkyl complex (for branched aldehydes). Since no isomerisation can be presumed to occur in this case due to the high resonance stabilisation energy of the benzene ring acting against de-aromatization, the bias towards the branched aldehyde can be aided by the formation of a η^3-Rh-olefin complex (**ii-b**) during the catalytic cycle (Scheme 5.3). This stable benzylic Rh-species intermediate co-exists at equilibrium with the generally accepted η^1-Rh-secondary alkyl complex (**ii-a**), further feeding into the channel for branched aldehydes upon CO coordination (further steps not shown for clarity).[70,71]

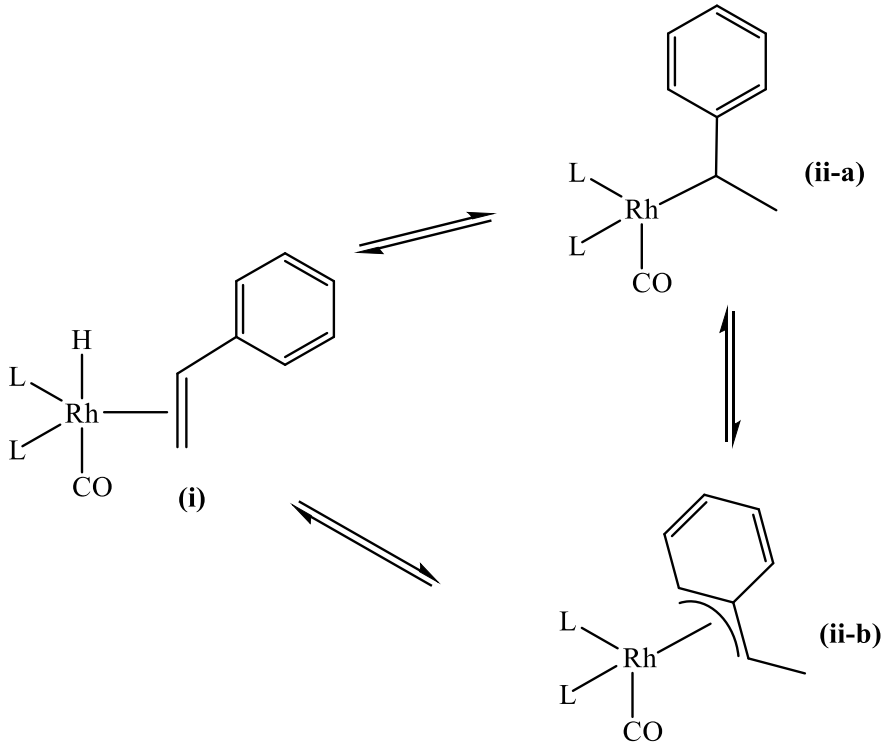

Scheme 5.3 Extract of the mechanism favouring branched aldehyde selectivity in styrene hydroformylation.[70,71]

In this work, both complexes were successfully evaluated in the hydroformylation of styrene, displaying good (**4.10**) to excellent (**4.9**) transformation of the substrate (77% and 98% respectively) (Table 5.5). It should be noted that no hydrogenation products (ethylbenzene or alcohols) were observed using catalyst precursors **4.9** and **4.10**, indicative of the good absolute aldehyde chemoselectivity of these complexes. The slightly reduced conversion (77%) and activity (479 h^{-1}) on styrene by precatalyst **4.10** can be attributed to the combined steric effects of the substrate and the bulky THPE-anchored precatalyst, leading to poor substrate accessibility of the active metal sites. The relatively less bulky mononuclear complex **4.9** provides ease of access to the active metal centre, leading to improved conversions (98%) and activity (615 h^{-1}) of the substrate. Interesting to note is the equivalent bias for branched aldehydes selectivity (*n/iso*, 26:74) with both catalyst precursors **4.9** and **4.10**, indicating that although there is poor access to the active sites of **4.10** by the substrate, the active metal centres could be acting as a single mononuclear entity. In that view, this is complimentary to the lower activity of **4.10** explained *vide supra*, with the steric bulk only lowering the rate of formation

of the 5-coordinate species (**i**) (Scheme 5.3 *vide supra*) and has less effect on controlling the regioselectivity of the system.

Table 5.5 Aqueous biphasic hydroformylation of styrene with **4.9** and **4.10** for 4 h[a].

Complex	Temp. (°C)	Pressure (bar)	Conv. (%)	Aldehydes (%)[b]	*n/iso*[c]	TOF (h^{-1})[d]
4.9	85	50	98	100	26:74	615
4.10	85	50	77	100	26:74	479

[a]Reactions carried out with ($CO–H_2$) (1:1) in H_2O:Toluene (5:5 mL) with 7.175 mmol of styrene and 2.87×10^{-3} mmol of Rh catalyst for **4.9**, and 9.57×10^{-4} mmol of Rh catalyst for **4.10**. The reactor was purged with syngas. GC conversions obtained using n-decane as an internal standard in relation to authentic standard aldehydes. [b]Total aldehydes formed, which includes the primary aldehyde product, nonanal, and the branched aldehyde. [c]The molar ratio of primary linear aldehyde product (*n*) and branched aldehyde (*iso*) formed. [d]TOF = (mmol of aldehydes per mmol of Rh)/time. Average error estimate = ± 0.62.

5.3 Summary

The success in recovery and reusability of a catalyst that displays good activity and selectivity forms an integral part of homogeneous catalysis. Several strategies have been investigated towards efforts to recover and reuse homogeneous catalysts, with aqueous biphasic catalysis being at the forefront.[72,73] This emanates from the alignment of the technique with the Green Chemistry principles on the use of non-toxic, relatively abundant and readily available solvent (for example, water). Moreover, successful application of this technique on an industrially relevant and economically significant reaction such as hydroformylation adds to the beneficiation of the metal of choice (rhodium) – a rare, expensive and fast depleting Platinum Group Metal. The use of water in biphasic hydroformylation of medium-to-long chain olefins (> C5) has long been a cumbersome process, owing to the poor solubility of the longer olefins in the aqueous – organic reaction media, consequently resulting in limitations of catalyst contact with the substrate, and inefficient catalytic performances.[74] In this work, we have successfully evaluated two new water-soluble catalyst precursors **4.9** and **4.10** in the aqueous biphasic hydroformylation of 1-octene, a good representation of the medium-to-long chain olefins. Both catalyst precursors have shown near-quantitative catalytic conversions of 1-octene, good activities (activity > 550 h^{-1}), and attractive chemoselectivity for aldehydes (90% (**4.9**) and 88% (**4.10**)) under the mild optimum conditions (85 °C / 50 bar / 4 h.). This overall catalytic performance is suggestive of good interaction of the substrate with the catalysts at the interface of the two immiscible solvents (water and toluene) under hydroformylation

conditions. Mercury poisoning experiments showed that the observed performance was to a dual extent, enhanced by the presence of Rh-nanoparticles in the system, a phenomenon that we have previously observed and reported on when using related catalyst precursors.[53,55–57] The reusability of the active metal species was successfully conducted over 5 cycles, with a gradual decline in catalytic performance of both catalysts. The decline was primarily attributed to catalyst leaching to the organic layer, and partly to catalyst degradation with constant subjecting to heat and pressure over the cycles. This has been observed and reported on previously in the literature.[53,55,57] Inductively coupled plasma optical emission spectroscopy (ICP-OES) experiments showed a 41% metal loss from the aqueous layer for **4.9**, and a 57% metal loss for **4.10**. Addition of the water-soluble trimeric ligand at various quantities (up to 12 equiv.) to the catalytic experiments with **4.10** improved the regioselectivity for the linear aldehyde nonanal, although lowering the catalytic conversions and activities of the substrate. In that view, this experimental strategy was not implemented in a recyclability approach. However, excess ligand has been reported to stabilise the active metal centre and help retain the catalyst in the aqueous phase, as reported for the water-soluble industrially employed [Rh-TPPTS] catalyst.[45–47] We have recently reported on good reusability of water-soluble catalyst precursors in a "neat" environment of water as the solvent, without the conventional organic solvent toluene.[68] With that motivation, our catalyst precursors **4.9** and **4.10** were successfully evaluated in the "neat" hydroformylation of 1-octene, and these showed good recyclability over 5 cycles. Interesting to note was the good stabilisation of the trinuclear dendritic catalyst precursor **4.10** over the mononuclear complex **4.9** in this reaction media, evidenced by the formation of black particulate matter in the case of **4.9**. This would explain the lower catalyst performance of **4.9** compared to **4.10** in the absence of toluene. A comparative study of the rigid THPE-anchored trinuclear complex **4.10** with our previously reported *in situ* synthesised tris-2-(aminoethyl)amine **4.11** shows superior catalytic performance of **4.10** over **4.11**, attributed to a limited access of the metal active sites when using **4.11**. The ability to design a versatile catalyst that can be used across a wide spectrum of substrates is very attractive from an economic perspective. The catalyst precursors **4.9** and **4.10** were successfully evaluated in the aqueous biphasic hydroformylation of styrene, a good representation of substituted olefins. Both catalyst precursors **4.9** and **4.10** showed good catalytic performance by displaying sole chemoselectivity for aldehydes (no hydrogenation products present). The mononuclear complex **4.9** showed better activity (615 h^{-1}) than the trinuclear complex **4.10** (479 h^{-1}). This was attributed to the limited access of the active metal centres of the sterically hindered dendritic complex **4.10** by the relatively bulky styrene substrate. Assessment of the aqueous-

biphasic hydroformylation of internal olefins would be interesting in evaluating the versatility of the mono- (**4.9**) and trinuclear complexes (**4.10**).

5.4 References

1 R. L. Pruett, *J. Chem. Educ.*, 1986, **63**, 196–198.

2 G. D. Frey, *J. Organomet. Chem.*, 2014, **754**, 5–7.

3 J. Halpern, *Pure Appl. Chem.*, 2001, **73**, 209–220.

4 T. Vanbesien, F. Hapiot and E. Monflier, *Lipid Technol.*, 2013, **25**, 175–178.

5 B. Cornils, W. A. Herrmann and M. Rasch, *Angew. Chem. Int. Ed.*, 1994, **33**, 2144–2163.

6 B. Cornils, in *Topics in Current Chemistry*, Springer-Verlag Berlin Heidelberg, Berlin, Germany, 1999, vol. 206, pp. 133–149.

7 R. Franke, D. Selent and A. Börner, *Chem. Rev.*, 2012, **112**, 5675–5732.

8 G. T. Whiteker and C. J. Colbey, *Top Organomet Chem*, 2012, **42**, 35–46.

9 B. Cornils, *J. Mol. Catal. A Chem.*, 1999, **143**, 1–10.

10 B. R. James, P. W. N. M. van Leeuwen and C. Claver, in *Rhodium Catalyzed Hydroformylation*, Kluwer Academic Publishers, New York, 1st edn., 2002, pp. 6–277.

11 J. Hagen, in *Industrial Catalysis*, Wiley-VCH Verlag GmbH & Co. KGaA, Weinheim, 2nd edn., 2006, pp. 9–14.

12 C. Li, W. Wang, L. Yan and Y. Ding, *Front. Chem. Sci. Eng.*, 2018, **12**, 113–123.

13 M. Lombardo and C. Trombini, in *RSC Green Chemistry Series: Eco-Friendly Synthesis of Fine Chemicals*, Royal Society of Chemistry, 1st edn., 2009, pp. 1–79.

14 I. Vural Gürsel, T. Noel, Q. Wang and V. Hessel, *Green Chem.*, 2015, **17**, 2012–2026.

15 D. J. Cole-Hamilton and R. P. Tooze, in *Catayst Separation, Recovery, and Recycling*,

Springer, Dordrecht, 1st edn., 2006, vol. 30, pp. 4–35.

16 V. S. Shende, V. B. Saptal and B. M. Bhanage, *Chem. Rec.*, 2019, **19**, 2022–2043.

17 X. Jin, J. Feng, S. Li, H. Song, C. Yu, K. Zhao and F. Kong, *Mol. Catal.*, 2019, **475**, 110503.

18 B. Cornils, W. A. Herrmann, I. T. Horvath, W. Leitner, S. Mecking, H. Olivier-Bourbigou and D. Vogt, in *Multiphase Homogeneous Catalysis*, Wiley-VCH Verlag GmbH & Co. KGaA, Weinheim, 2nd edn., 2005, pp. 3–21.

19 A. E. C. Collis and I. T. Horváth, *Catal. Sci. Technol.*, 2011, **1**, 912–919.

20 W. Keim, *Green Chem.*, 2003, **5**, 105–111.

21 T. Rösler, T. A. Faßbach, M. Schrimpf, A. J. Vorholt and W. Leitner, *Ind. Eng. Chem. Res.*, 2019, **58**, 2421–2436.

22 Y. Huang, E. Perperi, G. Manos and D. J. Cole-Hamilton, *J. Mol. Catal. A Chem.*, 2004, **210**, 17–21.

23 L. Maqeda, B. C. E. Makhubela and G. S. Smith, *Polyhedron*, 2015, **91**, 128–135.

24 A. P. Dobbs and M. R. Kimberley, *J. Fluor. Chem.*, 2002, **118**, 3–17.

25 L. P. Barthel-Rosa and J. A. Gladysz, *Coord. Chem. Rev.*, 1999, **190**–**192**, 587–605.

26 R. H. Fish, *Chem. Eur. J.*, 1999, **5**, 1677–1680.

27 D. F. Foster, D. J. Adams, D. Gudmunsen, A. M. Stuart, E. G. Hope and D. J. Cole-Hamilton, *Chem. Commun.*, 2002, 722–723.

28 W. Chen, L. Xu and J. Xiao, *Chem. Commun.*, 2000, 839–840.

29 D. J. Adams, D. J. Cole-Hamilton, E. G. Hope, P. J. Pogorzelec and A. M. Stuart, *J. Organomet. Chem.*, 2004, **689**, 1413–1417.

30 S. L. Desset, U. Hintermair and D. J. Cole-Hamilton, *Top. Catal.*, 2010, **53**, 963–968.

31 J. Walkowiak, G. Franciò and W. Leitner, in *Applied Homogeneous Catalysis with*

Organometallic Compounds, Wiley-VCH Verlag GmbH & Co. KGaA, Weinheim, 3rd edn., 2018, pp. 1221–1258.

32 M. Haumann and P. Wasserscheid, in *Applied Homogeneous Catalysis with Organometallic Compounds*, Wiley-VCH Verlag GmbH & Co. KGaA, Weinheim, 3rd edn., 2018, pp. 999–1067.

33 D. R. Palo and C. Erkey, *Ind. Eng. Chem. Res.*, 1999, **38**, 3786–3792.

34 A. C. J. Koeken, L. J. P. van den Broeke, B. J. Deelman and J. T. F. Keurentjes, *J. Mol. Catal. A Chem.*, 2011, **346**, 1–11.

35 X. Jin, J. Feng, Q. Ma, H. Song, Q. Liu, B. Xu, M. Zhang, S. Li and S. Yu, *Green Chem.*, 2019, **21**, 3267–3275.

36 Q. Lin, W. Jiang, H. Fu, H. Chen and X. Li, *Appl. Catal. A Gen.*, 2007, **328**, 83–87.

37 Y. Xu, Y. Wang, Y. Zeng, J. Jiang and Z. Jin, *Catal. Letters*, 2012, **142**, 914–919.

38 F. Joó and Á. Kathó, *J. Mol. Catal. A Chem.*, 1997, **116**, 3–26.

39 E. A. Karakhanov and A. L. Maksimov, *Russ. J. Gen. Chem.*, 2009, **79**, 1370–1383.

40 B. Cornils, *Org. Process Res. Dev.*, 1998, **2**, 121–127.

41 L. C. Matsinha, S. Siangwata, G. S. Smith and B. C. E. Makhubela, *Catal. Rev. - Sci. Eng.*, 2019, **61**, 111–133.

42 P. T. Anastas and J. B. Zimmerman, *Environ. Sci. Technol.*, 2003, **37**, 95–101.

43 R. A. Sheldon, *Green Chem.*, 2005, **7**, 267–278.

44 R. A. Sheldon, *Curr. Opin. Green Sustain. Chem.*, 2019, **18**, 13–19.

45 B. Cornils and E. G. Kuntz, *J. Organomet. Chem.*, 1995, **502**, 177–186.

46 C. W. Kohlpaintner, R. W. Fischer and B. Cornils, *Appl. Catal. A Gen.*, 2001, **221**, 219–225.

47 A. Bényei and F. Joó, *J. Mol. Catal.*, 1990, **58**, 151–163.

48 C. De, R. Saha, S. K. Ghosh, A. Ghosh, K. Mukherjee, S. S. Bhattacharyya and B. Saha, *Res. Chem. Intermed.*, 2013, **39**, 3463–3474.

49 H. Fu, M. Li, H. Mao, Q. Lin, M. Yuan, X. Li and H. Chen, *Catal. Commun.*, 2008, **9**, 1539–1544.

50 L. Obrecht, P. C. J. Kamer and W. Laan, *Catal. Sci. Technol.*, 2013, **3**, 541–551.

51 J. Leblond, J. Potier, S. Menuel, H. Bricout, D. Landy, S. Tilloy, E. Monflier and F. Hapiot, *Catal. Sci. Technol.*, 2017, **7**, 3823–3830.

52 E. B. Hager, B. C. E. Makhubela and G. S. Smith, *Dalton Trans.*, 2012, **41**, 13927–35.

53 Y. Brunsch and A. Behr, *Angew. Chem. Int. Ed.*, 2013, **52**, 1586–9.

54 S. Paganelli, M. Marchetti, M. Bianchin and C. Bertucci, *J. Mol. Catal. A Chem.*, 2007, **269**, 234–239.

55 S. Siangwata, N. Baartzes, B. C. E. Makhubela and G. S. Smith, *J. Organomet. Chem.*, 2015, **796**, 26–32.

56 S. Siangwata, S. Chulu, C. L. Oliver and G. S. Smith, *Appl. Organomet. Chem.*, 2017, **31**, e3593.

57 L. C. Matsinha, S. F. Mapolie and G. S. Smith, *Dalton Trans.*, 2015, **44**, 1240–1248.

58 M. Vilches-Herrera, L. Domke and A. Börner, *ACS Catal.*, 2014, **4**, 1706–1724.

59 C. P. Lenges and M. Brookhart, *Angew. Chem. Int. Ed.*, 1999, **38**, 3533–3537.

60 C. Williams, M. Ferreira, E. Monflier, S. F. Mapolie and G. S. Smith, *Dalton Trans.*, 2018, **47**, 9418–9429.

61 Y. Dangat, M. Ahmad, P. Pandey and K. Vanka, *J. Organomet. Chem.*, 2016, **801**, 30–41.

62 M. Rosales, O. Soto, B. González, I. Pacheco and P. J. Baricelli, *Transit. Met. Chem.*, 2018, **43**, 451–461.

63 D. Astruc and F. Chardac, *Chem. Rev.*, 2001, **101**, 2991–3023.

64 B. C. E. Makhubela, A. M. Jardine, G. Westman and G. S. Smith, *Dalton Trans.*, 2012, **41**, 10715–10723.

65 N. C. Antonels, B. Therrien, J. R. Moss and G. S. Smith, *Inorg. Chem. Commun.*, 2009, **12**, 716–719.

66 R. N. Butler and A. G. Coyne, *Chem. Rev.*, 2010, **110**, 6302–6337.

67 C. A. Tolman, *Chem. Rev.*, 1977, **77**, 313–348.

68 N. N. Omosun and G. S. Smith, *Eur. J. Inorg. Chem.*, 2019, 2558–2564.

69 O. L. Eliseev, T. N. Bondarenko, S. N. Britvin, P. P. Khodorchenko and A. L. Lapidus, *Mendeleev Commun.*, 2018, **28**, 264–266.

70 S. Yu, Y. M. Chie, Z. H. Guan, Y. Zou, W. Li and X. Zhang, *Org. Lett.*, 2009, **11**, 241–244.

71 C. Bertucci, C. Botteghi, D. Giunta, M. Marchetti and S. Paganelli, *Adv. Synth. Catal.*, 2002, **344**, 556–562.

72 M. Benaglia, in *Recoverable and Recyclable Catalysts*, John Wiley & Sons, Ltd., Chichester, 1st edn., 2009, pp. 1-458.

73 B. Cornils, W. A. Herrmann and R. W. Eckl, *J. Mol. Catal. A Chem.*, 1997, **116**, 27–33.

74 S. K. Sharma and R. V. Jasra, *Catal. Today*, 2015, **247**, 70–81.

Chapter 6

Experimental

6.1 General details

All reactions were carried out in air unless otherwise stated. All chemicals and solvents were reagent grade and used as received from Sigma-Aldrich/Merck, unless otherwise stated. Propylsalicylaldimine (**2.1**),[1] *N*-3-bromopropylsalicylaldimine (**2.3**),[2] phenyl propargyl ether (**2.8**),[3] 1,1,1-tris(4-propargyl ether phenyl)ethane (**2.11**),[4] 3,5-bis(propargyl ether)benzyl alcohol (**2.14**),[5] and 3,5-bis(propargyl ether)benzyl bromide (**2.15**)[5] 5-sulfonato salicylaldehyde (**4.1**),[6] ^{t}butyl(3-bromopropyl)carbamate (**4.2**),[7] ^{t}butyl(3-phenoxypropyl)carbamate (**4.3**),[8] 3-phenoxypropylamine (**4.5**),[9] were prepared according to modified previously reported literature procedures. Nuclear Magnetic Resonance (NMR) spectra were recorded on either a Bruker Biospin GmbH (^{1}H: 400.22 MHz; ^{13}C: 100.65 MHz) or a Varian XR300 MHz (^{1}H: 300.08 MHz; ^{13}C: 75.46 MHz) spectrometer. NMR chemical shifts were reported relative to the internal standard tetramethylsilane (δ 0.00). FT-IR spectra were recorded using Attenuated Total Reflectance Infrared spectroscopy. Elemental analyses were conducted with a Fision EA 110 CHNS Analyser. Melting points were determined using a BÜCHI melting point apparatus B-540. Mass spectrometry was carried out using a Waters API Quattro Micro Triple Quadrupole electrospray ionisation mass spectrometer in the positive- and negative-ion modes. The mobile phase for LCMS analyses was prepared using solvents and reagents of HPLC-grade obtained from Sigma-Aldrich (ammonium acetate as an additive), Merck (glacial acetic acid) and Microsep (acetonitrile and methanol). Low Resolution-ESI-MS was acquired on an Agilent 1260 Infinity HPLC system (Agilent® 1260 Infinity Binary Pump, Agilent® 1260 Infinity Diode Array Detector (DAD), Agilent® 1290 Infinity Column Compartment, and Agilent® 1260 Infinity Standard Auto sampler) coupled to Agilent 6120 Quardrupole MS system and Peak Scientific® Genius 1050 Nitrogen Generator. Phenomenex Kinetex® 2.6 μm EVO C18 100 Å (30 x 2.1 mm) reverse phase analytical column was used. The chromatographic method included a column temperature of 40 °C, an injection volume of 2 μL, flow rate of 0.7 mL/ min and maximum column back pressure set at 600 bars. The mass spectrum was acquired using electrospray ionisation (ESI) in the positive ionization mode.

6.2 Series 1 (leading to non-water-soluble complexes of Chapter 2)

Part of Section 6.2 of this Chapter is presented in a publication titled "*Olefin hydroformylation and kinetic studies using mono- and trinuclear N,O-chelate rhodium(I)-aryl ether precatalysts*", cited as: **S. Siangwata**, N. C. C. Breckwoldt, N. J. Goosen and G. S. Smith., *Appl. Catal. A Gen.* 2019, **585**, 117179.

6.2.1 Preparation of propylsalicylaldimine ligand (2.1)[1]

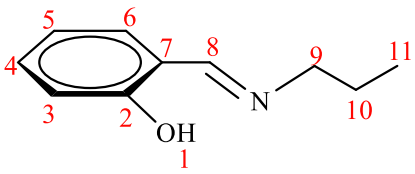

Propylamine (0.334 g, 5.65 mmol) was dissolved in dry methanol (20 mL) and added to a stirring solution of salicylaldehyde (0.656 g, 5.37 mmol) in methanol (30 mL). The yellow solution was left stirring at room temperature for 1 h, and the solvent was removed under reduced pressure to reveal a yellow oil. The oil was re-dissolved in dichloromethane and excess propylamine was removed through a dichloromethane-water extraction. The organic layer was collected and dried over anhydrous magnesium sulfate and the solvent was removed to yield the product (**2.1**) as a yellow oil which was collected and dried *in vacuo*. Yield: (0.850 g, 97%). ^{1}H NMR (DMSO-d$_6$, δ): 13.66 (s, 1H, H$_1$), 8.54 (s, 1H, H$_8$), 7.44–7.41 (m, 1H, H$_3$), 7.35–7.30 (m, 1H, H$_5$), 6.90–6.86 (m, 2H, H$_{4,6}$), 3.58–3.53 (t, ^{3}J = 6.9 Hz, 2H, H$_9$), 1.71–1.59 (sept, ^{3}J = 7.2 Hz, 2H, H$_{10}$), 0.95–0.90 (t, ^{3}J = 7.2 Hz, 3H, H$_{11}$). ^{13}C{^{1}H} NMR (DMSO-d$_6$, δ): 166.1 (C$_8$), 161.4 (C$_2$), 132.6 (C$_5$), 132.0 (C$_3$), 119.0 (C$_7$), 118.8 (C$_6$), 117.0 (C$_4$), 60.37 (C$_9$), 24.07 (C$_{10}$), 11.95 (C$_{11}$). FT-IR (ν_{max}/cm^{-1}): 2970 (O–H), 1635 (C=N). Anal. Calcd. For: C$_{10}$H$_{13}$NO, C: 73.59, H: 8.03, N: 8.58. Found: C, 73.64; H, 7.96; N, 8.05.

6.2.2 Preparation of Rh(I)-propylsalicylaldimine complex (2.2)

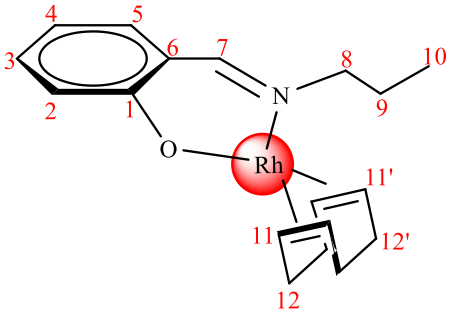

Triethylamine (0.272 g, 2.49 mmol) was added to a stirring solution of propylsalicylaldimine ligand **2.1** (0.203 g, 1.25 mmol) in dichloromethane (15 mL) and the reaction was left stirring for 1 h. A half molar equivalent of [RhCl(COD)]$_2$ (0.307 g, 0.623 mmol) was then added and the reaction was left stirring overnight at room temperature. The yellow solution was transferred into a 100 mL separating funnel and the triethylammonium chloride salt as well as excess triethylamine were removed from the solvent

through a dichloromethane-water extraction. The organic phase was collected and dried over anhydrous magnesium sulfate, filtered by gravity and the solvent in the filtrate was removed to yield the product (**2.2**) as a brown viscous oil which solidifies on drying *in vacuo*. Yield: (0.458 g, 99%). M.P.: 79 – 81 °C. ^{1}H NMR (DMSO-d$_6$, δ): 8.18 (s, 1H, H$_7$), 7.33–7.30 (m, 1H, H$_2$), 7.28–7.22 (m, 1H, H$_4$), 6.65–6.62 (d, ^{3}J = 8.4 Hz, 1H, H$_5$), 6.55–6.50 (m, 1H, H$_3$), 4.39 (br s, 2H, H$_{11}$), 3.69 (br s, 2H, H$_{11'}$), 3.11–3.06 (t, ^{3}J = 7.5 Hz, 2H, H$_8$), 2.38 (br s, 4H, H$_{12}$), 1.86 (br s, 4H, H$_{12'}$), 1.69–1.57 (sept, ^{3}J = 7.5 Hz, 2H, H$_9$), 0.89–0.84 (t, ^{3}J = 7.2 Hz, 3H, H$_{10}$). ^{13}C{^{1}H} NMR (DMSO-d$_6$, δ): 166.1 (C$_7$), 165.4 (C$_1$), 135.8 (C$_2$), 134.6 (C$_4$), 121.0 (C$_5$), 119.5 (C$_6$), 114.3 (C$_3$), 84.29 (C$_{11}$), 71.17 (C$_{11'}$), 60.40 (C$_8$), 31.85 (C$_{12}$), 28.90 (C$_{12'}$), 27.36 (C$_9$), 11.54 (C$_{10}$). FT-IR (ν_{max}/cm^{-1}): 1602 (C=N). Anal. Calcd. For: C$_{18}$H$_{24}$NORh, C: 57.92, H: 6.48, N: 3.75. Found: C, 57.54; H, 6.86; N, 3.19.

6.2.3 Preparation of *N*-3-bromopropylsalicylaldimine (2.3)[2]

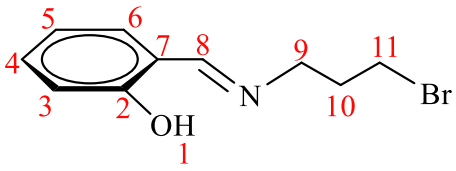

Salicylaldehyde (0.600 g, 4.91 mmol) was dissolved in ethanol (25 mL) in a 100 mL round-bottomed flask. 3-Bromopropylamine hydrobromide (1.20 g, 5.46 mmol) was dissolved in 25 mL of distilled water and added to the stirring solution. Sodium hydroxide pellets (0.200 g, 5.00 mmol) were dissolved in distilled water (0.5 mL) and added to the yellow solution. The reaction was stirred for 15 minutes at room temperature, after which distilled water (40 mL) was added and the product was extracted in a 100 mL separating funnel through a dichloromethane–water extraction. The organic layer was collected and dried over anhydrous magnesium sulfate, and the solvent was then removed under reduced pressure, yielding the product (**2.3**) as a viscous yellow oil which was collected and dried *in vacuo*. Yield: (1.07 g, 90%). ^{1}H NMR (DMSO-d$_6$, δ): 13.31 (s, 1H, H$_1$), 8.58 (s, 1H, H$_8$), 7.46–7.43 (m, 1H, H$_3$), 7.36–7.30 (m, 1H, H$_5$), 6.92–6.87 (m, 2H, H$_{6,4}$), 3.73–3.68 (t, ^{3}J = 6.6 Hz, 2H, H$_9$), 3.59–3.55 (t, ^{3}J = 6.3 Hz, 2H, H$_{11}$), 2.22–2.13 (quin, ^{3}J = 6.3 Hz, 2H, H$_{10}$). ^{13}C{^{1}H} NMR (DMSO-d$_6$, δ): 166.0 (C$_8$), 161.1 (C$_2$), 132.4 (C$_6$), 131.4 (C$_4$), 118.7 (C$_3$), 118.7 (C$_7$), 117.0 (C$_5$), 57.15 (C$_9$), 33.10 (C$_{10}$), 30.96 (C$_{11}$). FT-IR (ν_{max}/cm^{-1}): 2937 (O–H), 1629 (C=N). Anal. Calcd. For: C$_{10}$H$_{12}$BrNO, C: 49.61, H: 5.00, N: 4.93. Found: C, 50.39; H, 5.00; N, 4.93. EI-MS (positive ion-mode), (*m/z*) = 242.9505 [M]$^{+}$ and 240.9570 [M]$^{+}$ (calcd 242.0175).

6.2.4 Preparation of Rh(I)-bromopropylsalicylaldimine complex (2.4)

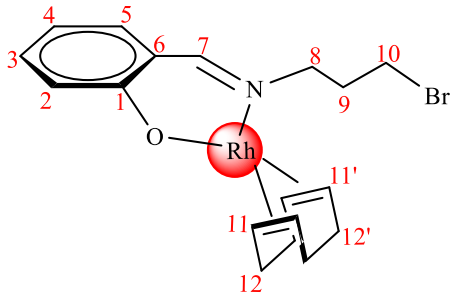

Triethylamine (8.19 x 10^{-2} g, 0.809 mmol) was added to a stirring solution of *N*-3-bromopropylsalicylaldimine ligand **2.3** (0.194 g, 0.803 mmol) in dichloromethane (25 mL) and the solution was allowed to stir for 30 minutes. A half molar equivalent of $[RhCl(COD)]_2$ (0.198 g, 0.402 mmol) was added and the solution was left stirring at room temperature for 24 h. The solvent was reduced (*ca*. 5 mL) and the triethylammonium chloride salt was extracted into water through a dichloromethane-water wash in a 100 mL separating funnel. The organic layer was dried over anhydrous magnesium sulfate, filtered by gravity and the solvent in the filtrate was reduced (*ca*. 3 mL), after which diethyl ether was added to precipitate the product (**2.4**) as a yellow solid which was collected by vacuum filtration and dried *in vacuo*. Yield: (0.276 g, 76%). M.P.: 120 – 121 °C. ^{1}H NMR (DMSO-d$_6$, δ): 8.21 (s, 1H, H$_7$), 7.32–7.23 (m, 2H, H$_{2,4}$), 6.65–6.62 (d, ^3J = 8.7 Hz, 1H, H$_5$), 6.55–6.51 (m, 1H, H$_3$), 4.39 (br s, 2H, H$_{11}$), 3.84–3.64 (m, 2H, H$_{11'}$), 3.56–3.52 (t, ^3J = 6.3 Hz, 2H, H$_8$), 3.26–3.24 (m, 2H, H$_{10}$), 2.38 (br s, 4H, H$_{12}$), 2.19–2.09 (quin, ^3J = 7.8 Hz, 2H, H$_9$), 1.86 (br s, 4H, H$_{12'}$). ^{13}C{^{1}H} NMR (DMSO-d$_6$, δ): 166.8 (C$_7$), 165.5 (C$_1$), 135.9 (C$_2$), 134.8 (C$_4$), 121.0 (C$_5$), 119.5 (C$_6$), 114.4 (C$_3$), 84.41 (C$_{11}$), 71.37 (C$_{11'}$), 57.31 (C$_{10}$), 36.62 (C$_9$), 32.13 (C$_8$), 31.84 (C$_{12}$), 28.85 (C$_{12'}$). FT-IR (ν_{max}/cm^{-1}): 1600 (C=N). Anal. Calcd. For: $C_{18}H_{23}BrNORh$, C: 47.81, H: 5.13, N: 3.10. Found: C, 47.90; H, 5.42; N, 2.80. EI-MS (positive ion-mode), (*m/z*) = 452.95 $[M + H]^+$ (calcd 453.21).

6.2.5 Preparation of Rh(I)-aryl ether low generation dendritic complex (2.5)

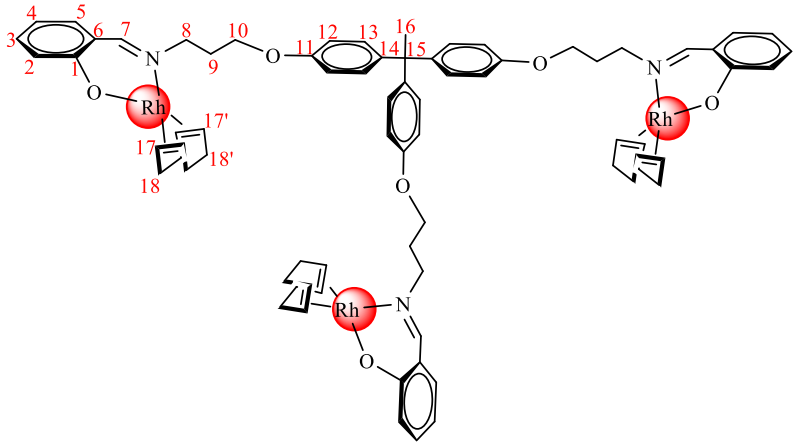

1,1,1-Tris(4-hydroxyphenyl)ethane (THPE), (2.26 x 10^{-2} g, 7.38 x 10^{-2} mmol) was dissolved in acetone (15 mL) in a 50 mL round-bottomed flask. K_2CO_3 (0.112 g, 0.812 mmol) and 18-crown-6 (1.00 x 10^{-2} g, 3.78 x 10^{-2} mmol) were then added,

and the mixture was allowed to stir for 1 h. Rh(I)-Bromopropylsalicylaldimine **2.4** (0.100 g, 0.221 mmol) was added and the reaction was refluxed for 72 h, after which the reaction was allowed to cool to room temperature, and then filtered by gravity. The filtrate was collected, and the solvent was removed to reveal a yellow viscous oily crude product. The crude product was re-dissolved in dichloromethane and washed with brine (2 x 100 mL). The organic layer was collected and dried over anhydrous magnesium sulfate, after which the solvent was reduced to a minimum (*ca*. 3 mL). Petroleum ether was added to precipitate the product (**2.5**) as a brown solid which was collected by vacuum filtration and dried *in vacuo*. Yield: (6.79 x 10^{-2} g, 22%). M.P.= decomposes without melting, onset occurs at 160 ºC. ^{1}H NMR (DMSO-d_6, δ): 8.20 (s, 3H, H_7), 7.27–7.22 (m, 6H, H_{Ar}), 6.96–6.92 (m, 6H, H_{Ar}), 6.85–6.82 (m, 6H, H_{Ar}), 6.67–6.61 (m, 4H, H_{Ar}), 6.53–6.48 (m, 2H, H_{Ar}), 4.37 (br s, 6H, H_{17}), 4.02–3.98 (m, 6H, H_8), 3.73 (br s, 6H, $H_{17'}$), 3.27 (br s, 6H, H_{10}), 2.30 (br s, 12H, H_{18}), 2.08–1.99 (m, 9H, $H_{9,16}$), 1.83–1.80 (m, 12H, $H_{18'}$). ^{13}C{^{1}H} NMR (DMSO-d_6, δ): 166.1 (C_7), 166.0 (C_1), 156.6 (C_{Ar}), 142.1 (C_{Ar}), 135.0 (C_{Ar}), 134.6 (C_{Ar}), 130.0 (C_{Ar}), 121.5 (C_{Ar}), 119.2 (C_{Ar}), 114.4 (C_{Ar}), 113.7 (C_{Ar}), 85.18 (C_{17}), 71.48 ($C_{17'}$), 63.71 (C_8), 41.36 (C_{10}), 36.09 (C_{15}), 31.77 (C_9), 30.90 (C_{18}), 29.70 (C_{16}), 28.96 ($C_{18'}$). FT-IR (ν_{max}/cm^{-1}): 1604 (C=N).

6.2.6 Preparation of Rh(I)-aryl ether first-generation benzyl alcohol complex (2.6)

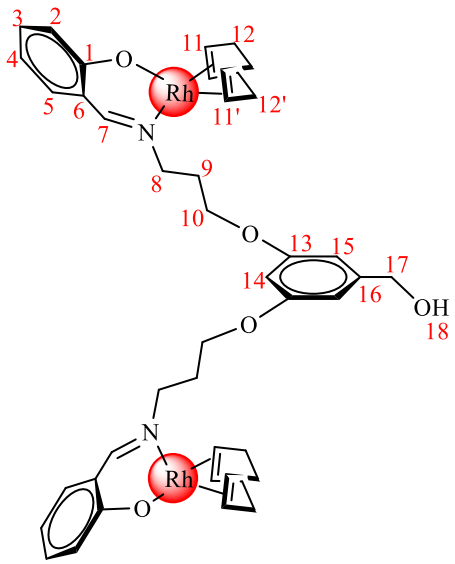

K_2CO_3 (0.590 g, 4.27 mmol) and 18-crown-ether (2.26 x 10^{-2} g, 8.53 x 10^{-2} mmol) were added to a stirring solution of 3,5-dihydroxybenzyl alcohol (0.120 g, 0.853 mmol) in dry acetone (15 mL). The mixture was left refluxing for 1 hour under N_2, and Rh(I)-bromopropylsalicylaldimine **2.4** (0.772 g, 1.71 mmol) was then added and the reaction was left heating under reflux for 48 h. The reaction mixture was allowed to cool to room temperature, and the solvent was removed, yielding a brown residue. The residue was re-dissolved in dichloromethane and transferred into a 100 mL separating funnel. A dichloromethane-water extraction was conducted (2 x 50 mL distilled water), and the organic layer was also washed with brine solution (1 x 50 mL). The organic layer was then collected and dried over anhydrous magnesium sulfate, and the solvent was reduced to a minimum (*ca*.

5 mL) and added dropwise into rapidly stirring hexane (350 mL). Precipitation of a brown solid product was observed, and this was triturated in diethyl ether, with periodic decantation of the resultant diethyl ether solution. Methanol was also used to triturate the same compound with periodic decantation of the resultant methanol solution. Finally, the brown solid product (**2.6**) was collected and dried *in vacuo*. Yield: (0.572 g, 38%). M.P.: decomposes without melting, onset occurs at 214 °C. ^{1}H NMR (DMSO-d$_6$, δ): 8.22 (s, 2H, H$_7$), 7.28–7.22 (m, 4H, H$_{2,5}$), 6.65–6.62 (d, ^{3}J = 8.4 Hz, 2H, H$_4$), 6.54–6.49 (m, 4H, H$_{3,15}$), 6.33 (s, 1H, H$_{14}$), 5.17–5.13 (t, ^{3}J = 5.4 Hz, 1H, H$_{18}$), 4.44–4.37 (m, 6H, H$_{17,11}$), 4.01–3.97 (t, ^{3}J = 5.7 Hz, 4H, H$_8$), 3.74 (br s, 4H, H$_{11'}$), 3.27 (br s, 4H, H$_{10}$), 2.34 (br s, 8H, H$_{12}$), 2.12–1.99 (quin, ^{3}J = 5.7 Hz, 4H, H$_9$), 1.83 (br s, 8H, H$_{12'}$). ^{13}C{^{1}H} NMR (DMSO-d$_6$, δ): 166.7 (C$_7$), 166.5 (C$_1$), 159.8 (C$_{13}$), 145.7 (C$_{16}$), 135.8 (C$_2$), 134.7 (C$_4$), 121.0 (C$_5$), 119.6 (C$_6$), 114.3 (C$_3$), 105.3 (C$_{15}$), 99.93 (C$_{14}$), 84.31 (C$_{11}$), 71.37 (C$_{11'}$), 65.11 (C$_8$), 63.24 (C$_{17}$), 55.47 (C$_{10}$), 33.49 (C$_9$), 31.81 (C$_{12}$), 28.91 (C$_{12'}$). FT-IR (ν_{max}/cm^{-1}): 1602 (C=N), 3325 (O–H).

6.2.7 Preparation of azidopropyl salicylaldimine ligand (2.7)

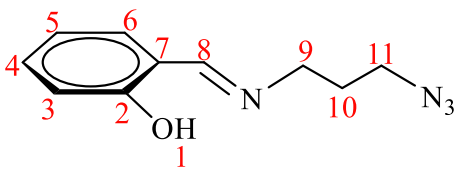

NaN_3 (0.303 g, 4.66 mmol) was added to a stirring solution of *N*-3-bromopropylsalicylaldimine (1.03 g, 4.23 mmol) in DMF (5 mL). The reaction was heated under N_2 at 80 °C overnight. The reaction was allowed to cool to room temperature and then filtered by gravity. The filtrate was then transferred to a 250 mL round-bottomed flask, and toluene was added to azeotropically remove the DMF. The resultant brown crude product was re-dissolved in ethyl acetate and washed with water (2 x 50 mL) and with brine solution (3 x 50 mL). The organic layer was collected and dried over anhydrous magnesium sulfate and filtered by gravity. The solvent was removed from the filtrate to produce (**2.7**) as a yellow oil which was dried *in vacuo*. Yield: (0.772 g, 89%). ^{1}H NMR (DMSO-d$_6$, δ): 13.35 (s, 1H, H$_1$), 8.57 (s, 1H, H$_8$), 7.45–7.42 (m, 1H, H$_3$), 7.35–7.30 (m, 1H, H$_5$), 6.92–6.87 (m, 2H, H$_{6,4}$), 3.67–3.63 (t, ^{3}J = 6.6 Hz, 2H, H$_9$), 3.45–3.41 (t, ^{3}J = 6.6 Hz, 2H, H$_{11}$), 1.95–1.86 (quin, ^{3}J = 6.9 Hz, 2H, H$_{10}$). ^{13}C{^{1}H} NMR (DMSO-d$_6$, δ): 166.8 (C$_8$), 166.1 (C$_2$), 132.7 (C$_5$), 132.1 (C$_3$), 119.1 (C$_7$), 119.0 (C$_6$), 116.9 (C$_4$), 56.0 (C$_9$), 49.1 (C$_{11}$), 30.0 (C$_{10}$). FT-IR (ν_{max}/cm^{-1}): 3056 (O–H), 2103 (–N$_3$), 1635 (C=N). LC-MS (ESI) (*m/z*) = 205.1 [M + H]$^{+}$ (calcd 205.1); purity (LC-MS) 99% (t_R = 2.23 min.).

6.2.8 Synthesis and characterisation of phenyl propargyl ether (2.8)[3]

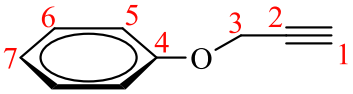

K_2CO_3 (3.46 g, 25.0 mmol) and 18-crown-ether (0.265 g, 1.00 mmol) were added to a stirring solution of phenol (1.57 g, 16.7 mmol) in dry acetone (30 mL). The reaction mixture was allowed to reflux for 45 minutes under N_2. Propargyl bromide (2.98 g, 25.0 mmol) dissolved in acetone (5 mL) was then added dropwise to the stirring mixture, and the reaction was allowed to reflux overnight under N_2. The solvent was removed under reduced pressure, and the resultant residue was re-dissolved in dichloromethane and transferred to a 100 mL separating funnel. A dichloromethane-water extraction was carried out (2 x 50 mL distilled water), and the organic layer was also washed with brine (1 x 50 mL), dried over anhydrous magnesium sulfate and filtered by gravity. The solvent in the filtrate was removed to yield the product (**2.8**) as a yellow oil which was dried *in vacuo*. Yield (1.90 g, 86%). ^{1}H NMR (DMSO-d$_6$, δ): 7.33–7.28 (m, 2H, H$_5$), 7.00–6.95 (m, 3H, H$_{6,7}$), 4.79–4.78 (d, ^4J = 2.4 Hz, 2H, H$_3$), 3.54–3.53 (t, ^4J = 2.4 Hz, H$_1$). ^{13}C{^{1}H} NMR (DMSO-d$_6$, δ): 157.7 (C$_4$), 129.9 (C$_5$), 121.7 (C$_7$), 115.3 (C$_6$), 79.77 (C$_2$), 78.52 (C$_1$), 55.80 (C$_3$). FT-IR (ν_{max}/cm^{-1}): 3266 (≡C–H), 2119 (C≡C).

6.2.9 Preparation of 4-(phenoxymethyl)-1*H*-1,2,3-triazol-1-yl-propylsalicylaldimine ligand (2.9)

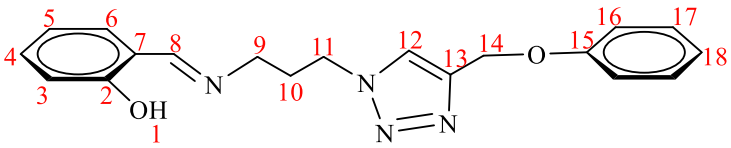

CuI (1.41 x 10^{-2} g, 7.41 x 10^{-2} mmol) was stirred in DIPEA (1.91 x 10^{-2} g, 0.148 mmol) at room temperature for 5 minutes in a 10 mL round-bottomed flask under N_2. A mixture of the alkyne-phenyl propargyl ether **2.8** (0.196 g, 1.48 mmol) and the azidopropyl salicylaldimine **2.7** (0.303 g, 1.48 mmol) was added, and the reaction was left stirring at room temperature under N_2, forming a paste. After 24 h, the reaction mixture was diluted with dichloromethane (3 mL) to bring the paste into solution and filtered by gravity. The filtrate was collected and washed in a 100 mL separating funnel with saturated NH_4Cl (3 x 50 mL) and the organic layer was then dried over anhydrous magnesium sulfate and filtered by gravity. The filtrate was reduced to a minimum (*ca.* 2 mL) and added dropwise into rapidly stirring diethyl ether (400 mL), yielding the product **2.9** as a dull yellow precipitate. Vigorous stirring was continued for 1 hour to triturate the product, which was collected by vacuum filtration, washed with diethyl ether, and then dried *in vacuo*. Yield: (0.423 g, 85%). M.P.: decomposes without melting, onset occurs at

124 °C. ^{1}H NMR (DMSO-d$_6$, δ): 13.26 (s, 1H, H$_1$), 8.52 (s, 1H, H$_8$), 8.27 (s, 1H, H$_{12}$), 7.44–7.42 (m, 1H, H$_{Ar}$), 7.36–7.27 (m, 3H, H$_{Ar}$), 7.04–6.87 (m, 6H, H$_{Ar}$), 5.11 (s, 2H, H$_{14}$), 4.49–4.44 (t, ^{3}J = 6.9 Hz, 2H, H$_9$), 3.60–3.56 (t, ^{3}J = 6.6 Hz, 2H, H$_{11}$), 2.27–2.18 (quin, ^{3}J = 6.9 Hz, 2H, H$_{10}$). ^{13}C{^{1}H} NMR (DMSO-d$_6$, δ): 167.0 (C$_8$), 161.0 (C$_2$), 158.6 (C$_{15}$), 143.4 (C$_{13}$), 132.8 (C$_5$), 132.1 (C$_3$), 130.0 (C$_{16}$), 124.9 (C$_{12}$), 121.3 (C$_{18}$), 119.1 (C$_7$), 119.0 (C$_6$), 116.9 (C$_4$), 115.2 (C$_{17}$), 61.57 (C$_{14}$), 55.83 (C$_{11}$), 47.85 (C$_9$), 31.24 (C$_{10}$). FT-IR (ν_{max}/cm^{-1}): 3087 (C–H, triazole), 3060 (O–H), 1627 (C=N). ESI-MS (positive ion-mode), (*m/z*) = 337.1747 [M + H]$^{+}$ (calcd 337.1666).

6.2.10 Preparation of 4-(phenoxymethyl)-1*H*-1,2,3-triazol-1-yl-propylsalicylaldimine-based Rh(I) complex (2.10)

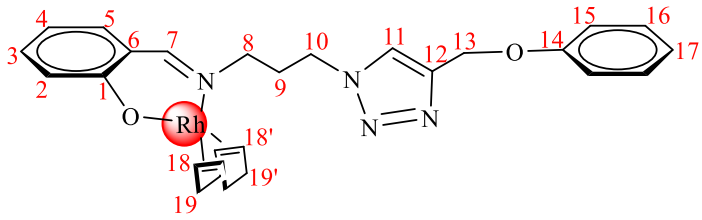

Triethylamine (1.37 x 10^{-2} g, 0.135 mmol) was added to a stirring solution of the 4-(phenoxymethyl)-1*H*-1,2,3-triazol-1-yl-propylsalicylaldimine ligand **2.9** (3.50 x 10^{-2} g, 0.104 mmol) in dichloromethane (5 mL) and the reaction was left stirring for 30 minutes. A half molar equivalent of [RhCl(COD)]$_2$ (2.56 x 10^{-2} g, 5.20 x 10^{-2} mmol) was added and the reaction was left stirring for 24 h at room temperature. The solution was diluted with dichloromethane (15 mL) and transferred into a 100 mL separating funnel in which triethylammonium chloride salt as well as excess triethylamine were removed from the organic solvent through a dichloromethane-water extraction (2 x 30 mL distilled water). The organic phase was collected and dried over anhydrous magnesium sulfate, filtered by gravity and the solvent in the filtrate was reduced to a minimum (*ca*. 2 mL). Diethyl ether was added (15 mL) to precipitate the product (**2.10**) as a yellow solid which was collected and dried *in vacuo*. Yield: (4.73 x 10^{-2} g, 83%). M.P.: decomposes without melting, onset occurs at 98 °C. ^{1}H NMR (DMSO-d$_6$, δ): 8.30 (s, 1H, H$_{11}$), 8.18 (s, 1H, H$_7$), 7.33–7.22 (m, 4H, H$_{Ar}$), 7.04–7.02 (m, 2H, H$_{Ar}$), 6.97–6.93 (m, 1H, H$_{Ar}$), 6.64–6.62 (m, 1H, H$_{Ar}$), 6.55–6.50 (m, 1H, H$_{Ar}$), 5.14 (s, 2H, H$_{13}$), 4.45–4.40 (m, 4H, H$_{8,18}$), 3.50 (br s, 2H, H$_{18'}$), 3.16–3.11 (t, ^{3}J = 7.5 Hz, 2H, H$_{10}$), 2.35 (br s, 4H, H$_{19}$), 2.22–2.13 (quin, ^{3}J = 6.9 Hz, 2H, H$_9$), 1.82–1.80 (m, 4H, H$_{19'}$). ^{13}C{^{1}H} NMR (DMSO-d$_6$, δ): 166.8 (C$_7$), 165.6 (C$_1$), 158.6 (C$_{14}$), 143.4 (C$_{12}$), 135.9 (C$_4$), 134.9 (C$_2$), 130.0 (C$_{15}$), 125.0 (C$_{11}$), 121.3 (C$_{19}$), 121.0 (C$_5$), 119.5 (C$_6$), 115.2 (C$_{16}$), 114.3 (C$_3$), 84.39 (C$_{18}$),

71.28 ($C_{18'}$), 61.60 (C_{13}), 55.74 (C_{10}), 47.51 (C_8), 34.24 (C_9), 31.73 (C_{19}), 28.94 ($C_{19'}$). FT-IR (ν_{max}/cm^{-1}): 1602 (C=N). ESI-MS (positive ion-mode), (*m/z*) = 547.1712 $[M + H]^+$ (calcd 547.1582).

6.2.11 Preparation of 1,1,1-tris(4-propargyl ether phenyl)ethane (2.11)[4]

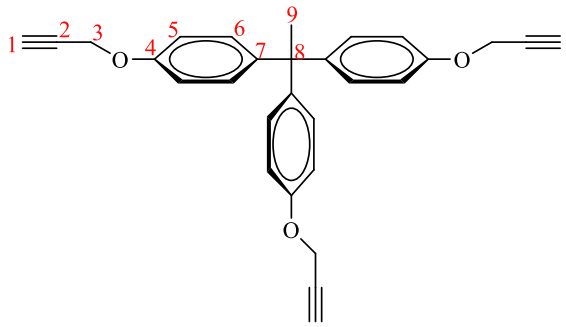

K_2CO_3 (6.30 g, 45.6 mmol) and 18-crown-ether (0.201 g, 0.760 mmol) were added to a stirring solution of 1,1,1-tris(4-hydroxyphenyl)ethane (THPE) (1.55 g, 5.07 mmol) in dry acetone (60 mL) and the mixture was refluxed for 45 minutes under N_2. Propargyl bromide (3.01 g, 25.3 mmol) dissolved in acetone (2 mL) was added dropwise to the stirring mixture, and the reaction was allowed to reflux for 24 h under N_2. The reaction was then allowed to cool to room temperature, filtered under gravity, and the solvent in the filtrate was removed under reduced pressure, revealing a brown oil which was re-dissolved in dichloromethane. A dichloromethane-water extraction was carried out (2 x 50 mL distilled water), and the organic layer was also washed with brine (1 x 50 mL) and dried over anhydrous magnesium sulfate. The solvent in the filtrate was removed to yield the product (**2.11**) as a light-brown oil which solidifies into a dirty-white solid when dried *in vacuo*. Yield: (1.93 g, 91%). M.P.: 82 – 84 °C. ^{1}H NMR (DMSO-d$_6$, δ): 6.97–6.87 (m, 12H, $H_{5,6}$), 4.76–4.75 (d, ^4J = 2.4 Hz, 6H, H_3), 3.54–3.52 (t, ^4J = 2.4 Hz, 3H, H_1), 2.05 (s, 3H, H_9). ^{13}C{^{1}H} NMR (DMSO-d$_6$, δ): 155.7 (C_4), 142.4 (C_7), 129.7 (C_5), 114.5 (C_6), 79.8 (C_2), 78.50 (C_1), 55.90 (C_3), 50.78 (C_8), 30.81 (C_9). FT-IR (ν_{max}/cm^{-1}): 3282 (≡C–H), 3266 (≡C–H), 2131 (C≡C), 2119 (C≡C).

6.2.12 Preparation of 1,1,1-tris(4-phenoxymethyl)ethane-1*H*-1,2,3-triazol-1-yl-propylsalicylaldimine ligand (2.12)

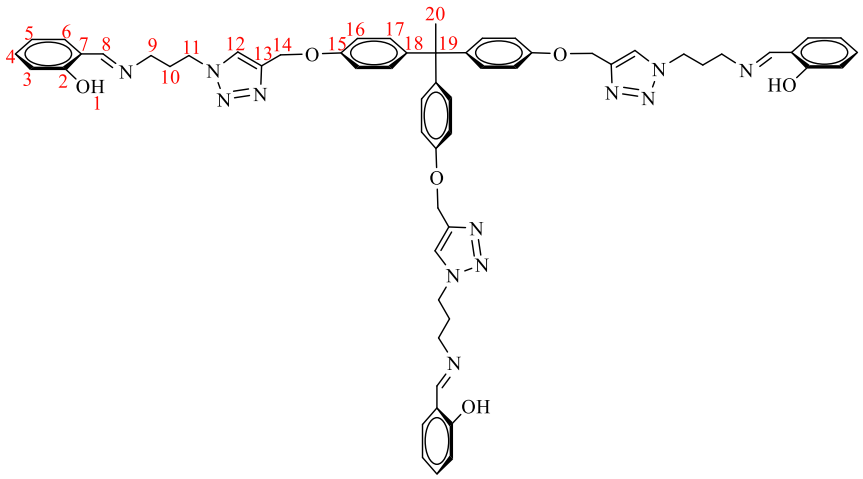

CuI (1.14 x 10^{-2} g, 5.98 x 10^{-2} mmol) was stirred in DIPEA (1.54 x 10^{-2} g, 0.119 mmol) at room temperature for 5 minutes in a 10 mL round-bottomed flask under N_2. The alkyne-1,1,1-tris(4-propargyl ether phenyl)ethane **2.11** (0.168 g, 0.398 mmol) was dissolved in dichloromethane (2 mL) and introduced into the flask, and the mixture was allowed to stir for a further 10 minutes, forming a paste. Azidopropyl salicylaldimine **2.7** (0.247 g, 1.21 mmol) was added and the reaction mixture was left stirring at room temperature for 72 h under N_2. Dichloromethane (5 mL) was added, and the mixture was stirred at 45 °C for 1 h under N_2. The reaction was allowed to cool to room temperature, and the mixture was filtered by gravity. The filtrate was collected and filtered through a pad of Celite™. The solvent was reduced to a minimum (*ca.* 2 mL) and added dropwise into rapidly stirring diethyl ether (400 mL), yielding the product (**2.12**) as a dull yellow precipitate. Vigorous stirring was continued for a further 30 minutes and the product was collected by vacuum filtration, washed with diethyl ether, and then dried *in vacuo*. Yield: (0.370 g, 90%). M.P.: decomposes without melting, onset occurs at 74 °C. ^{1}H NMR (DMSO-d_6, δ): 13.27 (s, 3H, H_1), 8.51 (s, 3H, H_8), 8.26 (s, 3H, H_{12}), 7.43–7.33 (m, 6H, H_{Ar}), 7.06–6.80 (m, 18H, H_{Ar}), 5.01 (s, 6H, H_{14}), 4.63–4.29 (br s, 6H, H_9), 3.66–3.52 (br s, 6H, H_{11}), 2.33–2.13 (br s, 6H, H_{10}), 2.04 (s, 3H, H_{20}). ^{13}C{^{1}H} NMR (DMSO-d_6, δ): 166.8 (C_8). 166.0 (C_2), 156.7 (C_{15}), 143.5 (C_{13}), 142.2 (C_{18}), 132.7 (C_5), 132.1 (C_3), 129.7 (C_{16}), 124.8 (C_{12}), 119.2 (C_7), 119.0 (C_6), 116.9 (C_4), 114.6 (C_{17}), 61.85 (C_{14}), 55.81 (C_{11}), 50.79 (C_{19}), 47.90 (C_9), 31.23 (C_{10}), 30.84 (C_{20}). FT-IR (ν_{max}/cm^{-1}): 3085 (C–H, triazole), 3052 (O–H), 1629 (C=N), 1611 (C=N). ESI-MS (positive ion-mode), (*m/z*) = 1055.4918 $[M + Na]^+$ (calcd 1055.4659).

6.2.13 Preparation of 1,1,1-tris(4-phenoxymethyl)ethane-1*H*-1,2,3-triazol-1-yl-propylsalicylaldimine-based Rh(I) complex (2.13)

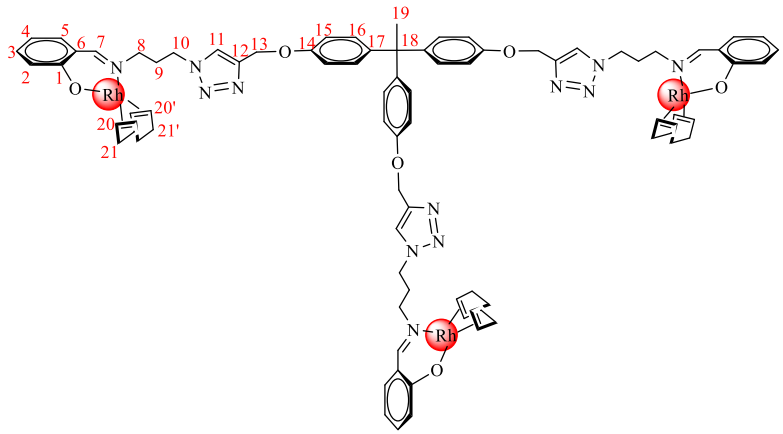

Triethylamine (2.88 x 10^{-2} g, 0.285 mmol) was added to a stirring solution of the 1,1,1-tris(4-hydroxyphenyl)ethane tris(triazolesalicylaldimine) ligand **2.12** (7.55 x 10^{-2} g, 7.31 x 10^{-2} mmol) in dichloromethane (5 mL) and the reaction was left stirring for 30 minutes. A one and a half molar equivalent of $[RhCl(COD)]_2$ (5.40 x 10^{-2} g, 0.110 mmol) was added and the reaction was left to stir for 24 h at room temperature. The solution was diluted with dichloromethane (15 mL) and washed with distilled water (2 x 30 mL). The organic phase was collected and dried over anhydrous magnesium sulfate, filtered by gravity and the solvent in the filtrate was then reduced to a minimum (*ca*. 2 mL). Diethyl ether was added (15 mL) to precipitate the product (**2.13**) as a yellow solid which was collected by vacuum filtration and dried *in vacuo*. Yield: (0.136 g, 99%). M.P.: decomposes without melting, onset occurs at 185 °C. ^{1}H NMR (DMSO-d_6, δ): 8.29 (s, 3H, H_{11}), 8.18 (s, 3H, H_7), 7.30–7.22 (m, 6H, H_{Ar}), 6.97–6.90 (br s, 12H, H_{Ar}), 6.65–6.62 (m, 3H, H_{Ar}), 6.55–6.50 (m, 3H, H_{Ar}), 5.11 (s, 6H, H_{13}), 4.50–4.30 (m, 12H, $H_{20,8}$), 3.54–3.38 (m, 6H, $H_{20'}$), 3.18–3.07 (m, 6H, H_{10}), 2.41–2.29 (m, 12H, H_{21}), 2.22–2.13 (m, 6H, H_9), 2.08–2.01 (s, 3H, H_{19}), 1.86–1.74 (m, 12H, $H_{21'}$). ^{13}C{^{1}H} NMR (DMSO-d_6, δ): 166.7 (C_7), 165.6 (C_1), 156.6 (C_{14}), 143.5 (C_{12}), 142.1 (C_{17}), 135.9 (C_4), 134.8 (C_2), 129.7 (C_{15}), 125.0 (C_{11}), 121.1 (C_5), 119.5 (C_6), 114.4 (C_{16}), 114.3 (C_3), 84.48 (C_{20}), 71.31 ($C_{20'}$), 61.66 (C_{13}), 55.72 (C_{10}), 50.70 (C_{18}), 47.51 (C_8), 34.24 (C_9), 31.74 (C_{21}), 30.81 (C_{19}), 28.86 ($C_{21'}$). FT-IR (ν_{max}/cm^{-1}): 1604 (C=N). ESI-MS (positive ion-mode), (*m/z*) = 736.4466 $[M + H + Na]^{2+}$ (calcd 735.1296).

6.2.14 Preparation of 3,5-bis(propargyl ether)benzyl alcohol (2.14)[5]

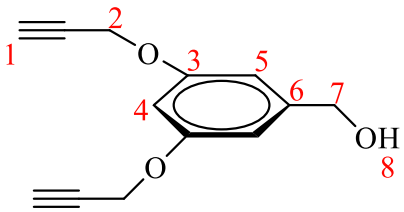

K_2CO_3 (2.71 g, 19.6 mmol) and 18-crown-ether (2.59 x 10^{-2} g, 9.80 x 10^{-2} mmol) were added to a stirring solution of 3,5-dihydroxybenzyl alcohol (0.549 g, 3.92 mmol) in DMF (5 mL). The reaction mixture was allowed to stir at 80 °C for 30 minutes under N_2. Propargyl bromide (1.17 g, 9.80 mmol) was dissolved in DMF (2 mL) and added dropwise to the stirring mixture, and the reaction was left to stir at 80 °C under N_2. After 24 h, the DMF was removed *via* azeotropic distillation with toluene, and the resultant residue was re-dissolved in ethyl acetate. The organic layer was washed with distilled water (4 x 40 mL) and brine (3 x 40 mL) and dried over anhydrous magnesium sulfate. The solvent was removed to yield the product (**2.14**) as a brown oil which was dried *in vacuo*. Yield (1.65 g, 96%) ^{1}H NMR (DMSO-d_6, δ): 6.58–6.57 (m, 2H, H_5), 6.48–6.47 (m, 1H, H_4), 5.21–5.17 (t, ^3J = 5.7 Hz, 1H, H_8), 4.76–4.75 (d, ^4J = 2.4 Hz, 4H, H_2), 4.45–4.43 (d, ^3J = 5.7 Hz, 2H, H_7), 3.54–3.52 (t, ^4J = 2.4 Hz, 2H, H_1). FT-IR (ν_{max}/cm^{-1}): 3382 (≡C–H), 3286 (≡C–H), 3329 (O–H), 2122 (C≡C).

6.2.15 Preparation of 3,5-bis(propargyl ether)benzyl bromide (2.15)[5]

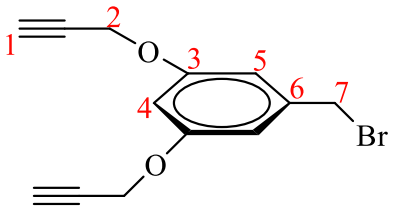

A solution of PBr_3 (96.1 µL, 1.02 mmol) in dry THF (2 mL) was added dropwise over 10 minutes to a stirring solution of 3,5-bis(propargyl ether)benzyl alcohol (0.553 g, 2.56 mmol) in a 20 mL Schlenk tube maintained at 0 °C under N_2. Stirring was continued for a further 30 minutes at 0 °C, and at room temperature. After 24 h, the brown solution was poured into ice-cold water (30 mL) and extracted with ethyl acetate (4 x 50 mL). The organic extracts were combined and dried over anhydrous magnesium sulfate and the solvent was removed under reduced pressure at 20 °C, revealing a brown viscous oil. Purification of the oil was conducted by silica gel chromatography, eluting with hexane:ethyl acetate (9:1) to give the product (**2.15**) as a light yellow viscous oil which was dried *in vacuo*. Yield: (0.669 g, 94%). ^{1}H NMR (DMSO-d_6, δ): 6.71–6.70 (m, 2H, H_5), 6.59–6.57 (m, 1H, H_4), 4.79–4.78 (d, ^4J = 2.4 Hz, 4H, H_2), 4.61 (s, 2H, H_7), 3.57–3.55 (t, ^4J = 2.4 Hz, H_1). FT-IR (ν_{max}/cm^{-1}): 3386 (≡C–H), 3258 (≡C–H), 2119 (C≡C).

6.2.16 Preparation of 3,5-bis(oxymethylene-1*H*-1,2,3-triazol-1-yl-propylsalicylaldimine) benzyl bromide (2.16)

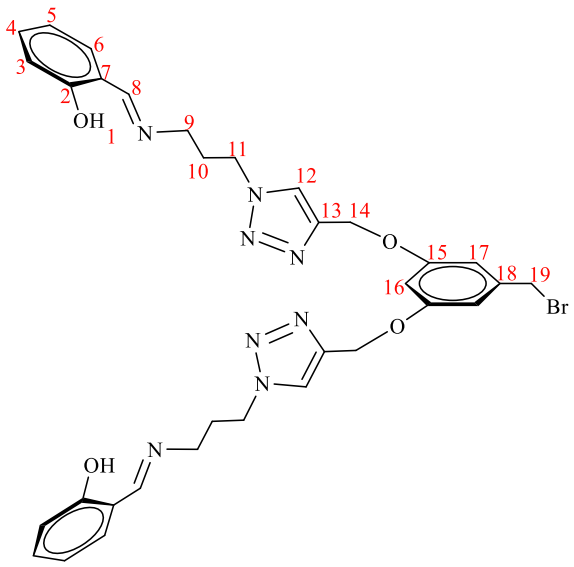

CuBr (6.74 x 10^{-3} g, 4.70 x 10^{-2} mmol) was stirred in DIPEA (1.21 x 10^{-2} g, 9.39 x 10^{-2} mmol) at room temperature for 5 minutes in a 10 mL round-bottomed flask under N_2. The alkyne-3,5-bis(propargyl ether)benzyl bromide **2.15** (0.131 g, 0.470 mmol) was dissolved in dichloromethane (0.1 mL) and added to the mixture, and this was allowed to stir for a further 10 minutes. Azidopropyl salicylaldimine **2.7** (0.192 g, 0.939 mmol) was dissolved in dichloromethane (0.1 mL) and added to the stirring mixture, and the reaction was left stirring at room temperature under N_2, forming a paste. After 48 h, the reaction mixture was diluted with dichloromethane (5 mL) to bring the paste into solution, and then filtered by gravity. The filtrate was washed with saturated NH_4Cl (3 x 40 mL), dried over anhydrous magnesium sulfate and filtered by gravity. The filtrate was reduced to a minimum (*ca.* 2 mL) and added dropwise into rapidly stirring petroleum ether (400 mL), yielding the product (**2.16**) as a dull yellow precipitate. The product was stirred vigorously for a further 30 minutes, and then collected by vacuum filtration, washed with petroleum ether and dried *in vacuo*. Yield: (0.196 g, 61%). M.P.: 92 – 95 °C. ^{1}H NMR (DMSO-d_6, δ): 13.19 (s, 2H, H_1), 8.52 (s, 2H, H_8), 8.24 (s, 2H, H_{12}), 7.42–7.32 (m, 4H, $H_{6,3}$), 7.01–6.55 (m, 7H, $H_{5,4,17,16}$), 5.24–4.95 (br s, 4H, H_{14}), 4.55–3.99 (m, 6H, $H_{9,19}$), 3.59 (br s, 4H, H_{11}), 2.22 (br s, 4H, H_{10}).). FT-IR (ν_{max}/cm^{-1}): 3080 (C–H, triazole), 3065 (O–H), 1629 (C=N), 1596 (C=N).

6.2.17 Preparation of 3,5-bis(oxymethylene-1*H*-1,2,3-triazol-1-yl-propylsalicylaldimine) benzyl azide (2.17)

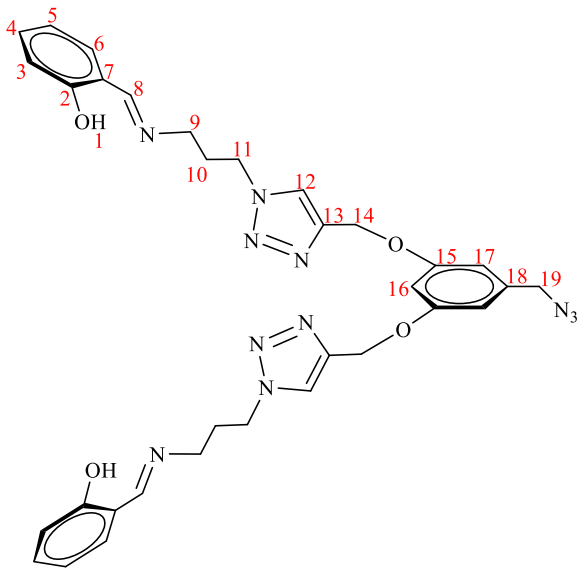

NaN_3 (8.84 x 10^{-2} g, 1.36 mmol) was added to a stirring solution of **2.16** (0.850 g, 1.24 mmol) in DMF (5 mL) and the reaction was left to stir at 80 °C. After 24 h, the reaction was allowed to cool to room temperature and then filtered by gravity. The filtrate was washed with distilled water (3 x 40 mL) and brine (5 x 40 mL) and the organic extracts were combined and dried over anhydrous magnesium sulfate. The solvent in the filtrate was reduced to a minimum (*ca*. 2 mL) and petroleum ether was added to yield the product (**2.17**) as a dull yellow solid which was collected by vacuum filtration and dried *in vacuo*. M.P.: 75 – 77 °C. ^{1}H NMR (DMSO-d_6, δ): 13.27 (s, 2H, H_1), 8.51 (s, 2H, H_8), 8.25 (s, 2H, H_{12}), 7.41–7.32 (m, 4H, $H_{6,3}$), 6.94–6.55 (m, 7H, $H_{5,4,17,16}$), 5.23–4.95 (br s, 4H, H_{14}), 4.56–4.24 (m, 6H, $H_{9,19}$), 3.56 (br s, 4H, H_{11}), 2.22 (br s, 4H, H_{10}). FT-IR (ν_{max}/cm^{-1}): 3084 (C–H, triazole), 3063 (O–H), 2127 (–N_3), 1620 (C=N), 1597 (C=N).

6.2.18 Synthesis and characterisation of the hexameric ligand (2.18)

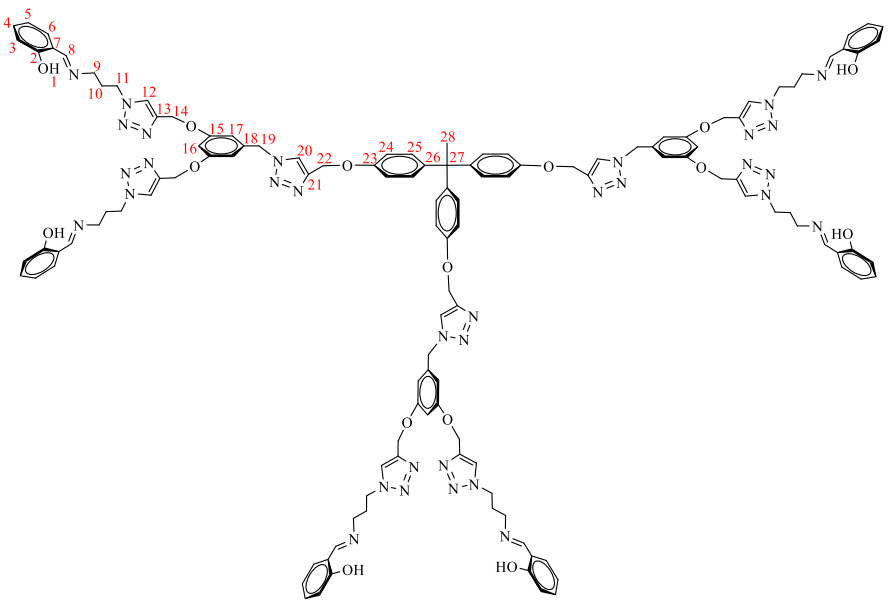

CuI (2.53 x 10^{-3} g, 1.33 x 10^{-2} mmol) was stirred in DIPEA (3.45 x 10^{-3} g, 2.66 x 10^{-2} mmol) at room temperature for 5 minutes in a 10 mL round-bottomed flask under N_2. The alkyne-1,1,1-tris(4-propargyl ether phenyl)ethane **2.11** (3.72 x 10^{-2} g, 8.85 x 10^{-2} mmol) was dissolved in dichloromethane (0.5 mL) and added to the mixture, and this was allowed to stir for a further 10 minutes. The azide **2.17** (0.173 g, 0.266 mmol) was dissolved in DCM (0.5 mL) and added to the reaction mixture, and this was left to stir at room temperature under N_2, with DCM solvent replenished as necessary. After 72 h, the reaction mixture was filtered by gravity and the filtrate was collected and washed with saturated NH_4Cl (3 x 40 mL) and brine (2 x 40 mL), and the organic extracts were combined and dried over anhydrous magnesium sulfate. The solvent in the filtrate was reduced to a minimum (*ca*. 2 mL) and petroleum ether was added, revealing the product (**2.18**) as a dull yellow solid which was collected and dried *in vacuo*. ^{1}H NMR (DMSO-d_6, δ): 13.27 (s, 6H, H_1), 9.33 (br s, 3H, H_{20}), 8.53 (s, 6H, H_8), 8.27 (s, 6H, H_{12}), 7.44–7.31 (m, 15H, H_{Ar}), 7.00–6.46 (m, 43H, H_{Ar}), 5.20–5.04 (m, 12H, H_9), 4.56–4.35 (m, 12H, H_{11}), 3.66–3.49 (m, 24H, $H_{14,22}$), 2.31–2.16 (m, 15H, $H_{10,28}$).

6.3 Series 2 (leading to water-soluble complexes of Chapter 4)

This Section of Chapter 6 forms part of a publication titled "*Aqueous olefin hydroformylation using water-soluble mono- and trinuclear N,O-chelate rhodium(I)-aryl ether precatalysts*", cited as: **S. Siangwata**, N. J. Goosen and G. S. Smith., *Appl. Catal. A Gen*. 2020, **603**, 117736.

6.3.1 Preparation of 5-sulfonato salicylaldehyde (4.1)[6]

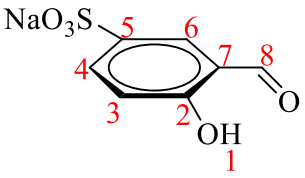

The sulfonated aldehyde was prepared following a literature procedure involving a series of protection, sulfonation and deprotection steps as outlined below.

Step 1: Aniline (3.53 g, 37.9 mmol) was added to a stirring solution of salicylaldehyde (4.63 g, 37.9 mmol) in methanol (50 mL), and the reaction was allowed to stir overnight at room temperature. The solvent was then reduced to a minimum (10 mL), yielding a yellow crystalline product (*N*-phenyl-salicylaldimine) which was collected by vacuum filtration, washed with cold methanol and dried *in vacuo*.

Step 2: The crystalline product (*N*-phenyl-salicylaldimine) (3.41 g, 17.7 mmol) was added to concentrated sulfuric acid (10 mL) slowly with stirring, and the reaction mixture was heated at 105 °C for 2.5 h. The hot solution was poured carefully into a beaker containing ice water (*ca*. 100 mL), revealing a yellow precipitate which was re-dissolved by heating to give a bright orange solution. The solution was filtered by gravity and the filtrate left to stand at room temperature to allow crystallisation, giving a dull yellow product (*N*-phenyl-5-sulfonatosalicylaldimine), which was filtered by vacuum, and washed with small portions of cold water and dried *in vacuo*.

Step 3: Sodium carbonate (0.600 g, 5.62 mmol) was added to a solution of *N*-phenyl-5-sulfonatosalicylaldimine (1.49 g, 5.37 mmol) in distilled water, and this was brought to boil in an open flask for 2 h with periodic replenishment of water when necessary. The resultant solution was cooled, followed by addition of glacial acetic acid (6 mL) and ethanol (10 mL), and the solution was cooled in an ice-bath for several hours to reveal a beige precipitate product (monosodium 5-sulfonatosalicylaldehyde, **4.1**). This was collected using a Büchner funnel and washed with cold ethanol and dried *in vacuo*. Yield: (0.775 g, 64%). M.P.: 330 – 334 °C. ^{1}H NMR (D_2O, δ): 11.62 (s, 1H, H_1), 9.97 (s, 1H, H_8), 8.20 (d, ^{4}J = 2.4 Hz, 1H, H_6), 7.99 (dd, ^{3}J = 8.4 Hz, ^{4}J = 2.4 Hz, 1H, H_4), 7.16 (d, ^{3}J = 8.6 Hz, 1H, H_3).

6.3.2 Preparation of ᵗbutyl(3-bromopropyl)carbamate (4.2)[7]

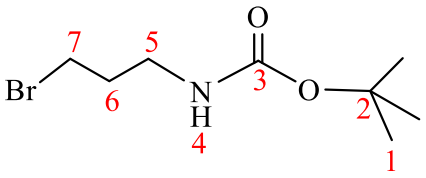

Triethylamine (1.19 g, 11.7 mmol) was added to a stirring solution of 3-bromopropylamine hydrobromide (1.51 g, 6.90 mmol) in methanol (15 mL). A solution of $(Boc)_2O$ (2.30 g, 10.4 mmol) in methanol (15 mL) was added dropwise over 30 minutes, and the reaction was left to stir at room temperature. After 16 h, the solvent was removed, revealing a white residue which was re-dissolved in distilled water (100 mL) and extracted with dichloromethane (4 x 50 mL). The organic extracts were combined and washed with brine (3 x 50 mL) and dried over anhydrous magnesium sulfate and then filtered by gravity. The solvent in the filtrate was removed revealing a colourless oil. Excess unreacted $(Boc)_2O$ was removed by azeotropic distillation with methanol, yielding the product (**4.2**) as a colourless oil which turns to a white solid when dried *in vacuo*. Yield: (1.58 g, 96%). M.P.: 38 – 39 °C. ^{1}H NMR ($CDCl_3$, δ): 4.65 (br s, 1H, H_4), 3.45–3.41 (t, ^3J = 6.6 Hz, 2H, H_7), 3.29–3.23 (q, ^3J = 6.3 Hz, 2H, H_5), 2.09–2.00 (quin, ^3J = 6.6 Hz, 2H, H_6), 1.44 (s, 9H, H_1). $^{13}C\{^1H\}$ NMR ($CDCl_3$, δ): 156.1 (C_3), 79.59 (C_2), 39.17 (C_5), 32.87 (C_6), 30.89 (C_7), 28.53 (C_1). FT-IR (ν_{max}/cm^{-1}): 3378 (N–H), 1684 (C=O).

6.3.3 Preparation of ᵗbutyl(3-phenoxypropyl)carbamate (4.3)[8]

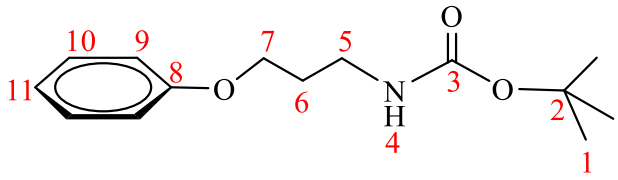

Phenol (0.300 g, 3.19 mmol), K_2CO_3 (1.32 g, 9.56 mmol), and 18-crown-ether (0.211 g, 0.797 mmol) were stirred in acetone (15 mL) under reflux for 30 minutes. To this mixture was added ᵗbutyl(3-bromopropyl)carbamate **4.2** (0.835 g, 3.51 mmol) and the mixture was refluxed overnight under N_2. The reaction was allowed to cool to room temperature and the solvent was removed under reduced pressure. The resultant residue was re-dissolved in distilled water (100 mL) and extracted with dichloromethane (4 x 50 mL). The organic extracts were combined and dried over anhydrous sodium sulfate and filtered by gravity. The solvent in the filtrate was removed to reveal the product (**4.3**) as a clear oil which solidifies to a white solid on drying *in vacuo*. Yield: (0.656 g, 82%). M.P.: 74 – 75 °C. ^{1}H NMR ($CDCl_3$, δ): 7.33–7.28 (m, 2H, H_9), 6.99–6.91 (m, 3H, $H_{10,\,11}$), 4.79 (br s, 1H, H_4), 4.07–4.03 (t, ^3J = 6.0 Hz, 2H, H_7), 3.38–3.32 (q, ^3J = 6.3 Hz, 2H, H_5), 2.04–1.96 (quin, ^3J = 6.3 Hz, 2H, H_6), 1.47 (s, 9H, H_1). $^{13}C\{^1H\}$ NMR ($CDCl_3$, δ): 158.9 (C_8), 156.2 (C_3), 129.6 (C_{10}), 121.0 (C_{11}), 114.7 (C_9), 79.35

(C_2), 65.89 (C_7), 38.28 (C_5), 29.71 (C_6), 28.56 (C_1). FT-IR (ν_{max}/cm^{-1}): 3302 (N–H), 1679 (C=O).

6.3.4 Preparation of 1,1,1-tris(ᵗbutyl-4-phenoxymethyl)ethane-propylcarbamate (4.4)

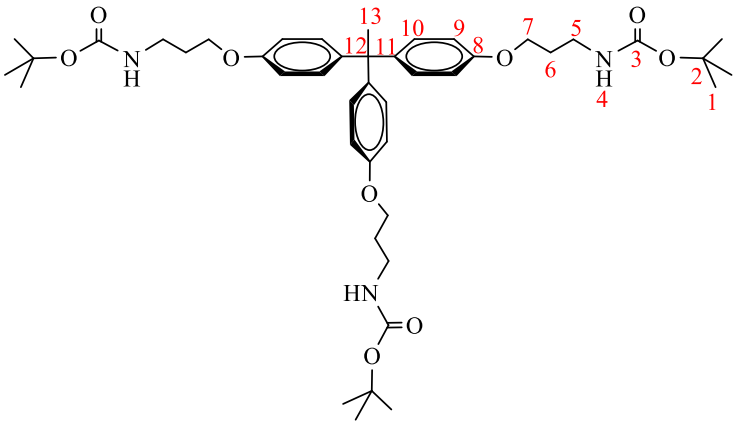

THPE (0.462 g, 1.51 mmol), K_2CO_3 (1.88 g, 13.6 mmol), and 18-crown-ether (9.97 x 10^{-2} g, 0.377 mmol) were stirred in acetone (20 mL) under reflux for 30 minutes. To this was added ᵗbutyl(3-bromopropyl)carbamate **4.2** (1.29 g, 5.43 mmol) and the mixture was refluxed under N_2. After 20 h, the reaction was allowed to cool to room temperature and the solvent was removed under reduced pressure. The resultant residue was re-dissolved in distilled water (100 mL) and extracted with dichloromethane (4 x 50 mL). The organic extracts were combined and dried over anhydrous sodium sulfate and filtered by gravity. The solvent was removed from the filtrate, yielding the crude product as a colourless viscous oil which was purified *via* silica gel column chromatography, eluting the product as a clear oil using toluene:ethyl acetate (85:15) as eluent. The colourless oil product (**4.4**) turns to a white solid upon drying *in vacuo*. Yield: (0.985 g, 84%). M.P.: 61 – 63 °C. ^{1}H NMR ($CDCl_3$, δ): 6.99–6.96 (m, 6H, H_9), 6.79–6.76 (m, 6H, H_{10}), 4.77 (br s, 3H, H_4), 4.02–3.97 (t, ^3J = 6.0 Hz, 6H, H_7), 3.41–3.24 (q, ^3J = 4.5 Hz, 6H, H_5), 2.09 (s, 3H, H_{13}), 2.00–1.92 (quin, ^3J = 6.0 Hz, 6H, H_6), 1.44 (s, 27H, H_1). ^{13}C{^{1}H} NMR ($CDCl_3$, δ): 156.9 (C_8), 156.2 (C_3), 142.1 (C_{11}), 129.8 (C_{10}), 113.8 (C_9), 79.34 (C_2), 65.94 (C_7), 50.77 (C_{12}), 38.32 (C_5), 30.94 (C_{13}), 29.71 (C_6), 28.56 (C_1). FT-IR (ν_{max}/cm^{-1}): 3353 (N–H), 1687 (C=O).

6.3.5 Preparation of 3-phenoxypropylamine (4.5)[9]

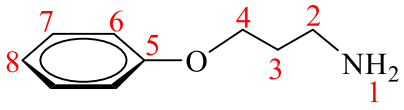

Trifluoracetic acid (1.29 g, 11.3 mmol) was added to a stirring solution of ^{t}butyl(3-phenoxypropyl)carbamate **4.3** (0.356 g, 1.42 mmol) in dichloromethane at 0 °C. The solution was allowed to stir to room temperature and then heated at 30 °C with periodic replenishment of dichloromethane as necessary. After 24 h, the reaction solution was added to a vigorously stirring 1:1 (v/v) mixture of ethyl acetate : NaOH (1M). The mixture was transferred to a 250 mL separating funnel and the aqueous layer was washed with ethyl acetate (3 x 50 mL). The organic extracts were combined and dried over anhydrous magnesium sulfate and filtered by gravity. The solvent was removed under reduced pressure, yielding the product (**4.5**) as a yellow oil which was collected and dried *in vacuo*. Yield: (0.150 g, 71%). ^{1}H NMR ($CDCl_3$, δ): 7.33–7.27 (m, 2H, H_6), 6.98–6.91 (m, 3H, $H_{7,8}$), 4.10–4.06 (t, ^{3}J = 6.0 Hz, 2H, H_4), 2.97–2.92 (t, ^{3}J = 6.6 Hz, 2H, H_2), 2.00–1.91 (quin, ^{3}J = 6.6 Hz, 2H, H_3), 1.55 (br s, 2H, H_1). $^{13}C\{^{1}H\}$ NMR ($CDCl_3$, δ): 158.0 (C_5), 130.9 (C_7), 121.5 (C_8), 114.3 (C_6), 66.02 (C_4), 37.40 (C_2), 30.91 (C_3). FT-IR (ν_{max}/cm^{-1}): 3319 (N–H), 3038 (N–H).

6.3.6 Preparation of 1,1,1-tris(4-phenoxymethyl)ethane-propylamine (4.6)

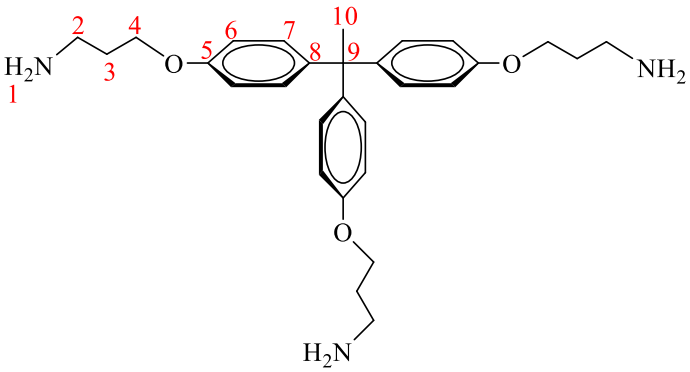

TFA (1.58 g, 13.8 mmol) was added to a stirring solution of 1,1,1-tris(*tert*-butyl-4-phenoxymethyl)ethane-propylcarbamate **4.4** (0.359 g, 0.461 mmol) in dichloromethane at 0 °C. The solution was allowed to stir to room temperature overnight and then heated at 30 °C for an additional 24 h, with periodic replenishment of dichloromethane as necessary. The reaction was allowed to cool to room temperature and then added to a vigorously stirring 1:1 (v/v) mixture of ethyl acetate : NaOH (1M). The aqueous layer was washed with ethyl acetate (4 x 50 mL) and the organic extracts were combined, dried over anhydrous magnesium sulfate and filtered by gravity. The solvent was removed under reduced pressure, revealing the product (**4.6**) as a clear oil which was collected and dried *in vacuo*. Yield: (0.164 g, 74%). ^{1}H NMR ($CDCl_3$, δ): 7.01–6.98 (m, 6H, H_6), 6.81–6.79 (m, 6H, H_7), 4.07–4.03 (t, ^{3}J = 6.0 Hz, 6H, H_4), 2.95–2.90 (t, ^{3}J = 6.0 Hz, 6H, H_2), 2.12 (s, 3H, H_{10}), 1.98–1.89 (quin, ^{3}J = 6.3 Hz, 6H, H_3), 1.60 (br s, 6H, H_1). $^{13}C\{^{1}H\}$ NMR ($CDCl_3$, δ): 157.3 (C_5),

142.9 (C_8), 129.4 (C_7), 113.0 (C_6), 66.81 (C_4), 50.76 (C_9), 37.38 (C_2), 30.91 (C_{10}), 29.83 (C_3). FT-IR (ν_{max}/cm^{-1}): 3361 (N–H), 3282 (N–H).

6.3.7 Preparation of 5-sulfonato phenoxypropylsalicylaldimine (4.7)

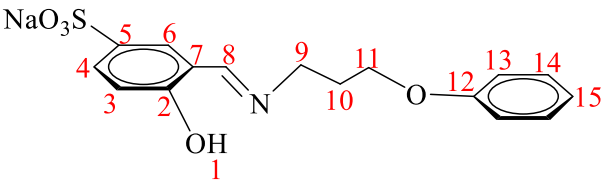

A solution of 3-phenoxypropylamine **4.5** (0.795 g, 5.26 mmol) in dry methanol (15 mL) was added to a stirring solution of 5-sulfonato salicylaldehyde **4.1** (1.18 g, 5.26 mmol) in dry methanol (60 mL), and the reaction was left to reflux overnight under nitrogen. The reaction was then allowed to cool to room temperature and filtered by gravity. The solvent was reduced to a minimum (*ca*. 3 mL), yielding a yellow precipitate which was collected by vacuum filtration, and washed with minimum cold methanol and diethyl ether to remove unreacted 3-phenoxypropylamine. The yellow solid was then recrystallised by re-dissolving in minimum methanol and chilling at 0 ºC in the refrigerator. The resultant yellow solid product (**4.7**) was collected *via* filtration by vacuum and washed with minimum cold methanol, and diethyl ether. Yield: (1.26 g, 67%). M.P.: decomposes without melting, onset occurs at 298 °C. ^{1}H NMR (DMSO-d$_6$, δ): 13.70 (br s, 1H, H_1), 8.64 (s, 1H, H_8), 7.70–7.68 (m, 1H, H_6), 7.56–7.52 (m, 1H, H_4), 7.30–7.23 (m, 2H, H_{13}), 7.17–7.13 (m, 1H, H_3), 6.90–6.86 (m, 2H, H_{14}), 6.80–6.77 (m, 1H, H_{15}), 4.08–4.04 (t, ^3J = 6.0 Hz, 2H, H_9), 3.84–3.79 (t, ^3J = 6.6 Hz, 2H, H_{11}), 2.20–2.11 (quin, ^3J = 6.6 Hz, 2H, H_{10}). ^{13}C{^{1}H} NMR (DMSO-d$_6$, δ): 166.5 (C_8), 161.5 (C_2), 155.5 (C_{12}), 140.0 (C_5), 130.4 (C_6), 129.3 (C_{13}), 126.5 (C_4), 123.4 (C_{15}), 117.6 (C_7), 116.1 (C_3), 112.6 (C_{14}), 65.77 (C_{11}), 55.42 (C_9), 31.87 (C_{10}). FT-IR (ν_{max}/cm^{-1}): 3294 (O–H), 1649 (C=N). ESI-MS (negative ion-mode), (*m/z*) = 334.0746 $[M]^-$ (calcd 334.0749). $H_2O_{solubility/25°C}$ = 21.4 mg/mL.

6.3.8 Preparation of 1,1,1-tris(4-phenoxymethyl)ethane-propyl-5-sulfonato salicylaldimine ligand (4.8)

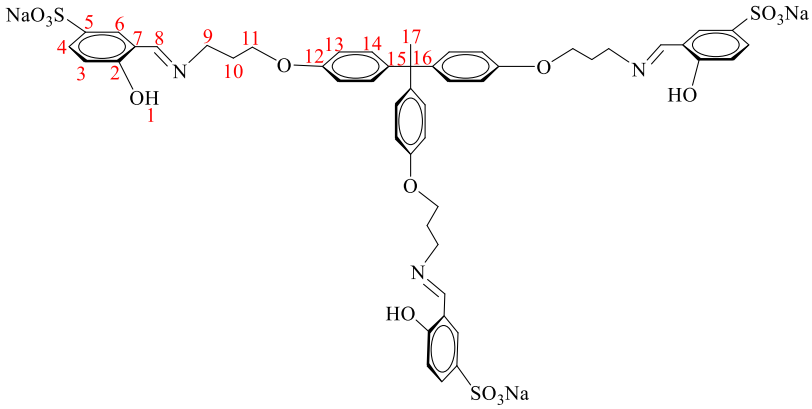

A solution of 1,1,1-tris(4-phenoxymethyl)ethane-propylamine **4.6** (0.399 g, 0.836 mmol) in dry methanol (10 mL) was added to a stirring solution of 5-sulfonato salicylaldehyde **4.1** (0.562 g, 2.51 mmol) in dry methanol (50 mL), and the reaction was left to reflux overnight under nitrogen. The reaction was then allowed to cool to room temperature and filtered by gravity. The solvent was removed under reduced pressure, to give an orange solid product which was re-dissolved in distilled water and filtered through a 0.22-micron hydrophilic PTFE syringe filter. The filtrate was lyophilised to yield the product as an orange solid which was then re-dissolved in minimum methanol and chilled at 0 ºC in the refrigerator. The resultant orange solid product (**4.8**) was collected by vacuum filtration and washed with minimum cold methanol, and diethyl ether and dried *in vacuo*. Yield: (0.661 g, 72%). M.P.: decomposes without melting, onset occurs at 307 °C. ^{1}H NMR (DMSO-d$_6$, δ): 13.64 (br s, 3H, H$_1$), 8.64 (s, 3H, H$_8$), 7.73–7.67 (m, 3H, H$_6$), 7.55–7.52 (m, 3H, H$_4$), 6.95–6.85 (m, 12H, H$_{13,\,14}$), 6.80–6.77 (m, 3H, H$_3$), 4.07–4.03 (t, ^{3}J = 6.0 Hz, 6H, H$_9$), 3.78–3.74 (t, ^{3}J = 6.6 Hz, 6H, H$_{11}$), 2.15–2.06 (quin, ^{3}J = 6.3 Hz, 6H, H$_{10}$), 2.03 (s, 3H, H$_{17}$). ^{13}C{^{1}H} NMR (DMSO-d$_6$, δ): 166.4 (C$_8$), 161.8 (C$_2$), 157.0 (C$_{12}$), 142.0 (C$_5$), 139.8 (C$_{15}$), 130.4 (C$_6$), 129.7 (C$_{13}$), 129.3 (C$_4$), 117.6 (C$_7$), 116.2 (C$_3$), 114.3 (C$_{14}$), 65.91 (C$_9$), 55.21 (C$_{11}$), 50.75 (C$_{16}$), 30.93 (C$_{17}$), 30.67 (C$_{10}$). FT-IR (ν_{max}/cm^{-1}): 1637 (C=N), 1609 (C=N). ESI-MS (negative ion-mode), (*m/z*) = 1084.2738 [M + Cl]$^{-}$ (calcd 1084.6675). $H_2O_{solubility/25°C}$ = 19.6 mg/mL.

6.3.9 Preparation of 5-sulfonato phenoxypropylsalicylaldimine Rh(I) complex (4.9)

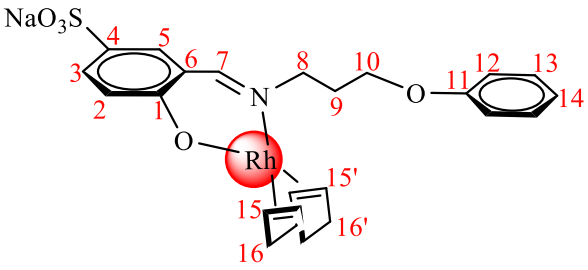

NaH (1.31 x 10^{-2} g, 0.547 mmol) was added to a stirring suspension of 5-sulfonato phenoxypropylsalicylaldimine **4.7** (0.107 g, 0.299 mmol) in dichloromethane (15 mL), and the reaction mixture was stirred for 30 minutes. A half molar equivalent solution of the dimer $[Rh(COD)Cl]_2$ (7.36 x 10^{-2} g, 0.149 mmol) in dichloromethane (5 mL) was added to the stirring suspension, and the reaction was left stirring at room temperature. After 12 h, methanol (5 mL) was added to quench the NaH, and the mixture was stirred for a further 30 minutes. The solvent was then reduced to a minimum (*ca*. 3 mL), yielding the product (**4.9**) as a yellow solid which was collected by vacuum filtration, washed with minimum cold methanol and diethyl ether, and dried *in vacuo*. Yield: (0.160 g, 94%). M.P.: decomposes without melting, onset occurs at 397 °C. ^{1}H NMR (DMSO-d_6, δ): 8.28 (s, 1H, H_7), 7.63–7.57 (m, 1H, H_5), 7.47–7.44 (m, 1H, H_3), 7.32–7.27 (m, 2H, H_{12}), 6.95–6.93 (m, 3H, $H_{13,\,14}$), 6.56–6.53 (m, 1H, H_2), 4.36 (br s, 2H, H_8), 4.05–4.00 (m, 4H, $H_{15,\,15'}$), 3.77 (br s, 2H, H_{10}), 2.40–2.27 (m, 4H, H_{16}), 2.12–2.02 (m, 2H, H_9), 1.91–1.76 (m, 4H, $H_{16'}$). ^{13}C{^{1}H} NMR (DMSO-d_6, δ): 166.2 (C_7), 164.9 (C_1), 158.2 (C_{11}), 134.5 (C_4), 132.4 (C_5), 132.0 (C_3), 129.3 (C_{12}), 120.5 (C_{14}), 119.4 (C_6), 117.1 (C_2), 114.3 (C_{13}), 83.70 (C_{15}), 70.94 ($C_{15'}$), 64.30 (C_{10}), 54.69 (C_8), 32.90 (C_9), 31.18 (C_{16}), 28.21 ($C_{16'}$). FT-IR (ν_{max}/cm^{-1}): 1606 (C=N). ESI-MS (negative ion-mode), (*m/z*) = 578.9556 $[M + Cl]^-$ (calcd 579.5195). $H_2O_{solubility/25°C}$ = 15.7 mg/mL.

6.3.10 Preparation of 1,1,1-tris(4-phenoxymethyl)ethane-propyl-5-sulfonato salicylaldimine Rh(I) complex (4.10)

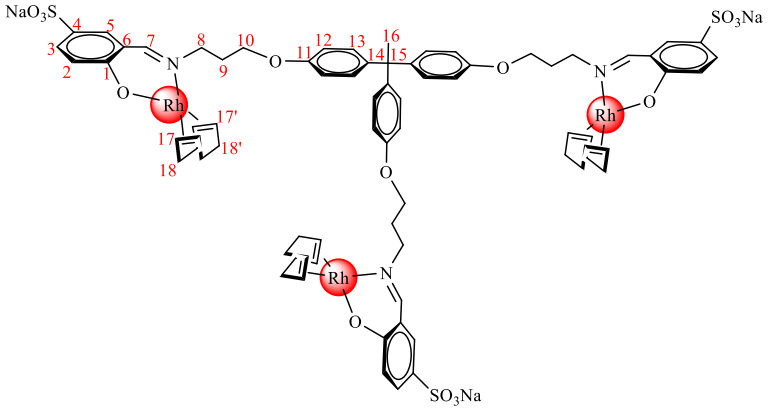

NaH (9.41 x 10^{-3} g, 0.392 mmol) was added to a stirring suspension of 1,1,1-tris(4-phenoxymethyl)ethane-propyl-5-sulfonato salicylaldimine ligand **4.8** (7.82 x 10^{-2} g, 7.13 x 10^{-2} mmol) in dichloromethane (15 mL), and the reaction mixture was stirred for 30 minutes. A one and a half molar equivalent solution of the dimer $[Rh(COD)Cl]_2$ (5.28 x 10^{-2} g, 0.107 mmol) in dichloromethane (5 mL) was added to the stirring suspension, and the reaction was left stirring at room temperature. After 12 h, methanol (5 mL) was added to quench the NaH, and the mixture was stirred for a further 30 minutes. The solvent was reduced to a minimum (*ca*. 3 mL), yielding the product (**4.10**) as a yellow solid which was collected by vacuum filtration, washed with minimum dichloromethane, methanol and diethyl ether, and then dried *in vacuo*. Yield: (1.20 g, 98%). M.P.: decomposes without melting, onset occurs at 296 °C. ^{1}H NMR (DMSO-d_6, δ): 8.29 (s, 3H, H_7), 7.68–7.57 (m, 3H, H_5), 7.49–7.45 (m, 3H, H_3), 6.99–6.73 (m, 20H, $H_{12,13}$), 6.61–6.49 (m, 3H, H_2), 4.52–4.17 (br s, 6H, H_8), 4.14–3.89 (br s, 12H, $H_{17,17'}$), 3.87–3.62 (br s, 6H, H_{10}), 2.39–2.23 (br s, 12H, H_{18}), 2.09–1.99 (br s, 9H, $H_{9,16}$), 1.87–1.75 (br s, 12H, $H_{18'}$). ^{13}C{^{1}H} NMR (DMSO-d_6, δ): 165.3 (C_7), 164.6 (C_1), 157.0 (C_{Ar}), 143.7 (C_{Ar}), 135.2 (C_{Ar}), 134.2 (C_{Ar}), 133.9 (C_{Ar}), 124.0 (C_{Ar}), 121.5 (C_{Ar}), 119.3 (C_{Ar}), 113.8 (C_{Ar}), 88.20 (C_{17}), 74.28 ($C_{17'}$). 65.34 (C_8), 40.01 (C_{10}), 35.49 (C_{15}), 30.19 (C_9), 29.64 (C_{18}), 29.36 (C_{16}), 28.04 ($C_{18'}$). FT-IR (ν_{max}/cm^{-1}): 1605 (C=N), 1586 (C=N). ESI-MS (positive ion-mode), (*m/z*) = 863.5983 $[M + 2H]^{2+}$ (calcd 863.5079). $H_2O_{solubility/25°C}$ = 8.6 mg/mL.

6.4 General hydroformylation procedure

6.4.1 Series 1 (homogeneous catalysis presented in Chapter 3)

$RhCl_3.3H_2O$ was purchased from Heraeus South Africa (Pty) Ltd. 7-Tetradecene was prepared *via* the metathesis of 1-octene using the Hoveyda-Grubbs second generation pre-catalyst, and then purified by removing the metathesis catalyst *via* organic solvent nanofiltration. The unreacted 1-octene was then boiled off to yield 7-tetradecene in high purity (> 98%).[10] Carbon monoxide and hydrogen gas were supplied by Afrox Ltd. Hydroformylation studies were conducted in a 100 mL stainless steel pipe reactor equipped with a Teflon interior. The conditions of the study (temperature and syngas pressure) were based on our previously reported work on the hydroformylation of 1-octene using analogous Rh(I) catalyst precursors bearing *N*,*O*-bidentate ligands.[6,11–13] In a typical experiment, the reactor was charged with toluene (7.5 mL), 1-octene (1.21 g, 10.7 mmol), dodecane as the internal standard (100 μL) and the precatalyst (2.87×10^{-3} mmol of Rh (**2.10**); or 9.57×10^{-4} mmol of Rh (**2.13**), substrate : Rh ratio 2500 : 1). The reactor was heated to the desired temperature, flushed with syngas ($CO:H_2$ = 1:1) and pressurised to the appropriate syngas pressure. Samples were analysed after 4 h using gas chromatography (GC-FID) equipped with a Zebron ZB-1701 capillary column (60 m x 250 μm x 0.25 μm). Authentic iso-octenes and aldehydes, alcohols and *n*-octane were used to confirm the products. Inductively coupled plasma optical emission spectroscopy experiments were conducted on a Varian 730 ES ICP-Optical Emission Spectrophotometer. Recyclability experiments presented in Section 3.2.4 of Chapter 3 were carried out after 2 h using the organic solvent nanofiltration technique (OSN) under the optimised conditions of temperature and pressure. In a typical recovery experiment, after the first catalytic run, the reaction components were cooled to room temperature, and diluted with toluene (7.5 mL). The solution was emptied into a stainless-steel dead-end separation cell mounted with a pre-conditioned Duramem® 200 membrane, and the cell was pressurised to 25 bar with nitrogen gas to enable the feed to flow through the membrane. The permeate was collected over time and the cell was de-pressurised when the feed was reduced to a minimum (negligible volumes). The catalyst-containing retentate was decanted from the cell with thorough rinsing using a portion of fresh toluene, and then reintroduced into the catalytic reactor bearing fresh substrate and the remainder of the toluene. The catalytic reaction was repeated under the same conditions of temperature, pressure and time, and subjected to the OSN technique after each cycle. Kinetic studies on the hydroformylation of 1-octene were conducted using the mononuclear catalyst

precursor **2.10** through varying the temperature, time, catalyst loading and total syngas pressure.

6.4.2 Series 2 (homogeneous catalysis presented in Chapter 5)

Carbon monoxide and hydrogen gas were supplied by Air Liquide. Hydroformylation studies were conducted in a 90 mL stainless steel pipe reactor. The conditions of the study (temperature and syngas pressure) were based on our previously reported work on the hydroformylation of 1-octene using analogous Rh(I) catalyst precursors bearing *N*,*O*-bidentate ligands.[6,11–13] In a typical experiment, the reactor was charged with the substrate (1-octene, 7.175 mmol), internal standard (*n*-decane, 1.435 mmol) and toluene (5 mL). The catalyst precursor (2.87×10^{-3} mmol of Rh (**4.9**); or 9.57×10^{-4} mmol of Rh (**4.10**) substrate : Rh ratio 2500 : 1) was dissolved in distilled water (5 mL) and introduced into the catalytic reactor. Degassing of the reactor was carried out twice with nitrogen, and twice with syngas ($CO:H_2$ = 1:1), after which the reactor was heated and pressurised to the desired temperature and syngas pressure. Samples were analysed after 4 h using a Perkin Elmer Clarus 580 GC instrument equipped with a flame ionisation detector and SGE Analytical capillary column (30 m x 0.25 mm). Authentic iso-octenes and aldehydes, alcohols and *n*-octane were used to confirm the products. Inductively coupled plasma optical emission spectroscopy experiments were conducted on a Varian 730 ES ICP-Optical Emission Spectrophotometer. In a typical recyclability assessment presented in Section 5.2.3 of Chapter 5, the product-containing organic phase was decanted for analysis by gas chromatography, while a fresh sample of 1-octene and *n*-decane (internal standard) was dissolved in toluene (5 mL) and added to the same catalyst-containing aqueous layer. This was repeated for each successive catalytic reaction using the same aqueous phase. On the other hand, the "neat" recyclability studies presented in Section 5.2.5 of Chapter 5 involved following the above procedure, but with the exclusion of toluene during the reaction. When the desired reaction time was reached, toluene was introduced to extract the organic products, and these were immediately decanted from the catalyst-containing aqueous-phase and analysed by gas chromatography. A fresh sample of 1-octene and internal standard (*n*-decane) was then added to the same catalyst-containing aqueous layer and charged back into the reactor. This was repeated for each successive catalytic reaction using the same aqueous phase.

6.5 References

1 H. Oie, A. Sudo and T. Endo, *J. Polym. Sci. Part A Polym. Chem.*, 2011, **49**, 3174–3183.

2 R. W. Kluiber and G. Sasso, *Inorg. Chim. Acta.*, 1970, **4**, 226–230.

3 P. K. Biswas, S. Saha, T. Paululat and M. Schmittel, *J. Am. Chem. Soc.*, 2018, **140**, 9038–9041.

4 M. Sun, H. Y. Zhang, Q. Zhao, X. Y. Hu, L. H. Wang, B. W. Liu and Y. Liu, *J. Mater. Chem. B*, 2015, **3**, 8170–8179.

5 P. Antoni, D. Nyström, C. J. Hawker, A. Hult and M. Malkoch, *Chem. Commun.*, 2007, 2249–2251.

6 E. B. Hager, B. C. E. Makhubela and G. S. Smith, *Dalton Trans.*, 2012, **41**, 13927–35.

7 H. Li, M. A. Hao, L. Wang, W. Liang and K. Chen, *Org. Prep. Proced. Int.*, 2009, **41**, 301–307.

8 P. Hidalgo Ramos, P. Saisaha, J. A. A. W. Elemans, A. E. Rowan and R. J. M. Nolte, *Eur. J. Org. Chem.*, 2016, 4487–4495.

9 E. Robinson, E. Leung, A. M. Matuszek, N. Krogsgaard-Larsen, D. P. Furkert, M. A. Brimble, A. Richardson and J. Reynisson, *Med. Chem. Commun.*, 2015, **6**, 239–246.

10 P. van der Gryp, S. Marx and H. C. M. Vosloo, *J. Mol. Catal. A Chem.*, 2012, **355**, 85–95.

11 S. Siangwata, S. Chulu, C. L. Oliver and G. S. Smith, *Appl. Organomet. Chem.*, 2017, **31**, e3593.

12 S. Siangwata, N. Baartzes, B. C. E. Makhubela and G. S. Smith, *J. Organomet. Chem.*, 2015, **796**, 26–32.

13 L. C. Matsinha, S. F. Mapolie and G. S. Smith, *Dalton Trans.*, 2015, **44**, 1240–1248.

Chapter 7

Overall summary, conclusions and future outlook

7.1 Synthesis and characterisation of aryl ether-based mononuclear and multinuclear salicylaldimine Rh(I)-complexes

The main objectives of this study were to prepare a series of new aryl ether salicylaldimine-based mononuclear, trinuclear and hexanuclear complexes of Rh(I), and evaluate these in the hydroformylation of higher olefins. Recyclability studies of the complexes were to be performed using the organic solvent nanofiltration strategy. In addition, kinetic studies were to be conducted using the complexes, to gain insights into the driving forces of our catalytic system.

A series of new aryl ether salicylaldimine-based Rh(I) mononuclear (**2.2**) and trinuclear (**2.5**) complexes were prepared following Schiff base condensation synthesis, complexation with the rhodium dimer $[RhCl(COD)]_2$ *via* a bridge splitting reaction, and Williamson ether synthesis. A dinuclear aryl ether salicylaldimine-based wedge (**2.6**) to the haxanuclear complex was also prepared and characterised using various spectroscopic and analytical techniques. However, the trinuclear complex (**2.5**) and the dinuclear wedge (**2.6**) were obtained in unfavourably low yields, which is counter to the objective of beneficiating the rhodium metal, as one of the rare, fast-depleting and relatively expensive Platinum Group Metals. The low yields were attributed to the tedious purification procedure that was required for **2.5** (22%) and **2.6** (34%), with product loses occurring at each step. The high yielding approach of Click Chemistry was then conducted in the preparation of new monomeric (**2.9**) and trimeric (**2.12**) ligands, as well as a dimeric wedge (**2.17**) and a hexameric ligand (**2.18**). These aryl ether salicylaldimine triazolyl-based ligands were obtained in good yields (> 75%) and characterised using ^{1}H NMR, ^{13}C NMR and infrared spectroscopy. Subsequently the ligands **2.9** and **2.12** were reacted with $[RhCl(COD)]_2$ *via* a bridge splitting reaction to afford in good yields, the mononuclear complex **2.10** (83%) and the trinuclear complex **2.13** (99%) respectively. The complexes were characterised using ^{1}H NMR, ^{13}C NMR and infrared spectroscopy, high resolution electrospray ionisation mass spectrometry (positive ion-mode), and melting point determinations. The hexameric ligand **2.18** could not be purified further despite several attempts, and this was

attributed to insolubility challenges in various available solvents. However, the ^{1}H NMR spectrum of the ligand (**2.18**) showed with certainty the presence of the desired signals that would be expected in the proposed structure of **2.18**.

The mononuclear and trinuclear Rh(I) complexes were successfully evaluated in the hydroformylation of higher olefins, with 1-octene as the model substrate. The mononuclear complex (**2.10**) gave good catalytic performance in the hydroformylation of 1-octene under mild optimum reaction conditions (85 °C, 40 bar for 4 h). These conditions gave good aldehyde chemoselectivity (90%), excellent conversion of the substrate (99%) and good catalytic activity (554 h^{-1}). Such catalyst performance is attractive since 1-octene is the simplest representation of the medium to long chain olefins that bring about the corresponding highly desirable medium to long chain aldehyde products.[1–3] The trinuclear dendritic complex (**2.13**) was then evaluated in the hydroformylation of 1-octene against the mononuclear complex (**2.10**) under milder conditions (85 °C, 20 bar for 4 h) and comparable performance was obtained for both precatalysts. This performance was ascribed to the poor solubility of the dendritic complex **2.13** in the solvent of choice (toluene), which potentially limited the interaction of the precatalyst with the substrate. The mercury poisoning experiment using catalyst precursor **2.10** revealed a nanoparticle-assisted catalytic system, indicating that the reaction is not entirely homogeneous, a phenomenon that we have also observed in our previous studies.[4,5] However, despite the reaction proceeding as a nanoparticle-mediated system, it should be mentioned that no hydrogenation products were observed in the hydroformylation studies using **2.10** and **2.13**, which is a significant result towards reducing unwanted product formation.[5] The versatility of precatalyst **2.10** was also evaluated in the hydroformylation of internal olefins, 7-tetradecene and *trans*-4-octene. Good conversions of both internal olefins were obtained (> 80%), which is attractive to the surfactant industry.[6–8] To establish further the avenues of beneficiating the Rh(I) precatalyst **2.10** and **2.13**, recyclability studies were conducted following the greener strategy of organic solvent nanofiltration. The complexes could be recycled for at least 5 times in the hydroformylation of 1-octene, with consistently good catalytic performance. The efficiency of the membrane to recover the metal was attested to *via* ICP-OES analysis, revealing a near-perfect (99%) rejection of the rhodium metal. This is vital for the downstream products, and also reflects on the process efficiency of the OSN membrane recovery technology.[9–11] Kinetic studies were conducted using precatalysts **2.10** and **2.13**, which lead to the determination of the activation energy of 62 kJ mol^{-1}. The studies also revealed that the observed reaction rate constants corelate well with a modified fundamental mechanistic-based

rate model, validating the experimental data obtained for precatalysts **2.10** and **2.13**, and giving a better insight of the driving forces of our system.

The advantages of the present Rh catalysts include:

(i) Operation under mild reaction conditions to give good catalytic activity and excellent chemoselectivity for aldehydes in the hydroformylation of the often-strenuous higher olefins.

(ii) Versatile, robust and stable precatalysts that can also be used for the hydroformylation of internal olefins, which are the feedstocks for the surfactant and detergent industries.

(iii) Good recyclability over multiple cycles with consistently appreciable catalytic performance.

(iv) Conforms to the Green Chemistry principles through the ease of catalyst recovery using the non-destructive and less energy intensive OSN technology.

7.2 Synthesis and characterisation of water-soluble aryl ether-based mononuclear and multinuclear salicylaldimine Rh(I)-complexes

The main objectives of this study were to prepare a series of new water-soluble aryl ether salicylaldimine-based mononuclear and trinuclear complexes of Rh(I), and to evaluate these in the aqueous biphasic hydroformylation of higher olefins. Recyclability studies of the complexes were to be performed using the aqueous biphasic strategy, a greener approach owing to the use of water as a solvent.

In this work, we have reported the preparation of precursor compounds that lead to water-soluble aryl ether salicylaldimine-based mono- and trinuclear ligands. The precursors to the ligands were prepared following a series of protection and deprotection procedures (amine and Boc-type), Schiff base condensation reactions, and finally Williamson ether synthesis. This afforded the monomeric ligand (**4.7**) and the trimeric ligand (**4.8**) in good yields (67% and 72% respectively). The ligands possess good solubility properties in water (21.4 mg/mL (**4.7**) and 19.6 mg/mL (**4.8**)). The reduced solubility of **4.8** could be ascribed to the hydrophobic character imparted by the THPE core of the trimeric structure. The ligands were characterised using ^{1}H NMR, ^{13}C NMR and infrared spectroscopy, high resolution electrospray ionisation mass spectrometry (positive and negative ion-mode), and melting point determinations. Complexation of the ligands **4.7** and **4.8** with the appropriate quantity of the rhodium dimer

$[RhCl(COD)]_2$ afforded the mononuclear complex (**4.9**) and trinuclear *N*,*O*-chelate rhodium(I) complex (**4.10**) in good yields (94% and 98% respectively). The complexes show appreciably good solubility in water, 15.7 mg/mL (**4.9**) and 8.6 mg/mL (**4.10**). The complexes were further characterised using various analytical and spectroscopic techniques.

Preliminary aqueous biphasic hydroformylation experiments were successfully performed using **4.9** as the model catalyst precursor, and 1-octene as the model substrate. Both catalyst precursors **4.9** and **4.10** gave good catalytic performance under optimum conditions (85 °C, 50 bar for 4h), suggestive of good interfacial interaction with the substrate. The catalyst precursors posted near-quantitative catalytic conversion of 1-octene, good activities ($> 550\ h^{-1}$) and attractive aldehyde chemoselectivity (90% (**4.9**), and 88% (**4.10**)). The mercury drop test was suggestive of a system that has a dual influence, from the homogeneous catalytic species as well as from the heterogeneous Rh-nanoparticles. This behaviour is similar to our previous observations in the literature for similar systems.[12,13] Recyclability experiments were successfully conducted over 5 cycles, with a gradual decline in catalytic performance for both complexes. It is recognised that aqueous biphasic systems are often confounded with catalyst leaching from the aqueous layer to the organic phase.[14] This was attested to *via* ICP-OES experiments, which showed moderate losses of the metal from the aqueous phase (41% (**4.9**), and 57% (**4.10**)). The linear aldehyde selectivity was increased by addition of excess bulkier trimeric ligand (**4.8**) to the catalytic system of precatalyst **4.10**. "Neat" monophasic catalytic experiments were successfully performed in water using the catalyst precursors **4.9** and **4.10**, as part of the attempts to alleviate the leaching of the catalyst precursors to the organic layer. The dendrimer-stabilised trinuclear catalyst **4.10** showed improved recyclability in the "neat" hydroformylation experiments, while the mononuclear precatalyst **4.9** showed a reduced overall performance. This was attributed to degradation of the mononuclear precatalyst, as evidenced by the black particulate matter after the reaction, which is indicative of degradation. A comparative study revealed that the rigid core-bound catalyst precursor **4.10** showed superior catalytic performance to our previously reported flexible core-bound catalyst precursor,[12] prepared *in situ* from the *tris*-ligand (**1.25**) and appropriate quantity of $[RhCl(COD)]_2$ dimer. The versatility of the catalyst precursors (**4.9** and **4.10**) was evaluated in the hydroformylation of styrene under aqueous biphasic environment. Both catalyst precursors showed good catalytic activity ($> 450\ h^{-1}$) and a total bias to aldehyde chemoselectivity (no hydrogenation products).

The advantages of the present water-soluble Rh catalysts include:

(i) Mild reaction conditions that give good catalytic activity and excellent chemoselectivity for aldehydes in the hydroformylation of the medium to long chain representative substrate, 1-octene.

(ii) Good catalytic performance in the presence of the relatively abundant, non-toxic, user-friendly and less toxic greener solvent, water.

(iii) Facile catalyst recovery *via* the biphasic approach, giving moderate to good recyclability of at least five cycles, consequently reducing the associated costs of catalyst deactivation at early stages.

(iv) Versatile catalytic system that performs well with the substituted aryl olefin representative, styrene.

7.3 Future outlook

The present recovery techniques reported in this work are a fundamental component of a drive aimed at beneficiation of the often-expensive PGM-based catalyst precursors. Moreover, the techniques are aligned well with the Green Chemistry principles on the use of energy-efficient systems (for example, OSN recovery technique), harmless solvents (for example, "water"-organic recovery technique), atom-efficient processes (hydroformylation), value-adding transformations (≥ C8 linear and internal olefins) and the overall speeding up of reactions (*via* catalysis).

As part of the strategies to complement the above-mentioned recovery techniques on catalyst efficiency, it could be useful to design complexes that possess electron-donating and electron-withdrawing substituent groups. These have in the past been shown to have a degree of influence in the reaction rates and selectivity of a catalyst.[13] Furthermore, phenyl groups with bulky substituents (for example, ^{t}Bu) could be incorporated close to the metal centre as these have previously been reported to be essential in channelling the regioselectivity towards high *n*:*iso* ratios.[12] Conducting high pressure NMR studies could assist in ascertaining the structural integrity of the complexes under hydroformylation conditions. This could be extended to the recycling studies using both techniques (OSN and aqueous biphasic strategies), to better understand the species responsible for the catalytic performance with constant reuse of the catalyst-containing solution. Further to that, a thermomorphic solvent system approach can be adopted using the present catalysts (with appropriate modification) in the rhodium-catalysed

hydroformylation of higher olefins, since this approach is not hampered by mass transfer limitations that are associated with the aqueous biphasic strategy.[14–19] This approach takes advantage of the phase change during a reaction as a result of an alteration in temperature. The catalyst is soluble in the respective solvents at elevated temperature, allowing for effective interaction with the substrate, and insoluble at a lower temperature allowing for effective phase separation for catalyst reuse.[20–23] Moreover, thermomorphic solvent systems can be successfully merged with the OSN recovery technique,[24,25] and this could be an interesting avenue to pursue using the appropriately modified catalysts of the present study.

7.4 References

1 M. Beller, B. Cornils, C. D. Frohning and C. W. Kohlpaintner, *J. Mol. Catal. A Chem.*, 1995, **104**, 17–85.

2 C. De, R. Saha, S. K. Ghosh, A. Ghosh, K. Mukherjee, S. S. Bhattacharyya and B. Saha, *Res. Chem. Intermed.*, 2013, **39**, 3463–3474.

3 L. I. Kaoxue, W. Yanhua, J. Jingyang and J. I. N. Zilin, *Chinese J. Catal.*, 2010, **31**, 1191–1194.

4 S. Siangwata, S. Chulu, C. L. Oliver and G. S. Smith, *Appl. Organomet. Chem.*, 2017, **31**, e3593.

5 S. Siangwata, N. Baartzes, B. C. E. Makhubela and G. S. Smith, *J. Organomet. Chem.*, 2015, **796**, 26–32.

6 G. T. Whiteker and C. J. Colbey, *Top Organomet Chem*, 2012, **42**, 35–46.

7 L. A. van der Veen, P. C. J. Kamer and P. W. N. M. van Leeuwen, *Angew. Chem. Int. Ed.*, 1999, **38**, 336–338.

8 B. Cornils and W. A. Herrmann, *J. Catal.*, 2003, **216**, 23–31.

9 D. Ormerod, B. Sledsens, G. Vercammen, D. van Gool, T. Linsen, A. Buekenhoudt and B. Bongers, *Sep. Purif. Technol.*, 2013, **115**, 158–162.

10 M. Christian and D. Vogt, *Green Chem.*, 2011, **13**, 2247–2257.

11 P. Marchetti, M. F. J. Solomon, G. Szekely and A. G. Livingston, *Chem. Rev.*, 2014, **114**, 10735–10806.

12 E. B. Hager, B. C. E. Makhubela and G. S. Smith, *Dalton Trans.*, 2012, **41**, 13927–35.

13 L. C. Matsinha, S. F. Mapolie and G. S. Smith, *Dalton Trans.*, 2015, **44**, 1240–1248.

14 M. Benaglia, in *Recoverable and Recyclable Catalysts*, John Wiley & Sons, Ltd., Chichester, 1st edn., 2009, pp. 1-458.

15 P. Tundo and A. Perosa, *Chem. Soc. Rev.*, 2007, **36**, 532–550.

16 M. S. Shaharun, B. K. Dutta, H. Mukhtar and S. Maitra, *Chem. Eng. Sci.*, 2010, **65**, 273–281.

17 Y. Brunsch and A. Behr, *Angew. Chem. Int. Ed.*, 2013, **52**, 1586–9.

18 A. Behr, Y. Brunsch and A. Lux, *Tetrahedron Lett.*, 2012, **53**, 2680–2683.

19 J. Tijani and B. E. Ali, *Appl. Catal. A Gen.*, 2006, **303**, 158–165.

20 J. Bianga, K. U. Künnemann, T. Gaide, A. J. Vorholt, T. Seidensticker, J. M. Dreimann and D. Vogt, *Chem. Eur. J.*, 2019, **25**, 11586–11608.

21 T. Gaide, A. Jörke, K. E. Schlipköter, C. Hamel, A. Seidel-Morgenstern, A. Behr and A. J. Vorholt, *Appl. Catal. A Gen.*, 2017, **532**, 50–56.

22 E. Schäfer, Y. Brunsch, G. Sadowski and A. Behr, *Ind. Eng. Chem. Res.*, 2012, **51**, 10296–10306.

23 J. Markert, Y. Brunsch, T. Munkelt, G. Kiedorf, A. Behr, C. Hamel and A. Seidel-Morgenstern, *Appl. Catal. A Gen.*, 2013, **462**–**463**, 287–295.

24 B. Scharzec, J. Holtkötter, J. Bianga, J. M. Dreimann, D. Vogt and M. Skiborowski, *Chem. Eng. Res. Des.*, 2020, **157**, 65–76.

25 J. M. Dreimann, F. Hoffmann, M. Skiborowski, A. Behr and A. J. Vorholt, *Ind. Eng. Chem. Res.*, 2017, **56**, 1354–1359.